2020

Retinal Repair for Macular Degeneration

A thesis submitted for the Degree of Doctor of Philosophy

JOANA FILIPA CLAUDIO RIBEIRO

Department of Genetics

UCL Institute of Ophthalmology

Primary Supervisor: Professor Robin Ali

Declaration

I, Joana Filipa Claudio Ribeiro, confirm that the work presented in this thesis is my own. Where information has been derived from other sources, I confirm that this has been indicated in the thesis.

Abstract

Current treatments for macular degeneration, such as gene therapy, pharmacological approaches and neuroprotective approaches require the present of the target cells, the photoreceptors, in order to achieve a successful outcome. This leaves several patients, where the retinal degeneration is too advanced, without any viable therapeutic alternative. Photoreceptor transplantation aims to replace the lost cells, providing a potential option for such cases.

For photoreceptor replacement to succeed, transplanted photoreceptors must mature and establish synaptic connection with the host retina. The remodeling of the host retina must be considered, as its interneurons and synaptic circuits rearrange following photoreceptor degeneration. Additionally, an ethical and renewable source is required. Studies have shown that mouse and human embryonic stem cells (ESC) can be differentiated to photoreceptor and transplanted into models of retinal dystrophy. However, no unambiguous evidence of synaptic connectivity and rescue of vision have been achieved.

Here a detailed characterization of the remodeling events following photoreceptor lost in *Aipl1*$^{-/-}$ animals is described. *Aipl1*$^{-/-}$ were chosen due to the severe and fast emerging phenotype. As expected, typical features of remodeling were identified in these retinas and potential morphological elements were selected for analysis, following transplantation. The transplantation conditions, specifically the number of transplanted cells, were optimized using mouse ESC-derived photoreceptors. Here was no evident cell maturation or integration in the host's synaptic circuit, following transplantation. Interestingly, when transplanting human (h) ESC-derived cones indication of such events was seen. To increase the period post-transplantation *Aipl1*$^{-/-}$ and *Rd*^{1}, another well-established model of end-stage retinal degeneration, mice were crossed with immuno-compromised animals. Twelve weeks following transplantation into immuno-compromised *Rd*^{1} mice, hESC-derived cones matured and established functional synapses with the host retina, achieving rescue of vision. Alternative explanations for the rescue seen can be excluded due to the use non-functional human induced pluripotent (hiPS)-derived cones as a sham control.

Impact Statement

Macular degeneration, by photoreceptor loss, is the primary cause of blindness in the western world; age-related macular degeneration (AMD) is a major contributor, along with other inherited retinal diseases. Macular degeneration is a major public health problem in developed countries. The macula is a cone rich area of the retina which is responsible for central vision mediated by cone photoreceptor cells, accounting for almost 10% of the entire visual field. Therefore, any damage to the macula that leads to photoreceptor loss has a major impact in one's quality of life as well as their families. Loss of vision reduce people's ability to perform daily tasks independently, such as reading, which impairs their contribution and interaction with the society. Beyond overwhelming and detrimental for the patient's mental health it jeopardises patient's employment and capacity of taking care of them self and their dependents. Furthermore, visual impairment associated with age or inherited macular degeneration also has a high socio-economic impact. The costs of supporting patients suffering from this debilitating pathology are high and the prevalence of an age-related disease such as this will increase as the life span increases.

Current treatments for macular degeneration, such as gene therapy, pharmacological approaches and neuroprotective approaches have in common the necessity of the target cell being present for the therapy to work. This leaves several patients, where the retinal degeneration is too advanced and very few photoreceptor cells are present, without any viable therapeutic option. Efforts to develop electrical-retinal-implants have achieved promising results, however the long-term damage of such devices to the inner retina still needs to be addressed. The size of the implant, the necessity of an intact inner retina and the risk to produce thermal damage to the retina call for the necessity to explore other approaches, such as cell replacement therapy.

The macula is an ideal area of the eye to explore the potential of cell replacement as it is small and accessible. In the present study we aim to optimise transplantation of human stem cell-derived cones into an end-stage degeneration retina, where the lack of photoreceptors and the remodelling of the interneurons is severe, mimicking several human conditions of advance retinal degeneration.

In this project transplantation conditions were optimised and long-term cell survival and maturation of the transplanted cone photoreceptors, as well as establishment of synaptic connections between transplanted cone photoreceptors and host retina was achieved. Importantly, the results suggest that the transplanted cells are able to

detect light and to connect with the host retina, propagating the signal through the host's circuit, which results is a rescue of visual function.

Despite the necessity to further investigate and improve connectivity between transplanted cells and the host retina, this study provides proof-of-concept that retinal repair for macular degeneration, using a cell replacement strategy, is feasible.

Once available as a therapy for macular degeneration, this strategy could help millions of people suffering from blindness, having a great impact in their lives, their family and in modern society.

Acknowledgments

The findings described in this thesis would not have been possible without the help and support of several people, to who I will always be grateful.

I wish to express my gratitude to my primary supervisor Professor Robin Ali for the opportunity of developing this project and be part of a great team of scientists, as well as for the support and guidance. I am also deeply appreciative of Dr Alexander Smith for all the valuable advice and constructive criticism that contribute for my development as a scientist. To Professor Rachael Person and Professor James Bainbridge I would like to thank for the availability, guidance and advice as well as for performing the sub-retinal injections that were required during this project.

I am thankful to Dr Christopher Procyk for collecting and analysing the Multielectrode Array data for this project, giving it an electrophysiological output. I am also appreciative of his patience and time spend teaching me the required basic knowledge to interpret such data sets. A word of appreciation for Dr Mateo Rizzi and Dr Kate Powel for the valuable advice. To Michelle O'Hara-Wright, I am grateful for the help with several experiments over the last year, which allowed me to conclude the writing of these thesis. A special thank you to the Stem cell group for all the help and support, specially to Arifa Naeem that introduced me to the "world of stem cell work" and to Dr Emma West, who as support me and given me valuable advice specially during the last year. A heartfelt thank you to my office girls that have given me a much-needed moral support and shoulder to cry on whenever necessary.

I must express my deepest gratitude to my secondary supervisor, Dr Anai Gonzalez-Cordero, for building this project with me. For being always supportive and available even with half a world of distance between us. Dr Anai Gonzalez-Cordero is an inspired and inspiring person that contaminates those around her with her enthusiasm for science. Thank you for pushing me to always want to do better and for being such a great example of what can be achieved through hard work. I will forever be grateful for the honour to work and learn from you.

Finally, I would like to thank my family for believing in me and always supporting me. A very special thank you to my, soon to be, husband, Enrico Walser, who endure four year of my extremely demanding working hours and emotional stress. Thank you for making my life easier and for being the constant force that helped me to keep going.

Without all these people, and others that I probably forgot to mention, getting this far would not have been possible.

Abbreviations list

AAV – adeno-associated virus

ALT - advanced Long-Term Medium

AMD – age-related macular degeneration

BMP - bone morphogenic protein

BPCs – bipolar cells

BRB - blood-retinal barrier

cGMP - cyclic guanosine monophosphate

COS – cone outer segments

Crx - cone-rod homeobox protein

DAPI - 4′,6-diamidino-2-phenylindole

dd – differentiation day

DM - differentiation medium

Dnmt1 - DNA methyltransferase 1

E – embryonic day

EB – embryonic body

EFTFs - eye field transcription factors

EM - Expansion Medium

ERG - electroretinogram

ESCs – embryonic stem cells

FACS - fluorescence-activated cell sorting

FGF - fibroblast growth factor

FM - Freezing Medium

GCL – ganglion cell layer

GCPAs - guanylate cyclase-activating proteins

GC - guanylate cyclase

GFP – green florescence protein

GMP - good manufacturing practice

h – human

Hh – hedgehog

iGluR – ionotropic glutamate receptor

ILM - inner limiting membrane

INL – inner nuclear layer

IPL – inner plexiform layer

ipRGCs – intrinsically photosensitive retinal ganglion cells

iPSCs – induced pluripotent stem cells

IRBP - interphotoreceptor retinoid binding

L-AP4 - L-2-amino-4-phosphonobutyric acid

L-CCG-1 - L-2-(Carboxycyclopropyl)glycine

LRAT - lecithin retinol acyltransferase

m – mouse

MEA – multi-electrode array

Meta II - metarhodopsin II

mGluR - Glutamate receptor, metabotropic

NRVs – neuro-retinal vesicles

NOD - Non-obese diabetic

Nrl - neural retina leucine zipper

OC – optic cup

OLM - the outer limiting membrane

ONL – outer nuclear layer

OPL – outer plexiform layer

OV – optical vesicles

p – postnatal day

PBS - phosphate-buffered saline

PCs – principal components

PSCs – pluripotent stem cells

PDE – phosphodiesterase

pMEA - perforated Multi Electrode Array

RA - retinoic acid

rd – retinal degeneration

RdCVF - rod-derived cone viability factor

RDH - retinol dehydrogenases

RDM - Retinal Differentiation Medium

Rec – Recoverin

RGCs – Retinal ganglion cells

RMM - Retinal Maturation Medium

RORβ- retinoid-related orphan receptor

ROS – rod outer segments

RP – Retinitis Pigmentosa

RPCs – retinal progenitor cells

RPE – retinal pigment epithelium

SCID – Severe combined immunodeficiency

Sd – standard deviation

Shh - Sonic hedgehog

SRS – subretinal space

STGD1 - Stargardt disease type 1

TEM – transmission electronic microscopy

TRβ2 - thyroid hormone receptor β2

Table of Content

Figures

Tables

Chapter 1: Introduction

Cell transplantation as a therapy for retinal degeneration has been the subject of many studies during the last decade and there have been several reports of rescue of vision following transplantation of photoreceptor cells. A number of studies (described in section 1.4) suggested that transplanted photoreceptor cells are able to migrate, integrate into host retina and restore vision by making new functional synapses. However, it was recently discovered that transplanted photoreceptor cells are able to engage in cytoplasmic material transfer with host cells, by a mechanism not yet known. Considering this novel finding, most of these photoreceptor transplantation published studies had to be re-evaluated. At the time the project described in this thesis started, the future of cell transplantation as a therapy seemed uncertain. It is imperative to ascertain unambiguously if *de novo* synapses can be established between transplanted photoreceptors and host retina, by addressing and minimizing the possibility of rescue by any alternative mechanism.

The focus of my thesis is on photoreceptor transplantation for the treatment of end stage retinal degeneration, when majority of photoreceptor in the treated area are lost. In the absence of host photoreceptors, rescue by material transfer can be excluded. We can therefore determine whether transplanted photoreceptors are able to make functional connections with the host retina and thus provide a treatment for advanced retinal degeneration.

Other therapies, such as gene therapy, gene editing, or pharmacological approaches, are already in clinical trials. However, these therapies are not suitable for advanced degeneration, where the target photoreceptor cells are no longer present. This leaves a major proportion of patients suffering from retinal degeneration without a possible treatment. Other alternative strategies to treated advanced retinal degeneration are the use of a light-sensitive prosthetic device and optogenetic tools. The use of light-sensitive prosthetic devices has been tested in a clinical trial setting, but due to their size very limited spatial resolution can be achieved compared with light-sensitive cells. Therefore, further optimization is required. Similarly, optogenetic tools present great potential alternative, as those strategies would aim to confer light-sensitiveness to the remaining interneurons of the retina, following photoreceptor degeneration. However, the optogenetic tools currently available still do not present the necessary sensitiveness to provide a level of vision comparable to that photoreceptor cells provide. Consequently, exploring and addressing the potential of photoreceptor

replacement, now with renewed focus on connectivity between host and transplanted cell as well as exclusion of material transfer, is extremely valuable for the field.

In this study we evaluate the efficacy of photoreceptor cell transplantation in an end-stage retinal degeneration mouse model to determine what can currently be achieved and what requires further optimisation to achieve an effective therapy for advanced retinal degeneration. As this is a project with a strong translational perspective and strong focus in technical optimisation to achieve cell survival, maturation and functional rescue following transplantation, it is imperative to explore the current literature and concepts that allow formulation of hypotheses and interpretation of results. As such, an overview of eye development, retinal cell types as well as the principles of vision is provided here. There is an emphasis on the retinal circuit and how the retinal morphology and organisation are essential for the synaptic connections to be established in development and how they are affected following retinal degeneration. By introducing the transplanted photoreceptor cells, we are likely to influence the microenvironment of the host retina and perhaps replicate the necessary signals to induce formation of new, functional synapses between the transplanted cells and the host's interneurons. As this work aims to lead to future studies for repairing the macula, a small, but very important area of retina for human vision, special attention has been given to the cone pathway in the retinal circuit. Finally, to in order to establish an effective therapy for widespread use, a renewable cell source is required and thus the basic concepts regarding embryonic stem cells and differentiation of retinal organoids are also explored in this introduction chapter.

1.1 The mammalian eye: anatomy and structure

The mammalian eye is composed of three different layers: the external corneoscleral layer that comprises the cornea, sclera and uveal tract; the intermediate layer comprising the iris, ciliary body and choroid; and the internal layer, the retina, where the sensory cells of the eye are located (Figure 1). The eye is divided into three fluid chambers: the anterior chamber which is located between the cornea and the iris; the posterior chamber which is located between the iris and the lens; and the vitreous chamber, the largest of the three, that is located between the lens and the retina. The anterior and posterior chambers contain aqueous humour while the vitreous chamber is filled with vitreous humour, a more viscous liquid.

The corneoscleral layer provides protection against ocular trauma. The sclera is a layer of collagen and elastin that covers the whole eye, with exception of the front where the cornea is located. The cornea is formed by five layers of transparent tissue which allows passage of light into the eye. The uveal tract, comprising the iris, ciliary body and choroid, is a thin, pigmented and vascular layer that lines the corneoscleral layer from the pupil to the optic nerve. The iris contains the pupillary muscles responsible for adjusting the size of the pupil, regulating the amount of light that enters the eye. The ciliary body has two regions, the anterior pigmented pars plicata and the posterior non-pigmented pars serrata, this being in continuity with the ora serrata, the area where the neural retina begins. The ciliary processes present in the pars plicata are responsible for aqueous humour production, and in the pars plana, the ciliary epithelium secures the lens in place enabling focusing of the eye. The choroid lines the interior surface of the sclera and is a pigmented, thin layer with a vast network of blood vessels that provides nutritional support to the outer layers of the retina. The pigment of the choroid absorbs the extra light that passes through the retina, preventing internal reflection that would disturb vision. The retina is the innermost layer of the eye and is formed by two layers: the neural retina, where the cells that respond to light are located, and the retinal pigmented epithelium (RPE), the non-neural retina. These two layers are not anatomically connected but are adjacent to each other, and support and interact with each other in very close proximity. All the other structures in the eye are responsible for maintaining its shape, protecting it from external damage, and mainly allowing and focussing the passage of light, so that it can reach the neural retinal and initiate the neural impulses that are transmitted to the brain to be converted into an image.

Figure 1 - Schematic of the structure of the eye.

From Webvision under a Creative Commons License

http://webvision.med.utah.edu/book/part-i-foundations/simple-anatomy-of-the-retina/

The eye is composed of three layers, which perform distinct functions. The external layer consisting of sclera and the cornea create a barrier from the external environment and provides structural support. The intermediate layer consists of the iris, ciliary body and the vascular network of the choroid. Pupillary muscles of the iris regulate the size of the pupil and therefore the amount of light passing to the retina. The lens, behind the iris, is adjusted to focus, through the action of ciliary muscles, the light. The retina is the light-sensitive layer, consisting of 7 different types of cells, that extracts and performs initial processing of visual information.

The neural retina is itself composed of 5 layers (Figure 2). The first layer, from the back of the eye to the vitreous cavity, is the outer nuclear layer (ONL). This layer is where the cell bodies of the photoreceptor cells, both cones and rods, are found. The photoreceptor axons terminate in the outer plexiform layer (OPL), the region where synapses between photoreceptors and the interneurons form. The interneuron cell bodies form the inner nuclear layer (INL), comprising bipolar, amacrine and horizontal cells. Also found in the INL are the Müller glia cell bodies, a specific type of glial cell that is responsible for supporting all the other neuro-retinal cells. The processes of the Müller cells extend throughout all the retinal layers. The interneurons connect to ganglion cells in a synaptic region, the inner plexiform layer (IPL). Finally, the ganglion cell layer, in contact with the vitreous cavity, contains the ganglion cell bodies. Their axons, that converge to form the optic nerve, form a nerve fibre layer. An inner limiting membrane separates the retina from the vitreous cavity.

Figure 2 - Layers of the neural retina.

From Webvision under a Creative Commons License

http://webvision.med.utah.edu/book/part-i-foundations/simple-anatomy-of-the-retina/

Schematic representation of the retina (left) and correspondent layers in light microscope image of human retina (right). Photoreceptors, cones and rods, are the sensory neurons of the retina. Photoreceptors form synapses with interneurons: bipolar cells and horizontal cells. An additional interneuron, the amacrine cell, which together with the bipolar cells form synapses with retinal ganglion cells. Retinal neurons are organised into three nuclear layers: outer nuclear layer, where photoreceptor nuclei reside (ONL), inner nuclear layer (INL), in which interneuron and Müller glia nuclei are located, and ganglion cell layer (GCL). Photoreceptor function is supported by retinal pigment epithelium (RPE).

1.1.1 Eye development

As a highly specialised extension of the brain, the eyes start developing in early embryonic stages. They originate from the anterior region of the neural plate and, through a series of complex morphogenic movements and different pathway signals, generate the ocular tissue and all the cell types contained within it (Figure 3). Critical, precisely coordinated steps are necessary during eye development, including the formation of the eye field, specification of the neural retina and RPE, and retinogenesis (for reviews see Forrester et al., 1996; Martinez-Morales and Wittbrodt, 2009).

During neurulation, the anterior region of the neural plate becomes committed to form an eye and becomes the eye field; it is from this anterior region that the neural tube will later emerge. Through several evaginations of the optic primordial (Figure 3), optic vesicles (OV) are formed and extend towards the overlaying ectoderm, that will eventually originate the lens and cornea. The forming OV and ectoderm share inductive signals that lead to the formation of the lens placode, as the ectoderm's surface thickens once in contact with the OV. The synchronised evagination of the lens placode and OV leads to the formation of the lens vesicle and a double-layered optic cup (OC). The inner layer of the OC continues developing to form the neural retinal, whereas the outer layer goes on to form the retinal pigmented epithelium (RPE). At this point, the laterally growing edges of the OC fuse to form the choroidal fissure, that provides a channel for the blood vessels and axons (for review see Adler and Canto-Soler, 2007). The cornea is formed by the surface of the ectoderm, that overlies the lens and the mesenchymal cells, derived from the neural crest at the distal tip of the OC where the inner and the outer layer meet, eventually form the iris and ciliary body (Beebe, 1986).

Figure 3 - Schematic of early mammalian eye development.

From Eiraku et al., 2012, under Creative Commons License

The optic vesicle forms by lateral evagination of the neuroectoderm wall, where committed precursor cells are located. By the evagination and invagination of the epithelium that forms the optic vesicle, a double-walled cup structure (optic cup) is formed, with the inner and outer walls being the future neural retina and retinal pigment epithelium, respectively. Simultaneously, the surface ectoderm adjacent to the optic vesicle differentiates into the lens placode by inductive signals from the retinal progenitors, and then invaginates to form a lens vesicle.

Several signalling pathways are known to be involved in eye development and retina specification. These signals include, for example, hedgehog (Hh), WNT, fibroblast growth factor (FGF), and bone morphogenic protein (BMP) signalling pathways. These interact and participate at different stages of development, inducing activation of specific transcription factors, which results in generation of all the layers of the eye and its specialised cells (for review see Adler and Canto-Soler, 2007). These key molecular players are also responsible for the morphogenic changes, such as the evagination of the anterior region of the optic primordia, where the already committed retinal precursors are located, and the later formation of optic vesicles and consequently optic cup. Once the optic cup has developed, differentiation of the proliferative multipotent retinal progenitor cells (RPCs) initiates. To achieve neuro retinal development, six neural cell types and a glial cell type must arise from the retinal progenitors. Firstly, ganglion cells are generated and the last ones to arise are rod photoreceptor and Müller glial cells. Several molecular cues, at the right time and in correct order, are necessary to generate all the cell types and structures that compose the eye (for reviews see da Silva and Cepko, 2017; Livesey and Cepko, 2001)

The first morphological evidence of eye formation in humans is at the 4th week of gestation when bilateral evagination of neuroepithelium within the anterior neural plate takes place, to form the optic vesicles. There is molecular evidence that the eye primordium is specified at an earlier stage (reviewed in Heavner and Pevny, 2012)).

During neural induction, ectoderm cells in the dorsal ectoderm adopt a neural fate, forming the neural plate. The anterior region of the neural plate gives rise to the retina, establishing the eye field. During eye formation, the eye field transcription factors (EFTFs) are expressed in specific patterns, overlapping temporally and spatially, resulting in activation of important genes for eye development. The EFTFs, such as *ET, Rx1*, *Pax6*, *Six3*, *Optx2/Six6* and *Lhx2* (Andreazzoli, 2009; Eiraku et al., 2012; Zuber et al., 2003)*,* establish the genetic network necessary to control cell specification within the eye field. Inhibition of Activin/Nodal and bone morphogenetic protein (BMP) signalling in the TGFβ signalling pathway, is also required as these pathways inhibit neural development and their activity must be suppressed in the ectoderm in order to establish and maintain neural fate (Fuhrmann, 2010, 2008; Wong et al., 2015).

1.1.2 Histogenesis of retinal cell types

The committed retinal progenitor cells (RPCs), inherently multipotent cells present in the optic cup, give rise to all cell types of the neural retina (Holt et al., 1988; Turner et al., 1990; Turner and Cepko, 1987). Intrinsic and extrinsic determinants restrict linage choices and shift the competence of the RPCs to generate the different retinal cells (Swaroop et al., 2010). Initially, the RPCs start to undergo extensive proliferation in order to create a robust pool of multipotent progenitor cells for later differentiation (Figure 4). Some of the extrinsic factors that were previously involved in earlier stages of eye development, such as FGF, have also been shown to contribute to the maintenance of the pool of multipotent progenitors (R. M. Anchan et al., 1991; Chen et al., 2013; A. M. Jensen and Wallace, 1997; L. Lillien, 1995; L. Lillien and Cepko, 1992; Swaroop et al., 2010). A high concentration of Notch maintains the cycling RPCs by regulating neurogenic basic helix-loop-helix (bHLH) transcription factors such as the expression of downstream intrinsic transcription factor genes, for example downregulating *Hes1* and upregulating *Hes5*, which in turn act to repress neurogenic bHLH activators, such as NeuriD1 and Mash1. This events promote proliferation and inhibit neural differentiation (Hatakeyama and Kageyama, 2004).

RPCs must acquire the competence to undergo differentiation and sequential production of all retinal cell types before retinal neurogenesis is initiated. It has been shown that this competence heavily depends on the ratio of two transcription factors, Sox2 and Pax6 (Xiang, 2013). In fact, in the absence of Pax6, following genetic removal of expression from RPCs, all retinal cell types, except for a subtype of amacrine cells, are lost. This highlights the importance of conferring RPCs multipotency (Marquardt et al., 2001). Pax6 acts on the neurogenic bHLH and homeodomain transcription factors that regulate commitment to specific fates. Similar to Pax6, loss of Sox2 leads to loss of neurogenic potential and fate switch during eye development through the loss of neurogenic transcription factor expression and *Notch1* expression. Incidentally, it is also associated with an increase in expression of Pax6, further emphasising that a balance of activity of both Pax6 and Sox2 is required for proper retinal neurogenesis (Glaser et al., 1994; Marquardt et al., 2001; Matsuo et al., 1995; Taranova et al., 2006). In addition, Vsx2 expression is also required to prevent differentiation into RPE cells, due to *Mift* expression, and assure competence to form the neural retina (Parvini et al., 2014; Rowan et al., 2004).

After the RPC pool is created, Notch is downregulated and pro-neuronal genes become activated, such as *Neurogenin2* (*Ngn2*), *Neurod1*, *Mash1* and *Math5.* Genes associated with the cell cycle, like *CyclinD1*, become downregulated allowing retinal

cell differentiation to occur (Hatakeyama and Kageyama, 2004; Jadhav et al., 2006). Cell differentiation progresses with some RPCs exiting the cell cycle and differentiating into post-mitotic retinal cells. By the proposed model in which this occurs, RPCs pass through intrinsically determined competence stages and during each stage are capable of differentiating into a limited subset of retinal cells when the right extrinsic signals are present (Figure 4). Therefore, different types of retinal cells are “born” in a distinctive order that is highly conserved across vertebrates: retinal ganglion cells, followed by horizontal cells, amacrine cells of at least one class and cone photoreceptors are born first; the remaining amacrine cells are next, followed by bipolar cells, rod photoreceptors and finally and Müller glia cells.

Figure 4 - Chronological order and transcriptional regulation of retinal cell birth

From Bassett and Wallace, 2012. Licensed by Elsevier and Copyright Clearance Center

Based on embryonic and post-natal age in mouse development. GCs are generated first, and Müller glia cells are generated last. Progenitor-identity in RPCs is maintained by Pax6 and Sox2 expression, involved in the Hedgehog pathway (box on the right). Various transcription factors (left) direct the specification of each cell type and subtype.

Cells that leave the cell cycle of the RPCs go into differentiation and must have the correct intrinsic and extrinsic signals to allow them to differentiate. For example, early post-mitotic photoreceptor precursors must co-express the homeobox genes cone-rod homeobox (*Crx*) and orthodenticle homeobox 2 (*Otx2*), along with the bHLH genes, *NeuroD* and *Mash1* (Hatakeyama and Kageyama, 2004). Otx2 plays a role in regulating the expression of *Crx*, a key transcription factor, and consequently its target genes that are necessary for differentiation, maturation and maintenance of both rod and cone photoreceptors (Hennig et al., 2008). Another example is the retinoid-related orphan receptor (RORβ), that is likewise essential for development and maturation of both rods and cones, having a role in outer segment and synapse formation (Jia et al., 2009). After the cell is committed to a photoreceptor fate, additional transcription factors are necessary to generate either cone or rod photoreceptors (Figure 5).

Figure 5 - Cooperation of bHLH and homeodomain genes for retinal cell type specification.

Adapted from Hatakeyama and Kageyama, 2004. Licensed by Elsevier and Copyright Clearance Center

Hes1 maintains cell cycles of progenitor cells by inhibiting neuronal differentiation via Notch signalling. Once *Hes1* expression is lost, differentiation starts. Likely homeodomain factors regulate layer specificity while bHLH activators determine neuronal fate within the layers. Cells that retain expression of *Hes1* during neurogenesis adopt the final available cell fate, becoming Müller glial cells.

For rod fate specification, the main key transcription factor is neural retina leucine zipper (Nrl). *Nrl* belongs to the Maf subfamily of transcription factors, is preferentially expressed in rod photoreceptors, shortly after terminal mitosis, and is regarded as the earliest rod-specific photoreceptor marker (Akimoto et al., 2006). It interacts with several transcription factors, including Crx to activate the Rhodopsin promoter and promote a rod lineage. At the same time, Nrl activates orphan nuclear receptor Nr2e3, which in turn activates other rod-specific genes, and supresses the expression of cone-specific genes, thereby irreversibly committing the *Nrl*-expressing post mitotic cell to a rod fate (Oh et al., 2008).

Cone lineage specification is less well understood than rod linage, and despite identification of several important regulators, a clear pathway remains unknown. RORβ has been shown to interact synergistically with Crx to initiate S-opsin transcription in cones (Srinivas et al., 2006). S-opsin is the ancestral vertebrate visual pigment present in S cones (Lamb et al., 2007; Larhammar et al., 2009) and recent evidence suggests that transcription factor Onecut1 participates in the binary fate choice between rod and cone precursors, by promoting a cone fate. Onecut1 participates by inducing the expression of the early cone marker thyroid hormone receptor β2 (*Trβ2*). In the chicken retina, Onecut1 is required to repress Nrl and L-Maf, and in the mouse retina overexpression of this factor results in an increase number of immature cone precursors and a decrease in rod precursors (Emerson et al., 2013). Another identified transcription factor is Sall3 of the Spalt family, as it activates expression of multiple cone genes and plays a particular role in the initiation of *Opn1sw* expression *(S-opsin*) (de Melo et al., 2011). Development of S cones was also found to depend on the expression of DNA methyltransferase 1 (*Dnmt1*) (Nasonkin et al., 2013). Trβ2 nuclear receptor, in the thyroid hormone signalling pathway, is crucial for induction of *Opn1mw* expression *(M-opsin*) (Lu et al., 2009; Roberts et al., 2006). To date, this data suggests that whilst S-opsin is the default visual pigment in mammals, the number of mature cone cells is determined by the activity of positive regulators as well as the repressive activity of the rod differentiation pathway inducers (Figure 6).

Figure 6 - Model of photoreceptor cell fate determination.

From Swaroop et al. 2010. Licensed by Springer Nature and Copyright Clearance Center.

(A) This model suggests that RPCs divide producing additional RPCS (thick circular arrow) or originate cells that become restricted in their competence to generate specific cell types (thin circular arrow). After cell cycle exit, post-mitotic precursors remain plastic and depend on extrinsic signals to specify into one cell type. During cell type specification of photoreceptors, precursors are directed to become cones or rods. The panel on the far-left lists key transcription factors and signalling proteins that maintain RPCs multipotency and proliferation. The panel on the far-right lists key transcription regulatory proteins that are involved in cone and rod differentiation and maintenance. **(B)** OTX2 and other non-yet identified factors control photoreceptor genesis. The model suggests that the S-cone pathway is the default pathway, and intervening action of other transcription factors is necessary to generate rods and M/L cones.

1.1.3 Neural Retina and Retinal Pigmented Epithelium

The retina has a neural component and a non-neural component that must work together for the correct functionality of this layer: a breakdown in this relationship is the irreversible cause of degeneration and blindness. The light sensitive cells, the photoreceptors, are divided into two types, rods and cones. Their visual pigments, the light absorbing molecules that initiate the visual cascade, are located in their outer segments. Light must travel across all the neural retinal layers to reach the outer segments, where the phototransduction takes place, allowing the light stimuli to be converted into an electric signal that is passed through the bipolar cells, with modulation from horizontal and amacrine cells, to the retina ganglion cells and from there to the visual cortex of the brain.

Bipolar cells transmit the signal from photoreceptor to ganglion cells, having a central cell body from where two processes, one in each pole, arise. The spatial distribution of these cells varies throughout the retina. In the fovea the ratio of cones to bipolar to ganglion cells is 1:1:1, but in the periphery, one bipolar cell gets input from up to 100 photoreceptor cells. Amacrine cells are associative neurons located in the inner part of the INL, towards the GCL, and have a characteristic morphology, with a larger cell body than bipolar cells, oval shape and shorter, highly branched processes that extend in the GCL direction. These cells modulate the signal that reaches the ganglion cells.

Other cells present in the retina, forming the INL, are the horizontal, bipolar and amacrine cells. The horizontal cells get their name from their morphology, with long horizontal processes. They can be classified in two subtypes: type A, which connects only to cone photoreceptors, and type B, that have longer axons, with more branches. Some of the branches of type B horizontal cells contact only with cone, but in addition to those, they have axons with extensive arborisation that connect only with rods. Each rod cell connects with at least two horizontal cells and each cone with up to four. Horizontal cells have an integrative role in processing the input of several light-sensitive cells.

Ganglion cells are the last link between the visual pathway in the eye and the transmission of the signal to the brain. The density of ganglion cells in the human eye varies, being densely packed in the fovea (area of high cone photoreceptor cell density, responsible for high acuity vision) where up to seven rows of ganglion cell nuclei can be found; and down to one row in the periphery of the eye (for review see da Silva and Cepko, 2017). All ganglion cells present some similar features such as

a large cell body and Golgi apparatus. However, there are morphological differences that allow the sub-classification of these cells as α, β or γ, each being functionally diverse with respect to contrast, chromacity or spacial resolution. Each ganglion cell receives input from several light-sensitive cells, approximately one-hundred rods and four to six cones per ganglion cell. Ganglion cells receive their input from bipolar and amacrine cells, through the synapses formed in the IPL where their dendrites branch forming the “dendritic tree”, that can also vary in complexity according to the area of the eye.

Three classes of glial cells are found in the retina: neuroglia, astrocytes and microglia. The neuroglia in the retina are called Müller cells. They are the main supporting glial cell of the retina, extending across all layers of the neural retina. These cells maintain the environment by extracellular matrix production and provision of oxygen and nutrients for the retinal cells that lack a direct blood supply. Furthermore, Müller glia cells form the inner and outer limiting membranes. The retina’s inner limiting membrane (ILM) is composed of lateral contacts between Müller glia cell-end feet and basement membrane constituents, and separates the vitreous cavity from the retinal layers, forming a diffusion barrier. Likewise, the outer limiting membrane (OLM), formed by the apical processes of Müller cells attached to each other and to the inner segments of the photoreceptor cells, forms a barrier between the ONL and the sub-retinal space, where the inner and outer segments of photoreceptor cells project to be in close contact with RPE cells. Astrocytes are also found in the retina, mainly in the GCL and IPL and are mainly thought to provide structural support and ion homeostasis. Microglia cells have a different function, as they are not supporting cells. Retinal microglia are a highly specialised sub-population of monocytes that reside in the central nervous system; upon injury to the retina these cells become activated and acquire phagocytic function.

The retinal pigment epithelium (RPE), located between the photoreceptor’s outer segments and choroid, is a monolayer of cuboid epithelial cells that contain melanin granules. These cells allow absorption of light, reducing the amount of light that is reflected back into the eye, thereby improving image resolution. It is responsible for supporting the cells of the ONL by providing oxygen and recycling phototransduction molecules. The basal side of RPE layer resides on top of the Bruch’s membrane, a thin layer on connective tissue that separates RPE layer from the choroid. RPE layer and Brunch’s membrane are separated only by the RPE basement membrane.

1.1.3.1 Photoreceptor cells

In the human eye, there are approximately 115 million rods and 6.5 million cones. Rods are responsible for sensing contrast, brightness and motion, and are required for night or dim light vision (scotopic conditions). Cones are responsible for fine resolution, spatial resolution and colour vision and respond to bright daylight (photopic) conditions. Rods are inactivated by bright light and cones are not functional in dim light. Whilst cones represent only 5% of the photoreceptor cells in the human retina, it is nevertheless imperative to have both types of photoreceptors for visual perception across different light intensities. The ratio of cones to rods is similar for human and mice, but the human retina, unlike the mouse retina has a macula region in the central part of the retina, above the optic nerve. Here the cone density is up to 5 times higher than in the periphery which has a cone density of approximately 30,000 per mm^2. In the centre of the macula is the fovea which provides high acuity vision. It is a rod-free area with a cone density of 150,000 per mm^2 (Forrester et al., 1996).

All photoreceptors are highly polarised, long and narrow cells, with rods being longer and narrower than cones, with an inner and an outer segment joined by a connecting cilium. The outer segments contain membrane disks where the visual pigments reside, responsible for light absorption and initiation of the visual cascade, and they give these cells their names, as rod outer segments have a rod-like like morphology and cone outer segments resemble cones. The inner and outer segments extend beyond the outer limiting membrane while the photoreceptor nuclei are in the ONL. Both rods and cones have one axon that extends into the outer plexiform layer where it forms synapses with bipolar cells. The synaptic terminals of rods and cones are different, with rods having a spherule synaptic terminal, that forms a single ribbon synapse, an electron-dense structure that holds synaptic vesicles close to the active zone. In contrast, cones have a pedicle synaptic terminal, where multiple ribbon synapses are formed (Figure 7) (for review see Schmitz et al., 2012).

Figure 7 - Photoreceptors form ribbon synapses with horizontal and bipolar cells

From Schmitz et al, 2012, under Creative Commons License

(A) Schematic of rod (R) and cone (C) photoreceptors and its synaptic ribbons (sr) with bipolar (b) and horizontal (h) cells. (B) Schematic of rod and cone photoreceptor presynaptic terminals. Rod synapses possess only a single synaptic ribbon (sr) and cones possess multiple active zones (20–50). (C–E,) Electron micrographs of photoreceptor terminals. (C) Cross-sectioned synaptic ribbon, with its typical bar-shaped appearance in a rod terminal, associated with large numbers of synaptic vesicles (sv) (D). Higher magnification on rod photoreceptor synaptic ribbon showing the synaptic ribbon (sr) with synaptic vesicles (sv) at the base (small white arrows). The dashed circle indicates the site where the postsynaptic dendrites (po) enter the postsynaptic cavity formed by the invagination of the presynaptic photoreceptor terminal (pr). (E) Tangential view of the synaptic ribbon. White arrows denote the ribbon plate which is bended along the presynaptic plasma membrane in a horseshoe-like manner. (F) Super-resolution structured illumination microscopy (SIM) image of the horseshoe-shaped in (E) immunolabeled with anti-RIBEYE antibodies, (white arrows in E and F). White arrowheads show synaptic spheres (ss).

Rod outer segments contain the visual pigment rhodopsin, which has a peak spectral sensitivity at 496 nm. Rhodopsin is bound to the membrane disks of the rod outer segment, each cell can present up to one thousand disks, with 10-15 nm thickness, enclosed by a single cell membrane. Each outer segment is approximately 1 µm wide and 25 µm long. The disks are generated near the connecting cilium and over the course of ten days make their way to the tip of the outer segment, which is enclosed by the apical microvilli of the RPE. At the other end, the rods have their synaptic terminal, the spherules. Each rod spherule can be connected to up to five interneurons, having up to four dendrites of bipolar cells penetrating the spherule as well as horizontal cells, these with dendrites more deeply embedded into the rod spherule.

In contrast, in most diurnal mammals the cone outer segments contain either of two visual pigments, generating two different sub-types of cones: S-cones, that contain the visual pigment S-opsin (blue-sensitive opsin), which in humans has peak sensitivity at 430 nm (short wavelength); and M-cones, that have the visual pigment M-opsin (green-sensitive opsin), which has peak sensitivity at 530 nm (medium-long wavelength). In primates and humans, a third type is present, the L-cones, containing L-opsin (red-sensitive opsin), which has a peak spectral sensitivity at 561 nm (long wavelength), conferring trichromatic colour vision. Cone outer segments are shorter than rods and have a conical shape (6 µm at the base and 1.5 µm at the tip in humans). Unlike rod outer segments, cone disks are not enclosed by a cell membrane, being in direct contact with long melanin containing RPE processes. At the synaptic terminal, cones have pedicles; these are broader than spherules and have a pyramidal shape (Figure 7). In each cone pedicle there are up to twelve indentations, each with three neuronal terminals, known as a triad. In the centre of each triad is a connection to a dendrite of a midget bipolar cell, a bipolar subtype that connects specifically to cones and that might have several connections within the same pedicle. Several bipolar cells might also connect to the same pedicle. The connection to horizontal cells in the pedicle modulates the signalling between cells. Up to twenty-five synaptic ribbons can be found in a single pedicle.

Renewal of photoreceptor outer segments occurs by synthesising new disks that are rich in the visual pigments, by invagination of the plasma membrane at the outer limiting membrane region and shedding and phagocytosis of the outer segment tips by the RPE. Visual pigments are formed in the endoplasmic reticulum and Golgi and transported in vesicles to the newly formed membrane where they fuse, originating new outer segment disks.

1.1.3.2 Retinal Pigment Epithelium

The RPE is a monolayer of cuboid/columnar epithelial cells that extends from the optic nerve insertion to the ora serrata, where it continues with the epithelium of pars plana. Despite these cells not being light sensitive, they have several major functions in the visual process, from physical to metabolic roles. Its physical function is maintaining the neural retina attachment, by engulfing the photoreceptor outer segments and also by synthesising inter-photoreceptor extracellular matrix. The RPE is also part of the outer blood-retinal barrier (BRB) and forms a selective barrier, regulating the movement of solutes and nutrients from the choroid to the sub-retinal space. The RPE is also involved recycling of the chromophore part of the visual pigment back into the visual cycle; it is responsible for phagocytosis of photoreceptor's outer segments and reduces light scatter within the eye, improving image resolution.

The RPE are organised as a monolayer of hexagonal shaped cells, resembling a honeycomb structure. This epithelium varies in shape and size, depending on where the cells are located in the retina as well as its age. They tend to have a more columnar shape near the central retina and get flatter in the periphery as they get wider. These cells are polarised, having their basal side sitting on the Bruch's membrane, where RPE cells have a basal infolding, and their apical microvilli which are in close association with photoreceptor's outer segments. The RPE layer has a low regenerative capacity, and cell loss, either by age or injury, leads to hyperplasia of the remaining cells, resulting in the loss of the hexagonal shape and a greater variety of cell sizes (reviewed in Fuhrmann et al., 2014)).

1.1.3.3 Phototransduction

The main function of the retina is to convert energy from light photons into electric signals that can be interpreted by the brain to form an image. This is only possible due to photochemical events that occur in photoreceptor cells, this process is called phototransduction. All molecules necessary for phototransduction are present in the photoreceptors' outer segments, where this cascade takes part (Figure 8) (for review see Pugh and Lamb, 2000). The phototransduction cascade is best described in the rod photoreceptor, due to electrophysiology and genetic studies performed in several animal models, mainly mice. The general process of phototransduction is similar in rods and cones, as the cones have been shown to have homologous proteins to the ones founds in rods (for a review see Kefalov, 2010). Nevertheless, some distinctions between the rod and cone phototransduction pathway have been identified by using

knockout mouse models that allow to evaluate the contribution individual proteins specifically in rod and cone photoreceptors (Baehr et al., 2007).

Phototransduction takes place in three general steps, photo-activation, reduction in the neurotransmitter release, and recovery. Photo-activation is when light is absorbed by the chromophore, 11-*cis*-retinal, that is bound to an opsin protein, leading to its isomerisation to all-*trans*-retinal. This change in the chromophore triggers a conformational change in the opsin protein and subsequent binding to transducin, a G-coupled protein. This initiates downstream signalling, by exchanging GDP to GTP, activating the α-subunit of transducin that dissociates from the complex and activates a membrane-associated phosphodiesterase (PDE) through removal of its two regulatory γ-subunits. Once activated, PDE hydrolyses cyclic guanosine monophosphate (cGMP), lowering its cytosolic concentration. In the dark, cGMP concentrations are high and cations flow into the photoreceptor. When a photon of light is absorbed, PDE causes lowering of the cGMP concentration through its hydrolysis. This results in cGMP-gated cation channel closure and subsequently a decrease in cytosolic cations (including Ca^{2+}) and hyperpolarisation of the photoreceptor. Reduction in neurotransmitter release takes place in response to the hyperpolarisation, blocking glutamate release at the synaptic terminal, which is interpreted by the INL interneurons as light detection. Finally, there is the recovery stage of the cascade: after light stimulation the phototransduction cascade must be terminated, cytosolic levels of cGMP restored and cationic channels re-opened, returning the cell to the basal dark-adapted state. This is achieved through a series of quenching and termination reactions. Once the Ca^{2+} goes down following phototransduction, recoverin (Rec), a calcium-binding protein, that forms a complex and inhibits opsin kinase, releases Ca^{2+} and separates from the kinase that then phosphorylates and inactivates the opsin protein. The low levels of Ca^{2+} also stimulate the release of Ca^{2+} ions from guanylate cyclase-activating proteins (GCAPs), activating retinal guanylate cyclase (GC), membrane-associated enzymes that catalyse the formation of cGMP. Finally, all-*trans*-retinal in is released and is recycled to 11-*cis*-retinal, by RPE cells, in order for photoreceptors to maintain their ability to respond to light (for review see Pugh and Lamb, 2000) .

Figure 8 - Schematics of phototransduction cascade in vertebrates

From Pugh and Lamb, 2000. Licensed by Elsevier and Copyright Clearance Center.

(A) Activation steps of the cascade. After absorption of a photon of light (hυ) the opsin becomes active (R*), binds to the G-protein (G) and catalyses the conversion of GDP to GTP and consequently produces an active form of the G-protein (G*α), transducin. G*α activates the phosphodiesterase, PDE (E*) that catalyses the hydrolysis of cGMP (cG), reducing its cytoplasmic levels. This leads to closure of the cationic channels, reducing the circulating electric current. In response to low Ca^{2+} Guanine cyclase (GC) synthesises cG from GTP. Guanylyl cyclase activating protein (GCAP) binds to GC to increase its activity. Box α and box β refer to the rate of synthesis of cG by GC and its degradation by E*. **(B)** Inactivation steps of rod phototransduction cascade. When concentration of Ca^{2+} is low, Recoverin (Rec) releases the Ca ions that it was bound to; this allows dissociation of Rec from Rhodopsin kinase (RK), which then becomes active, binding to the Rhodopsin (RK R*), becoming inactive by phosphorylation of Rhodopsin (R-P). R-P binds preferentially to Arrestin (Arr). This rapidly reduces the amount of R* available for the activation of transducin, and thereby quenches R* activity.

1.1.3.4 Visual cycle

Visual pigments are formed of an opsin protein bound to a chromophore, 11-*cis*-retinal, a derivative of vitamin A. Chromophore and opsin are coupled via a Schiff base. The reactivity of the retinal aldehyde group allows it to be linked to opsin proteins, in which after photoisomerisation, it can induce conformational changes triggering downstream signalling, known as the visual cascade (described 1.1.3.3). When light is absorbed by the photopigment, 11-*cis*-retinal isomerises to its all-*trans* form and the visual pigment is converted to metarhodopsin II (*meta II*), its signalling form. The *meta II* visual pigment becomes unstable and all-*trans*-retinal is released from the protein. In vertebrates, once in an all-*trans*-retinal form, the chromophore is not able to absorb light again and isomerise back to 11-*cis* conformation. Therefore, there is a requirement for regeneration of the photopigment and those reactions take place in the RPE cells (Figure 9) in a process called the visual cycle (reviewed in Palczewski, 2012; Sung and Chuang, 2010).

The rod visual cycle is initiated after absorption of light in the outer segments, resulting in isomerisation of 11-*cis*-retinal of rhodopsin into the all-*trans* isoform. This creates an activated photoproduct, meta-rhodopsin II, which initiates downstream signalling as described in section 1.1.3.3. Once in all-*trans* isoform, the chromophore and bound rhodopsin is hydrolysed, and the retinal molecule is released to the cytoplasm within the outer segment's disks. All-trans-retinal is then reduced, by all-trans-retinol dehydrogenases (RDH), to all-trans-retinol. This molecule is transported to the RPE, by chromophore binding proteins (IRBP and CRBP), where it is esterified, by lecithin retinol acyltransferase (LRAT), to retinyl-esters. Retinyl-esters are hydrolysed and isomerised to 11-*cis* retinol by the isomerohydrolase RPE65. Cellular retinal protein (CRALBP) binds to 11-*cis* retinol and RDH oxidises it to 11-cis-retinal. CRALBP carries 11-cis-retinal to the RPE apical processes where interphotoreceptor retinoid binding (IRBP) transports it back to the rod outer segments, completing the visual cycle. If the visual cycle is impaired the health of retinal cells is compromised, which results in retinal degeneration (reviewed in Maeda and Palczewski, 2013).

There are similarities between rods and cone regarding the activation of the visual pigments, however cones, by mediating day-time vision, need rapid recycling of their chromophore to regenerate their pigment. In order to sustain these fast responses in bright light conditions, cones have different physiological properties to rods, and it is likely that the way photopigment is recycled is one of those properties. It was biochemically shown that the canonical visual cycle pathway was too slow to be able to sustain photosensitivity in photopic light levels (Mata et al., 2002). Other studies

showed that proteins capable of synthetase 11-*cis*-retinal , were present in chicken Müller glial cells (Das et al., 1992; Kaylor et al., 2014; Muniz et al., 2006). Moreover, cone-specific photopigments regeneration by Müller glial cells, independently of RPE cells, was demonstrated in salamander retinal explants (Wang et al., 2009). Having that in consideration, currently, the model proposed for cone visual cycle pathway in mammals is that, as in rods, 11-*cis*-retinal after photon absorption isomerises into the all-*trans* conformation, activating the phototransduction cascade, followed by dissociation of all-*trans* retinal from the opsin and its reduction to all-*trans* retinol. The difference appears when it comes to where the all-*trans* retinol is transported. It is thought that Müller glia cells play a similar role to RPE in the cone visual cycle. It is not yet clear whether this is instead or in addition to the canonical visual cycle, but it is most likely in addition as mutations in RPE65 gene translate in reduced cone function. The process described suggested that in the Müller glia cells all-*trans*-retinol is isomerised into 11-cis-retinol and transported back to the cone outer segments. There 11-cis-retinol is oxidised to 11-*cis*-retinal, which binds to opsin reforming the visual pigment. Since rod photoreceptors cannot utilise 11-cis-retinol, this pathway gives cones a faster supply of chromophore without competition from the rods (for review see Wang and Kefalov, 2011). The exact molecular process and intermediate steps are still unknown.

Figure 9 - Schematics of the visual cycle

From Wang and Kefalov, 2011. Licensed by Elsevier and Copyright Clearance Center.

(A) Rod visual cycle. After a light exposure, rhodopsin is activated and the bound visual pigment becomes dissociated, originating free opsin and all-*trans* retinal (atRAL) that is later reduced to all-*trans* retinol (atROL) by the enzyme, retinol dehydrogenase (RHD). atROL is transported to the interphotoreceptor matrix (IPM), where it binds to the chromophore binding protein IRBP, that transports it to the RPE apical processes. Another chromophore binding protein, CRBP, transfers the atROL to the RPE cell body, where it is esterified by lecithin retinol acyltransferase (LRAT), becoming all-*trans* retinyl esters (atRE). atRE is then hydrolysed and isomerised to 11-*cis* ROL by the isomerohydrolase RPE65. CRALBP binds the 11-*cis* ROL, removing it from the reaction site to speed up the isomerisation. The CRALBP - 11-*cis* ROL complex is oxidised by RDH resulting in 11-*cis*RAL that, with assistance of scaffold proteins (e.g. EBP50/NHERF-1 and Ezrin), leave the RPE cell. IRBP binds to 11-*cis*RAL, bringing it back into the ROS where it is recombined with the opsin, regenerating the visual pigment, rhodopsin. **(B)** Cone visual cycle. After photoactivation, cone opsins also result in free opsin and all-*trans* retinal (atRAL). atRAL is reduced to all-*trans* retinol (atROL) retinol dehydrogenase (RHD) in the cone outer segment (COS). atROL can be either transported to the RPE and recycled to 11-*cis*RAL via by the visual cycle process explained in **(A)**; or transported to Müller glia cells, where a similar process occurs and atROL is converted to 11-*cis*ROL and transferred back to the cone. Once there, it is oxidised by an unidentified RDH protein to 11-*cis*RAL.

1.2 Development of retinal cell types and establishment of the synaptic network

Understanding how the retinal circuit is established and how the organisation of the retina impacts the formation of synapses is necessary to understand how the remodelling events, following photoreceptor loss, might impact the circuit. It will allow us to hypothesise how the presence of transplanted cells might affect the host network and assess whether the formation of new connections between transplant and host is likely. Only then it will be possible to consider if cell transplantation might be suitable as a therapy.

The retina is a highly organised structure where the synaptic connections occur exclusively in distinct layers. The photoreceptor cells contact the interneurons (bipolar and horizontal cells) in the OPL, while the inner retinal synapses, between the interneurons (amacrine and bipolar cells) and ganglion cells, occur in the IPL. There is not only an organisation when it comes to the layering of the retina, but within those layers there are further levels of organisation. Connections between ON bipolar and ganglion cells are mostly confined to the inner half of the IPL and the connections between OFF cells is confined to the outer half of the IPL. This is another level of organisation of the retina and demonstrates how highly organised the retinal circuit is (Euler et al., 2014; Morgan and Wong, 1995; Ribelayga, 2010). The exact mechanisms that lead to this specificity are still not completely understood, but functional and structural studies have provided some information about how the circuit develops, what the mechanisms involved are and what the sequence of circuit assembly is.

Studies suggest that retinal synaptogenesis in vertebrates, occurs in three major phases. The sequential pattern seems to be preserved across species, although the time scale in which the events occur is highly variable, ranging from a few hours to days or weeks depending in the species. Nevertheless, the sequence of events appears to be the same, with the retinal ganglion cells and amacrine cells differentiating first and establishing the earliest functional circuits in the IPL of the developing retina. The horizontal cells and photoreceptors follow, establishing contacts in a developing OPL. Lastly the bipolar cells, that establish the vertical connections between OPL and IPL, are differentiated and connect with both previously established plexiform layers (Blanks et al., 1974; Fisher, 1979; Olney, 1968).

The synaptic connections of the retinal circuit are highly restricted to the plexiform layers, reflecting their specificity. However, other structural features of each neuron also impact the formation of the synaptic circuit, as the patterns of lateral branching of the axons and dendrites that determine the spatial coverage of each cell. These represent the lateral and vertical organisation of the retinal circuit (Euler et al., 2014; Helmstaedter et al., 2013; Morgan et al., 2011; Yonehara et al., 2013).

The different cell types in the retina shape their dendritic stratification, allowing the circuit to form. Even within each type of retinal cell, sub-types can be identified based on cell morphology and dendrite localisation. In the adult retina, mammalian ganglion cells extend their dendrites into the IPL or horizontally in the GCL However, during development, these cells' dendrites are initially projected throughout the full depth of the IPL and stratification follows progressively, becoming static once cells are fully mature (Morgan and Wong, 1995). The mechanisms underlining this stratification process seem to be related to neurotransmission, meaning that for the circuit to form, it is necessary that some neuronal activity is present during development. This idea is supported by studies where pharmacological blocking of neurotransmitters and injection of glutamate receptor agonists, leads to a decrease of neurotransmitter, and consequently the mis-localisation of cell dendrites (Bodnarenko et al., 1995; Sernagor and Mehta, 2001; Wong et al., 2000).

Similar events are true for all the interneurons, as the stratification of their synaptic terminals and dendrites arises during development and cell maturation. Amacrine cells extend their dendrites in several directions prior to reaching the border of INL and IPL, where they are found in an adult retina (Hinds and Hinds, 1983, 1978; Prada et al., 1987). Furthermore, once at the right layer, amacrine cells arrange their dendrites to create sub-lamination, within the IPL, with two distinct areas of synaptic terminals corresponding to ON-centre (more internal half of the IPL) and Off-centre (more external half of the IPL) ganglion cells. Once the correct sub-lamination is established, the amacrine cells reorganise the dendrites to establish the lateral arborisation before becoming fully mature (Kay et al., 2004). The mechanisms that explain the development and organisation of amacrine cell are still mostly unknown. Nevertheless, it is clear that amacrine cells do not depend on the presence of ganglion cells, their post-synaptic target, to establish lamination. Evidence of that was shown in studies where the absence of ganglion cells, either caused by injury or in genetically modified animals, did not impact the lamination of amacrine cells (Brown et al., 2001; Chalupa and Günhan, 2004; Kay et al., 2004; Wang et al., 2001). Since bipolar cell differentiation happens following amacrine cell lamination, it is not likely

that bipolar cells will have a role in the initial stratification seen. It has therefore been hypothesised that the cues arise from Müller glial cells or their precursors and/or communications between the amacrine cells themselves, as they express neurotransmitters even before being localised to the INL/IPL border (Morgan and Wong, 1995).

There is not a vast knowledge and understanding of how dendrites and axons of bipolar cells are generated and mature, contributing to their retinal placement, as there are no known early markers that allow identification of bipolar cells. However, studies using silver staining technique, the Golgi method to visualise nervous tissue, suggest that bipolar cells start by extending their pre- and post-synaptic axons across the full width of the retina, reaching the inner and outer limiting membranes. Once the axons are in place, arborisation starts taking place in the areas where mature synaptic connection will occur, in the OPL and INL (Quesada et al., 1981). It is thought that this arborisation takes place in response to interactions with amacrine cells in the IPL, which at this time are already in place and present mature lamination. Bipolar cells then retract the extended axons, restricting their pre-synaptic terminals to the IPL and post-synaptic terminals to the OPL (Günhan-Agar et al., 2000; Rice et al., 2001). Horizontal cells also undergo dramatic changes during development, similar to what happens in bipolar cells, starting with elongated processes that seem to aid the cell body to localise in the correct layer (vertical or radial organisation), and once in the correct layer, horizontal cells expand their dendritic network laterally. Studies show that this lateral organisation is achieved in the absence of cone photoreceptors (Reese et al., 2005), but abnormalities were detected in the absence of rod photoreceptors (Donovan and Dyer, 2004). This data suggested that horizontal cells might need some signally from rod photoreceptors to maturate and achieve the final arborisation of their dendrites. Since rod photoreceptors are only starting to differentiate when the peak of horizontal cell differentiation has already taken place (Marquardt and Gruss, 2002), it is possible that these cells do not require an input to achieve the radial/vertical organisation, but might depend in some rod derived input to achieve the lateral organisation. Despite the lateral extension of the dendrites of horizontal cells not being impacted by the absence of cones, cone photoreceptors might be involved in the branching pattern of horizontal cells' dendrites. This is suggested by studies that showed changes in the branching patterning in absence of cone photoreceptors, suggesting that cone photoreceptors might be involved in the initiation or maintenance of the branching of the dendrites in horizontal cells (Reese et al., 2005). The proposed maturation events are summarised in Figure 10.

Figure 10 – Proposed sequence of dendritic development in retinal interneurons

Adapted from Webvision under a Creative Commons License

https://webvision.med.utah.edu/book/part-vi-development-of-cell-types-and-synaptic-connections-in-the-retina/development-of-cell-types-and-synaptic-connections-in-the-retina/

(A) Ganglion cell's dendrites initially extend across the whole thickness of the retina, with stratification and dendritic arborisation taking place progressively as the cell matures. **(B)** Amacrine cell initially extend dendrites in all direction, until the right layer of the retina is reached, and the cells localise to the correct place. Once there, amacrine cells retract the dendrites that extend into the INL and extend an organised horizontal dendritic network in the IPL. **(C)** In early stages of development bipolar cells extend their pre- and post-synaptic axons from the ILM to the OLM, across the retina's width. In the areas where synaptic connections will occur, IPL and OPL, arborisation of the axons occurs, followed by retraction of the axons, restricting their presence to the plexiform layers. **(D)** Initially**,** horizontal cells elongate their axons in several directions until the cell body reaches the correct position. Once in place lateral expansion and organisation of the dendrites takes place. Simultaneously, misplaced dendrites are retracted.

In summary, despite some hypotheses, the mechanisms behind the formation and organisation of the synaptic circuit in the retina are still largely unknown. Nevertheless, it is apparent that different types of retinal cells depend on signals from other cell types in order to acquire the normal structure and organisation that leads to establishing the synaptic circuit.

1.2.1 Synaptic circuits and the cone pathway

As the aim of this project is to transplant cone photoreceptors, understanding how these cells establish their connections and propagate information is relevant for interpreting the results.

Rods and cones have a different morphology and are active under different light conditions. Not surprisingly, the synapses they form with bipolar cells and the way that the signals are propagated though the retinal circuit to the ganglion cells are also different. Unlike rods, that make a connection with a single bipolar cell, cone photoreceptors establish connections with several cone bipolar cells. There is only one type of rod bipolar cell (an ON bipolar cell), whilst there are several subtypes of cone bipolar cells that can be distinguished by the size of their dendritic field, being classified as diffused or midget types. Midget bipolar cells contact with a single cone photoreceptor and diffuse bipolar cells contact multiple cones. They can be classified further depending on the placement of their dendritic terminal, either on the surface, flat bipolar cells, or penetrating within the photoreceptor's synaptic terminals, invaginating. Studies involving physiological response, morphology analyses and specific protein markers in mice (Ghosh et al., 2004; Wässle et al., 2009), rabbit (MacNeil et al., 2004) and primates (Hopkins and Boycott, 1997) have allowed the discovery of twelve types of cone bipolar cells. It is thought that all major bipolar cell types present in the mammalian retina have now been discovered.

In darkness, photoreceptor cells are depolarised and therefore they release glutamate continuously. Light leads to hyperpolarisation of photoreceptors, suppressing the release of glutamate (Trifonov, 1968). The constant release of glutamate has an effect on cone bipolar cells, leading to depolarisation or hyperpolarisation depending if the bipolar cell is an ON or OFF cell (Nelson and Kolb, 1983; Werblin and Dowling, 1969). The same is not true for rod bipolar cells, as in the presence of light, therefore in response to a decrease in the release of glutamate by rod photoreceptors, rod bipolar cells always depolarise (Dacheux and Raviola, 1986).

The synapses established between cone photoreceptors and cone bipolar cells are highly specialised and organised, having a cone photoreceptor cell making central ribbon contacts with an ON bipolar cell and wide-cleft basal junction contacts with an OFF bipolar cell (see Figure 11) (for review see D'Orazi et al., 2014).

Figure 11 - Schematic representation of synapses formed by cone photoreceptors

Adapted from D'Orazi et al. ,2014. Licensed by Elsevier and Copyright Clearance Center.

Schematic representation of the cone's pedicle (pink) and post-synaptic terminals of horizontal (HC, in orange) and cone ON (ON-CBC, in light blue) and OFF (OFF-CBC, in yellow) bipolar cells. Each cone pedicle has glutamate vesicles (white circles) at the synaptic terminal, most concentrated at the ribbon synapse area (black). Here the cone releases glutamate that is picked up by the ionotropic glutamate receptors (iGluRs) (dark blue) on HC and OFF-CBC and by metatropic glutamate receptor 6 (mGluR6) (in red), on ON-CBC.

Both ON and OFF types of bipolar cells have glutamate receptors, ON bipolar cells express metabotropic glutamate receptor 6 (mGluR6) and OFF bipolar cells express ionotropic α-amino-3-hydroxy-5-methyl-4-isoxazole-propionic acid (AMPA)/kainate (KA) receptor channels. OFF bipolar cells also present receptors for another neurotransmitter, gamma-aminobutyric acid (GABA) (for a review in neurotransmitter in the retina see Yang, 2004). However, these cells differ in the response they have to glutamate, the neurotransmitter released by photoreceptor cells. In ON bipolar cells the presence of glutamate has an inhibitory effect, while it has an excitatory effect in OFF bipolar cells. Since in dark conditions photoreceptor cells are depolarised, they release glutamate. The glutamate being released will result in firing of the OFF bipolar cells, that will release neurotransmitter, sending signals to the ganglion cells, while ON bipolar cells will be inhibited by the presence of glutamate, therefore not releasing neurotransmitters. In the presence of light, the opposite takes place, as photoreceptor cells will become hyperpolarised and stop releasing glutamate, therefore the ON bipolar cells will no longer be inhibited by the glutamate, become depolarised and release neurotransmitters, signalling the ganglion cells (Figure 12).

Figure 12 – ON and OFF channels at the photoreceptor/bipolar synaptic terminal

From Ribelayga, 2010, under Copyright Clearance Center's RightsLink®

Schematic representation of synaptic connection between photoreceptor and bipolar cells in darkness. Photoreceptor cells release glutamate in darkness, as they are depolarised under those conditions. In an OFF channel (on the left), bipolar cells express an AMPA/KA receptor, that once bound to glutamate leads to an excitatory response and depolarisation of the OFF bipolar cells and consequent release of neurotransmitter at its pre-synaptic terminal, propagating the signal. In an ON channel (on the right), bipolar cells express mGluR6, to which glutamate has an inhibitory effect, leading to hyperpolarisation of the bipolar cell upon binding to glutamate, consequently no neurotransmitters are released by the bipolar cells at the pre-synaptic terminal and there is no signal propagation. The reverse occurs in response to light. The ON channel is used by cones and rods while the OFF channel is cone exclusive.

More details about the circuit that is established between cone photoreceptor cells and the interneurons are still to be discovered. From what has been established so far it is known that the major difference between the cone and rod pathways is that the cone bipolar cells can make direct synapses with ganglion cells, without the need of amacrine cell modulation. Therefore, narrow-field and convergent pathway than the rod pathway. There are fewer cones than rods and there are fewer cones converging to each cone bipolar cell, despite the same cone photoreceptors contacting and delivering their input to several cone bipolar cells. The cone bipolar cells also converge, having a relatively small number of cone bipolar cells converging to ganglion cells. This is particularly noticeable at the fovea where each cone feeds input to 1 to 3 ganglion cells and each ganglion cell, localised in the perifovea, receives input from a single cone and (reviewed in Masland, 2012).

Reinforcing the role of the organisation of the retina in the circuit formation, the various cell types, over sixty different types and subtypes, are regularly spaced and cover the retinal surface evenly. This way the visual inputs can be sampled efficiently and all the possible information created by a photoreceptor can be carried to the brain and form the most complete visual scene possible (Cook, 1996; Wässle et al., 1981; Wässle and Riemann, 1978). It is important to clarify that the cells are evenly spaced in respect to the other subtypes of the same cell type but, randomly positioned with respect to other cell types (Rockhill et al., 2000). This arrangement is not only seen at the cell body level but also at the dendritic level, as dendrites of the same subtype do not overlap much despite the overlap of different subtypes being common. Different subtypes of cone bipolar cells sample and transmit different information. Therefore, it is believed that each of the approximately twelve subtypes of cone bipolar cells that contact a given cone, transmits to the inner retina a different component extracted from the output of that cone (Wässle et al., 2009) (see figure 13). This allows an efficient coverage of the photoreceptor output, that can be seen morphologically and physiologically (Devries and Baylor, 1997; Gauthier et al., 2009).

Figure 13 – Synaptic coverage of cone photoreceptors by bipolar cells

Adapted from Masland, 2012, under Copyright Clearance Center's RightsLink®

(A) Schematic representation of a bipolar cell extending dendrites and contacting every cone photoreceptor cell within its reach. **(B)** Two bipolar cells contacting every cone photoreceptor cell within their reach, and overlapping in two points, sharing a set of cones. Both bipolar cells are showed in red as they are the same sub-type of bipolar cell, transmitting the same type of information. **(C)** same situation described in B, but now each bipolar cell represents a different sub-type (red and blue), meaning each transmits a different set of information collected from the shared cone photoreceptors. **(D)** Four different sub-types (red, blue, green and yellow) of bipolar cells contacting one cone terminal (black arrow), carrying different information from the same cone photoreceptor. This overlap occurs at any point of the retina and the dendritic terminals of the ~12 sub-types of bipolar cells sample each cone. For simplification only 4 sub-types and its overlap with a single cone are represented in the figure. **(E)** Confocal reconstruction showing an example of structural diversity of 3 different sub-types of bipolar cells in a mammalian retina. These 3 bipolar cells sample an identical area, overlapping and sharing a set of cones. ON bipolar cells (red) and OFF bipolar cells (green and blue) are present.

The term “receptive field” is used to refer to the area of retina that is covered by a ganglion cell and in which a light stimulus alters its frequency of discharge. The size of receptive fields in the human retina varies from 200 to 600 µm in diameter and they are likely to be arranged in a hexagonal array, as this conformation allows a more efficient coverage of an area, with minimal overlap (reviewed in Forrester et al., 1996). These receptive fields are dynamic and not static, as initially thought, as they can be influenced by the context of the visual scene, such as response to “looming” stimuli or anticipatory responses to a moving stimulus. Ganglion cells anticipate and start responding earlier than expected, according to the mapping of their static receptive field, as they adapt to predict the stimulus based on the neighbouring cells (Hosoya et al., 2005; Münch et al., 2009; Roska and Werblin, 2003).

The dynamic state of ganglion cells’ receptive fields is a relevant topic for this thesis, as it indicates that these cells might be able to adapt following retinal degeneration and cell transplantation and thereby respond to the input of transplanted photoreceptor cells, even if the circuit has suffered remodelling. Moreover, there is also evidence that the brain can correctly interpret novel input transmitted by previously established circuits. One example comes from an experiment in which viral-vector mediated transfer of red opsin to cones of a dichromatic adult non-human primate that does not naturally express this opsin. Behavioural tests showed that following introduction of a red opsin molecule to a subset of cones, the treated animals had now trichromatic vision, without any direct modification to the circuit (Mancuso et al., 2009). This suggests that the brain is able to learn how to interpret new input without requiring a propose-built neurocircuit for red/green colour vision. Similar results were obtain in mice, with gene transfer experiments, creating a new trichromatic mouse strain (Jacobs et al., 2007).

We can hypothesise that the circuit could adapt and react in a similar way following transplantation, having new cells connecting and using the previous established circuit to rescue vision.

1.2.2 Synapses and Neurotransmitters in the retinal circuit

Neurons communicate with each other electrically via gap junctions, or chemically using neurotransmitters. Chemical synaptic connections allow cells to communicate and transmit signals that are electronically isolated from each other. The neurotransmitters are synthesised in the pre-synaptic cells, stored in vesicles in the presynaptic terminal and release to the extra cellular space upon stimulation. The

presynaptic space between pre- and post-synaptic cell is called the synaptic cleft and is typically more than ten nanometres across. Once in the synaptic cleft the neurotransmitter binds to its specific receptors in the post-synaptic cell, stimulating this cell to open its calcium channels and consequently propagating the signal throughout the synaptic circuit. To regulate and clear the excess of neurotransmitters from the cleft, the pre-synaptic cells have receptors and transporters that will also bind to the neurotransmitters. Glutamate is the main neurotransmitter used by the retina's neurons along the vertical pathway, photoreceptor to ganglion cells. The post-synaptic cells in the retina have glutamate receptors. These receptors can be classified as ionotropic or metabotropic. Both types of receptors are similar, as both bind to glutamate and that leads to changes in the cell permeability to ions, by influencing the ion channels, but they differ in the mechanism used to achieve that end. The ionotropic receptors influence the ion channels directly as the receptor and ion channel form a complex. This type of receptor mediates fast synaptic transmission between neurons. The OFF responses of cone bipolar cells are mediated by ionotropic receptors, mainly AMPA/Kainate receptors (for review see Dhingra and Vardi, 2012).

Unlike the ionotropic receptors, the metabotropic glutamate receptors (mGluR) do not form a complex with the ion channel. The mGluRs are associated with the ion channel via a second messenger pathway, with the binding of glutamate leading to activation of the receptor and consequent activation of a G-protein that initiates an intracellular cascade that leads to the activation of the ion channel (Lees, 1994; Slaughter and Miller, 1983, 1981). To date, eight mGluRs have been discovered and they can be classified in one of three groups according to their characteristics and agonist, as all receptors bind to glutamate but not all receptors bind to the same glutamate agonists. mGluR1 and mGluR5 belong to group I, the activation of such receptors leads to the hydrolysis of fatty acids and consequent release of intracellular calcium. The known agonists for this group are quisqualate and trans-1-Amino-1,3-dicarboxycyclopentane (ACPD). Both Group II, consisting of mGluR2 and mGluR3, and group III, consisting of mGluR4, mGluR6, mGluR7 and mGluR8, are considered inhibitory, as they lead to the downregulation of cyclic nucleotide synthesis. The known agonists for these groups are L-2-(Carboxycyclopropyl) glycine (L-CCG-1) and trans-ACPD, for Group II, and L-2-amino-4-phosphonobutyric acid (L-AP4) for group III. mGluRs are present in post-synaptic cells as well as in pre-synaptic terminals, where they help to clear up and decrease the glutamate release to the cleft, modulating the synaptic transmission (Dhingra and Vardi, 2012; Pin and Duvoisin, 1995).

All mGluRs have been shown to be present in the retina, with the exception of mGluR3. Each retinal cell type often expresses more than one mGluR however, there seems to be a level of specificity, with the same type of receptor being expressed exclusively by ON or OFF cell types in post-synaptic terminals or a single receptor type being present in pre-synaptic terminals. In the retina mGLuR8 is the only mGluR present in photoreceptor cells as an auto-receptor at the pre-synaptic terminal, modulating the levels and release of glutamate. mGluR8 is also present in a few amacrine cells, also in the pre-synaptic terminal. Another mGluR present in presynaptic terminals in the retina is mGluR7, present in the presynaptic terminals of bipolar and amacrine cells. Rod bipolar cells show presence of RNA and positive staining for mGluR1, 5 and 6. Cone ON bipolar cells are positive for only one of the mGluRs, mGluR6 (Vardi et al., 2000; Vardi and Morigiwa, 1997, p. 6), making this an interesting marker to evaluate the interaction between the transplanted cones and host retina. Interestingly, mGluR6 is also the better characterised of the mGluR receptors in mammalian and primate retinas (Vardi et al., 2000). It is the dominant receptor in the OPL, since is present in both rod and ON cone bipolar cells. Both knockout (Masu et al., 1995) and naturally (Maddox et al., 2008) occurring mutant mice lacking mGluR6 do not present an ERG b-wave, meaning all cone bipolar cell-derived ON responses are abolished in these strain . A similar phenotype was identified in patients with mutations in the *GRM6* gene which encodes mGluR6 (Xu et al., 2009; Zeitz et al., 2005).

The restricted localisation of mGluR6 to the post-synaptic dendritic terminal is essential for several other proteins that are required to initiate the synaptic cascade following binding of glutamate to the receptor and it might even be involved in stabilisation of this proteins (Cao et al., 2009). The localisation of mGluR6 is altered following photoreceptor degeneration, even during early stages, with mGluR6 being present but diffused in the cell's cytoplasm instead of restricted to the dendrite's tips (Nomura et al., 1994). Several studies show that these alterations result from absence or altered pre-synaptic proteins in photoreceptor cells. Mutations in presynaptic proteins such as bassoon,Cacna1(Specht et al., 2009), ELFN1 (Cao et al., 2015) and LRIT (Sarria et al., 2018) lead to a decrease in correctly localised mGluR6 positive structures in the post-synaptic dendrites of bipolar cells. These data re-enforce the theory that intact photoreceptor signals are required in order to establish and maintain the synaptic circuit, influencing the localisation of post-synaptic proteins to the post-synaptic terminal (reviewed in Dhingra and Vardi, 2012).

1.3 Retinal Degeneration

Retinal degeneration comprises a vast group of pathologies, including genetically inherited retinal diseases, such as retinitis pigmentosa (RP) or Stargardt disease, or complex disorders like age-related macular degeneration (AMD) that are due to a combination of genetic and environmental factors. Retinal degeneration can also result from trauma to the eye/retina.

In developed countries, AMD and inherited retinal degenerations that result in loss of photoreceptor cells, are the leading cause of blindness (Owen et al., 2012). Although not life-threatening, loss of vision represents therefore a severe debilitating condition, with considerable socio-economic repercussions. The mammalian retina, like other parts of the nervous central system, is unable to repair/regenerate effectively once cell loss occurs, unlike some lower vertebrate species that show repair and regeneration mechanisms. Photoreceptor cell loss in mammals results in permanent vision impairment.

Retinal degeneration can be classified as: rod-degenerative conditions, where rod photoreceptors are the main/primary affected cell type, and cone photoreceptors preserve function, at least temporarily; cone-degenerative conditions, where cones are affected and rods preserved; rod/cone and cone/rod-degenerative forms, where both rods and cones are affected, sometimes the cone degeneration being a consequence of rod photoreceptor death (Michaelides et al., 2006; Pontikos et al., 2020). Along with photoreceptor cell loss, the retina also undergoes remodeling of the remaining neurons (Jones and Marc, 2005). Usually, the INL and GCL remain intact for several years after the ONL is lost, but significant synaptic remodeling occurs (Jones and Marc, 2005; Marc et al., 2003a; Strettoi et al., 2003a), and gliosis might occur (Barber et al., 2013; Hippert et al., 2015; Rodrigues et al., 1987). The fact that the interneurons that compose the INL and GCL, still survive after degeneration of the photoreceptor layer offers an opportunity for possible therapeutic intervention to restore vision.

The retinal changes that occur following the progressive loss of photoreceptor cells result in neuronal rewiring and reprogramming events, including alteration in gene expression and metabolic rate of some cells, as well as the migration of neurons across the vertical axis of the retina. Regardless of the cause, once photoreceptors are lost, particularly cones, a sequence of progressive events takes place, inducing remodelling of the retina (Figure 14) (Jones et al., 2006, 2003; Marc et al., 2008, 2003b; Marc and Jones, 2003; Strettoi, 2015; Strettoi and Pignatelli, 2000).

Figure 14 - Schematic of retinal remodelling following photoreceptor degeneration

Adapted from Webvision under a Creative Commons License

https://webvision.med.utah.edu/book/part-xii-cell-biology-of-retinal-degenerations/retinal-degeneration-remodeling-and-plasticity/

Normal organisation of the retina can be seen on the left, with organised layering of retinal cells and their dendrites. Phase 1 of remodelling starts before photoreceptor cell loss occurs and gets more pronounced as photoreceptor cells show abnormalities and fully degenerate. Müller glia cells extend their feet past the OLM and sprouting of horizontal cell dendrites occurs. RPE becomes unhealthy. In phase 2, when all rod and most cone photoreceptors are absent, sprouting of interneuron dendrites and establishment of a new circuit takes place. Some Müller cells become activated. RPE cells lose their apical microvilli. By phase 3, remodelling is complete in an end degeneration situation, where complete photoreceptor loss has occurred. Interneurons retract their dendrites, RPE invades the neural retina and most Müller cells become activated and form glial scar.

The presence and localisation of synaptic markers is affected by the remodelling events from early stages. Bipolar cells are the most severely affected as they are the first to lose their synaptic connection as a consequence of photoreceptor degeneration (Figure 15). In cases the where the rod photoreceptors are present but not functional, the rod bipolar cells will extend their synaptic terminals and try to establish new point of contact (Figure 15A, on the left). When there is loss of rods, the rod bipolar cells will display absence or redistribution of mGluR6, throughout their cell bodies and axons. If functional cone photoreceptors are present, the rod bipolar cells may, at a later stage, establish new connection with these photoreceptors. Therefore, mGluR6 might re-localise to the post-synaptic terminals (Figure 15A, on the right). Cone bipolar cells also suffer remodelling (Figure 15B) with the ON pathway being more severely affected. OFF cone bipolar cells retract the dendritic terminals that no longer contact a photoreceptor and, in this case, the iGluRs in that terminal is lost. Some dendrites remain in place with no alteration to the iGluRs. Most ON cone bipolar cells retract their dendrites and lose their mGluR6 (Figure 15B, middle), others seem to rewire and start presenting iGluRs, characteristics of the OFF pathway, when a substantial number of cones are still present. The same has been described for rod bipolar cells; in the complete absence of cones, rod bipolar cells also present iGluRs on their post-synaptic terminals (Figure 15B, left) (D'Orazi et al., 2014).

Figure 15 - Structural and functional rewiring during retinal remodelling

Adapted from D'Orazi et al. ,2014. Licensed by Elsevier and Copyright Clearance Center.

(A) In a healthy retina rod bipolar cells (RBC) connect to rod photoreceptors, with the glutamate receptor mGluR6 in its dendritic tips, across the synaptic ribbons. (Left) In retinas where rod photoreceptors are present but transmission-defective, RBC's dendrites sprout to the ONL, developing new locations of contact. (Right) Rod degeneration leads to retraction of the RBC dendrites and a simultaneous loss or redistribution of mGluR6 to the cell body and axon. RBC dendritic retraction may precede the formation of synapses with novel partners, such as cones. **(B)** In a heathy retina OFF cone bipolar cells (OFF-CBC) contact cones, establishing synaptic connections via iGLuRs. ON cone bipolar cells (ON-CBC) establish synaptic connection vis mGluR6. (Middle) In the presence of few cones the ON-CBC retract their dendrites and mGluR6 is absent. The OFF-CBC are mostly preserved however, retraction of some of its dendrites is seen. (Right) In the presence of cone photoreceptors, but absence of rod photoreceptors, abnormal presence of iGluRs in ON-CBC and RBC is seen.

Studies have shown that mutations in many different genes, including rhodopsin, peripherin, and cGMP phosphodiesterase genes, result in photoreceptor cell death. It is also known that that this process occurs mainly by apoptosis. However, little is known about the link between these genetic mutations and the subsequent death of photoreceptors by apoptosis (Hao et al., 2002; Portera-Cailliau et al., 1994). A better understanding of such link and mechanism may provide potential ways to intervene and prevent or delay retinal degeneration.

Apoptosis occurs in normal development and is a necessary mechanism of programmed cell death that is mediated by a signalling cascade that involves the activation of caspase enzymes by proteolytic cleavage of proteins. This mechanism can be initiated intrinsically, in response to damage within the cell, such as in response to a genetic mutation as happens in the inherited retinal dystrophies; or it can be in response to an extrinsic signal from other cells (Portera-Cailliau et al., 1994). In photoreceptor cells, the homeostasis of calcium seems to be of central importance to initiate apoptosis in response to a calcium overload of the photoreceptor cells. Studies suggest that mutations associated with certain retinal dystrophies likely lead to a metabolic stage that mimics constant darkness, giving this hypotheses the name, “equivalent dark hypotheses” (Fain and Lisman, 1999). The retinal degeneration (*rd*) mouse is a model of rapid degeneration caused by a null mutation in the *Pde6b* gene. The mutation leads to a loss of activity of the β-subunit of phosphodiesterase (PDE) and, consequently, elevated levels of cGMP in these mice. The high levels of cGMP result in a continuous influx of calcium ions through the cGMP-gated channels (Bauer, 2013; Fain and Lisman, 1999). Mutations in other genes, such as *AIPL1* and *PDE6A* genes, that result in photoreceptor cell death are also associated with disruption of PDE and increased cGMP-gated calcium channel activity, suggesting that an apoptotic mechanism leading to retinal degeneration is initiated by high calcium levels within the photoreceptor cells (Liu et al., 2004; Sakamoto et al., 2009).

An alternative explanation for the photoreceptor cell death in retinal degeneration is the “equivalent light hypothesis”. This hypothesis postulates that some mutations lead to the overstimulation of the phototransduction cascade, resulting in signals being sent to the interneurons of the INL that are similar to those produced when light is detected by the photoreceptor cells. In these circumstances, photoreceptor cell death occurs in a similar way to that seen in light damage models of retinitis pigmentosa, where photoreceptor loss is induced following exposure to short intense intervals of light or prolonged lower intensity light (Fain and Lisman, 1993; Lisman and Fain,

1995). Some studies suggest that the equivalent light hypothesis may be the main cause for cell death in Retinitis Pigmentosa dystrophies. This evidence was mainly obtained by studying the *Rpe65*$^{-/-}$ mouse strain, where the rod photoreceptor cells, that carry the mutation, behave as they are constantly in presence of a light background and present reduced circulating current in response to light stimulation, reduced light sensitivity and accelerated turn-off of photo response. In this model, the lack of RPE65 protein lead to photoreceptor loss due to accumulation of opsin protein that does not bind to 11-*cis* retinal in the outer segments, causing activation of the phototransduction cascade, effectively causing an equivalent light background. (Woodruff et al., 2003). Other studies supporting the equivalent light hypotheses were carried out using the arrestin knockout mouse (*Sag*$^{-/-}$) and the rhodopsin kinase knockout mouse (*Rhok*$^{-/-}$). In these animals, photoreceptor cells degenerate rapidly when the animals are placed in constant dim light, which would not lead to retinal degeneration in wild-type animals. Those studies also showed that these strains, *Sag*$^{-/-}$ and *Rhok*$^{-/-}$, do not suffer retinal degeneration if kept in constant darkness (C. K. Chen et al., 1999; J. Chen et al., 1999; Xu et al., 1997).

Interestingly, further investigation to prove if the retinal degeneration seen in *RPE65*$^{-/-}$, *Sag*$^{-/-}$ and *Rhok*$^{-/-}$ strains was due to constitutive activation of the phototransduction cascade, a second mutation was introduced in these mice by crossing them with the *Gnat1*$^{-/-}$ strain that lacks α-transducin, thereby blocking the phototransduction cascade. Both studies showed that blocking of the phototransduction cascade in the double knockout mice resulted in a protective effect, since no retinal degeneration was detected when mice were exposed to constant dim light. These results supported the “equivalent light hypothesis”, by showing that even in presence of light, if there is no overstimulation of the phototransduction cascade and consequent hyperpolarisation of the photoreceptor cells, photoreceptor apoptosis does not occur (Hao et al., 2002; Woodruff et al., 2003).

It has been hypothesised that permanent hyperpolarisation might lead to apoptosis by either intrinsic or extrinsic mechanisms. The intrinsic mechanism would be an intra-cellular, autonomous response within photoreceptors due to the low levels of calcium, as the overstimulation of the phototransduction cascade results in calcium no longer being transported inside the cell. This leads to a permanent hyperpolarisation of the photoreceptor cells that prevents glutamate release, simulating a permanent exposure to light. The exact mechanism that leads to apoptosis in presence of low calcium levels is not completely understood, but it is known that neurons appear to require their calcium levels to be within a restricted range, and it is proposed that the

same is true for photoreceptors (Lipton and Kater, 1989). If cultured neurons, are unhealthy because they have been deprived of growth factor, they can be rescued by depolarisation caused by exposure to a high concentration of potassium that leads to opening of calcium channels (Franklin and Johnson, 1994a, 1994b; Moulder et al., 2003). The possibility that a low concentration of calcium could lead to photoreceptor apoptosis is supported by the mechanisms known to be used by photoreceptor cells to regulate the rate of phototransduction, therefore keeping the calcium levels within certain limits. The regulation of calcium concentration by the sodium/calcium, potassium exchanger (Schnetkamp et al., 1991), light dependent translocation of transducing and arrestin in order to decrease activation in bright light levels (Sokolov et al., 2002; Zhang et al., 2003) and the modulation of cGMP channels by calcium binding proteins (Hsu and Molday, 1993) are examples of known mechanisms that photoreceptor cells use to maintain the calcium homeostasis.

Another possible intrinsic mechanism that leads to activation of apoptosis mechanism in photoreceptor cells, in a context of hyperpolarisation, is oxidative stress (Travis, 1998). Photoreceptor cells have a high metabolic activity and therefore contain a large number of mitochondria in their inner segments. Possible mutations that lead to a reduction in metabolic activity have as consequence an increase in production of mitochondrial free radicals, such as reactive oxygen species. While in other tissues this would not necessarily be a problem, as the oxygen supply could be modulated by vasoconstriction, the choroid's vasculature is largely unable to constrict, resulting in the same amount of oxygen being supplied to the photoreceptor cells, despite their altered metabolic state. The reactive oxygen species induce oxidative damage to the photoreceptor's mitochondria, leading to activation of caspase proteins and ultimately apoptosis (Greenlund et al., 1995).

Extrinsic mechanisms that lead to apoptosis should also be considered, as it is known that the microenvironment during retinal degeneration can have a negative effect on surrounding photoreceptor cells, leading to the death of cells that do not carry the mutation. This can be observed in models like the *rd1* strain, where the rods carry a fatal mutation, but cones also degenerate following the loss of rods. It was described using this model, that rods secrete a cone viability factor, that is capable of improving survival of the cone-only *rd1* retinas *in vivo*, when delivered subretinally (Mohand-Said et al., 1998), and *in vitro*, when added to cultured *rd1* retinal explants (Léveillard et al., 2004). Another study showed how the microenvironment can initiate an extrinsic mechanism of apoptosis, by generating a chimeric mouse from albino *Prph2*$^{RD2/RD2}$ and a pigmented wild-type strain. In the chimeric animals they saw

pigmented areas, therefore of wild-type origin, where photoreceptor degeneration was evident (Sanyal and Zeilmaker, 1984). Other study integrated a transgene encoding the PRPH2 gene in the X chromosome of *rds*$^{-/-}$ mice. Hemizygote transgenic females displayed a mosaic phonotype, with patches of genetically normal retina and patched where there was no PRPH2 expression. Interestingly, thinning of the outer nuclear layer in this hemizygote transgenic females was similar to what was observed in untreated *rds*$^{-/-}$ mice. Despite the mosaic phonotype, cells expressing the PHPR2 gene degenerated at the same rate as *rds*-mutant cells. In contrast, homozygote transgenic animals did not display retinal degeneration, corroborating rescue of the *rds*$^{-/-}$ phenotype by introduction of the PHPR2 transgene (Kedzierski et al., 1998). These results are similar to what is seen in *rd1* mice, where genetically intact cone photoreceptors degenerate in consequence of the loss of rod photoreceptors, which carry the mutation. Together this data suggests that the proportion of mutant to wild type cells may play a role and genetically healthy photoreceptor cells may degenerate due to an abnormal microenvironment caused by loss of the mutated photoreceptors and remodelling of the neural network.

1.4 Therapies for Retinal Degeneration

Several alternative approaches are being explored for the treatment of retinal degeneration: gene therapy, electronic retinal prosthesis, and cell therapy.

Retinal diseases that are caused by known genetic mutations can be diagnosed and possibly treated with a gene therapy approach. There are currently over 200 genes that have been linked to inherited retinal degeneration, the majority being specifically expressed in photoreceptor cells and RPE (reviewed in Veleri et al., 2015a). Some diseases also present a heterogeneity in mutations within large genes, making gene therapy more challenging. Moreover, in some cases patients can show different clinical manifestations and phenotypes despite mutations the same gene (Boye et al., 2013; Michaelides et al., 2006, 2004; Pontikos et al., 2020; Smith et al., 2001). Nevertheless, gene therapy has been a successful therapeutic approach for several inherited retinal pathologies in pre-clinical and clinical studies (Bainbridge et al., 2015, 2008; Boye et al., 2013; Ripamonti et al., 2015; Tan et al., 2009). In order for gene therapy to work, the photoreceptor cells (or other target cells) need to be sufficiently healthy at the time of intervention, as gene therapy is able to limit the progression of the disease but cannot restore visual function once the photoreceptor cells are lost. Other challenges of gene therapy are the size of the therapeutic gene, as some genes that cause retinal degeneration exceed the packaging size capacity of the most effective viral vectors currently available for use, the adenovirus associated vectors. Strategies to overcome this challenge are currently being studied, and rapid progress is being achieved, especially by exploring the potential of CRISPR/Cas9 technology (Colella et al., 2014; Maeder and Gersbach, 2016). Even if some supplementation gene therapies are effective and prevent retinal degeneration, they would have to be developed for many different forms of retinal dystrophies and this is likely to be impractical for the foreseeable future. An alternative gene therapy approach that might be effective for advanced degeneration is the use optogenetic strategies. These involve the delivery of genes encoding for light-sensitive proteins into surviving non-light sensitive retinal cells, like bipolar or ganglion cells, “hijacking” its function to become photoreceptor-like. This strategy has the advantage of targeting cell that are already part of the synaptic network. However, the sensitivity of the currently available optogenetic tool is low and the amount of light required to induce a response might be damaging to the cells. Despite improvement in the available tools, the kinetics of these still slower than a heathy photoreceptor cell, and therefore the visual rescue obtained might not be sufficient to perform daily tasks. The use of special equipment (light-stimulation goggles) that record, process and then project into a specific area

of the retina might be required to overcome some of these pitfalls of this approach (for a review on optogenetic therapy for retinal degeneration see (Baker and Flannery, 2018; Busskamp et al., 2012). Further research to improve the current or develop new optogenetic tools is required and worth pursuing. The broad spectrum, light sensitiveness and temporal high resolution of human vision makes recapitulation of human vision, using an optogenetic approach, an ambitious goal. The simultaneous use of different optogenetic tools will be necessary to achieve such results. Furthermore, bypassing part of the retinal circuit, interfering with the natural modulation of the response, will impact image formation, which might be a limiting factor for the extension of rescue achieved. Nevertheless, an optogenetic approach would comprise the advantages of gene therapy replacement, having the delivery method and most good manufacturing practice (GMP) already approved, with the advantage of other therapeutic strategies that allow a broad application, independent of genetic cause for retinal degeneration.

Other approaches for the treatment of blindness include the use of electronic retinal prostheses. Several groups have tested, in clinical trials, the implantation of light-sensitive devices (e.g., Argus®II, Alpha-IMS, IMI, IRIS and EPI-RET 3) that generate and pass electrical stimuli to the retina's INL or GCL (for a review see Bloch et al., 2019). This approach works independently of advanced degeneration of the photoreceptor layer and utilises the remaining retinal circuitry. Epiretinal prostheses are implanted on the surface of the retina, on top of inner limiting membrane, in contact with the axons of ganglion cells. Due to the its proximity to the ganglion cell nerve fibres, occasional random stimulation of the retinal circuit occurs, which interferes with the proper visual stimulus and reduces spatial resolution. I will use Argus®II as an example for type of prosthetics as it is the most promising and widely used epiretinal prosthesis, however other have been developed and tested, (IRIS II and EPI-RET III). Argus®II was approved by European and American regulatory entities in 2011 and 2013, respectively. Over 250 patients have received this implant since then. It is composed of the epiretinal device, which is comprised of 60 microelectrodes, that receives an electrical output from the glasses-mounted camera and processing unit, the external component to Argus®II. This is a complex system as the signal acquired by the camera, process and then transmitted via radio frequency to a coil position in the sclera, which decodes the signal back into an electrical one which finally reached the epiretinal implant and initiates the retinal response. Some of the patients showed implant-mediated light responses and visual perception in daily light (Stingl et al., 2013), ability to identify letters and small words

(da Cruz et al., 2013), and some have even shown long-lasting improvements, years after surgical implantation (Ho et al., 2015). These are promising results, but the size of the small field of vision, 20°, and low-resolution leads to a partial rescue of vision that might be useful for patients with very severe retinal degeneration and complete loss of light perception. However, for patients with macular degeneration it might not be the most suitable as the remaining peripheral vision will be more useful than the vision mediated by the prosthesis. In addition to epiretinal prosthetic other strategies have been studied, such as subretinal, to attempt to use the retinal circuit to modulate and process the visual stimulus, and suprachoroidal prosthetics aiming to make the surgical procedure easier and the implant more accessible for repairs. Both strategies require further investigation, as few patients have received each of the several available implants of subretinal or suprachoroidal retinal prosthesis. Nevertheless, all prosthetics are faces with the same overall limitations: low spatial and temporal resolution. Therefore, the visual rescue and acuity that can be achieved with retinal implants is rudimentary and much inferior to natural vision. This is not an easy problem to address since the number and size of electrodes would have to be increased in order to improve the outcome. However, the heat generated by having more/bigger electrodes would cause damage to the retinal tissue. Other limiting factors are the imaging processing software and appropriate measurements of outcome. Despite several improvements over the last decade the electronic retinal prostheses still far from to confer visual rescue that recapitulates normal vision.

Since in the majority of visually impaired patients, loss of vision is the consequence of the loss of photoreceptor cells, direct photoreceptor replacement is a rational strategy to restore visual function in advanced degeneration. Several characteristics of the retina and eye itself facilitate this approach. Firstly, the eye, being part of the central nervous system, has immune privilege. It therefore has limited immune and inflammatory responses to surgical procedures and transplanted cells. The photoreceptor cells themselves have characteristics that suggest cell transplantation as a promising strategy, since photoreceptors are afferent neurons that do not receive any incoming connections and only require extension of a short axon and single synaptic connection to the interneurons to be able to contribute to the retinal circuit. The following section describes the various photoreceptor replacement strategies that have been investigated to date.

1.4.1 Photoreceptor Cell Transplantation for Retinal Degeneration

A variety of cell replacement strategies for the retina have been investigated over the past decades. The main strategies being explored differ regarding source of cells, donor cells vs mouse or human pluripotent stem cells (PSCs), and delivery method, dissociated cells in suspension vs retinal sheets. In this chapter an overview of the transplantation field is provided. Studies that had direct impact in the experimental set of the present thesis are mentioned in detail later, in the short introduction to each chapter of results. Replacement strategies for retinal degeneration are summarised in Figure 16.

Figure 16 - Schematic of cell replacement strategies

Adapted from Jayakody et al., 2015 (A) Licensed by Elsevier and Copyright Clearance Center. and Santos-Ferreira et al., 2017 (B and C) under Creative Commons License

(A) Transplantation of mouse photoreceptor cells from *Nrl*.GFP$^{+/+}$ or *Crx.GFP*$^{+/+}$ donor mice or *Crx* GFP ESC-derived retinal organoids. After dissociating the embryonic retinas or ESC-derived optic cups, GFP positive cells are sorted by FACS, isolating photoreceptor precursor cells that are then transplanted into the sub-retinal space of a mouse model. These cells can then be found in the host retina, expressing proteins that the host cells lack. **(B)** Transplantation of human ESC- or iPCS-derived photoreceptors. Cells are plated; to get iPS cells a reprogramming step is necessary to restore pluripotency and differentiated into retinal organoids. The neuroretina layer can be isolated by cutting a retinal sheet that can be transplanted into the sub-retinal space of a mouse. Photoreceptors can also be isolated by FACS, either by using antibody staining or virus label with a reporter molecule, or by MACS, using antibody cell markers, to obtain a pure population of photoreceptor precursors that can then be transplanted into a mouse model. **(C)** Once in the sub-retinal space, transplanted cells, can integrate the host retina and/or engage in a process of cytoplasmic transfer of material to the host cells by an unknown mechanism. Note that retinal sheets can also be obtained from mESC-derived retinal organoids despite not shown in this schematic.

1.4.1.1 Transplantation of Donor-derived Dissociated Cells in Suspension

The possibility of photoreceptor cell transplantation using isolated post-natal photoreceptors from donor animals was first performed in the 1990s. These experiments showed that transplanted photoreceptors were able to grow outer segment-like structures towards the RPE layer, and expressed presynaptic markers facing the INL. However, no rescue of visual function was reported (Gouras et al., 1991). Transplantation of retinal progenitor cells (RPCs) (Klassen et al., 2004) and neural-stem precursors (Banin et al., 2006) have also been investigated. Whilst the cells survived, they were unable to differentiate into mature photoreceptors.

Most of the studies over the past two decades have used neonatal donor cells as a source for transplantation, more specifically rod photoreceptor cells, for practical reasons since the mouse has a rod-dominant retina. Furthermore, many of these studies have used the transgenic *Nrl.GFP*$^{+/+}$ mouse as a source for photoreceptors, as in these animals GFP is expressed under transcriptional control of the neural retinal leucine zipper gene (*Nrl*), that becomes activated specifically in post-mitotic rod photoreceptors, allowing easy identification and isolation of post-mitotic photoreceptors by fluorescence-activated cell sorting (FACS) (Akimoto et al., 2006). Several studies demonstrated that the best transplantation outcome was obtained by FACS isolating early post-mitotic rod photoreceptors at post-natal day 4 to 8 (P4-8), as these cells are committed but still not yet fully differentiated and injecting them as a cell-suspension into the sub-retinal space. Different recipient mice were used for such experiments. Some studies transplanted 400,000 *Nrl.GFP*$^{+/+}$ cells into *rd1, rds* and *rho*$^{-/-}$ mice (MacLaren et al., 2006), showing that transplanted cells integrate and mature following transplantation. Others used wild type mice as recipient for transplantation of 100,000 *Nrl.GFP*$^{+/+}$ cells at a later stage, comparing the integration capacity of photoreceptor precursors with adult photoreceptor cells (Gust and Reh, 2011). The importance of the recipient retina to the transplantation outcome was also investigated by transplanted 200,000 *Nrl.GFP*$^{+/+}$ cells into different models of retinal degeneration (*Prph2*$^{+/\Delta 307}$, *Crb1*$^{rd8/rd8}$, *Gnat1*$^{-/-}$, *Rho*$^{-/-}$, *rd1* and *Prph2*$^{rd2/rd2}$) and quantifying the number of integrated cells (Barber et al., 2013). The process of when and how this transplanted cells migrate, integrate and mature was examined by histological analysis across a period of time of 6 weeks following transplantation of 200,000 *Nrl.GFP*$^{+/+}$ cells into wild-type mice (Warre-Cornish et al., 2014). The integration of the transplanted cells seemed to be well characterised and established. All results appeared extremely promising with rescue of function, assessed by pupillometry and extracellular field potential recordings (MacLaren et al., 2006) or

optomotor reflex (Barber et al., 2013; Warre-Cornish et al., 2014), being reported. In 2012 very strong evidence of rescue of rod-mediated vision, following transplantation of 400,000 *Nrl.GFP*$^{+/+}$ was reported by Pearson *et al*. This study differs from all the previously mentioned as it was focus of establishing and characterising the level of rescue of visual function. The recipient model were night-blind mice, (lacking *Gnat1* gene that encodes rod alpha-transducin protein). Following transplantation, the GFP+ labeled early post-natal rod photoreceptors were found correctly oriented within the host ONL with inner and outer segments in contact with the RPE layer, inner processes with presynaptic proteins facing the INL. Nearly all the GFP+ cells expressed the Gnat1 protein that was missing in the endogenous cells of these mice. Rescue of function was shown by electrophysiology with suction-pipette recordings ERG recordings and intrinsic signal optical imaging (showing that the visual signals generated in the retina reached the visual cortex) being performed. Furthermore, behavioral tests, optomotor reflex and water maze, were also used to established rescue of vision under scotopic conditions(Pearson et al., 2012).

Despite very promising, replicable and extensively analysed by several groups, all the results of these previously mentioned studies would have to be reinterpreted This is due to recent discoveries which disprove integration was the main responsible mechanism for the reported rescue. Such findings will be discussed later in this chapter. Is worth firstly mention another study, by Lakowski and colleagues in 2010, that, unlike the ones previously mentioned, explored the transplantation capacity of cone photoreceptor precursors. For this study a new donor strain was used. *Crx.GFP*$^{+/+}$ mice, that had recently been generated in order to mark, with GFP, both rod and cone photoreceptors (Samson et al., 2009). The stage of isolation of such cells was the key factor that allowed for a cone enrichment. Cells were transplanted at an early embryonic stage (E14-E15), coinciding with the differentiation peak of cone precursors. The peak or rod differentiation is much later, around post-natal day 4. This allows for an enrichment for cones but does not guaranty a pure cone population, as rods are still being born during embryonic stage. Cells were isolated, by FACS, at a range of development stages (E13.5, E14.5, E15.5, E16.5, E17.5, P2 and P3) and 200,000 *Crx.GFP*$^{+/+}$ cells were transplanted into wild-types and retinal degeneration mouse models. After transplantation, independently of the development stage, only a few of these cells resembled cone photoreceptors. Most having a more rod-typical morphology. This led to the question of whether this was due to plasticity of the transplanted donor cells, or due to rod photoreceptors being

more likely to integrate the host retina than cone photoreceptors (Lakowski et al., 2010).

As I mentioned previously, all these results would have to be reinterpreted considering novel findings. Until recently it was thought that transplanted photoreceptor cells migrated into the host retina where they integrated, as GFP expressing cells were observed located in the host ONL. This notion was challenged by two studies published in 2016. These independent studies showed that only a minority of the GFP+ photoreceptor cells seen in the host ONL were truly integrated transplanted cells. The majority of the GFP+ cells were host photoreceptors that engaged, using an unknown mechanism, in a process of cytoplasmic material transfer with the cells that remained in the sub-retinal space (Pearson et al., 2016; Santos-Ferreira et al., 2016). It still not clear by what mechanism this material transfer occurs, or what exactly is transferred, the most likely candidates being RNA or proteins or a combination of both. What is known is that it is not a classic cell-fusion process, and that this mechanism allows host photoreceptors to contain proteins that were lacking prior to transplantation. For example, in addition to the fluorescent reporter GFP used to mark and identify the transplanted cells, rod α-transducin was detected in the host *Gnat1*$^{-/-}$ mouse model. With these findings it is necessary to reinterpret almost all of the literature published so far regarding photoreceptor transplantation (for review see Ortin-Martinez et al., 2017). Other studies since, have indicated that the host environment is also relevant to transplantation outcome, and the number of integration and cytoplasmatic material transfer events varies between mouse models (Waldron et al., 2018). Identification of the cellular mechanism behind material transfer might open novel therapeutic approaches to target retinal degeneration. However, it will still not be applicable to end-stage degeneration scenarios.

Majority of the previously mentioned studies were performed using slow degeneration or stationary models, with a relatively intact ONL. As a proof-of-concept for visual rescue following transplantation in such models, rescue should be less complicated as their retinas do not present the challenges of an end-stage degenerate retina, where the thinning retinal layers make the surgical approach harder, and where it is still uncertain if the remaining retinal circuitry is healthy enough to connect with the transplanted photoreceptor cells. Nonetheless, end-stage degeneration is more clinically relevant and therefore the more appropriate target for cell replacement therapy. More studies are necessary to understand if material transfer will have an impact under these circumstances, however, since very few host photoreceptor cells

are left, these models are more likely to show if transplanted cells can rescue vision by forming synaptic connections with the host retina.

1.4.1.2 Transplantation of PSC-Derived Dissociated Cells in Suspension

For photoreceptor transplantation to be considered a viable therapy is imperative that a renewable and ethical source of cell is used (see chapter 1.4.3). Therefore, donor cells can inform regarding the feasibility of cell transplantation, but human PSCs are the ideal choice for future clinical application.

In 2012, our group reported transplantation into healthy (*wild-type*) and retinal degeneration mice models (*Rho*$^{-/-}$, *Gucy2e*$^{-/-}$, and *Gnat1*$^{-/-}$), using mESC-derived photoreceptor precursors derived from an optimised adherent, two-dimensional (2D) culture system. There was no indication of these cells having integrated into the host retina following transplantation. This led to the conclusion that the precursor photoreceptor cells generated by this 2D ESC culture systems did not fully recapitulate embryonic developmental processes, despite expressing a selection of photoreceptor markers. Therefore, cells generated by this protocol were unlikely to provide a robust source of photoreceptor precursors equivalent to those from the developing retina (West et al., 2012a). Later, in line with the progress made in differentiating embryonic stem cells towards photoreceptor lineages in vitro (see section 1.4.3) our group adapted the protocol published by Eiraku *et al.* in 2011 and were able to generate and isolate mESC-derived photoreceptor precursors. This optimised protocol allowed for the organoid-generating process to be scaled up, enabling the transplantation of a purified population of photoreceptor precursors at defined stages of development (Gonzalez-Cordero et al., 2013). A schematic of this differentiation protocol can be seen in Figure 20, under the methods section 2.1. Using this protocol, neuroepithelium-like structures were identified at dd5 and by dd7, optic vesicle-like structures were seen. Between dd9 and dd12, RPE cells could be detected and the optic vesicle-like structures developed further, showing an optic cup-like structure, similar to the developmental stages seen *in vivo*. Gene expression profiles were analysed, by microarray, along with immunohistochemistry and, in order to further investigate the similarities between the mESC-derived rod photoreceptor precursors and post-natal retinas (Figure 17A).

Figure 17 - Characterisation and assessment of transplantation capacity of mESC-derived photoreceptor precursors generated by 3D culture system

From Gonzalez-Cordero *et al.*, 2013. Licensed by Springer Nature and Copyright Clearance Center

(A) Time course of photoreceptor genesis in 3D culture system using E16 cell line. Temporal expression of Crx and Rhodopsin **(A1)**, and Recoverin- and Rhodopsin-positive **(A2)** photoreceptors at different time points. **(A3)** Hierarchical clustering and heat map of 12 photoreceptor-associated transcripts at days 26 and 34 ESC-derived and P12 donor-derived Rhop.GFP^{+} cells. **(B)** Integration and connectivity of mESC-derived photoreceptor precursors using 3D culture system. **(B1)** Rhop.GFP^{+} integrated photoreceptors showing mature morphology with outer segments (OS) stained for rod α-Transducin (**a**, inset) and spherule formation in the outer plexiform layer (OPL). **(B2-4)** Integration of ESC-derived Rhop.GFP^{+}/Gnat1^{+}photoreceptors into the *Gnat1*$^{-/-}$ (**e**), *Prph2*$^{rd2/rd2}$ (**f**) and *Rho*$^{-/-}$ (**g**) degenerate models as demonstrated by rod α-Transducin, Peripherin-2 and Rhodopsin segment staining, respectively. **(B5)** Rhop.GFP^{+}/Gnat1^{+} integrated rod spherule in close proximity to bipolar cells (PKCα^{+}) **(B6)** Rhop.GFP^{+} rod spherule localised with ribbon synaptic marker Dystrophin. **(B7)** 3D confocal image of *Gnat1*$^{-/-}$ retinal flatmount showing Rhop.GFP^{+} integrated rod stained for rod α-Transducin and synaptic marker Ribeye. **(B8)** Histogram showing the number of Rhop.GFP^{+}/Gnat1^{+} ESC-derived integrated rods from transplants of days 26, 29 and 34 of culture. Error bars, mean ± s.e.m; ANOVA, **P* < 0.05, ****P* < 0.001

Cells were infected with a viral vector driving GFP expression under a Rhodopsin promotor, in order to facilitate their isolation. The capacity of these cells to integrate and connect with the host retina, as well as mature post-transplantation was then analysed (Figure 17B). Approximately 200,000 Rhop.GFP+ FACS-sorted photoreceptor precursors (dd26-29) were transplanted into the subretinal space of adult *Gnat1*$^{-/-}$ mice. Three weeks post-transplantation, integration of the mESC-derived cells was thought to have occurred, as presence of both identifying molecules (GFP as well as the protein absent in the host mouse model, Gnat1) was detected. However, these findings, mainly regarding the number of real integration events, need to be revaluated in light of the more recently reported material transfer between transplanted and host photoreceptor cells (Pearson et al., 2016; Santos-Ferreira et al., 2016). Authors claimed that cells transplanted at dd 26-29, the equivalent to an early post-natal retina, showed greater integration potential than cells transplanted at dd 34, the equivalent to a late post-natal retina. Which indicated that the developmental stage of the transplanted photoreceptor cells determines their ability to integrate, as seen previously with donor cells (Gonzalez-Cordero et al., 2013). In summary, this report showed that the optimised protocol of 3D culture system established in our laboratory provides a robust and consistent method of differentiation of mESC into photoreceptor precursors, , supporting the possible utility of ESC-derived cell for photoreceptor cell replacing therapies.

In 2014, Decembrini and colleagues generated a *Crx.GFP*$^{+/+}$ mouse stem cell line. In this line photoreceptor precursors produce GFP which facilitates isolation, as there is no requirement for viral transduction. Retinal organoids were generated and GFP+ cell isolated, with 200,000 GFP+ cells being transplanted into NOD/SCID mice. Following transplantation cells appear to integrate and mature (Decembrini et al., 2014). Other study developed a cell surface biomarker panel of for isolation of post-mitotic rod precursors from mouse ESC-derived retinal organoids. Same number of cells was transplanted and the transplantation outcome was similar to what was previously reported by the previous studies, with transplanted cell integrating and maturing following transplantation (Lakowski et al., 2015). Remember that now we know that the majority of those “integrated cells” were actually host cells that engaged in material transfer with the transplanted cells and not truly integrated cells. More recently, characterisation and optimisation of culturing protocol, to increase cone differentiation in the *Crx.GFP*$^{+/+}$ mouse stem cell line, was achieved. The retinal

organoids were then infected with a viral vector (2.1.GFP) under a M/L OPSIN promotor, which allow isolation of a pure population of cones by FACS. Following transplantation of 200,000 GFP+ mESC-derived cones precursors into an end-degeneration model. Cells survived in the subretinal space and matures, displaying mature cone markers, such as Mopsin (Kruczek et al., 2017). By transplanting in severely degenerated retina, where only few photoreceptor host photoreceptors were present, this work demonstrated beyond doubt that ESC-derived photoreceptors can survive and mature following transplantation. However, no connectivity with host retina was assessed beyond the proximity with host bipolar cells and present of pre-synaptic proteins in the transplanted cones. Further detail regarding this article and its impact in work developed in this thesis is discussed in chapter 4.

In parallel the use of human PSCs as a source of photoreceptors, as that will eventually be the one of interest for clinical use, was also investigated by several groups. Is important to mention that mouse cell cultures are much shorter than human, as the cell development is obviously quicker. This means that mouse PSCs still provide a valuable tool to study photoreceptor transplantation, as it allows optimisation of transplantation conditions in a shorter time frame.

Several protocols were optimised in order to generate retinal cells from human PSCs (see chapter 1.4.3). In 2009 Lamba and colleagues reported the transplantation of hESC-derived cells for the first time. In this study cell culture were infected with a virus expressing GFP under an CMV or hEF1a promotors, which are both highly expressed in retinal cells and not photoreceptor specific. 50,000 to 80,000 cells were transplanted in the intravitreal space of newborn wild-type mice and in the subretinal space of *Crx*$^{-/-}$ mice and samples were analysed 1 to 6 weeks following transplantation. The authors report that cells transplanted into the intravitreal space prior to post-natal day 2, migrate into all the layers of the retina, including ONL, where rod-like morphology and markers was seen in GFP+ cells. Cells transplanted into the subretinal scape migrate exclusively in to the INL showing similar features to the host photoreceptors (Lamba et al., 2009). Rescue of some retinal function was reported by using ERGs However, the probability that so few cells, a mix retinal cell population from each only up to 80% were actually photoreceptors, could induced an ERG response is low. The same approach was then reported using hiPSC-derived cells, displaying similar results (Lamba et al., 2010). It is extremely likely that the GFP+

cells seen were, once more, due to cytoplasmatic transfer and not true cell integration. All the images shown in this article show GFP+ cells that look similar to host mouse photoreceptors. In another publication further optimisation and new differentiation protocol, using 3D cell culture to generate human ES and iPSC derived retinal organoids, were reported. Interestingly, this group adopted a different strategy as organoids were frozen prior to transplantation. This is a valuable concern in a clinical setting, as long-term store and cell shipment will be required. Unfortunately, the authors do not provide extensive data regarding experiment set up and outcome. At the time of transplantation retinal organoids are thaw and cultured for a week until dissociated and transplanted. Cell viability was regularly checked and batches under 70% viability were discarded. Prior to transplantation cells were infected with a viral vector in order to express GFP, this was use as a tool to identify these cells following transplantation and to FACS the photoreceptors. 200,000 cells were transplanted into the subretinal space of wild-type mice and collected 7 days following transplantation. The authors claim that no GFP+ cells were seen in the host INL, therefore excluding that these cells engage in cytoplasmatic material transfer with the host. Having that as a control for material transfer transplantation into a model of severe retinal degeneration, 10-12 weeks of age *rd1* mice, was performed. Following transplantation maturation of few rod photoreceptor cells was shown. Connectivity with the host's INL was assumed based on proximity with host's bipolar cells and presence of presynaptic protein, synaptophysin, in the GFP+ cells. Rescue of basic visual function was assessed by Optomotor reflex and light avoidance test. Curiously, optomotor test showed a significant difference in contrast sensitivity between treated and untreated eyes. However, such difference was not seen in the light avoidance test, when including all transplanted animals. By excluding, post analysis, animals that were considered to have fewer transplanted cells in the sub-retinal space (4 out of 8 animals) a difference in light avoidance was detected (Barnea-Cramer et al., 2016). The fact that some samples were excluded after analysis is not an ideal experimental set up, as exclusion criteria should be set prior to avoid skewing the results. Is also peculiar that a clear difference was seen in contract sensitivity but not in light avoidance, which is a less complex behavior and more simple visual process. It is worth mentioning that he optomotor reflex was not measured in the typical way where a staircase of contrast is automatically set by the software and presence of optomotor reflex is scored, by the software or researcher that is blind to the direction

of the stimulus. Stimulus are presented to the animals several times until the threshold of detection is established, by absence of optomotor reflex. Right and left eye contrast sensitivity can be differentiated optomotor reflex is triggered by temporal to nasal movement, with the head of the animal following the stimulus direction. To establish the threshold several repetitions are required. Barnea-Cramer and colleagues report the average number of head movements during a stimulus, but they do not specify if such movement is in the expected direction for the stimuli presented. Another important publication reporting transplantation of hESC-derived photoreceptors is Gonzalez Cordero *et al*., 2017. This publication describes an optimised 3D protocol that generated retinal organoids that recapitulate human development (see 1.4.3.1). A pure population of cone photoreceptors was isolated by FACS and transplanted into wild-type and mice with severe retinal degeneration. Cell maturation and some true integration into the host's INL were shown, but no rescue of function was detected. Since this publication is the base for the work developed in this thesis a detailed description of the findings is provided in chapter 4.

1.4.1.3 Transplantation of Retinal Sheets

Transplantation of retinal sheets is another cell replacement strategy that can be used. Rather than dissociating the retina into single cells and transplanting a photoreceptor cell suspension, the photoreceptor layer of a fetal retina or retinal organoid is dissected and transplanted as a unit. The isolation of the photoreceptor layer is done manually which allows for possible human error. Furthermore, due to the early stage of development at which such isolation takes place, the retinal layers are still not well defined and mostly retinal projectors are isolated. This means that the retinal sheets should not be perceived as a photoreceptor sheet, but rather a sheet of retinal progenitor cells, that despite being enriched for photoreceptors cells also contain other retinal cell types. This strategy has various advantages and disadvantages. For example, synaptic connection of the graft with the host retina will be more difficult due to the presence of the host INL or INL cells in the retinal sheet. Moreover, the area of treatment will be limited to the size of the graft, which in turn is limited by the size of the fetal eye or retinal organoid and surgical delivery method, unlike cell suspension which can spread a cover a larger area. Conversely transplantation of an organised structure, that can include an RPE layer, might be beneficial to cell survival and maturation.

Retinal sheets can be isolated from human fetal donors or derived from PSCs. Human fetal retinal-sheets have been successfully transplanted into retinal degenerated rats humans, with clinical trials for RP (Radtke et al., 2002, 1999) and AMD patients (Seiler and Aramant, 2012). These trials reported a modest improvement in visual acuity in several patients. However, the studies lacked objective assessments and it was therefore difficult to conclude there was an improvement in vision. Moreover, human fetal tissue is not a renewable cell source and ethical issues prevent this strategy to be widely applicable.

The first study using mouse ES and iPSC-derived retinal sheets was reported in 2014. In this study mouse ES and iPSCs were differentiated into retinal organoids and the neuroblastic layer, containing neural retinal progenitors, was manually dissected and transplanted, subretinally, into *rd1* mice. Following transplantation, retinal sheets survived and mature, with clear areas of the graft self-organising into rosettes. Mature outer segments developed in the centre of the rosettes. They report that the structure of the graft lead to different integration patterns. A possible pattern is the direct contact of photoreceptor cells present in the retinal sheet with the host INL; other possible pattern is the interneurons of the retinal sheet preventing the contact of grafted photoreceptors with host's INL; and the third pattern described is when the retinal sheet loses structural organisation. In the case of loss of organisation of the retinal sheet it is hypothesised that individual photoreceptors could migrate and integrate the host's circuit, in a similar way to what is seen when transplanted dissociated cells in suspension. and the individual photoreceptor (Assawachananont et al., 2014).

In 2016, Shirai et al, demonstrated the ability of hESC-derived retinal sheets to survive and mature to form ONL-like structures in rosettes, with inner and outer segments, following transplantation into nude rats and two primate models of retinal degeneration (Shirai et al., 2016).The retinal-sheets were isolated from retinal organoids at different differentiation stages and transplanted into nude rats, with no retinal degeneration, to assessed the best optimal stage for transplantation. Retinal sheets transplanted between dd50 and dd150 showing the most mature structures at 100 to 200 days following transplantation. They report that younger grafts resulted in thicker ONL-like structures and substantial numbers of cone photoreceptors. More rosettes were seen in retinal sheets transplanted at an earlier differentiation stage

and although inner retinal cells may block contact between the host INL and the photoreceptors of the graft, rosettes in hESC-retinal sheets transplanted at dd50–60 made contact with host bipolar cells at a comparable with that of older grafts. Therefore, they concluded that the ideal stage for transplantation of retinal sheets is ~dd60. Next, they performed transplantation of dd60 hESC-retinal sheets into SD-Foxn1 Tg(S334ter)3LavRrrc rats, an immunocompromised, end-stage degeneration, due to a mutation in the Rhodopsin gene, strain. The results were similar to what had been previously observed in immunocompromised rats with intact retina. The transplanted retinal sheets expressed Ribeye and in the host retina, the sprouting of once-retracted bipolar processes was seen. Finally the pilot study using primates shown that, following causing retinal degeneration, by laser or chemical damage, hESC-retinal sheets could be transplanted, survived and matured as previously reported (Shirai et al., 2016). In summary, this report characterised the maturation process of hESC-retinal sheets in detail, demonstrating cell survival and maturation as well as possible connectivity between graft and host retina. The presence of rosette formation might be a disadvantage as it might prevent contact between host and transplanted photoreceptors and these structures are not normally seen in healthy retina. Recently, another publication from the same laboratory showed similar results following transplantation of hESC-retinal sheets into an immune-deficient end-stage *rd1* mouse model of retinal degeneration. The transplanted grafts showed signs of photoreceptor maturation with inner segment and outer segment formation. Synaptogenesis and light responses from hESC-retinal sheets following transplantation, recorded by micro ERGs were reported (Iraha et al., 2018). However, due to presence of pre- and post-synaptic cell within the graft I such results are ambiguous as is s not possible to differentiate interactions between graft/host and cell within the graft itself.

To date no study has been published that has compared transplantation of cell suspension and retinal sheets in a comprehensive and systematic way. Such study would be extremely valuable in order to establish which is the most valuable strategy, which is more likely to succeed in clinical trials.

1.4.2 Transplantation of RPE for Retinal Degeneration

While photoreceptor transplantation is still very much at the pre-clinical stage, substantially faster advances have been made with ESC-derived RPE cells (for a review see Vitillo et al., 2020). The first FDA-approved allogenic trial using hESC-derived RPE was initiated in 2011 by Schwartz et al. In this phase I/II trial hESC-derived RPE cells were subretinally injected into patients with either Stargardt disease or the atrophic form of AMD. The primary aim of this trial was assessment of safety, and so far, no major adverse events have been reported. Longer follow-up assessments are required to establish the true long-term outcomes of this trial (Schwartz et al., 2016, 2015).

The first Asian clinical trial, where the same hESCs-RPE used by Schwarts, were transplanted into four patients also showed no safety issues and improvement of visual acuity was observed in some of the treated patients (Song et al., 2015). An alternative approach has been explored in Japan, where an autologous iPSC-derived RPE sheet was transplanted. No safety issues were reported and one-year post transplantation the RPE cell sheet is still intact. This approach proved to be too complex to implement on a bigger scale, due to the costs and labour associated with developing a cell line for each patient. Therefore no more patients are expected to be enrolled (Mandai et al., 2017).

More recently the first European safety trial using ESC-derived RPE for macular repair in patients with advanced Stargardt type 1 (STGD1) disease was performed. An escalating dose of cells, between 50,000 and 200,000, was administered in one eye to different groups of patients in order to determine the safe dose for future studies. In this study a detailed analysis of retinal structure and function of the treated area was performed, something that previous studies were lacking. A 12 month follow-up of twelve transplanted patients, children and young adults, has been published. In this study it was demonstrated that the transplanted RPE cells survive, with focal areas of hyperpigmentation being present in all patients in a dose-dependent manner, even following the withdrawal of immunosuppression after thirteen weeks (Figure 18). No unexpected adverse events were detected, as no uncontrolled proliferation or inflammatory responses were identified. Detection of small visual improvements was not sustained or were matched by similar improvements in the untreated eye. In one of the patients who received the highest

dose of cells, localised thinning and reduced sensitivity in the area of hyperpigmentation were reported, suggesting potential harm of high dose. A longer follow-up is necessary to further investigate the safety and possible long-term impact on vision (Mehat et al., 2018).

Figure 18 - Fundus photographs 12 months following RPE transplantation

Mehat et al., 2018. under Creative Commons License

Areas of hyperpigmentation can be seen in all patients. The extension of the area of pigmentation appears to be dose-dependent, with the exception of patient 6 (P6). Retinotomy site is indicated by the green dot, and the area of subretinal administration is outlined by the dotted black line.

Together these studies support the potential of ES and iPS cells as a source for future cell therapy applications, demonstrating encouraging results. However, transplantation of RPE cells will not, in most cases, be sufficient to improve or reverse visual impairment. A therapy for end-stage degenerative retina would still require transplantation of photoreceptor cells and, in some cases, replacement of both photoreceptor and RPE cells, in order to achieved long-term sustained improvements.

1.4.3 Pluripotent Stem Cells as a Source for Cell Transplantation

Embryonic stem cells (ESC) have the ability to self-renew indefinitely and to differentiate into any cell type, including photoreceptor cells. These cells, as well as induced pluripotent stem cells, are considered the most attractive source of cells for retinal cell therapy as they represent a virtually inexhaustible source of cells that, after being differentiated into a post-mitotic cell type, can be transplanted. Technologies for defined large scale culture of PSCs are rapidly being developed (for review see Carpenter and Rao, 2015). Moreover, these cells also allow i*n vitro* studies of development, disease modelling and drug screening, thereby limiting the dependence on donor-derived material and reducing the need for animal models.

Isolation and characterisation of PSCs were first described using mouse blastocysts, and reports showed that these cells could be maintained *in vitro* in an undifferentiated state for an undetermined period of time. This studies also showed that these cells could differentiate into cell lineages of all three germ layers (Evans and Kaufman, 1981; Martin, 1981). Some years later the equivalent population of cells has been isolated from human embryos opening new possibilities for regenerative medicine (Thomson et al., 1998).

PSCs can be differentiated using 2 main methods: a 3D culture in suspension, where embryonic bodies are formed, or in 2D cultures where ESC grow as a monolayer on stromal cells or on extracellular matrix (Keller, 2005). Several protocols have been successfully developed in order to differentiate ESCs into retinal cells, for both mouse and human cells. The same protocols can also be applied to induced pluripotent stem cells (iPSC) which proved to be a solution to the problem of finding an ethical source of ESCs, as these can be obtained by reprogramming adult cells to a pluripotent state, showing similar differentiation potential as observed for ESCs.

1.4.3.1 Stem cell derived photoreceptors and RPE

In 1995, for the first time, a protocol showed that embryonic bodies (EBs) formed from mouse ESCs, when exposed to retinoic acid, could develop into neuronal cells expressing markers such as βIII tubulin, neurofilaments and various voltage-gated ion channels, that are hallmarks of neuronal identity. This protocol consisted of a 3D culture system, where the EBs were induced to form neuronal cells in suspension, followed by dissociation and plating the cells as a monolayer to differentiate further (Bain et al., 1995). The importance of a stepwise induction, where cells are alternately cultured as a 2D monolayer or 3D organoids was explored from the very beginning and used in the first protocols to generate retinal lineage cells derived from ESC (Bain et al., 1995; Kawasaki et al., 2000; Lee et al., 2002; Zhao et al., 2002).

Zhao *et al,* were the first group to report the differentiation of mouse ESC-derived retinal cells using retinoic acid, insulin-transferrin-selenium-fibronectin (ITSFn) with fibroblast growth factor 2 (FGF2) to induce initial neural differentiation of mouse ESC aggregates in a 3D suspension culture. These were then dissociated and plated as a monolayer, a 2D culture, on top of mouse P0 retinal cells. This co-culture allowed for further differentiation, as the P0 retinal cells secreted factors necessary for retinal differentiation. Expression of early markers of retinal progenitors (Nestin, Pax6, Notch1, Rx), and then photoreceptor precursors (NeuroD, Crx, Nrl), was observed. Subsequently, some mouse ESC-derived photoreceptor progenitors also showed signs of maturation with expression of markers such as Rhodopsin, Rhodopsin kinase and Peripherin2, but these were rare events. This study provided proof-of-concept for the feasibility of photoreceptor differentiation from ESCs (Zhao et al., 2002). Next, it was required to improve protocols to generate mouse ESC-derived retinal cells more efficiently. A big step in achieving this was the use of a serum-free neural induction protocol, where the serum was substituted with a knockout serum replacement (KSR). By using KSR, after around seven days in culture, 70 % of the cells expressed the neural precursor marker, Nestin, and a similar proportion expressed the neuroectodermal marker *Sox1* (Watanabe et al., 2005). Efficiency was further improved through addition of Wnt antagonist and head inducer Dickkopf-1 (Dkk1) and Nodal inhibitor LeftyA for the first five days of neural induction. This enhanced neural differentiation with up to 90 % efficiency, as it addressed the *in vitro* lack of regional specification that would be present *in vivo* during embryonic development, by timely addition of embryological-relevant patterning factors (Watanabe et al., 2005).

The search for a protocol that induced further differentiation into photoreceptors cells continued with several groups contributing with new discoveries in the field. Ultimately a study by the Sasai and Takahashi laboratories reported improved efficiency of differentiation towards retinal lineages, by using a mouse ESC line with a GFP reporter in the *Rx* locus, a gene that encodes the retinal homeobox protein Rx and is necessary for retinal cell fate. When the *Rx* gene was activated in these cells, the fluorescent reporter allowed for purification of the Rx:GFP+ retinal progenitor cells. The dissociation and purification of this population, by FACS, was performed after 9 days in culture. Following FACS the cells were re-plated and 7% of them further differentiated, expressing *Crx* by day 20 in culture. The percentage was still low and to improve generation of Crx-positive photoreceptor precursors, the Notch pathway was inhibited, simulating what happens *in vivo.* This led to a significantly increased proportion of cells differentiating into *Crx*-expressing photoreceptor precursors, as well as Pax6+/Islet1+ retinal ganglion cells. Moreover, addition of fibroblast growth factors, taurine, Sonic hedgehog (Shh) and retinoic acid (RA) was found to further increase the number of Rhodopsin-positive cells without significantly increasing the abundance of Crx-positive cells in culture. This protocol allowed differentiation of ESC-derived photoreceptor precursors expressing a panel of cone and rod maturation markers (Osakada et al., 2008).

Another landmark study in ESC-derived retinal progenitors was reported by Sasai's laboratory in 2011, when not only stepwise differentiation was achieved, but also recapitulation of retinal morphogenesis *in vitro* (Eiraku et al., 2011). In this protocol embryonic bodies (EBs) were generated following dissociation of mouse ESCs, and maintained in a suspension 3D culture, by using low binding plates. After the first week of culture, vesicles evaginated from the aggregates. The vesicles flattened and then invaginated forming a cup shape. The proximal portion of the vesicles showed expression of low levels of *Rx* and activation of Mitf, a marker for RPE, and the distal portion of the vesicles showed strong expression of *Rx* as well as other neural retina markers, such as *Pax6*, *Six3* and *Chx10*/*Vsx2*. In summary, Eiraku *et al,* were able to generate optic cups *in vitro,* with an inner portion of invaginated neural retina epithelium, surrounded by a rigid outer shell of RPE precursors, resembling development *in vivo* (Eiraku et al., 2011). This indicated that there is an intrinsic self-organisation mechanism driving morphogenesis of the optic cup, with neural retina and RPE domains (Eiraku et al., 2012, 2011; Eiraku and Sasai, 2012).

Furthermore, our laboratory showed that the photoreceptor precursors generated from mouse ESC could be isolated and transplanted into a murine retina and were the first group to optimise and scale-up the 3D retinal organoid protocol. This provided conclusive evidence that ESCs could be a viable source of photoreceptors for cell transplantation, following recapitulation of the development and differentiation of these cells (Gonzalez-Cordero et al., 2013).

The increasing understanding of ESCs, their differentiation into a retinal-lineage and organoid culture, led to the establishment by different groups of differentiation and culture protocols for human ESCs (hESC) (Boucherie et al., 2013; Gonzalez-Cordero et al., 2017; Mellough et al., 2015; Meyer et al., 2009; Nakano et al., 2012; Reichman et al., 2014; Zhong et al., 2014). In 2006 Lamba *et al.* showed, using a 2D culture protocol, that 80 % of the ESC-derived retinal progenitors, from a H1 hESC line, shared a similar genetic profile to human foetal retina (Lamba et al., 2006). Furthermore, it was shown by other groups, that cell fate specification and maturation followed a time course that recapitulated human development *in vivo*. It was also shown that it is possible to alter retinal differentiation to obtain different retinal cell types, by manipulation of endogenous developmental signalling pathways (Meyer et al., 2009).

The field has continued to evolve, and in 2012, Nakano *et al.* reported a protocol that produced self-forming optic cups, with stratified neural retina from hESC, by using a 3D suspension protocol (Nakano et al., 2012). Other protocols were also reported, using iPSCs, where not just 3D retinal cups were obtained, but the photoreceptor cells matured to form photosensitive outer-segments (Zhong et al., 2014). In addition, the authors found efficient formation of human neural retinal vesicles (also called embryonic bodies) and RPE from the same starting population (Reichman et al., 2014). In 2017, Gonzalez-Cordero *et al.* published a modified 2D/3D protocol that produced both RPE cells and neural retinal vesicles with well-formed outer nuclear layer-like structures, containing rods and cones, and showing nascent outer segments and presynaptic structures (Figure 19). This cell culture system recapitulated human photoreceptor development and allowed isolation and transplantation of a pure population of ESC-derived cone photoreceptors, that survived and showed some evidence of becoming incorporated within the host retina (Gonzalez-Cordero et al., 2017).

Figure 19 - Time course of photoreceptor development in 2D/3D differentiation cultures

From Gonzalez-Cordero *et al*., 2017 under Creative Commons License

(A-C and E) Characterisation of expression of photoreceptor markers at neuroepithelial regions. Scale bars, 25 μm **(D)** Summary of temporal expression of photoreceptor markers during human eye development at indicated foetal week (Fwk).

Research Aims and Objectives

This project aims to provide a comprehensive understanding of the capacity of hES-derived cone precursors to, following transplantation, establish connection with the host retina and rescue visual function, in advanced retinal degeneration. This will provide valuable insight into the development of possible future cell therapies for conditions such as AMD and Stargardts Disease.

By asking if ES-derived cells can rescue visual function in an advanced degeneration model this study will:

(1) Comprehensively characterise the *Aipl1*$^{-/-}$ mouse strain, with particular interest in assessment of remodelling events and function of the retinal circuit following retinal degeneration.

(2) Optimise cell transplantation conditions into the *Aipl1*$^{-/-}$ mice, by looking for cell maturation and visual function, following transplantation, comparing both transplantation strategies (dissociated cells vs retinal sheets).

(3) Evaluate long term cell maturation, connectivity with the host and rescue visual function, following transplantation into immunocompromised mice with advanced retinal degeneration.

(4) Exclude the possibility of rescue of visual function due to material transfer between transplanted cells and host remaining photoreceptors.

The present study will determinate the potential of using cell transplantation as a therapy for retinal pathologies that lead to loss of photoreceptor cells.

Chapter 2: Methods

2.1 Mouse ESC cultures

2.1.1 Maintenance of ESC cultures

A mouse Crx.GFP ESC line (Decembrini et al., 2014) (a kind gift of Prof. Y. Arsenijevic) was maintained mouse Maintenance Medium (mMM) (Gonzalez-Cordero et al., 2013).

Cell were grown in 100 mm petri dishes coated with 0.1% gelatine (Sigma, G2625). Dishes were coated on the day of use, by adding 6 ml of the gelatine solution to each plate. Cells were split/passaged every Monday, Wednesday and Friday. Cells were split when under confluent (30 to 70%). mMM was aspirated and a PBS wash was performed, followed by addition of 2 ml of 0.25% Trypsin-EDTA (Gibco, 25200-072), pre-warmed to 37°C. Trypsin solution was incubated at 37°C for five minutes and then the same amount of mMM was added to the plate to inactivate the enzymatic treatment. Cells were gently pipetted, collected into a 15 ml falcon tube and centrifuged at 1000rpm (180g) for five minutes at room temperature. The supernatant was aspirated, and cells were resuspended in 2 ml of mMM. Live cells were counted using a haemocytometer and, using the formula previously published by Gonzalez-Cordero *et al* in 2013, 4.2 x 10^5 cells were added to 9 ml of mMM with 18µl of 10% LIF solution, and plated in a new gelatine coated dish. Dishes were incubated at 37°C with 5% CO_2

2.1.2 Freezing/thawing mouse ESCs

A 60 mm petri dish was coated with gelatine thirty minutes before cells were plated.

One cryovial was partially thawed in the water bath for twenty seconds and its content was pipetted, carefully, into a falcon tube containing 2 ml of pre-warmed mMM. The cryovial was then washed with an extra 1ml of mMM and that was added to the falcon tube that was centrifuged at 100 rpm (180g) for three minutes at room temperature. Supernatant was aspirated and cells were resuspended in 4 ml of mMM with 8 µl of 10% LIF solution. Cells were plated in 60 mm dish. Next day the media was replaced by fresh mMM containing LIF. Cells were slipped and passaged next following the protocol previously described in the previous section.

Early passages were frozen in order to keep a stock of mESCs. Cells were frozen down at the time of splitting/passaging, using the same protocol described previously. When planning on freezing cells an extra plate, for such purpose was plated during the previous passaging. Following trypsin treatment and centrifuging of the cells (see section 2.1.1) the supernatant was aspirated and 750 µl of pre-cooled mouse Freezing Medium (mFM) was added to resuspend the cells. Cryovial, previously labelled with the cell line, passage number, date and name of the user, were filled with 250 µl of the mFM containing the cells and immediately transferred to a pre-cooled (on ice) freezing container. The container was placed at -80°C overnight and cryovial were then stored in liquid nitrogen.

2.1.3 Differentiation into retinal organoids

For differentiation of 3D neuroretinal organoids, also known as embryonic bodies (EBs) (Figure 20), on day zero of differentiation, usually a Wednesday, cells were passaged using the protocol previously described in section 2.1.1. Following trypsin treatment and centrifuging, supernatant was aspirated and mESCs were resuspended in 2 ml of mouse Differentiation Medium (mDM). Cells were counted using a haemocytometer and 3 x 10^5 cells were added to 10 ml of mDM, for each 96-well plate we aimed to differentiate (for this projected usually 20 plated were differentiated at the time). 100 µl per well was added to low-binding 96-well (Nuclon Sphera, 174925) plates and incubated at 37°C with 5% CO_2. On the following day, differentiation day 1 (dd1), growth factor-reduced Matrigel (BD Biosciences) was added to each well to a final concentration of 2% (v/v). By dd9, whole neuroretinal organoids were transferred to low-binding 24-well plates at a density of 12 organoids per well and cultured in 1 ml of mouse Retinal Maturation Medium (mRMM). The Medium was changed every 2 days (3 days over the weekend), with the addition of 1mM taurine (Sigma, T8691) and 500nM retinoic acid (Sigma, R2625), per millilitre of Medium, from dd14 onward.

Figure 20 - Schematic of early and late mouse retinal 3D differentiation

Adapted from Gonzalez-Cordero et al. 2013.

At dd0 ESCs were plated in a 96 well plate, 2% Matrigel was added the next day. By day 9, optic cup was formed and the neurotretinal organoids were transferred to 24-well plate and Medium changed to initiate late retinal differentiation. By day 14 neural retina and RPE was visible.

2.2 Human iPSC reprogramming

The reprograming was performed with help from Mr Milan Fernando.

On day zero, a vial of peripheral blood mononuclear cells (PBMCs) containing 2x 10^6 cells was defrosted and 10mL of Stemspan 3000 with Penicillin/ Streptomycin (Medium SS), prewarmed to 37°C, were added. This mixture was carefully added, drop by drop, to 10ml of Expansion Medium (EM), prewarmed at 37°C. Tube was centrifuged at 300g for five minutes, the supernatant discarded, and the pellet resuspended in 2ml of EMCells were then plated in one well of a 12-well plate.

On day three remove medium containing cells and place in a 15ml falcon tube with 2ml of prewarmed SS Medium. Spin at 300g for five minutes. Discard the supernatant and resuspend in 2ml of EM Medium. Cells were then plated in one well of a 12-well plate.

On day six/seven, as cell have now been expanded, reprograming takes place. Medium containing the cells was removed from the well and placed in a 15ml falcon tube. Cell were counted using a haemocytometer and solution containing 200.000 cells was transferred into a new falcon tube. 12ml of PBS were added to the 200.000 cells and centrifuged at 300g for five minutes. In the meantime, the Lonza P3 Nucleofection buffer (P3 buffer), from P3 Primary Cell 4D-Nucleofector™ X Kit L (Lonza™, V4XP-3024), was prepared in a ratio of 1:4.5 to give a volume of 20ul per electroporation reaction. 0.33 ug of each Yamanaka's episomal plasmids (Addgene, #27080, #27078 and #27077) to give total of just under 1.0ug DNA per 200.000 cells was added to P3 buffer. Following centrifugation, the supernatant was aspirated, and the cell pellet was resuspended in the P3 buffer containing Yamanaka's plasmids. Cells were then transferred to the cuvette strip (Lonza™, V4XP-3024). Using Amaxa 4D-Nucleofector™ System (Lonza), cells were electroporated using program EO-115. Following electroporation cells were kept at room temperature for five minutes and then 80µL of Roswell Park Memorial Institute (RPMI) 1640 (Gibco™ ,11875085) was added to the cuvette strip and it was placed at 37°C for ten minutes. Cells were then added to 1 well of a 6-well plate, previously coated with Geltrex (1:100), in 2ml of EM.

Cell were kept in EM until day 8. From day 8 to day 10 cells were fed daily with a 1:1 E8/EM mix. After day 10 cells were fed daily with E8 medium and followed the protocol described to maintain hESCs and hiPSCs (see section 2.3.1).

2.2.1 Staining for pluripotency markers

Cell were gown in chamber slides (Thermo Scientific, 154526) previously coated with Geltrex (Invitrogen, A1413302). Medium was aspirated and 1ml PBS per well was added carefully avoid lifting off any cells. Chamber slide was transferred out of the Stem cell laboratory in order to fix the cells by adding 250µL of 4% PFA per well, at room temperature for fifteen minutes. After removing PFA, a PBS wash was performed, followed by addition of blocking buffer (3% goat serum, and 1% bovine serum albumin in PBS with 0.1% Triton X-100). Blocking buffer was incubated for two hours at room temperature and then removed. Primary antibodies were diluted in blocking buffer, without goat serum added, according to Table 1, and incubated over night at 4°C. A negative control where only the blocking buffer was added was run in parallel. The primary antibodies were aspirated, and three PBS washed of five minutes each were performed. Alexa-Fluor 488 (Invitrogen-Molecular Probes) at a 1:500 dilution, was incubated for two hours at room temperature, and then samples were counterstained with DAPI (Sigma-Aldrich, D9542).

Antigen	Host species	Concentration used	Supplier
c-Myc	rabbit	1 in 800	Cell Signalling Technology (5605)
LIN28A	rabbit	1 in 400	Cell Signalling Technology (3695)
Nanog	rabbit	1 in 800	Cell Signalling Technology (4903)
Oct-4A	rabbit	1 in 400	Cell Signalling Technology (2840)
Sox1	rabbit	1 in 400	Cell Signalling Technology (3579)

Table 1 - Primary Antibodies for Pluripotency Markers

Following staining the wells were removed carefully and slides were mounted using Florescent Mounting Medium (Dako, S302380-2) and imaged using a Leica DM5500Q confocal microscope. Images shown maximum projection images of xyz stacks. This characterization was performed by Dr Anai Gonzalez-Cordero.

2.3 Human ESC and iPSC cultures

Medium preparation protocols are under 2.2.2, prepared Medium is filter-sterilized and stored at 4°C. All cells were kept at 37°C with 5% CO_2.

2.3.1 Maintenance of ESCs and iPSCs cultures

The Human RB2 ESC cell line and Human iPSC line were maintained in Essential 8™ Medium (Invitrogen, A1517001), in 6-well tissue culture plates (Corning®Costar, 3516) coated with Geltrex (Invitrogen, A1413302). The Medium was changed (2 ml per well) every day until cells presented 90-100% confluency. One well per plate was used to split while the remaining five were differentiated. Cells were split twice a week, when 90% confluent. Medium was aspirated and 2ml PBS was added to wash. 1ml of Versine (Gibco, 15040033), prewarmed to 37°C, was added and plate was put back in incubator at 37°C for 5 minutes. Versine was carefully aspirated and 2ml E8 were added. By carefully pipetting up and down the cells were lifted off the plate and transferred to 15ml falcon. Cells were quantified using haemocytometer and 200.000 were plated in each well of 6-well plate containing 2ml of E8 and 2µL Rock Inhibitor (Live Technologies, 1254).

2.3.2 Freezing/thawing human ESCs and iPSCs

Some wells were used to freeze and keep earlier passages of the cell lines.

Cultures were kept was described above until 70-90% confluent and split with Versine (Gibco, 15040033), prewarmed to 37°C, was added and plate was put back in incubator at 37°C for five minutes. Versine was carefully aspirated and 2ml E8 were added. Cell were centrifuged at 180g (1000rmp) for five minutes at room temperature. Supernatant was aspirated and cells were resuspended in 2-4ml (depending on cell confluency and size of cell pellet following centrifugation) pre-cooled Freezing Medium (KSR 10% DMSO). 1ml of the cell suspension was added to each cryovial (labelled with cell line, passage number, user and date) and placed in a pre-cooled (on ice) cell freezing container. The container was placed at -80°C overnight and cryovial were then stored in liquid nitrogen.

When maintenance cultures were no longer growing or differentiating (after passage 45) a new vial of an earlier passage was taken from liquid nitrogen and partially defrosted at 37°C for a few seconds. Immediately the content of the vials was collected and added, drop by drop, to 10ml room temperature E8. Cells were centrifuged at 180g (1000rmp) for five minutes at room temperature, supernatant was aspirated, and cells were resuspended in 2-4ml (depending on size of cell pellet following centrifugation) of E8 and Rock Inhibitor (1µL /ml) (Live Technologies, 1254). And plated in 1 or 2 wells of a 6-well plate. Next day Medium was change to E8 without Rock Inhibitor and cells were split, as previously described in section 2.3.1. Cells were not split earlier than three days after thawing, independently of its confluency.

2.3.3 Differentiation into retinal organoids

When confluent, Medium was changed to Essential 6™ Medium (Invitrogen, A1516401) for two days, with Medium being changed every day. This change marks differentiation day one (dd1). On dd3 cells were transferred to Proneural Induction Medium (PIM). From this day on Medium was changed every two days (three at weekends). Cultures remain in PIM till retinal organoids start to develop, for a maximum of fourty days. When retinal organoids appeared, these were individually dissected and transferred to a low binding 96 well plate (Nuclon Sphera) for 3D culture in Retinal Differentiation Medium (RDM), until dd42. The PIM wells are then transferred into RDM Medium so that more RPE cells can be differentiated. These cells are then manually picked, dissociated using trypsin for fifteen minutes at 37 degrees, and plated in a laminin coated 48 wells plate. A monolayer of RPE cells are kept in RDM Medium. At dd42, factors were added to the Medium (RDM + Factors). After 70 days in culture individual retinal organoids were transferred to low binding 24 well tissue culture plates (Corning®Costar, 734-1584) at a density of 5 vesicles per well; Retinoic Acid (RA) was added fresh to the Medium at a concentration of 1µg/ml at each feeding. By dd90, RDM+Factors+RA Medium was replaced by a different formulation of Retinal Differentiation Medium (RDM90) (Figure 21). RA was added fresh to RDM90 before use at a concentration of 0.5µg/ml.

Figure 21 - Human retinal differentiation protocol
Adapted from Gonzalez-Cordero, 2017, under Creative Commons License
(A) Schematic of the retinal 2D/3D differentiation protocol. **(B)** Bright-field images of representative stages in culture, white arrows in 3 show RPE differentiation and black arrowhead show areas of neuroepithelia.

Cell grown for experiments described in chapter five, RFM+F, was substituted by a lipid enriched Medium which was called “Advanced Long-Term Medium Seventy” (ALT 70) from differentiation day seventy until differentiation day ninety. From differentiation day ninety onwards RDM90 was substitute by “Advanced Long-Term Medium Ninety” (ALT90).

2.4 Medium preparation

All Medium was filter using a 500ml vacuum filtration with PES membrane and 0.22µm pore size (Merk, 10074360), aliquoted in 50ml falcon tubes and stored at 4°C. Technical staff aid the media reparation.

Mouse Maintenance Medium (mMM)

500 ml GMEM (Gibco, 21210-082)

5.8 ml Non-Essential amino acids (GIbco, 11140-035)

5.8 ml Pyruvate (to final concentration of 1mM) (Sigma, S8636)

1.16 ml 2-Mercaptoethanol (to final concentration of 0.1mM) (Gibco, 21985023)

5.8 ml Knckout Serum Replacement (KSR) (Gibco, 10828028)

5.8 ml Fetal Bovine Serum (FBS) heat inactivated (Gibco, 10106-169)

Mouse freezing Medium (mFM)

900 µl MMM per 60mm dish

10 µl DMSO

Mouse Differentiation Medium (mDM)

500 ml GMEM (Gibco, 21210-082)

5.1 ml Non-Essential amino acids (GIbco, 11140-035)

5.1 ml Pyruvate (to final concentration of 1mM) (Sigma, S8636)

1.2 ml 2-Mercaptoethanol (to final concentration of 0.1mM) (Gibco, 21985023)

8.4 ml Knockout Serum Replacement (KSR) (Gibco, 10828028)

Mouse Retinal Maturation Medium (mRMM)

500 ml DMEM/F12 GlutaMAX (Gibco, 31331-093)

5 ml N2 Supplement (Gibco, 17507-048)

2.5 ml 100 µL Penicillin/ Streptomycin (Life Technologies, 15140122)

Expansion Medium (EM)

10 ml Stem SpanH3000 (StemCell, 9850)

100 µL Penicillin/ Streptomycin (Life Technologies, 15140122)

50 µL Ascorbic Acid (AA) (Sigma, A4544-25G)

10 µL of 50 ng/ml SCF (Miltenyi,130-096-692)

10 µL of 10 ng/ml IL-3 (Invitrogen, PHC0035)

10 µL of 2U/ml EPO (R&D, 287-TC-500)

4 µL of 40 ng/ml IGF-1 (Milteny,130-093-885)

10 µL of 1µM Dexamethasone* (Sigma, D8893-1MG)

*Keep dexamethasone protected from light (discard every 2 weeks)

Proneural Induction Medium (PIM):

500 ml Advanced DMEM/F12 (Life Technologies, 12634-010)

5 ml of N-2 Supplement (Life Technologies, 17502-048)

5 ml L-glutamine (Life Technologies,25030-024)

5 ml MEM non-essential amino acids (Life Technologies, 11140-050)

5 ml Antimycotic Antibiotics (Life Technologies, 15240-062)

Retinal Differentiation Medium (RDM):

350 ml of DMEM High glucose (Life Technologies, 41965-062)

150 ml of F12 (Life Technologies, 12634-027)

10 ml of B27 supplement (Life Technologies, 12587-010)

5 ml of Antimycotic Antibiotics (Life Technologies, 15240-062)

Retinal Differentiation Medium with added factors (RDM+Factors):

350 ml of DMEM High glucose (Life Technologies, 41965-062)

150 ml of F12 (Life Technologies, 12634-027)

10 ml of B27 supplement (Life Technologies, 12587-010)

5 ml of Antimycotic Antibiotics (Life Technologies, 15240-062)

10 ml FBS (Life Technologies, 10500064)

1ml Taurine (Sigma Aldrich, T8691)

10ml Glutamax (Life Technologies, 35050-038)

Retinal Differentiation Medium with factors added at day 90 (RDM90):

350 ml of DMEM (Life Technologies, 10565-018)

150 ml of F12 (Life Technologies, 12634-027)

10 ml of B27 supplement (Life Technologies, 12587-010)

5 ml of Antimycotic Antibiotics (Life Technologies, 15240-062)

10 ml FBS (Life Technologies, 10500064)

1ml Taurine (Sigma Aldrich, T8691)

10ml Glutamax (Life Technologies, 35050-038)

5ml of N-2 Supplement (Life Technologies, 17502-048)

Advanced Long-Term Medium Seventy (ALT70)

500ml Advanced DMEM (Life Technologies, 12634-010)

10ml B27-vit A (Life Technologies ,12587-010)

5ml Antibiotic-Antimycotic (Life Technologies, 15240-062)

50ml FBS (Life Technologies, 10500-064)

10ml Glutamax (cat.no. 35050-038)

1ml Taurine (Sigma, T4571)

Advanced Long-Term Medium Nineteen (ALT90)

500ml Advanced DMEM (Life Technologies, 12634-010)

10ml B27-vit A (Life Technologies, 12587-010)

5ml Antibiotic-Antimycotic (Life Technologies, 15240-062)

5ml N2-supplement (Life Technologies, 17502-048)

10ml Glutamax (Life Technologies, 35050-038)

1ml Taurine (Sigma, T4571)

5.4ml Glucose (Sigma, G6152)

500ul Lipid Mixture (Sigma, L5146)

2.5 Production of ShH10.Mopsin.GFP virus and infection of retinal organoids

Viral production was performed with aid of technical staff, specialists in viral production. Michelle O'Hara-Wright generated most the plasmid and aid viral production.

A ShH10, an engineered capsid protein, adeno-associated viral vector (AAV) (Klimczak et al., 2009) with a GFP reporter under the control of a previously described 2.1PR promoter (Wang et al., 1992), that specifically labels L/M opsin cone photoreceptors, was used to infect retinal organoids at day 100. A pD10/2.1PR_L/Mopsin promoter-GFP, containing AAV-2 inverted terminal repeat (ITR), was used to generate ShH10(Y445F) L/Mopsin.GFP viruses. Recombinant AAV2/2 serotype particles were produced through a previously described triple transient transfection method in HEK293T cells (Nishiguchi et al., 2015), followed by purification of the ShH10(Y445F) serotype using AVB Sepharose column (GE Healthcare). Viral particles were eluted with 50 mM Glycine pH2.7 into 1 M Tris pH 8.8. Vectors were washed in 1 × PBS and concentrated to a volume of 100–150 µl using Vivaspin 4 (10 kDa) concentrators. Viral genome titres were determined by quantitative real-time PCR using a probe-based assay binding the SV40 poly-adenylation signal. Amplicon-based standard series of known amounts were used for sample interpolation. Final titres were expressed as vg/ml. Retinal organoids were infected with approximately $1.2x10^{11}$ viral particles per well in RDM90 or ALT90 (human retinal organoids). Virus (300µl) was added per well and plates were incubated overnight in the incubator and 700 µl of the same Medium was added next morning and left for 48 hours. This virus can also be called 2.1eGFP.

2.6 Dissociation of retinal organoids for cell sorting and preparation of cell suspension for transplantation

Retinal organoids were dissociated using the papain-based Neurosphere Dissociation Kit (Miltenyi Biotec, 130-095-943). Solutions were prepared according to manufacturer's instructions and 1 ml of the enzyme solution was added per every 72, mouse, or 30, human, retinal organoids. Vesicles were incubated with the papain-based enzyme solution for 15 minutes at 37ºC with agitation. Vesicles were then dissociated by gentle mechanical trituration using a 1000 ml pipette tip and incubated at 37ºC for a further 5 minutes. Cells were then centrifuged at 900 rpm for 7 minutes. Cell pellets were resuspended at 2-3 x 10^7 cells/ml in FACS buffer (66% MEM-E HEPES, 33% HBSS (+Mg^{2+}, -Ca^{2+}), 1% FBS, DNAse I (10 µL/ml)) and passed through a 35-µm mesh cell strainer (BD Falcon, UK; cat no 352235). GFP positive cells, identified by a 488-530/40nm detector, were sorted by fluorescence activated cell sorting (FACS) on a BD Influx Cell Sorter fitted with a 200mW 488nm blue laser to excite GFP, and sorted with a 70-µm nozzle at 50 psi. The GFP+ cells, on average >95% pure GFP-positive, were collected in 20% FBS in DMEM, centrifuged and resuspended at a final concentration of ~200,000 cells/µL, ~500,000 or 800,000 cells/µL in sterile EBSS (+Ca^{2+}, +Mg^{2+}) and DNAse I (0.05%).

2.7 Dissociation and preparation of hESC-derived RPE cells for transplantation

A PBS wash is done followed by incubation with 500µL of trypsin for fifteen minutes at 37 degrees. Following incubation 500µL RDM Medium was added to the well, resuspending the cells that were then centrifuged at 900 rpm for 7 minutes. Cell pellets were resuspended at 50.000 cells/µL in sterile HBSS ($+Ca^{2+}$, $+Mg^{2+}$) and DNAse I (0.05%).

2.8 In vivo experiments

2.8.1 Animals

Aipl1$^{-/-}$ mice (Dyer et al., 2004), Crl:NU(NCr)-Foxn1nu, homozygous cross of Crl:NU(NCr)-Foxn1nu with *Aipl1*$^{-/-}$ mice and homozygous cross of Crl:NU(NCr)-Foxn1nu with *Rd1* mice were used in this study. For control experiments wild-type CB57B/6 were used. For all experiments the ages stated are ± two days.

Animals were maintained on a standard 12hr light-dark cycle. Mice received food and water and were provided with fresh bedding and nesting weekly. Crl:NU(NCr)-Foxn1nu mice were maintained in the same condition but autoclaved cages, bedding, and water, along with radiated food was provided. Animals that received cell transplantation at 11-14 weeks of age and were kept from 3 up to 26 weeks post-transplantation, depending on the experiment, in the same conditions previously described. Treatment was performed in only one eye of each animal, while the other eye served as internal control for the experiments. Both male and female recipient animals were used in all experiments and no immunosuppression was administered. Animals were sacrificed by cervical dislocation.

All experiments were conducted in accordance with the United Kingdom Animals (Scientific Procedure) Act of 1986 and Policies on the Use of Animals and Humans in Neuroscience Research.

2.8.1.1 Genotyping

All mice were genotyped every four months or every litter, when generating a new crossed strain, by extracting DNA from ear clips using Extract™ DNA kit (Quantabio, 733-2160).

Aipl1$^{-/-}$ gene was genotype by electrophoresis, as knockout animals will show a smaller band than WT animals, following PRC using the following primers:

WTR – TTCCTCTCTTCAAATCCAGATGAC

G1 – CGTCAGACACTCAGCTAAGAGCAT

N1 – CGAGGCCAGAGGCCAGAGGCCACTTGTGTAGC

Rd1 animals, with point mutation in PDE6β gene were genotyped using a costume TaqMan SNP Genotyping Assay (Thermofisher, part number 4332077) according to manufacturer's instructions (Thermofisher, publication number MAN0009593).

All animals were always genotyped for *Aipl1* and *PDE6β*, as the retinal degeneration phenotype is similar, serving as a control for each other.

Genotyping for Foxn1^{nu} gene was done by phenotype, as homozygote for such gene results in alopecia, therefore homozygote animals can be identified by the lack of hair.

2.8.1.2 Animal Anaesthesia

Mice were anesthetised by intraperitoneal injection of 0.2ml of a mixture of Dormitor (1 mg/ml medetomidine hydrochloride; Pfizer Pharmaceuticals), ketamine (100 mg/ml; Fort Dodge Animal Health), and sterile water in the ratio 5:3:42. Tropicamide (1 %; Bausch & Lomb) was used to dilate the pupils and eyes were kept moist by using Viscotears (Novartis Pharmaceuticals UK Ltd). Anaesthesia was then reversed using Antisedan (atipamezole hydrochloride 0.10 mg/ml, Pfizer Pharmaceuticals, Kent UK), with the mice placed on heat mats and receiving softened food until fully recovered.

2.8.2 Transplantation of ES-derived photoreceptor precursor cells

Recipient mice were anesthetised A glass coverslip was placed over the eye and surgery was performed under direct visual control using an operating microscope (Carl Zeiss) as described previously (Pearson et al., 2012).

When transplanting dissociated mESC-derived photoreceptors precursors, after being sorted and prepared at a concentration of ~200,000 or ~5330,000 cells/µL in sterile EBSS (+Ca^{2+}, +Mg^{2+}) and DNAse I (0.05%), 1 to 1.5 µL were injected into the sub-retinal space of anesthetised recipients, using a sterile 8mm, 34-gauge needle Hamilton precision glass syringe. The procedure was similar for dissociated hESC-derived photoreceptor precursors; cells were sorted and prepared at a concentration of 200,000 cells/µL or 500,000 cells/µL, and 1µL was injected in the sub-retinal space using the 8mm, 34-gauge needle.

For transplantation of hES-derived neuroretinal sheets, the retinal organoids were examined using light microscopy and the photoreceptor rich area of neuroepithelia was dissected using a needle blade microsurgical knife (Sharpoint). The neuroretinal

sheets were injected into the sub-retinal space of mice with up to 2µL of sterile HBSS (+Ca^{2+}, +Mg^{2+}) and DNAse I (0.05%), using a sterile 8mm, 30-gauge needle.

All animal sub-retinal injections were performed by Professor Rachael Pearson or Professor James Bainbridge, with the assistance of the author.

2.9 Histology

Mice were euthanised by cervical dislocation. Eyes were dissected to remove the cornea, iris, and lens. All samples (retinal organoids and dissected eye cups) were fixed for 1h in 4% paraformaldehyde (PFA), cryopreserved in 20% sucrose (1h at room temperature or overnight at 4ºC) and embedded in OCT (TissueTek). Embedded samples were frozen in 2-methylbutane pre-cooled in liquid nitrogen. Samples were then cryosectioned at 12µm thickness and stored at -20ºC.

2.9.1 Immunohistochemistry

For immunohistochemistry, sections were blocked for 2h at room temperature with 3% goat serum, unless otherwise stated, and 1% bovine serum albumin (BSA) in PBS with 0.1% Triton X-100, followed by incubation with primary antibody (Table 2) at 4 °C overnight. Some antibodies (anti-mGluR6 and anti PSD95) required an antigen retrieval step (three minutes microwave, 600watts, in Unmasking Solution Citric based (Vector, H-3300).

Following PBS washes, samples were incubated with secondary antibody Alexa-Fluor 488, 546 and 633 (Invitrogen-Molecular Probes) at a 1:500 dilution, for 2h at room temperature, after washes with PBS, samples were counterstained with DAPI (1:1000, Sigma-Aldrich). Primary and secondary antibodies were diluted in serum free blocking solution.

After staining, samples were imaged using a Leica DM5500Q confocal microscope. Images shown are either single confocal sections or maximum projection images of xyz stacks through 12-mm thick xy sections taken at 1µm intervals, unless otherwise stated. LAS AF image software was used for image processing.

Antigen	Host species	Concentration used	Supplier
Anti-GFP antibody (FITC)	goat	1 in 250	Abcam (ab6662)
PKC-α	mouse	1 in 100	Santa Cruz (sc10800)
Cone Arrestin	rabbit	1 in 500	Milipore (ab15282)
Arrestin 3	rabbit	1 in 200	Novus (NBP1-19629)
Rhodopsin	mouse	1 in 1000	Sigma Aldrich (O4886)
Recoverin	rabbit	1 in 1000	Chemicon (AB5585)
S-opsin	rabbit	1 in 100	Milipore (AB5407)
M-opsin	rabbit	1 in 200	Milipore (AB5405)
HuC/HuD	mouse	1 in 100	ThermoFisher (A-21271)
mGluR6	rabbit	1 in 100	Sigma (SAB4501324)
VGLUT	Guinea pig	1 in 100	AB5905
CtBP2 (Ribeye)	mouse	1 in 100	BD Biosciences (612044)
Calbindin	rabbit	1 in 300	Millipore (AB1778)
Calretinin	rabbit	1 in 300	Abcam (ab702)
PSD95	mouse	1 in 1000	NeuroMab (75-028)
Human Nuclei	mouse	1 in 200	Millipore(MAB1282)
Peripherin2	rabbit	1 in 1000	Gift from Gabriel Travis
Synaptophysin	mouse	1 in 1000	Sigma Aldrich (S5768)
Phalloidin	donkey	1 in 1000	Invitrogen (A22287)
Bestrophin	mouse	1 in 300	Millipore (MAB5466)
F4/80	rat	1 in 150	Abcam (ab6640)
GFAP	rabbit	1 in 250	DAKO (Z0334)

Table 2 - Antibodies for Immunohistochemistry Characterisation

2.9.2 Cell quantification in retinal cross sections

Eyes were sectioned (12µm) and the whole sample was collected across a set of six "twin" microscope slides. Three out of the six "twin slides" were stained for the specific marker using the Immunohistochemistry protocol described (see 3.6.1).

To quantify PKC-α, Calbindin, Calretinin and HuC/D positive cells confocal images (162.5 x 162.5 µm) were taken from superior and inferior mid retina of three sections of each slide, making a total of six images per slide. Quantification was performed by counting the positive cells for each marker in the six projection images of the channel of interest (no DAPI to allow quantification to be blind). All counts included matched wild-type controls and were performed by the same researcher that was masked to the age and strain of the animals.

Since the number of expected Melanopsin positive cells in the retina is low, the quantification method was different from the one used for quantification of other cell types. The average number of melanopsin positive cells per eye was determined by counting all positive cells in three out of the set of six "twin slides", having no DAPI present, to allow researcher to be masked to age and strain. Total number was obtained by doubling the count at the end to estimate the total number of positive cells across the six slides. A strict selection criteria was applied, with only cells that showed positive cell body and at least one cell process were quantified.

2.9.3 Electron microscopy

Mice were euthanised as previously described. Eyes were dissected to remove the cornea, iris, and lens. Samples were fixed for 24 hours in Karnovky fixative (1 % PFA, 3 % glutaraldehyde, 0.08M sodium cacodylate-HCL). After washing with 0.1M cacodylate buffer (pH 7.4) samples were osmicated in 1% aqueous solution of osmium tetroxide, for 2 hours in the dark. Following washing with distilled water samples were dehydrated through ascending ethanol series (30 %, 50 %, 70 %, 90 %, 100 %, 10 minutes per solution with 3 repeats of the 100 % ethanol). To conclude dehydration, samples were incubated in propylene oxide (total of 30 minutes with 3 changes of solution) and left overnight with rotation in a 1:1 mixture of propylene oxide and araldite resin. The samples were then changed into 100 % araldite resin and left for 6 hours with rotation, until embedding and then incubated for 24 hours at 60 °C. Semi-thin (700 nm) and ultrathin (50-70 nm) sections were cut using a Leica ultracut S microtome with a diamond knife (Diatome histoknife Jumbo). Semi-thin sections

were collected onto slides, stained with 1% alcoholic toluidine blue and evaluated under light microscope and ultrathin sections were collected on to 100 mesh copper grids (Agar Scientific), counter-stained with lead citrate and imaged using a JEOL 1010 Transmission Electron Microscope.

2.10 Quantitative PCR

50 ng of cDNA was loaded per well of 96-well plate (Life Technologies Ltd., UK) mixed with 2x Fast Start TaqMan® Probe Master Mix (Roche Ltd., UK), gene-specific forward and reverse primers at a final 900 nM concentration and an appropriate hydrolysis probe binding to the amplified region at a final concentration of 250 nM (Roche Diagnostics Ltd., UK), all dissolved in DNase and RNase free water up to 20 µl final volume. Each cDNA sample was run in triplicate. The reactions were then run on an ABI Prism 7900HT Fast Real-time Sequence Detection System (Applied Biosystems Ltd., UK) equipped with SDS 2.2.2 software for amplification results analysis. From amplification curves Ct values were obtained for each sample. Expression levels were normalised to Brn3 mRNA levels for each sample to assess relative expression of particular genes in different experimental conditions. Cycling conditions were as follows 40 cycles of 95°C for 30 sec. and 60°C for 1 minute. Table 2 contains the list of gene-specific primer sequences used.

Gene Name	Left Primer (5'-3')	Right Primer (5'-3')	Amplicon size (nt)	Probe number
OPN4	cgcactgattgtcattcttctc	cgtcaggatgtgcgagtatc	94	56
Brn3b	cggagagcttgtcttccaac	ctctgggagacgatgtcca	107	42

Table 3 – qPCR Primers and Probes

2.11 Assessment of visual function

2.11.1 Electroretinogram method and analysis

All animals ERGs were performed my animal technicians, Justin Hoke and Aura Hare.

Electroretinogram measures the light-induced electrical activity of the eye. Typically, 2 waves can be identified, a-wave and b-wave. More components can then be identified under different conditions, however none of those was studied during these experiments (Einthoven and Jolly, 1908). The a-wave is the first to appear, immediately after the light stimulus, resulting of extracellular radial current produced by photoreceptor cells as a consequence of closer of cGMP-gated ionic channels and hyperpolarisation of photoreceptors in response to light. This is a negative wave as it translated a reduction of the dark current. A-wave is immediately followed by b-wave, a positive wave, which originated in the post-synaptic retinal cells, predominantly Müller and ON-bipolar cells. Hyperpolarisation of photoreceptor cells leads to a decrease in glutamate release, which consequently results in depolarisation of post-synaptic cells. This increases the level of extracellular potassium ions and generates an electrical current that depolarises post-synaptic cells and generates a corneal-positive deflation (Armington, 1988; Einthoven and Jolly, 1908; Gotch, 1903).

Electroretinograms (ERGs) were recorded from both eyes in both treated and untreated mice. All animals were dark adapted overnight (minimum sixteen hours) before ERG recordings, pupils were dilated using 2.5% phenylephrine and 1.0% tropicamide and kept hydrated with Viscotears (Novartis Pharmaceuticals Ltd), that also improved the contact with the electrodes. All manipulation prior to ERG procedure was conducted under dim red-light illumination. ERGs were recorded using commercially available equipment (Espion E2, Diagnosys, LLC, MA). Scotopic recordings were obtained at the following increasing light intensities: 0.0001, 0.001, 0.01, 0.1, 1, 10, 31.2 and 75.2 $cd\,s^{-1}\,m^{-2}$, and photopic light intensities used were 0.01, 0.1, 1, 10, 31.2 and 72.5 20 cd s−1 m−2, for an eight-step protocol.

The platinum electrodes were placed in the cornea of each eye and one reference electrode was placed sublingually. ERGs from both eyes were collected simultaneously. A midline reference and ground electrodes were placed subdermal in the centre of the forehead and on the tail of each animal. Electrode impedance were kept symmetrical and between five and ten kOhm. Recording were filtered from

zero to one kHz with a sampling frequency of 5kHz. Response to the light pulse was recorded for 400 ms and the initial 10ms of each recording was used to zero the trace.

The readings obtained were analysed by the author using the software provided by Tonnies Multiliner Vision.

2.11.2 Multi-Electrode Array (MEA) recordings

All MEA experiments were performed and analysed by Dr Christopher Procyk.

This state-of-the-art electrophysiology technique records focal neuronal network changes in presence to light, as each microelectrode can detect changes in the extracellular environment as a results of action potential of nearby by cells (Obien et al., 2015). MEA enables extracellular recording of several neurons simultaneously, with each electrode potential recording from a large number of individual cells.

As neurons, ganglion cells have a base like activity, which translates into spontaneous skipping activity. In response to light, photoreceptors initiate an action potential that, when it reaches the ganglion cells leads to a change on that base line spiking which can be measured as voltage changes by the electrodes in the MEA. This allows the study of the retinal circuit in response to light as well as the more detail characterisation of such responses. Furthermore, MEA allows assessment of effect of pharmacological compounds which provides further information regarding the synaptic network and cells involved in the light responses. MEA characterisation of the retina allowed to characterised not only the photoreceptor responses, by microERG/focal ERG, as it provides further information regarding the how synaptic information if passed thought out the network, by recording the activity of ganglion cells (Meister and Berry, 1999; Reinhard et al., 2014; Stett et al., 2003, 2000).

Eyes were collected, placed in Ames Medium (Sigma-Aldrich, A1420) and immediately enucleated. Retinal dissections were performed under dim red light (λmax = 650nm) in bicarbonate-buffered Ames Medium (Sigma-Aldrich, A1420) bubbled with carbogen (5% CO2 /95% O2).An area of interest, in case of transplanted eyes a GFP positive cell mass was first identified under the microscope and then dissected, was dissected and vitreous was carefully removed in order to allow good contact between ganglion cells and electrodes. Retina was mounted ganglion side down onto a perforated Multi Electrode Array (pMEA) (100/30iR-Ti, Multi-Channel Systems). A platinum harp (~0.75 g) was used to weight the retina down and good

electrode contact was maintained by applying negative pressure below the pMEA chamber until large amplitude spontaneous spiking activity was observed. To preserve physiological conditions, the pMEA recording chamber was continuously perfused with pre-warmed, oxygenated, bicarbonate buffered AMES (37 ± 1°C). The retina was left in the dark for half an hour to allow neuronal activity to stabilise and to dark adapt the retina, as previously described (Reinhard et al., 2014).

Full-field Light-stimuli were generated in MC_stimulus II (Multi-Channel Systems) which controlled a LED Driver (LEDD1B, Thorlabs, NJ, USA) connected to an LED light source (M505L3 - 505 nm, 440; Thorlabs). Light was passed through an adjustable neutral density filter wheel (Thorlabs) and delivered to the retina via a 7mm diameter flexible fibre optic light guide positioned approximately 5cm from the retina. Stimuli consisted of 20 repeats of a 100ms, 250ms, 500ms, 1s, and 10s light pulses. The interstimulus interval (ISI) was maintained at 10s except for the 10s pulses where this was 60s. For pharmacological manipulation, L-(+)-2-Amino-4-phosphonobutyric acid (L-AP4); 6,7-Dinitroquinoxaline-2,3-dione disodium salt (DNQX) and D-(−)-2-Amino-5-phosphonopentanoic acid (D-AP5) were added to the perfusion bath 60 minutes before recordings commenced.

Electrophysiological signals were acquired with MC_Rack software (Multi Channel Systems) through a MEA1060UP-BC amplifier and sampled at 12.5 kHz. To detect spiking activity, electrophysiological signals were high pass filtered at 300 Hz (second order Butterworth) with a threshold set to 3 standard deviations of the noise. For Micro ERGs, the signal was low pass filtered at 200Hz (second order Butterworth).

The recorded spikes were then analysed, as each electrode might recorded spikes from more than one cell. Following event detection, the recordings done during the experiment, the data must be analysed in order to isolate single cell responses. This is done by spike sorting using software Offline Sorter (Plexon) that clusters the data using “principal component analysis” (PCA), based in wave form differences. PCA is used to emphasise variation and bring out strong patterns in a dataset, making individual neurons easier to identify. The principal components (PCs) are axis generated by the software, where the actual points in the graph do not have a physical meaning and have aim to get the most variation possible from each data set. By plotting data using the PCs we obtain a different graphical representation of the same data. Several PCs, that can be 2D or 3D, are analysed and the cells that were

recorded by the same electrode can be isolated at the same time cells that were picked up by multiple electrodes are identified (Figure 22).

Figure 22 - Example principal component analysis for spike sorting MEA data

Adapted from Stratton et al 2012, under Creative Commons License

(A-C) Hybrid traces, with two different wave forms, generated by computer data to test spike sorting software. A, B and C represent different MEA channels, where multi-unit data is present. Different wave forms can be identified in A and B, but C appears to be a single wave form and therefore the recording a single cell. **(A1-C1)** PCA analysis, plotting the same data seen in wave form (A-C) in three different forms. In the middle and left images yellow and green dots correspond to the dots that were previously clustered together and classified as a potential wave form derived from a single cell (in this case is not a real cell is a computer-generated trace). In each PCA graphs the noise, dots that don't clutter according to the PCs, are excluded from the cluster. In B1 and C1, left images, new potential clusters were identified by the software (grey and red). **(A2-C2)** Same traces seen in A-C but now colour coded, identified two individual wave forms.

According to the characteristics of their wave form cells were classified as: non-light responsive, if no changes in spiking rate were identified following a light stimulus; transient, if cells suffered a quick change in spiking rate immediately following the light turning on or/and off; and sustained, if cells slowly increased their firing rate during the whole time of the light stimulus, followed by a slow relaxation and return to base line skipping once the light stimulus was tuned off (Meister et al., 1994). Typically, responses recorded from ganglion cells that originate in a photoreceptor response to the light stimulus are transient. Contrasting, melanopsin positive cells which are intrinsically photosensitive retinal ganglion cells (ipRGCs) display a transient response to light.

To distinguish between responses originated by photoreceptor cells or ipRGCs, further than the response profile, synaptic blockers were used. ipRGCs responses are not dependent on synapses and therefore are not obliterated in presence of synaptic blockers. However, photoreceptor originated light responses, which present a transient profile were eliminated following addition of synaptic blockers L-AP4, glutamate receptor agonist, responsible for blocking the synaptic input into ON-bipolar cells; DNQX, AMPA/kinase antagonist, which blocks synaptic input into OFF-bipolar cells (Borghuis et al., 2014).; and D-AP5, N-methyl-D-aspartate (NMDA) receptor antagonist present in bipolar and amacrine cells and involved in ON an d OFF pathway (L. Kalbaugh et al., 2009; Shen et al., 2006).

2.11.3 LOOM experiments

Mice, as prey species, have innate behaviours to avoided predators. Such behaviour is selected based on sensorial cues, including visual perception. The choice between initiating an escape or freezing depends on the stimulus, with a visual LOOM leading, most of the times, to an escape. This is because a LOOM stimulus simulates a predator approaching (De Franceschi et al., 2016; Yilmaz and Meister, 2013). Therefore, a change in behaviour can results of visual perception and consequently LOOM test can be used to assess rescue of visual function.

Mice were placed in an arena, 48 x 35 x 30 cm, with an opaque triangular refuge 20 cm wide and 12 cm maximum in height in one corner. A visual stimulus (1 cm black disk rapidly widening to 25.5 cm in 250 ms and remaining on-screen at this size for an additional 500 ms) was presented on a calibrated LCD monitor that filled most of the open top of the arena. Mouse movements were recorded with a camera and

acquired continuously in MATLAB (MathWorks), as previously described (De Franceschi et al., 2016). Mice were left to climatise for 5 minutes minimum before the presentation of the LOOM stimuli. Experiment was repeated in three consecutive days for each mouse. Behaviour change was analysed, by a researcher masked to age and strain of the mice, by viewing the videos and identifying as a response to the stimuli any change of behaviour (fleeing, freezing and rearing behaviour). Each animal was taken as an experimental unit, where an animal was taken as visual responsive, and their behaviour classified as “Response”, if it showed a change of behaviour to at least two out the three of the trials performed.

2.11.4 OptoMotor response (OMR)

This behavioural test analyses the head movement in response to the movement of the surrounding environment. It takes advantage of a reflex behaviour and therefore does not require a learning process. It can be used to measure contrast sensitivity and/or acuity (Abdeljalil et al., 2005; Shi et al., 2018; Thaung et al., 2002).

Optomotor test was performed to assess contrast sensitivity in mice. The spatial frequency was kept at 0.128 cycles per degree (c/d) and only the contrast of the vertical rotating bars displayed on the screens varied, from black and white to grey scale. Mice were place on a platform in the centre of the arena, surrounded by screens, and the stimulus was played. The observer, which was blinded to the direction of the rotation, as well as to the fact of the animals being treated or untreated, and which eye, for the treated animals, had been injected, in order to eliminate bias, then decided on what direction the animal moved its head due to tracking the visual stimulus. All mice were tested twice a day for a period of 4 days. Between mice, the arena and platform were cleaned with 70% ethanol. The experiment was conducted by the same investigator every time and both male and female mice, aged matched, were used. All experiments were conducted under normal light levels. Final values for contrast sensitivity were calculated according to the formula:

$$1 \div \left(\frac{Value\ Obtained\ given\ by\ Optomotor\ software}{100}\right.$$

Random Calibration data was collected previously by Dr Martha Robinson and consists of a computer code that randomly choses between right and left, without any animal or stimulus being present.

2.11.5 Light avoidance

As nocturnal animals, mice display a natural light aversion to acute light exposure, between ten and thirty minutes, in an open field (Semo et al., 2010). This light mediated behaviour can be used to assess restoration of light perception (Barnea-Cramer et al., 2016; Singh et al., 2013).

Mice were dark adapted overnight, and the experiment was conducted in a dark room until the recording of behaviour began. Mice's pupils were dilated with one drop of 1% tropicamide 10 minutes before they were placed in arena, 29 x 24 x 20 cm, with dark and light chambers of the same size, connected by an aperture, 6 x 7 cm, that allowed animals to transition freely between chambers. The light chamber was illuminated by an LED array on the top of the chamber, emitting 100 lux at the arena floor. Before every test, both chambers were thoroughly cleaned with ethanol 70%. After placing a mouse in the centre of the arena, in the light chamber, camera recording was commenced, and the LED light was turned on. Each trial lasted 10 minutes for each mouse and the animals were naïve to the test (single trial per mouse). It was considered an entrance into a different chamber when three paws had crossed to that chamber. Light avoidance was measured by the percentage of time spent in the dark chamber. Data was recorded by a digital camera and analysed manually by viewing the recordings.

2.11.5.1 Light avoidance set up for experiments described in Chapter 5

No dark adaptation or pupil dilation were performed. Mice were placed in newly built arena, 45 x 39 x 33 cm, with dark and light chambers of the same size, connected by an aperture, 6 x 7 cm, that allowed animals to transition freely between chambers. The light chamber was illuminated by an LED array on the top of the chamber, emitting 300 lux at the arena floor. This set up was built by Monica Freitas.

Before every test, both chambers were thoroughly cleaned with ethanol 70%. After placing a mouse in the centre of the arena, in the light chamber close to the aperture, camera recording was commenced, and the LED light projector was turned on. Each trial lasted 10 minutes for each mouse and the animals were naïve to the test (single trial per mouse). It was considered an entrance into a different chamber when three paws had crossed to that chamber. Light avoidance was measured by the percentage of time spent in the dark chamber. Data was recorded by a digital camera and analysed semi-automatically using AnyMaze software. The point of crossing

chambers was determined by 2 blinded evaluators, but the software timed the time spent in each zone of the arena and track the movement of the mice. Tracking of movement was not always perfect and that is why it couldn't be used to determine movement between chambers, due to the pigmentation of *Foxn1*^{nu} mice, that interferes with body detection software.

2.12 Statistical analysis

All means are presented ± s.d., unless otherwise stated; N, number of animals or independent experiments performed; n, number of eyes or retinal organoids examined, where appropriate. Statistical analysis is based on at least three independent experiments, e.g. three transplantation sessions (cell differentiation, preparation, FACS and transplantation). Statistical significance was assessed using GraphPad Prism 5 software to conduct appropriate statistical tests.

Chapter 3: Characterisation of the *Aipl1*$^{-/-}$ mouse model of retinal degeneration

3.1 Introduction

Mouse models of end-stage retinal degeneration provide insight regarding phenotype and disease progression. They also serve as a platform to evaluate potential treatment strategies to several diseases that affect human vision. For the purpose of the experiments described in this thesis a model with fast photoreceptor degeneration and retinal remodeling was necessary. By using a rapid end-stage retinal degeneration model we could not only mimic the severe remodeling phenotype but also address the cytoplasmatic transfer concern. Unlike, other models of retinal degeneration where photoreceptor cell are functionless but otherwise preserved, in end-stage retinal degeneration most photoreceptor cells are absent. Therefore, by using a strain which displayed such phenotype the confounding complications in interpretation that may arise from material transfer were largely removed.

The most well-known model of end retinal degeneration is the PDE6β$^{rd1/rd1}$ (commonly known as *rd1*). This RP model was the first mammalian retinal degeneration model to be described (Pittler et al., 1993). *Rd1* mice carry a naturally occurring mutation in the phosphodiesterase beta-subunit (*Pde6b*) gene that encodes the β-subunit of the rod-specific cGMP phosphodiesterase (β-PDE), resulting in disrupted phototransduction, and leads to dead of rod photoreceptors. Rod photoreceptors lacking PDE6β start to degenerate by p8-10, with complete loss being detected by 1 month of age. In this model cone photoreceptors are genetically undamaged, and degenerate due to the lack of structural and neurotrophic support from rod photoreceptors (Carter-Dawson et al., 1978). Cone degeneration can be seen by p12, with shortening of outer segments, and progress until 3 months of age, when degeneration appears complete (Lin et al., 2009). In retinal degeneration, following photoreceptor loss, a process of gradual morphological, molecular, and functional changes involving neurons, glia and blood vessels in the retina takes place (Marc et al., 2003b). This biological rearrangement is referred to as “remodeling” and its general features are largely independent from the underlying cause of photoreceptor degeneration. These general features of remodelling of the inner retina include dendritic and axonal rearrangements, such as dendritic pruning and projection refinement (for review see Strettoi, 2015). Degeneration and remodelling progression

is well characterised for *rd1* mice (Strettoi et al., 2002) and this has been, thus far, the selected strain for the study of photoreceptor transplantation as a therapy for into end-stage retinal degeneration. Several groups have transplanted into these mice and reported rescue of visual function, either by using mouse dissociated photoreceptor cell suspension (MacLaren et al., 2006), human dissociated photoreceptor cell suspension (Barnea-Cramer et al., 2016) or retinal sheets, derived from mouse (Mandai et al., 2017a) or human pluripotent stem cells (Iraha et al., 2018).

Despite the similar phenotype, *Aipl1*$^{-/-}$ mice have been far less studied. The aryl-hydrocarbon interacting protein-like 1 (*AIPL1*) gene is specifically expressed in photoreceptor cells, both rods and cones, and pineal-gland cells. Mutations in this gene were identified in patients with Leber Congenital Amaurosis (LCA). Details regarding the exact function of the Aipl1 protein are still being investigated, however studies suggest that AIPL1 acts as a chaperone for retinal protein folding, including stabilisation of PDE (Chapple et al., 2001; Kosmaoglou et al., 2008). This strain was generated and first described in 2004 by two independent groups, that created an *Aipl1*$^{-/-}$ mice, using slightly different strategies to silence/eliminate the gene of interest, and analysed its phenotype (Dyer et al., 2004; Ramamurthy et al., 2004). Only one follow up paper was later published, describing the remodeling events in the *Aipl*$^{-/-}$ mice generated by *Ramamurthy et al*. Even with these studies it is still unclear when complete loss of photoreceptors takes place, as the publish reports are contradicting. Is also necessary further characterisation of visual function in these mice, as such assessment have, so far, been limited to ERG recordings at 8 weeks of age.

Considering the time scale of the project described in this thesis, a fast model of retinal degeneration was essential. Furthermore, the lack of studies using *Aipl*$^{-/-}$ mice added interest, as achieving rescue function in this model could provide hope to patients with LCA. Gene therapy has been shown to work for this patients (Tan et al., 2009) and clinical trial are currently ongoing, but due to the very fast degeneration the intervention window is small presenting a major therapeutic challenge. Cell therapy could provide a viable treatment for these patients yet no studies have yet been performed in order to show that this approach would be feasible for such severe cases, where the retinal synaptic circuit might be too damage or not developed properly, due to lack of photoreceptor input from such an early stage.

Therefore, here a detailed description of the remodelling events following photoreceptor degeneration, in the *Aipl1*$^{-/-}$ retina, by histological, electrophysiological and behaviour analysis, is presented. The information collected was crucial to plan and interpreted the transplantation experiments described in the following chapters. For clarity, a summary of previously reported *Aipl1*$^{-/-}$ mice's phenotype is described next.

3.1.1 *Aipl1*$^{-/-}$ mouse model

In 2004 Ramamurthy *et al.,* reported the generation of an *Aipl*$^{-/-}$, by removing exons 2 to 5 of this gene. This group showed no morphological developmental changes were found in *Aipl1*$^{-/-}$ mice before post-natal day (p) eleven, with retinal lamina developing appropriately and no identifiable difference in the thickness of the outer nuclear seen at this age when compared to an age-match wild-type. With immunohistochemistry they showed that both rod and cone photoreceptors are formed and that no difference in number of mitotic cells between p24, could be found. By p12 they identified presence of morphological abnormalities in photoreceptor cells, followed by rapid degeneration of the ONL that is reduced to a single layer by p18. They stated that by four weeks of age degeneration is complete and that both rods and cones degenerate at the same rate. They also reported presence of apoptotic cells from p9 onwards. With TEM they examined the ultrastructure of *Aipl1* $^{-/-}$ photoreceptor outer segments, reporting no differences could be found between *Aipl1* $^{-/-}$ and wild-type mice at p8, when outer segments start being formed. However, by p11, photoreceptor outer segments of *Aipl1* $^{-/-}$ mice are shorter than normal, highly disorganised, and fragmented. No a or b-wave were detected at any age analysed, with p12 being the earliest age this technique was performed. Finally, they quantified the relative amounts of retinal proteins by immunoblot analysis at p8. The immunoblotting results show levels of most of the proteins analysed (Rhodopsin, Guanylyl cyclase GC-E, Rhodopsin Kinase, Transducing and Recoverin) are similar to what is found in wild-type animals, with exception of the three PDE subunits (α, β, and γ), that were reduced by 90% in *Aipl1* $^{-/-}$ mice. Interestingly, they also show, by RT-PCR analysis, that the mRNA levels for all subunits of PDE are normal, which contrasts with the phenotype of the *rd*/*rd* mouse, where PDE-β protein is completely absent and mRNA is significantly reduced (Ramamurthy et al., 2004).

Ten years after this model was created, Singh *et al*. reported early alterations in retinal neurons in *Aip1l*$^{-/-}$ mice. They reported that by one month of age, when they describe the retinal degeneration as complete, Ribeye was undetectable in *Aip1l*$^{-/-}$ mice, despite, at p8, showing the typical horseshoe-pattern. They concluded that these findings suggested that the presynaptic terminals of the photoreceptor cells develop normally prior to degeneration. Presence of Synaptophysin, another pre-synaptic protein, was also evaluated. Positive structures showed a discontinuous distribution in the OPL of *Aipl1*$^{-/-}$ animals from early ages and was weaker when photoreceptor degeneration was complete, by one month of age.

To evaluate integrity of the post-synaptic terminals of bipolar cells, presence and localisation of mGluR6 and VGLUT1 were analysed by immunohistochemistry. The OPL of *Aip1l*$^{-/-}$ mice showed 40% reduction of mGluR6 positive structures at p8, when compared to an age-matched a wild-type retina. Between p14 and p18, when degeneration of photoreceptors has started, mGluR6 was distributed abnormally with some positive structures being found along cell bodies and some bipolar cell axons. By 1 month of age no more mGluR6 positive structures were found in *Aip1l*$^{-/-}$ retinas. In the *Aip1*$^{-/-}$ animals, at p8, VGLUT1 staining was similar to what was seen in age matched wild-type. However, a visible reduction of VGLUT1 positive structures was identifiable by p14; by p18 only very limited staining was observed and VGLUT1 was absent by one month of age. Both rod and cone bipolar cells were studied. At p14 both *Aipl1*$^{-/-}$ and wild-type animals showed similar rod bipolar cell morphology. By p18 morphological differences were identified as the reduction and retraction of dendritic arborisation from the OPL in the *Aipl1*$^{-/-}$ retina. By one month of age retinas lacking Aipl1 the morphological differences were more exuberant and a reduction in number of rod bipolar cells was seen, significantly declining further between one and five months of age. The axons in the IPL also showed alteration in morphology, as *Aipl1*$^{-/-}$ animals presented smaller axonal terminal in the IPL from p18, and those appeared as rudimentary dots, by 3 months of age. Cone bipolar cells remained comparable to a wild-type retina until 1 month of age. However, by 2 months of age, disorganisation of the dendritic arborisation in the OPL was reported. From 3 months of age the cone bipolar cell dendrites were absent and cell bodies were discontinuously arranged and a significant reduction in cone bipolar cell number was observed. This study also reports changes in the horizontal cells of *Aipl1*$^{-/-}$ animals, from p14 onwards, with

sprouting and disorganisation of axons and dendrites. No noticeable differences in amacrine and ganglion cells were reported (Singh et al., 2014a).

Similar findings regarding photoreceptor degeneration were described by Dyer *et al.* who generated *Aipl1*$^{-/-}$ mice by removing exon 1 and 2 of the gene. In this report early central-to-peripheral photoreceptor degeneration, starting at p8-12, with loss of almost all photoreceptors by 8 weeks of age was described. At p12 cone photoreceptors displayed some morphological anomalies but, preserved typical cone-like features. At 8 weeks of age quantification of photoreceptor cells, using haematoxylin and eosin morphologic staining, showed that *Aipl1*$^{-/-}$ animals have 13% ±1% of the number of cells found in an age-matched wild-type. No obvious changes in horizontal cells, possible expansion or disorganisation of bipolar cells and activation of Müller Glia cells were reported. Immunohistochemistry and quantification of cell specific markers following dissociation suggested an increase of rod bipolar and amacrine cells. No detectable a or b-waves in ERG recordings, by 8 weeks of age, were present. This study concludes that the absence of gross abnormalities in early post-natal retinas, between p2 and p8, suggests that Aipl1 is not require to cell proliferation and commitment to photoreceptor cell fate, however lack of *Aipl1* in the final stages of photoreceptor differentiation and synapse formation is lethal to photoreceptor cells (Dyer et al., 2004). No further characterisation of these mice was performed following this original report and the progression of remodeling events was never assessed. Additionally, the quantification of retinal cell types described in this publication was done following retinal dissociation, therefore cell morphology and location within the retina was not considered. These were the mice used in this thesis.

3.2 Aims

The aims of the work described in this chapter were to (1) confirm ONL degeneration ; (2) establish progression of retinal remodeling; (3) identify potential morphological features that could be used to assess transplantation outcome; (4) determine the retinal and visual function of *Aipl1*$^{-/-}$ mice at an early and a late degeneration stage; and (5) determine the best age for transplantation of photoreceptor cells, to minimise the possibility of material transfer between transplanted and host photoreceptors.

3.3 Results

In order to confirm and further characterise the phenotype previously described by Dyer *et al.* *Aipl1*$^{-/-}$ mice were subjected to behavioural and electrophysiology experiments, to assess visual and retinal function, at p18 and 3 months of age (N > 3). Eyes were then collected to study presence and morphology of retinal cells and remodeling events, by using specific cell markers (N > 3). For simplicity, morphological evaluation will be presented first, followed by the characterisation of visual function, contrary to the order of experimental execution.

3.3.1 Morphology of the Aipl1$^{-/-}$ retina

3.3.1.1 Characterisation of the outer nuclear layer

To assess the morphology and organisation of the retina of *Aipl1*$^{-/-}$ mice, eyes were collected for immunohistochemistry at p19, 1 month, 3 months and 6 months of age and compared to age-matched wild-type controls (n = 3 eyes, N = 3 eyes, per strain and time point).

Firstly, degeneration progression of cone and rod photoreceptor cells in the ONL was investigated. The presence of cone photoreceptors was evaluated using the cone specific marker, cone Arrestin. Cones were detected at all ages analysed; however, degeneration was evident. At p19, retina showed a single layer of cone photoreceptors. By 1 month of age, the Cone Arrestin positive layer was intermittent and by 3 months only a few positive cells could be identified. These cells seem to remain even by 6 months of age (Figure 23). Rod photoreceptor loss was more pronounced. Only a few Rhodopsin positive cells were identified at p19 and these were no longer detected in older animals. Moreover, abnormalities in cone and rod photoreceptor cell morphology could be appreciated at all ages analysed, with shorter/non-existent cell processes as well as loss of typical photoreceptor features, such as inner and outer segments facing the RPE.

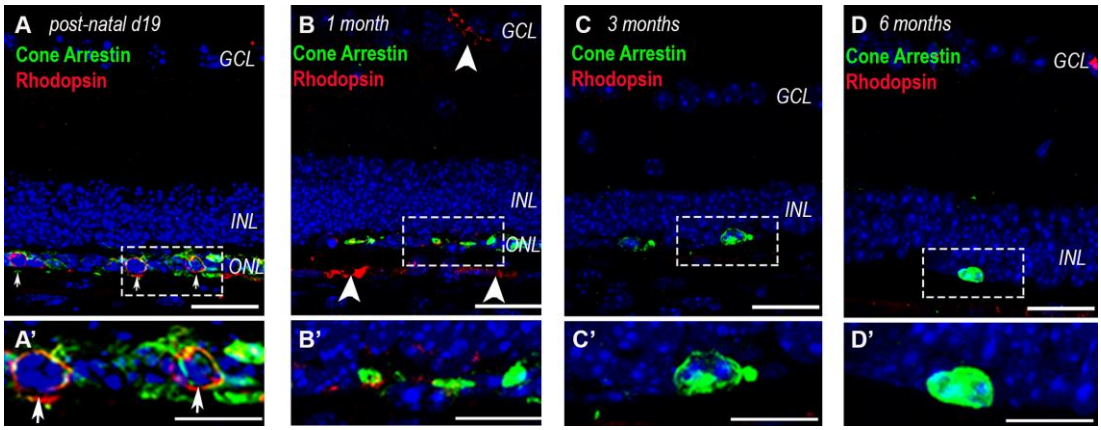

Figure 23 - Characterisation of *Aipl1*$^{-/-}$ ONL

(A-D) Representative confocal images of immunohistochemistry for photoreceptor markers, cone Arrestin and rhodopsin. **(A)** A single layer of cone Arrestin positive cells were present, with shorten or absent cell processes. Rhodopsin positive cells were rarely observed and only present at p19 (white arrows). **(B)** A similar but intermittent layer of cone photoreceptors was present at 1 month of age. **(C and D)** Rare photoreceptor cells could be identified at three and 6 months of age. These cells showed loss of cells polarity and absent cell processes. Rhodopsin antibody is raised in mouse, which explains staining seen in the retina's blood vessels at 1 month of age (white arrow heads) (scale bar = 25µm)

To establish if these remaining cone photoreceptor cells expressed Opsins, the proteins necessary to initiate the visual cycle, immunohistochemistry for M and S-opsins were performed (n = 3 eyes, N = 3 animals, per time point) (Figure 24). Wild-type eyes at p18 were stained as a positive control and showed Opsins localised to outer segments (Figure 24A and D). Only S-opsin could be co-stained with Cone Arrestin due to incompatibility of the commercially available antibodies. At p19 the cells in the ONL of *Aipl1*$^{-/-}$ retinas, showed a few Opsin positive buds, resembling underdeveloped or atrophic outer segment-like structures, which exhibited various shapes and sizes. S-opsin positive structures (Figure 24B) were observed more often than M-opsin positive structures (Figure 24E). Some cells did not present these proteins localised to a bud, having it mislocalised throughout their cell bodies. Nevertheless, it was clear that Opsin proteins were not present in all the remaining photoreceptor cells. By 3 months of age the remaining cones no longer presented outer segment-like Opsin positive structures. Both S (Figure 24C) and M-opsin (Figure 24F) proteins were present in the cell cytoplasm and membrane and not localised to a bud, unlike what was seen at p19.

Quantification was not performed, due to the misplacement of these proteins and their random distribution. These characteristics made the assessment unreliable, as it was impossible to distinguee structures that were attached to a single cell.

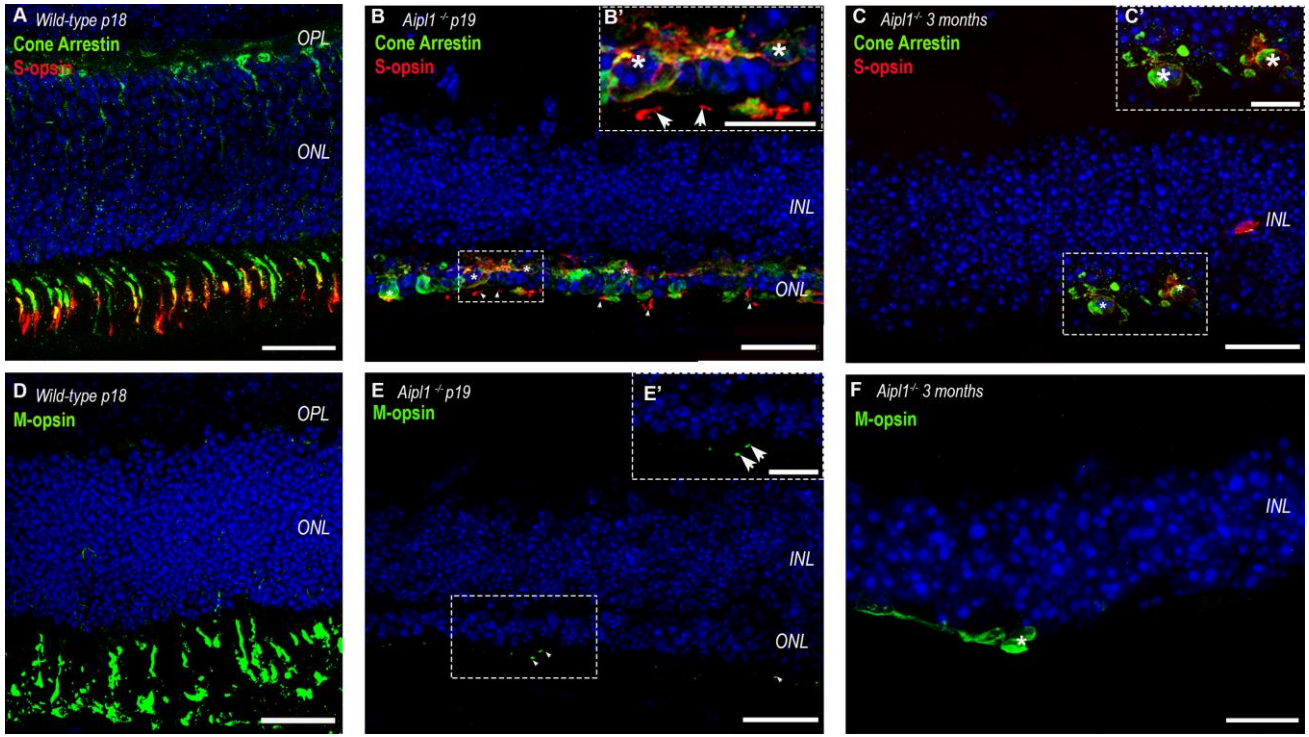

Figure 24 - Characterisation of *Aipl1*$^{-/-}$ Outer Segments

Representative confocal images of immunohistochemistry for proteins localised to outer segments of cone photoreceptor cells, S-opsin and M-opsin. **(A)** Wild-type retina at p18 shows Cone Arrestin localised to the synaptic pedicle and outer segment region. S-opsin cones show presence of protein localised to the OS. **(B)** Cone Arrestin and S-opsin protein can be identified in a p18 *Aipl1*$^{-/-}$ retina. The S-opsin protein is localised in the cell body (white asterisks) or in buds of different shape and size (white arrows). **(C)** At 3 months of age, no S-opsin positive buds were identified, with both Cone Arrestin and S-opsin being present in the cell cytoplasm and membrane (white asterisk) **(D)** Wild-type retina at p18 shows M-opsin localised to the OS. **(E)** M-opsin buds were seen in *Aipl1*$^{-/-}$ at p19 (white arrows) **(F)** By 3 months of age M-opsin was present in the cell body (white asterisk). (Scale bar 25µm, A-E; 12.5µm B, C', E'; 10µm, F)

Furthermore, to confirm the presence of atrophic/underdeveloped outer segments, Peripherin2 immunohistochemistry was performed (n = 3 eyes, N = 3 animals) (Figure 25). This marker could not be used in conjunction with another photoreceptor marker, due to incompatibility of the antibodies. For this reason, only p19 retinas were examined for the presence of this outer segments' protein. Outer segment-like structures could be identified in some of the cells that compose the remaining ONL. These structures were much shorter than what was seen in WT retinas (Figure 25A), confirming that *Aipl1*$^{-/-}$ outer segments were either underdeveloped or degenerated by this age (Figure 25B). Despite presence of Peripherin2 positive structures, these did not appear to be in contact with RPE cells, corroborating the loss typical photoreceptor cell polarity (Figure 23).

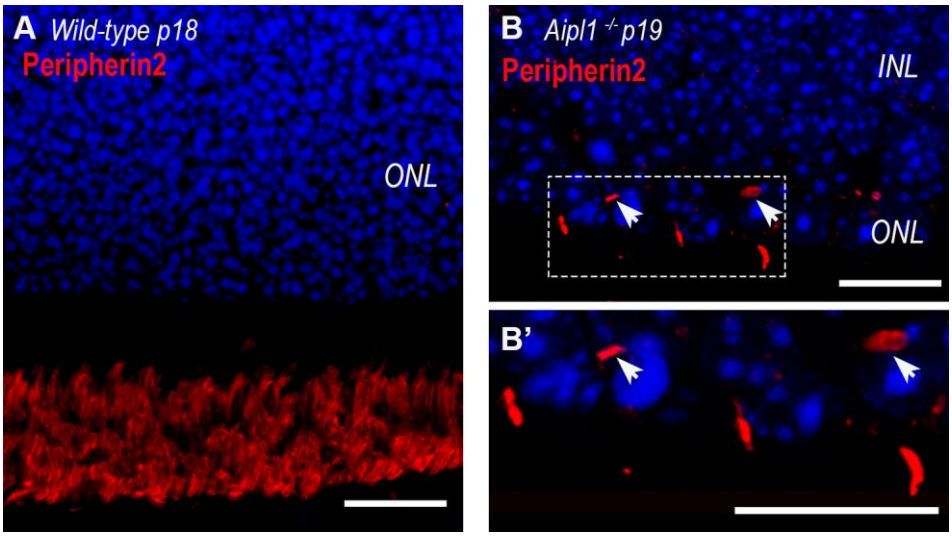

Figure 25 - - Presence of Peripherin2 in *Aipl1*$^{-/-}$ outer segments

Representative confocal images of immunohistochemistry for the outer segment protein, Peripherin2. **(A)** The wild-type control at p18 shows that Peripherin2 is exclusively present in the outer segment region. **(B-B')** At p19, the *Aipl1*$^{-/-}$ retina shows small buds positive for Peripherin2. These are shorter and vary in orientation, some facing away from RPE (white arrows). (Scale bar 25 µm, A; 12.5µm, B-B').

Next, in order to assess if some of the surviving cone photoreceptors were still connected or had the structures necessary to connect with the interneurons of the INL, immunohistochemistry staining for Ribeye was performed. Ribeye is a protein expressed in the pre-synaptic region of synaptic ribbons. This staining was done in junction with cone Arrestin to identify the remaining cone photoreceptor cells (Figure 26).

Post-natal day 19 *Aipl1*$^{-/-}$ retina showed a similar distribution of Ribeye to p18 wild-type retina. Since there were less photoreceptors cells, was not surprising that there were less Ribeye positive structures. Nevertheless, these dotted structures were localised to the correct layer and appear to be present in all the surviving cells (Figure 26A, A', D, D'). This dotted pattern differs from the typical horse-show shape Ribeye positive structures seen in wild-type retina (Figure 26 A'', D'') This difference was seen is all ages analysed. At one month of age the dotted Ribeye pattern was still present but further reduced in spread and intensity; fewer photoreceptor cells were present and not all of them appeared to contain Ribeye-positive structures (Figure 26E, E'). In contrast, the 1 month old wild-type retina seemed to have a stronger signal with a denser distribution of this synaptic protein (Figure 26B, B'). By 3 months of age the *Aipl1*$^{-/-}$ retina, unlike from the wild-type retina (Figure 26C, C'), was mostly depleted of photoreceptor cells and the rare surviving cone photoreceptors did not show clear Ribeye staining (Figure 26F-G'). Is relevant to mention that the anti-Ribeye antibody is raised in mouse, therefore staining strongly the retina's blood vessels and occasional background by attaching to unspecific sites. This makes the interpretation of the presence of this protein at 3 months of age problematic because of the unusual morphology, loss of cell polarity and mislocalisation of proteins in the few remaining photoreceptor cells.

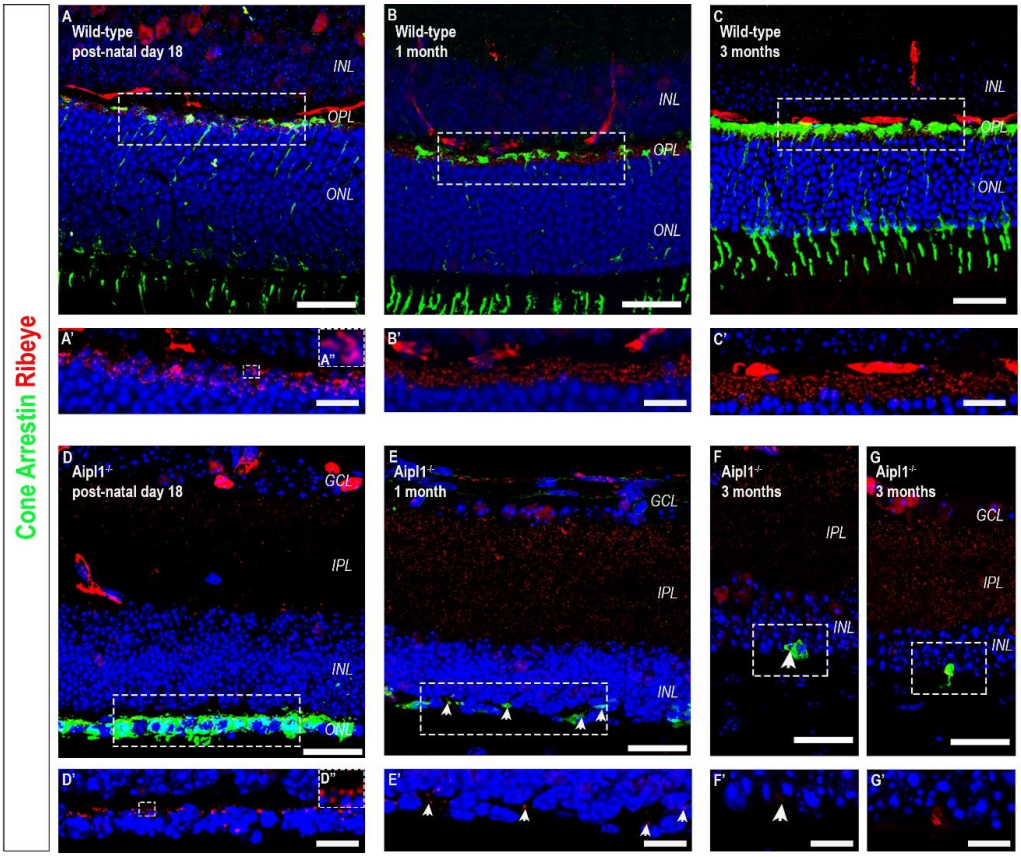

Figure 26 – Expression of Ribeye protein in *Aipl1*$^{-/-}$ OPL

Immunohistochemistry staining for Ribeye in cone photoreceptors in wild-type and *Aipl1*$^{-/-}$. **(A-C)** In wild-type retinas, Ribeye staining appears in a horse-shoe shape pattern (**A''**) in the OPL. **(D, D')** In *Aipl1*$^{-/-}$ retinas, at p18, the intensity of the Ribeye positive dots was comparable to age-matched wild-type retina, but no horse-shoe shaped pattern could be identified **(D''). (E, E')** By 1 month of age some Ribeye positive dots were still present in areas where cone photoreceptors were present (white arrows). **(F-G')** At 3 months of age, some of the rare cones still showed Ribeye positive dots (white arrows). **(G, G')** Most remaining photoreceptor cells did not show positive Ribeye dots **(F, F')**. The anti-Ribeye antibody is raised in mouse which explains the staining of retinal blood vessels by the secondary antibody used. This antibody also bound to some of the cells' nuclei. This stain can be disregarded. (Scale bars: 25µm, A- G; 12.5um, A'-G')

Finally, vesicular glutamate transporter1 (VGlut1), present in the vesicles that transport glutamate to the photoreceptor's synaptic terminal, was examined in combination with pre-synaptic marker Synaptophysin. Presence of VGLut1 and synaptophysin in the OPL of the wild-type retinas at p18 and at 3 months of age was detected (Figure 27A, B). Since these antibodies did not conflict with Recoverin, this marker was used to identify the remaining photoreceptor cells in the *Aipl1*$^{-/-}$ retinas. *Aipl1*$^{-/-}$ retinas showed presence and co-localisation of Synaptophysin and VGLut, at p18 in some areas where photoreceptor cells remained (Figure 27C). By 3 months of age no VGlut or Synaptophysin positive structures were identified in majority of the retina, where no photoreceptor cells were present (Figure 27D). However, in the few areas where there were surviving photoreceptor cells positive for both proteins were identified (Figure 27E).

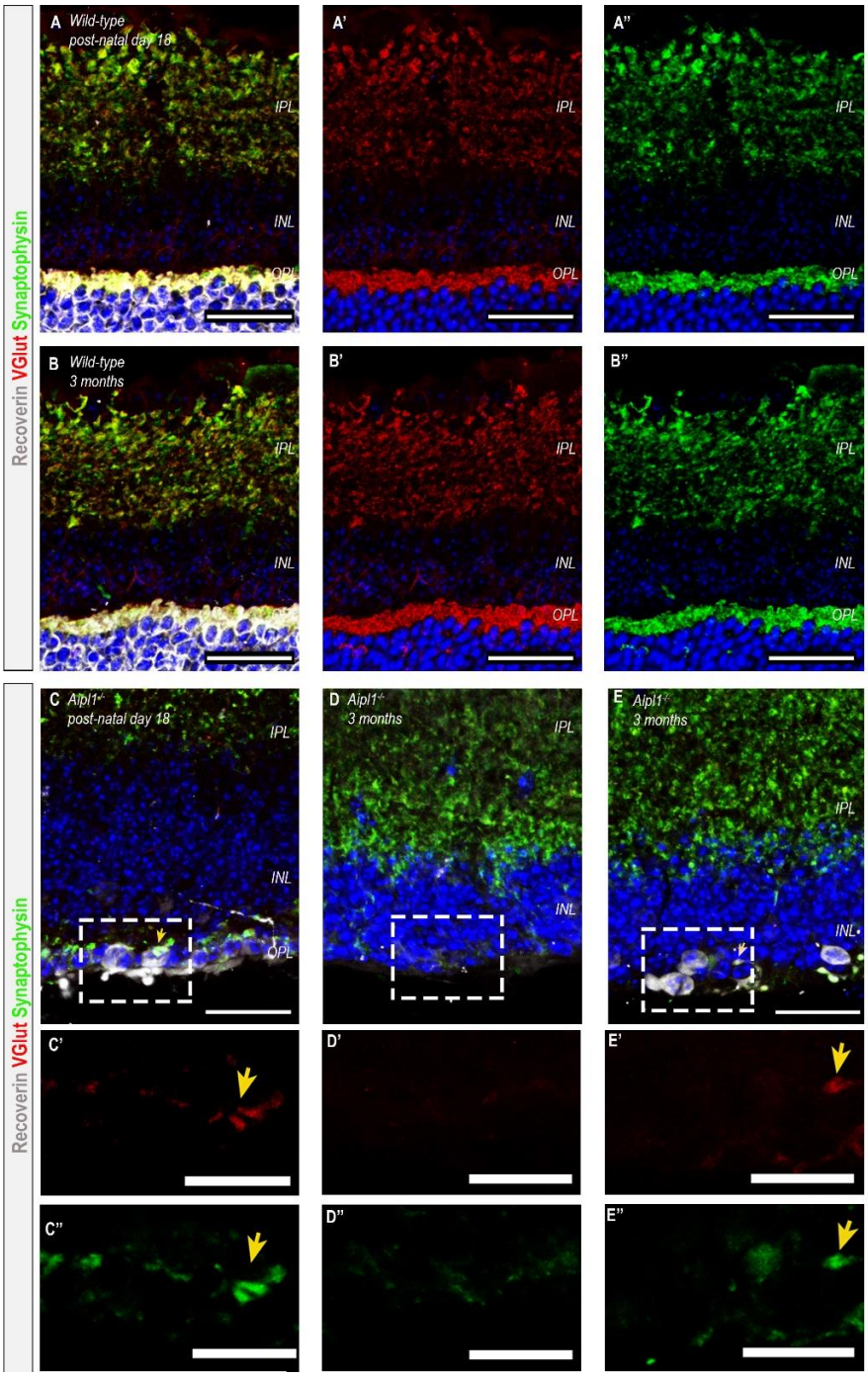

Figure 27 - Characterisation of VGlut1 and Synaptophysin in the OPL of *Aipl1*$^{-/-}$ retina

Immunohistochemistry for photoreceptor specific marker Recoverin (white), VGlut1, (red), and pre-synaptic protein, Synaptophysin (green). **(A-B'')** At p18 (A) and 3 months (B), wild-type retinas show strong staining for VGlut1 (A', B') and Synaptophysin (A''. B'') in the OPL and IPL **(C)** *Aipl1*$^{-/-}$ retinas at p18 displayed some positive structures (yellow arrow) for both VGlut1 (C') and Synaptophysin (C''), the staining of the latter being more intense. **(D)** At 3 months of age, majority of the *Aipl1*$^{-/-}$ retina lacked Recoverin positive photoreceptor cells and showed absence of VGlut1 (D') and Synaptophysin (D''). **(E)** In areas where surviving photoreceptor cells could be found by 3 months of age, *Aipl1*$^{-/-}$ retinas still displayed rare positive VGlut1 and Synaptophysin structures (yellow arrow) (E' and E''). (Scale bar 25µm).

In summary, *Aipl1*$^{-/-}$ mice showed rapid photoreceptor degeneration. Faster degeneration of rod photoreceptors was evident, with these cells being rare even at the earliest time point analysed, p19. At this stage, the ONL was mostly composed of a single layer of disorganised cone photoreceptor cells, which did not typical photoreceptor morphology and appeared to have lost cell polarity. By 3 months of age very few cone photoreceptor cells remained, and these displayed severe morphological abnormalities. At this age, the degeneration appeared to reach a plateau as no further obvious changes were seen in 6 months *Aipl1*$^{-/-}$ retinas.

3.3.1.2 Characterisation of the inner nuclear layer and ganglion cell layer

Remodelling of the INL was evaluated by assessing the number, morphology and organisation of rod bipolar, amacrine and horizontal cells.

In a healthy retina, rod bipolar cells are localised at the base (outer aspect) of the INL, where they connect to rod photoreceptor cells in the OPL. Immunohistochemistry for PKC-α was used to assess the morphology of rod bipolar cells. The few changes that could be identified in the *Aipl1*-deficient mice at p18 were at the OPL level, where the bipolar cells' post-synaptic terminals appeared less dense and more disorganised (Figure 28D, asterisks) when comparing with an age-matched wild-type (Figure 28A). At 1 month of age the changes in the OPL were more evident, with atrophy of the post-synaptic terminals' arborisation, as well as reduction of the arborisation of its pre-synaptic terminals in the IPL (Figure 28E), when compared to an aged-matched wild-type retina or a younger *Aipl1*$^{-/-}$(Figure 28B and D, respectively). Reduction in arborisation and disorganisation of the synaptic terminals at the OPL and IPL was more evident by 3 months of age, with the post-synaptic pedicle terminals being absent in the OPL. The cell bodies of some cells were displaced, localising far within the INL, near the IPL (Figure 28F).

Quantification of the total number of PKC-α positive rod bipolar cells (Figure 28G) and displaced rod bipolar cells (Figure 28H), defined as cells that were not within the first two nuclei layers in the INL, was performed as described in the methods section 3.6.2 (N≥3 animals). No difference was found in total number of rod bipolar cells at any of the time points analysed (2way ANOVA; n≥3 eyes for wild-type and n≥5 eyes for *Aipl1*$^{-/-}$ animals). However, the number of displaced PKC-α positive cells showed a significant increase in *Aipl1*$^{-/-}$ retinas compared to *wild-type* retinas at 1 month of age (**p<0.01, 2-way ANOVA; 0.45 ± 0.25 vs 3.02 ± 1.25*, wild-type*, n=3 eyes vs *Aipl1*$^{-/-}$, n=6 eyes) and 3 months of age (***p<0.001, 2-way ANOVA; 0.90 ± 0.35 vs 3.86 ± 1.57, *wild-type* vs *Aipl1*$^{-/-,}$ n=5 eyes). The number of displaced rod bipolar cells

increased with age, within the *Aipl1*$^{-/-}$ strain, with retinas at p19 being significantly different from *Aipl1*$^{-/-}$ retinas at 1 months and 3 months of age (***p<0.001, 2-way ANOVA). A slight increase was seen in *wild-type* animals; however, these differences were not statistically significant.

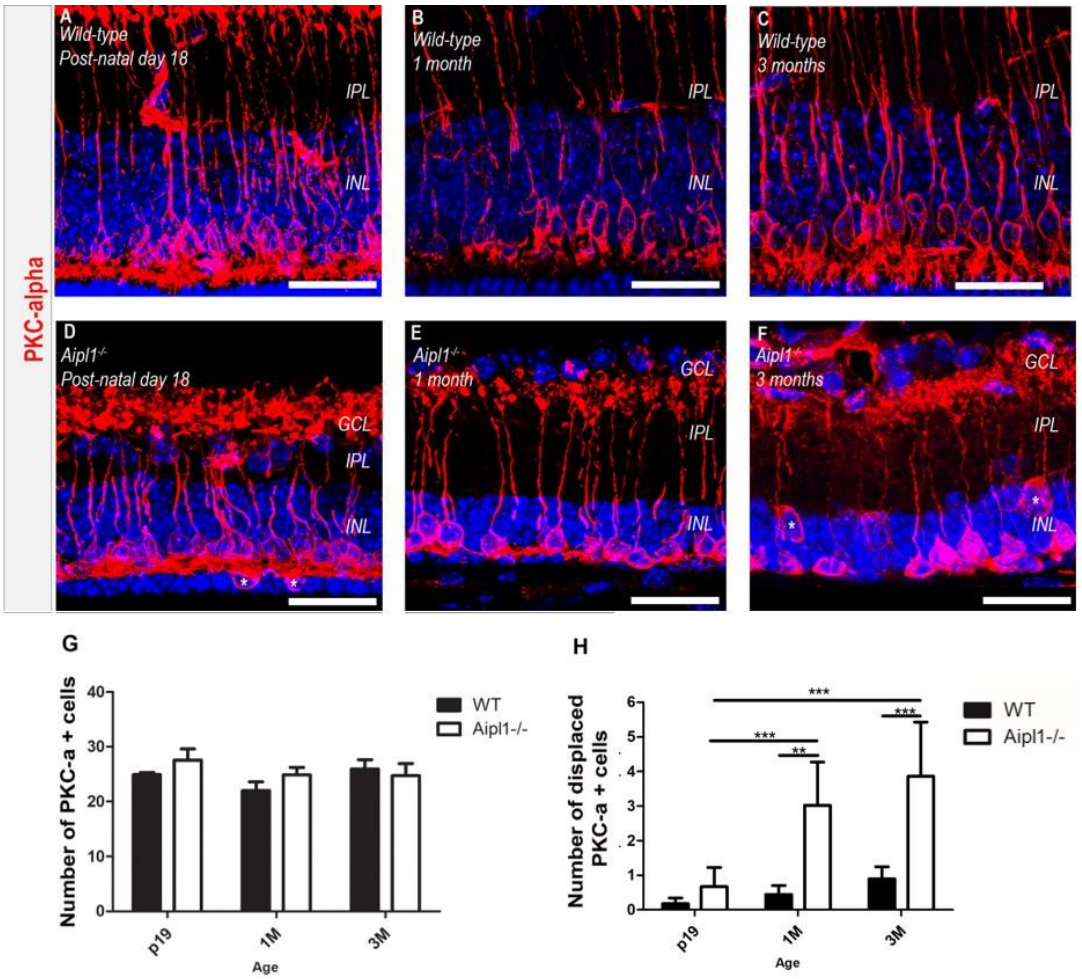

Figure 28 – Remodelling of the INL: rod bipolar cells in the *Aipl1*$^{-/-}$ retina

Retinas were stained for PKC-α, a rod bipolar cell marker. **(A-C)** *Wild-type* retinas showed typical distribution of rod bipolar cells with their cell bodies close to the OPL, where they extend dendrites to connect with rod photoreceptor cells. **(D)** *Aipl1*$^{-/-}$ retinas show that, at p18, rod bipolar cells have similar organisation and morphology to the *wild-type* retinas, except at the post-synaptic terminal in the OPL, where the dendrites' ramifications appear to be less defined. Some bipolar cells can be seen to be displaced and invading the ONL (white stars). **(E)** By 1 month of age, PKC-α positive cells are deeper within the INL. Dendritic arborisation appeared less dense. **(F)** At 3 months of age, some bipolar cells are placed far within the INL (white arrows) and post-synaptic pedicles in the OPL are absent. The anti-PKC-α antibody, in red, is raised in mouse therefore secondary antibody bound to the host IgGs. **(G)** No difference in total number of cells per field of view, with six fields analysed per retina, was detected in any of the investigated time points (2way ANOVA). **(H)** Number of PKC-α positive cells that were not within the first two layers of nuclei in the INL were quantified using the same fields of view as in B. At p19 no significant difference could be found between *wild-type* and an *Aipl1*$^{-/-}$ retina (2way ANOVA; n=3, N=3, *for wild-type*; n=6, N=6 for *Aipl1*$^{-/-}$). By 1 month of age a significant difference was found between this strain and age-matched *wild-type* (** p<0.01, 2way ANOVA; n=3, N=3, for *wild-type*; n=6, N=6, for Aipl1$^{-/-}$). A bigger difference was detected at 3 months of age (*** p<0.001, 2-way ANOVA; n=5, N=4, for *wild-type*; n=5, N=5, for Aipl1$^{-/-}$). The number of displaced cells increased in *Aipl1*$^{-/-}$ retinas between p19 and 1(*** p<0.001, 2-way ANOVA) and 3 months of age (*** p<0.001, 2-way ANOVA). No significant differences were identified between 1 and 3 months of age. (scale bars 25µm).

Different sub-types of bipolar cells were not analysing due to lack of adequate/specific antibodies. Since cone photoreceptors survive longer than rod photoreceptors, is possible that cone-bipolar cells undergo different remodelling events, or that similar remodelling events occur but at later stages.

Other classes of interneurons were also evaluated by immunohistochemistry staining (n=3 eyes, N=3 animals). Horizontal cells, that laterally interconnecting neurons, were identified by their calcium-binding protein, Calbindin and typical morphological features. Calbindin positive cells appear to have shorter cell processes with a less dense synaptic network in the *Aipl1*$^{-/-}$ OPL, at both ages analysed (Figure 29B, D), when compared to an aged-matched wild-type retina (Figure 29A, C). At 3 months of age the horizontal cells were flatten, with wrong orientation of their cell body, which appears to be in the same level as its cell processes in the OPL. High magnification images highlight this difference in morphology (Figure 29A'-D'). Quantification of horizontal cells was performed as described (see section 2.9.2). A small, but significant, reduction in number of cells was identified at 3 months of age, when comparing *Aipl1*$^{-/-}$ retinas with *wild-type* retinas (*p<0.05, 2way ANOVA; 7.4 ± 0.60 vs 5.1 ± 0.35, *wild-type* vs *Aipl1*$^{-/-}$, n = 3 eyes, n = 3 animals) (Figure 29E). No difference was identified between strains in p18 retinas (2way ANOVA; 9.0 ± 1.04 vs 8.1 ± 1.25, *wild-type* vs *Aipl1*$^{-/-}$, n = 3 eyes, N = 3 animals). With age, a decrease in number of horizontal cells was detected in *Aipl1*$^{-/-}$ retinas (**p<0.001, 2way ANOVA; *Aipl1*$^{-/-}$, p18 vs 3 months).

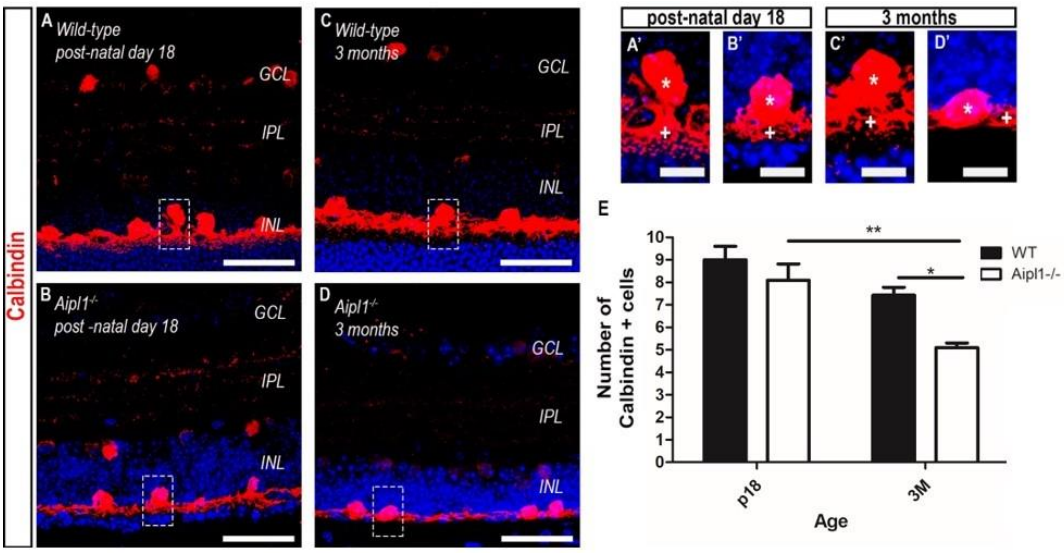

Figure 29 – Characterisation of the INL: horizontal cells in the *Aipl1*$^{-/-}$ retina

Immunohistochemistry for Calbindin, a marker for horizontal cells. **(A, C)** *Wild-type* retinas at p18 and 3 months of age (top panel) showed an even distribution of horizontal cells with their cell bodies within the INL and extending processes to the OPL, where they connect with the photoreceptors, forming a dense synaptic network. **(B)** *Aipl1*$^{-/-}$ retinas show that at p19 horizontal cells have similar organisation and morphology to the WT retinas, but with less ramification of its processes in the OPL. **(D)** At 3 months of age *Aipl1*$^{-/-}$ horizontal cells lose their characteristic orientation and retract their dendrites. **(A', B', D')** Characteristic morphology of horizontal cells is present in wild-type retinas, A' and C', and at p18 *Aipl1*$^{-/-}$ retinas, B', with the cell body (white asterisk) within INL, extending processes (white +) into the OPL. **(C')** Horizontal cells in 3 months old *Aipl1*$^{-/-}$ retinas have its cell body (white asterisk) and processes (white +) aligned, showing loss of orientation. **(B)** Quantification of calbindin positive cells per field of view. At p18 no significant difference could be found between *Aipl1*$^{-/-}$ and *wild-type* retinas (n=3 eyes, N=3 animals, per strain; 2-way ANOVA). By three months of age a significant difference was found between strains (*p<0.05, 2way ANOVA) and younger *Aipl1*$^{-/-}$ animals. (**p<0.001, 2way ANOVA). (scale bar 25µm, A-D; 6µm, A'-D')

A homologous calcium-binding protein to calbindin, calretinin, was used as a marker for amacrine cells. Staining for the neuronal protein HuC/D was used to identify ganglion cells (this antibody also weakly stained some amacrine cells in the INL), at p19 and 3 months of age (n = 3 eyes; N = 3 animals) (Figure 30). The *Aipl1*$^{-/-}$ retinas showed differences in the IPL, demonstrated by the calretinin positive cell processes. In *wild-type* retinas, these processes showed three clearly organised layers forming the synaptic circuit between INL and GCL, at both ages evaluated (Figure 30A, B). In contrast, *Aipl1*$^{-/-}$ retinas displayed a disorganised synaptic network. At p18, *Aipl1*$^{-/-}$ retinas displayed resemblance to three layer of cell process seen in *wild-type* animals, however by 3 months of age most of this organisation was lost (Figure 30C, D). There was no evidence of retraction of these processes, but rather an unsystematic growth/rearrangement. No obvious morphological differences in the HuC/D ganglion cells, between strains were identified by immunohistochemistry analysis (Figure 30). Upon quantification of calretinin positive cells within the INL (see methods, 2.9.2)., a significant reduction in number of amacrine cells was detected at both ages analysed, when compared with age-matched *wild-type* controls (***p<0.001, 2way ANOVA; 31.7 ± 1.4 vs 9.1 ± 1.3 at p18; 28.6 ± 2.5 vs 12.9 ± 4.00 at 3 months of age, *wild-type* vs *Aipl1*$^{-/-}$, n = 3 eyes, N = 3 animals).(Figure 30E). The quantification showed an increase in number of amacrine cells with age in *Aipl1*$^{-/-}$ retinas. However, the standard deviation seen in this strain at 3 months of age is substantial, and it is hard to envisage an increase in neuronal counts over time, suggesting that this is most likely an artefact with no true scientific value. It is known that the remodelling process can occur at slightly different rates between animals, explaining the bigger standard deviation seen.

The HuC/D positive cells in the GCL did not show any obvious morphological differences between strains and ages (Figure 30A-D). HuC/D antibody is raised in mouse consequently, the secondary antibody also highlighted the blood vessels. It also appeared to bind to cells in the INL. Some of those co-localised with calretinin positive cells, but majority did not. The morphology and size of these cells suggest that this antibody is binding something present in a few of the interneurons of the INL, but the exact subtype was not identified. Only the much stronger ganglion cell signal in the GCL was used for further quantification (methods, 2.9.2). No significant differences in number of HuC/D positive ganglion cells was identified between strains, at both ages analysed were found (2way ANOVA; 27.37 ± 0.8 vs 32.5 ± 3.0 p18; 31.8 ± 3.5 vs 29.5 ± 4.9 at 3 months of age, *wild-type* vs *Aipl1*$^{-/-}$, n = 3 eyes, N = 3 animals) (Figure 30F).

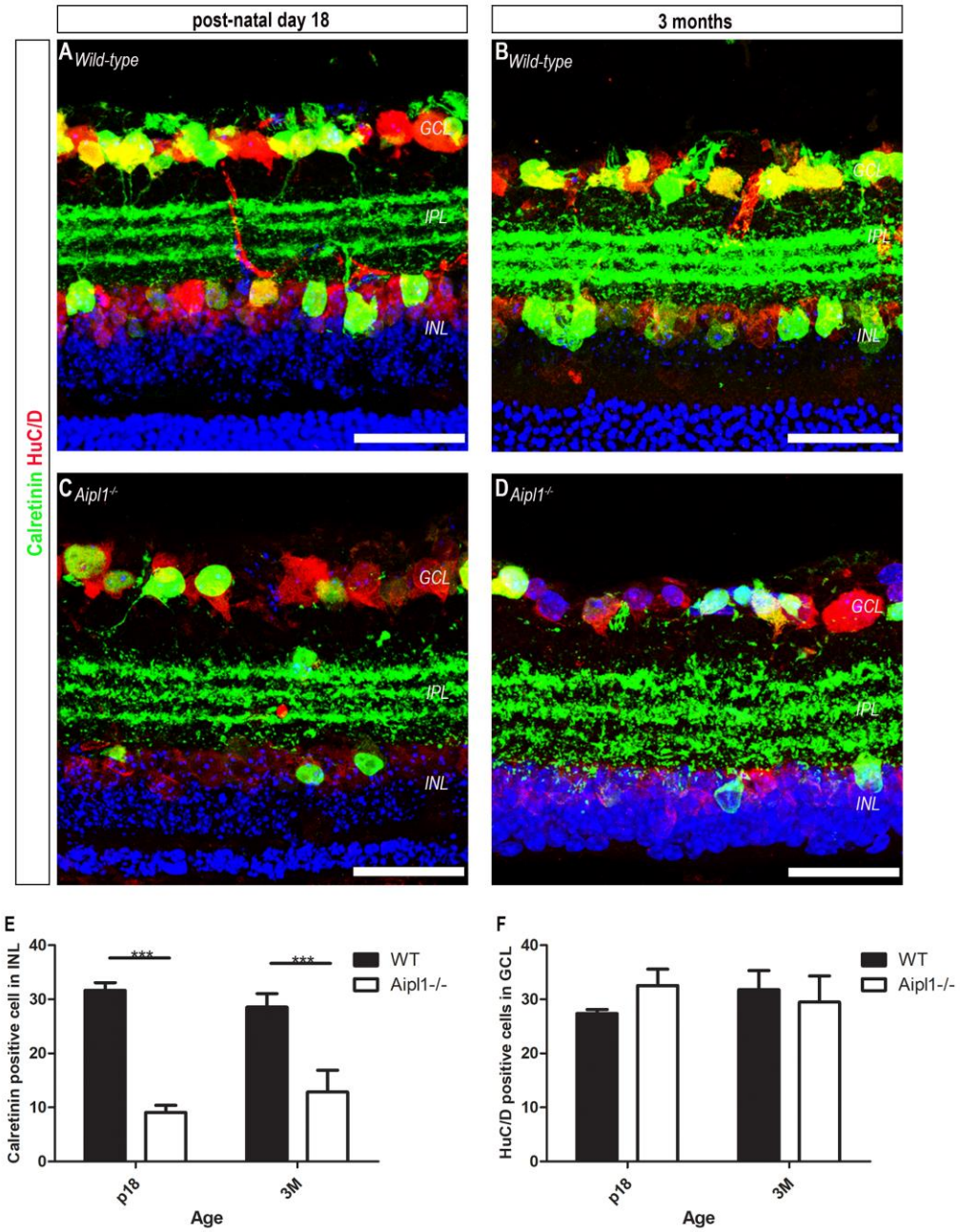

Figure 30 - Characterisation of the INL and GCL: amacrine and ganglion cells in the *Aipl1*$^{-/-}$ retina

Immunohistochemistry for calretinin (green), a marker for amacrine cells, and HuC/D (red), a marker for ganglion cells and quantification. **(A-B)** Wild-type retinas at p18 and 3 months of age showed even distribution of amacrine and ganglion cells. The IPL of wild-type retinas showed three organised layers of calretinin positive processes. **(C-D)** Amacrine cells appeared fewer, smaller, and less intense stained for calretinin in the *Aipl1*$^{-/-}$ retinas. HuC/D strongly stained cells in the GCL, these being ganglion cells, that showed no obvious differences between strains at both ages analysed. **(C)** A level of organisation of IPL similar to *wild-type* could be seen in *Aipl1*$^{-/-}$ retinas at p18. **(D)** By 3 months of age IPL showed disorganisation of calretinin positive processes. **(E)** Quantification of calretinin positive cells in the INL. A significant difference could be found between *Aipl1*$^{-/-}$ and *wild-type* retinas (n=3 eyes, N=3 animals; ***p<0.001; 2way ANOVA). **(F)** Quantification of HuC/D positive cells in GCL. No significant differences could be found between strains at the ages analysed (n=3, N=3; 2way ANOVA). (scale bar 25µm, A-D)

Finally, to evaluate if the remodelling events led to the formation of glial scarring, analysis of immunohistochemistry for glial fibrillary acidic protein (GFAP) was performed (n = 3 eyes, N = 3 animals). In *wild-type* retinas no GFAP positive Müller glia was observed and only positive astrocytes were present in the GCL (Figure 31A, B). In *Aipl1*$^{-/-}$ animals, retinas showed thin, GFAP positive Müller glia processes extended from the GCL towards the ONL (Figure 31C). By 3 months of age these processes appeared thicker and more abundant than those seen at early age (Figure 31D). However, no clear glial scarring was detected.

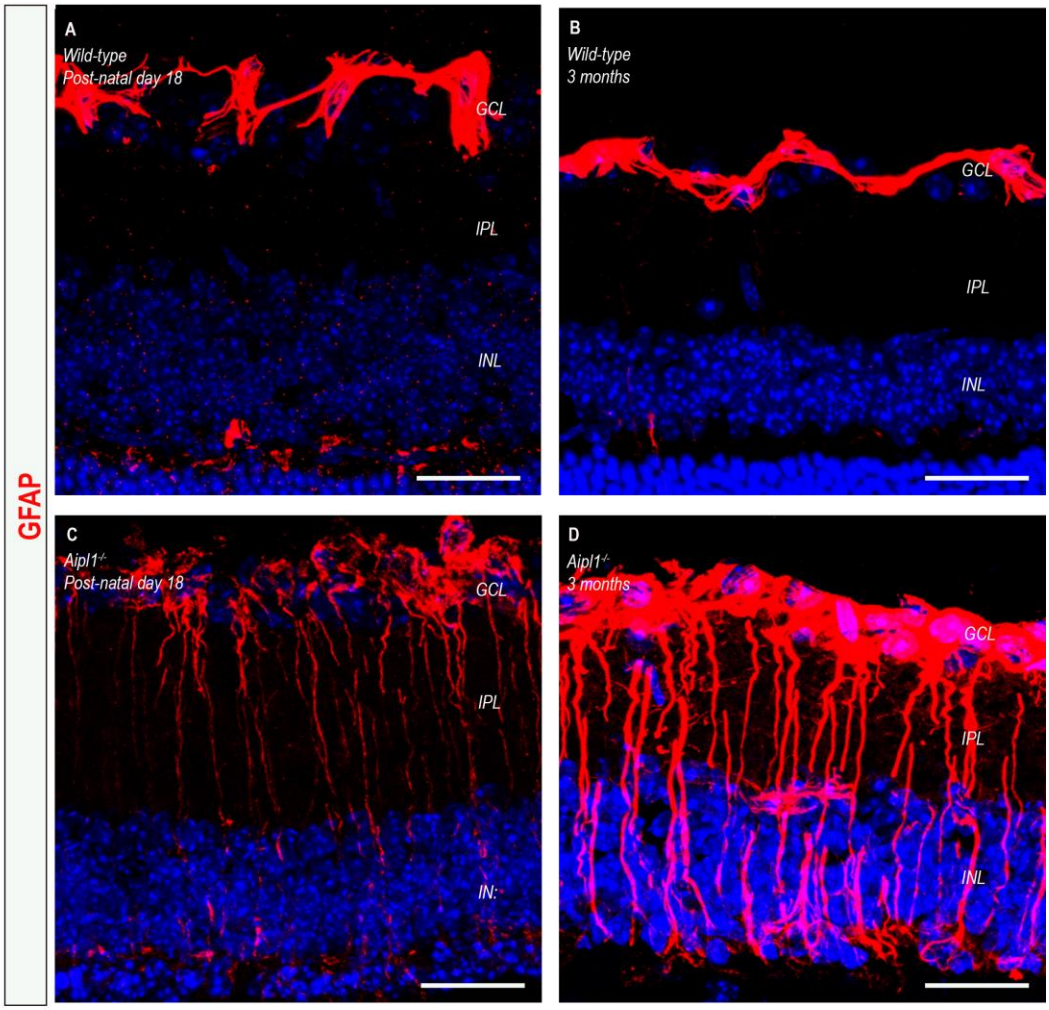

Figure 31 - Activated Müller glia cells in the *Aipl1*$^{-/-}$ retina

Immunohistochemistry for GFAP, marker for activated Müller glia cells and astrocytes. **(A and B)** In wild-type retinae, GFAP staining was restricted to astrocytes in the GCL. **(C)** In *Aipl1*$^{-/-}$ retinae, at p18, numerous GFAP positive Müller cell processes extending into the ONL were observed. **(D)** By 3 months of age increased GFAP expression in Müller glia processes was visible in the *Aipl1*$^{-/-}$ retinae. No identifiable gliotic scar was present at any of the ages analysed. (scale bar 25µm, A-D)

In summary, the INL of *Aipl1*$^{-/-}$ retinas display typical remodelling from an early age. No reduction in number of rod bipolar cells was detected. Nevertheless, there was evidence that rod bipolar cells suffered remodelling, with a significant number of rod bipolar cells displaced at 1 and 3 months of age. The number of displaced cells as well as the reduction of cell dendrites increased with age, as expected for remodelling events. A significant reduction of horizontal cells at 3 months of age, when compared to an age-matched *wild-type* control, was found. By 3 months of age, the morphology of horizontal cells was altered, showing atypical orientation. Calretinin was used to identify amacrine cells that were significantly fewer than *wild-type* controls at both ages analysed. Differences in the processes of amacrine cells were evident in the OPL at 3 months of age, with loss of organisation of synaptic layers. No differences were identified in total number of ganglion cells. Activation of GFAP in Müller cells was visible since p18 and increased with age, in *Aipl1*$^{-/-}$ animals.

3.3.1.3 Characterisation of post-synaptic proteins in the outer plexiform layer

To assess if the interneuron cells still presented post-synaptic proteins, essential for the synaptic connectivity with the photoreceptor cells, immunohistochemistry for PSD95 (Figure 32) and mGLuR6 (Figure 33) was performed (n=3 eyes, N=3 animals, per time point).

Wild-type retinas showed a dense PSD95 horse-shoe pattern at all ages analysed (Figure 32A - B'). PSD95 protein could not be detected in the *Aipl1*$^{-/-}$ retina at any stage. Even at p18, when a layer of cone photoreceptors was present and the dendritic morphology of rod bipolar cells was still normal, no PSD95 was observed (Figure 32C-D'). This protein could not be analysed in combination with a pre-synaptic marker or a bipolar-cell marker, due to antibody incompatibility.

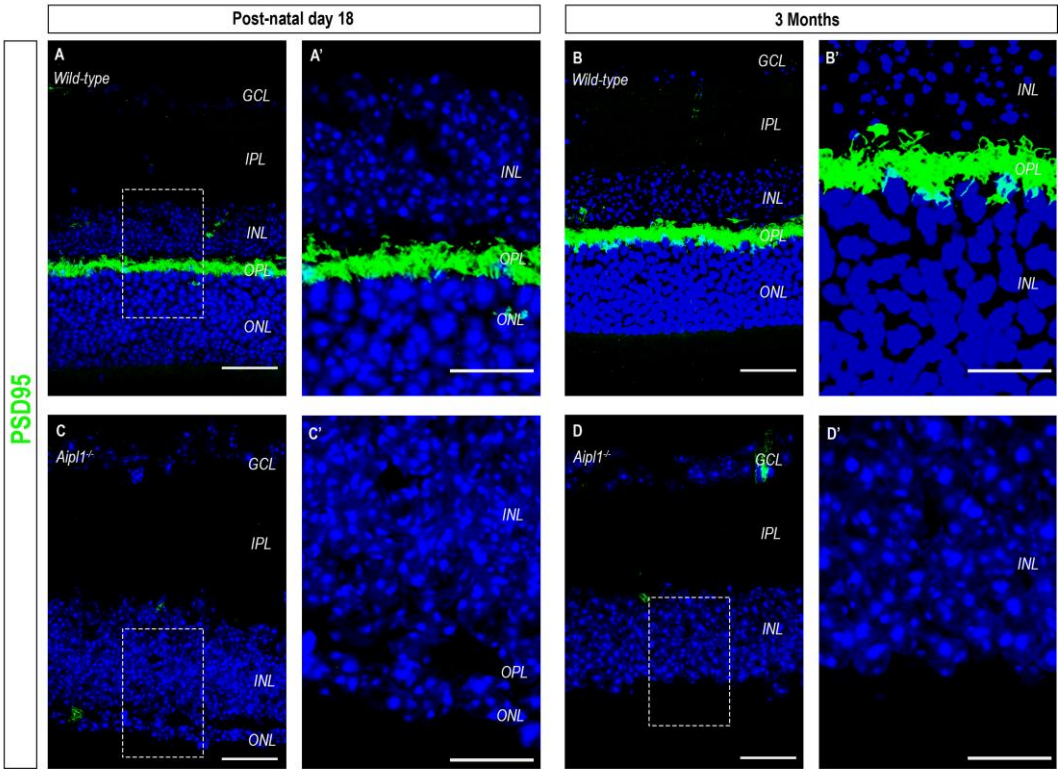

Figure 32 – Characterisation of post-synaptic marker PSD95 in the OPL of *Aipl1*$^{-/-}$ retina

(A-B) Wild-type retinas show strong staining for PSD95 in the OPL (Scale bar 12.5 µm). **(A' and B')** The shoe-horse-shoe pattern can be identified in the wild-type OPL. **(C - D')** No positive structures were identified in the OPL of *Aipl1*$^{-/-}$ retina at p18 and 3 months of age. (Scale bars: 12.5µm, A, B, C, D, 6µm, A', B', C', D').

Presence of the most abundant post-synaptic marker in the retina, mGluR6, was assessed. Since the *Aipl1*$^{-/-}$ retina does not always have a clear OPL due to the lack of ONL, mGluR6 and PKC-α were combined to provide a structural reference to where the post-synaptic protein should be seen, as mGluR6 should be present in the dendrites of bipolar cells. GluR6 showed a dotted pattern within the pedicles of the rod bipolar cells in *wild-type* retinas (Figure 33 A- B'). At p18 *Aipl1*$^{-/-}$ retinas did not show a clear mGluR6 pattern (Figure 33C, C') with a few positive structures (white asterisks) present (Figure 33C'), but not within the processes of rod bipolar-cells. As mGluR6 is also present in cone bipolar cells and the signal was in the right location, it is likely that the staining identified post-synaptic protein within cone bipolar cells. No positive mGluR6 structures were identified in *Aipl1*$^{-/-}$ by 3 months of age (Figure 33D, D').

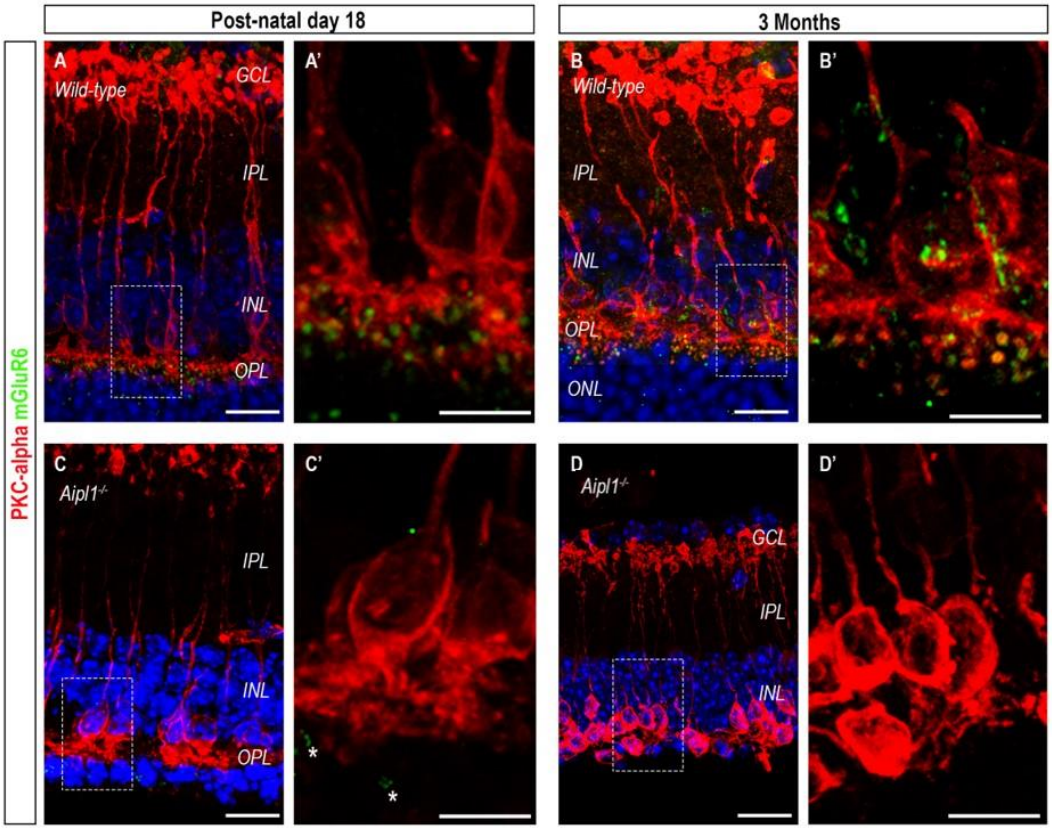

Figure 33 - Characterisation of post-synaptic marker mGluR6 in the OPL of *Aipl1*$^{-/-}$ retina

Immunohistochemistry for post-synaptic protein mGluR6, and PKC-α, marking rod bipolar cells. **(A-B)** Wild-type retinas show strong staining for mGluR6 in the OPL. **(A', B')** Presence of dotted pattern of mGluR6 positive structures (green) contained within the post-synaptic processes of PKC-α positive cells, rod-bipolar cells (red). **(C, C')** Few positive structures were identified in the OPL of at p18. **(D, D')** No mGluR6 positive structures were identified at 3 months of age in the *Aipl1*$^{-/-}$ retina. (Scale 12.5µm (A-D) and 6µm (A'-D')).

In summary, post-synaptic protein PSD95 is not identifiable in *Aipl1*$^{-/-}$ retinas from early stages. Presence of mGluR6 protein was perceptible in some areas of p18 *Aipl1*$^{-/-}$ but absent by 3 months of age.

3.3.2 Visual function of the *Aipl1*$^{-/-}$ mice

To establish retinal function, electrophysiology techniques, electroretinography (ERG) and Multielectrode array (MEA), were performed. In order to assess visual function behaviour tests such as optomotor, LOOM test and light avoidance assessments were completed (see section 3.8 for methods and a more detailed description of all techniques used to assess function). MEA records focal changes in retinal explants, therefore this technique was performed last. For simplicity, electrophysiology data will be presented first, followed by the behavioural data, which does not represent the real order in which experiments were performed. Some of the mice used for characterisation of visual function were later collected for the immunohistochemistry characterisation previously described.

3.3.2.1 ERG

All ERG data was collected by Justin Hoke and Aura Hare, and analysed by the author.

ERGs, which measures changes of electrical activity at the corneal surface, following a light stimulus, were performed at p18 and 3 months of age (N = 3 animals per time point, both eyes recorded). The changes in electrical activity, measured by the electrodes placed in the cornea of each eye, are induced by the light-mediated change in polarity of photoreceptor cells. Such technique has been well characterised in wild-type animals. An initial negative deflection is expected, denominated a-wave, which is derived from the hyperpolarisation of photoreceptor cells in response to the light stimulus. A larger positive deflection follows, due to the depolarisation of the inner retina. For more details on this technique and experiment set up please see the methods section.

No a or b-waves could be identified in any of the animals, as shown in a representative trace of an ERG recording from *Aipl1*$^{-/-}$ mice at p18 (Figure 34).

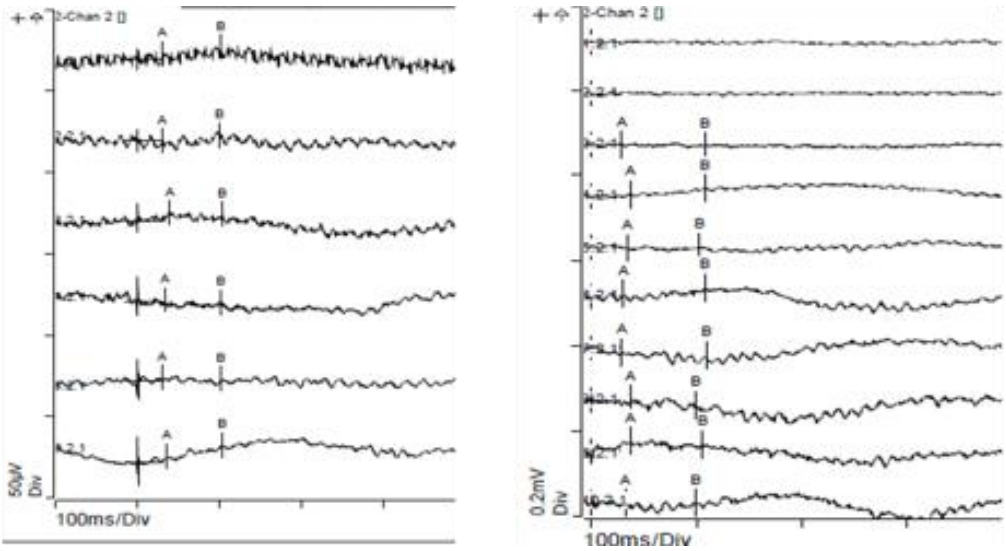

Figure 34 - ERG trace of *Aipl1*$^{-/-}$ mouse at p18

No A or B waves could be detected, either in photopic (on the left) or scotopic conditions (on the right).

3.3.2.2 MEA

Despite no global ERGs being detected it was hypothesised, considering the presence of opsins and atrophic/underdeveloped outer segment-like structures identified by immunohistochemistry, that the remaining cones in *Aipl1*$^{-/-}$ retinas could still exhibit some light sensitive. In order to investigate this hypothesis a more sensitive electrophysiology technique, Multi Electrode Array (MEA), was performed. For MEA experiments a small portion of retinal explants are placed on an array of electrodes which record changes in the extracellular action potential. RGCs are in contact with these electrodes their spiking activity and microERGs are recorded by the electrodes and can be analysed, adding another level of characterisation, as changes in the retinal circuit can be detected. Such changes might be small and not be detected by ERGs measured at the cornea surface, and not result in a measurable visual output, therefore not being detectable by the behaviour tests performed. For further details regarding this technique's principals and experimental set up please see the methods chapter (section 2.11.5). All MEA data was collected and analysed by Dr Christopher Procyk.

Both p19 and 3 month-old *Aipl1*$^{-/-}$ retinas were recorded (n = 5 retinas, N = 5 animals, for each age). As a reference, p17 wild-type retinas were also recorded (n = 3, N = 3). MicroERGs were recorded to a one millisecond light stimuli. RGC's spiking activity was recorded using a 1 second and 10 seconds light stimulus. The wild-type retinas displayed microERGs in most channels (Figure 35A), with identifiable a- and b-waves, analogous to what was described for ERGs measured at the corneal surface. In wild-type samples, channels with no ERG might be due to bad contact between retinal tissue and electrode. No microERGs were identified in any of the *Aipl1*$^{-/-}$ samples collected at either the time point analysed (Figure 35B, C).

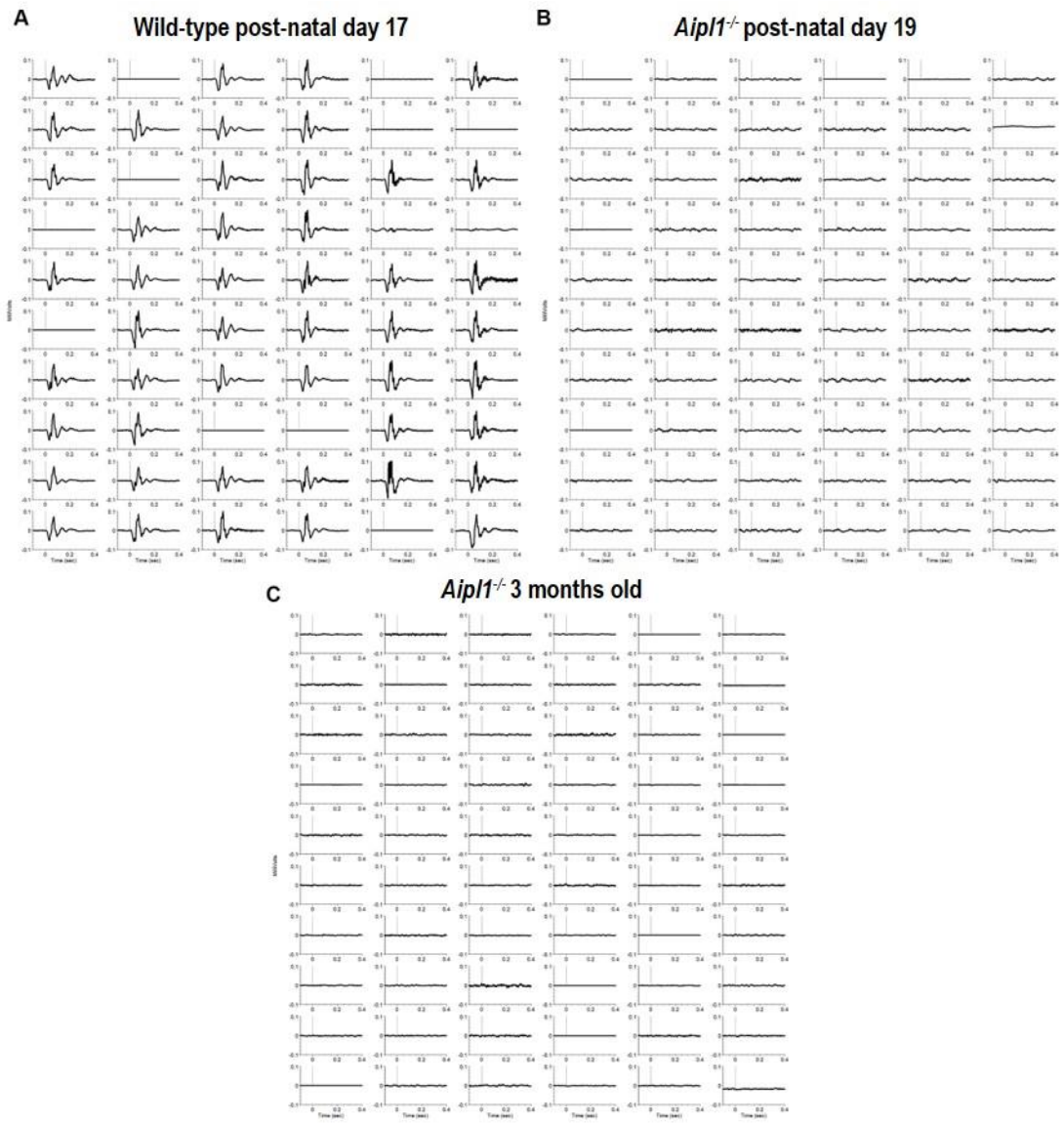

Figure 35 – Representative microERG recordings of *Aipl1*$^{-/-}$ retinas

Representative microERG showing amplitude of electric signal following a 1 millisecond light pulse. Time is represented in the x axis in seconds and y axis showed millivolts. The dashed vertical line shows the moment when light stimulus was presented, which was represented in the x axis as zero. 0.1 seconds were recorded before light stimulus was showed and 0.4 seconds were recorded after. All graphs are scale to the same voltage, ± 0.1 milliVolt. **(A)** In a young wild-type retina several channels recorded microERGs, with a clear a-wave, of various amplitudes with a minimum of -0.02 to a maximum of -0.1 milliVolts, immediately after the light stimulus. The a-wave was then followed by a b-wave, with the electrical signal rising up to 0.1 milliVolts and then returning to base line (zero). This were rapid responses happening within 0.1 seconds after light stimulus. **(B)** Such responses were not present in young *Aipl1*$^{-/-}$ retinas, with only some electrical noise being present but not influence by the light stimulus. **(C)** Adult *Aipl1*$^{-/-}$ retinas displayed similar results as the ones seen in younger animals.

Data recorded from *Aipl1*$^{-/-}$ RGCs showed presence of light-responses in all samples analysed. These responses did not look to be driven by photoreceptor cells, displaying a profile more consistent to what is expected from melanopsin positive retinal ganglion cells (Mure et al., 2016; O'Hearn et al., 2006; Sexton et al., 2012). Following spike sorting single cell responses were identified. All the cell displayed a similar response profile, with a slow on set that was initiated in response to light and took a few seconds to reach the peak firing rate, followed by a slow relaxation and return to base line firing rate following the light turning off (Figure 36A and D). Such responses were classified as sustained responses, since those cells responded for the entire period of the light stimulus, ten seconds (see methods section 2.11.5). To exclude that the light responses seen were being driven by the remaining cone photoreceptors, despite the unusual profile, the ON and OFF pathways of photoreceptors cells were blocked using pharmacology, by adding L-AP4, D-AP5 and DNQX to the recording bath. Following addition of synaptic blockers, the responses were still present and maintained the same profile as what was seen before adding the synaptic blockers (Figure 36B and E). Following washout out of the drugs the responses remained (Figure 36C and F).

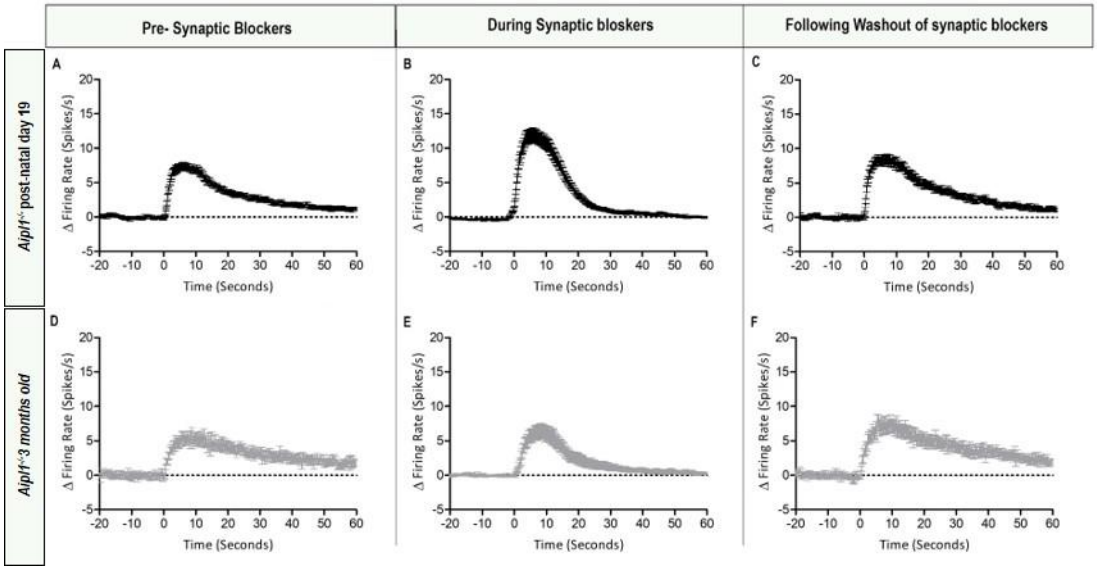

Figure 36 - MEA recording of light responses during synaptic blocking of ONL input

Firing rate of all spike sorted cells (average, SEM) is plotted over time. Cells were recorded for 80 seconds, 20 seconds before the light stimulus, 10 seconds of light stimulation (on the graph zero represent the moment the light stimulus was initiated) and 40 seconds after the light was turned off. Both p19 and 3 month-old retinas displayed similar profile and the sustained light responses were not eliminated by presence of synaptic blockers. **(A, D)** Before addition of synaptic blockers, the all cells showed a slow rise in firing rate following the light stimulus. The firing rate increase reached a peak and remained sustained until light stimulus was turned off. Firing rate then slowly decreased towards base line firing rate. **(B, E)** Following addition of the synaptic blockers, the responses to light remained and appeared to become more defined, due to the “silencing” of spontaneous firing of all other retinal cell neurons that communicate with RGCs via synapses. **(C, F)** After washout out of the synaptic blockers the sustained responses remained.

By not being supressed by the synaptic blockers, and having in consideration the profile seen, such responses were not consistent with responses being originated by photoreceptor cells. Those responses were therefore initiated by intrinsically photosensitive retinal ganglion cells (ipRGCs), which contain the photopigment, melanopsin. In total, 681 spiking RGCs were recorded from p19 *Aipl1*$^{-/-}$ retinas (n = retinas, N = 5 animals), with 169 out of those being light responsive. For *Aipl1*$^{-/-}$ analysed at 3 months of age, the total number of spiking RGCs across different experiments was 356 (n = retinas, N = 5 animals), and 56 out of those were light responsive. All the light responsive cells presented a similar profile, consistent with sustained light responses, and following addition of synaptic blockers, the number of light responsive cells remained unchanged. These results show that 25%, in young *Aipl1*$^{-/-}$ retinas, and 15%, for 3 month-old *Aipl1*$^{-/-}$ retinas, of the RGCs were ipRGCs.

Interestingly, in a wild-type retina ipRGCs has been reported to be a rare population, with only 5% of the RGCs presenting melanopsin (Graham and Wong, 1995). To further investigate these differences, not only between wild-type and *Aipl1*$^{-/-}$ retinas but also between *Aipl1*$^{-/-}$ retinas at different time points, immunohistochemistry and qPCR for Melanopsin were performed. Melanopsin positive cells were present at both p19 and 3 months of age. These cells displayed typical morphology, with some cells sending processes towards the INL and others sending process horizontally, into the GCL, demonstrating presence of the different sub types of ipRGCs cells. No morphological differences were detected between *Aipl1*$^{-/-}$ and *wild-type* retinas using this marker (Figure 37A). Quantification showed no significant difference between the total number of melanopsin positive cells at neither age analysed (2wayANOVA; 78.3 ± 9.4 vs 77.4 ± 5.3 at p19, wild-type vs *Aipl1*$^{-/-}$; n=3 eyes, N = 3 animas, per each strain; 75.2 ± 4.0 vs 88.2 ± 3.3 at 3 months of age, , wild-type vs *Aipl1*$^{-/-}$; n=3 eyes, N = 3 animas, per each strain) (Figure 37B). Immunohistochemistry for melanopsin protein is not optimal and some sub-types cannot be detected. Therefore, to further investigate differences in melanopsin qPCR analysis for expression the gene *OPN4* was performed (Figure 37C) (see methods in section 2.10). The expression of *OPN4* was normalised against *Brn3*, a gene present in vast majority of retinal ganglion cells. Results showed a significant difference in relative expression of *OPN4,* between strains, at 3 months of age (*p<0.05, 2wayANOVA; 1.0 ± 0.81 vs 2.74 ± 1.27; wild-type vs *Aipl1* $^{-/-}$ n=4 retinas, N = 3 animas, per strain). A significant different p19 and 3 month-old retinas were detected for wild-type animals (**p<0.01, 2wayANOVA) but no significant difference was present between young and adult *Aipl1*$^{-/-}$ mice.

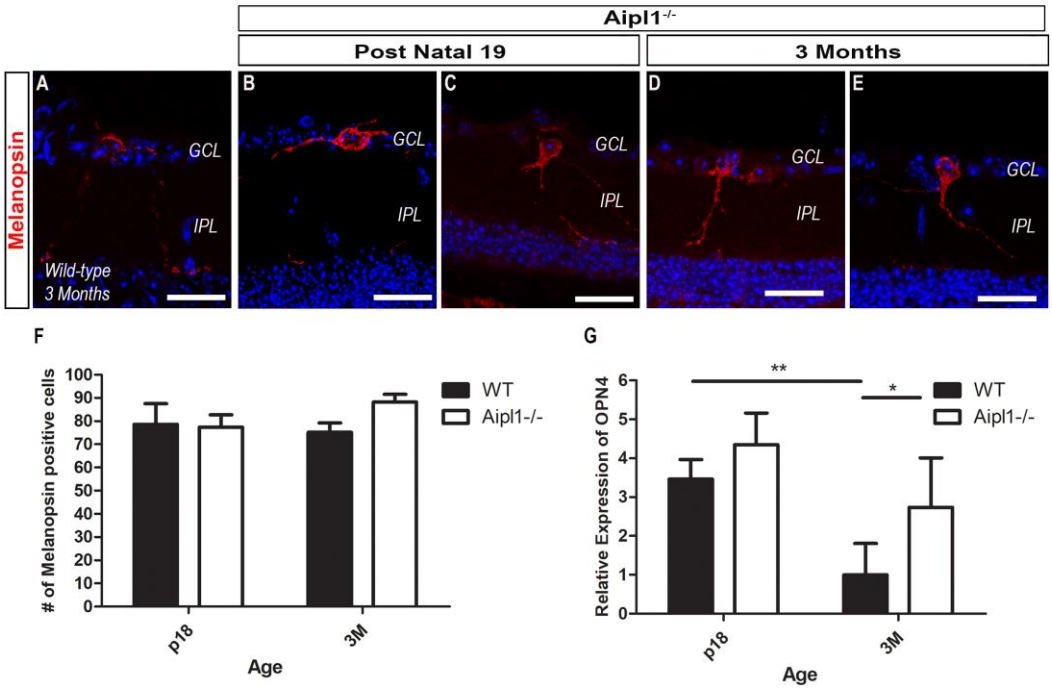

Figure 37 - Characterisation of the GCL: ipRGCs in the *Aipl1*$^{-/-}$ retina

(A) Representative confocal images of Melanopsin-positive cells in the *Aipl1*$^{-/-}$ retina. In the image of a 3 month retina is possible to see both sub-types in the same image. **(B)** Quantification of Melanopsin positive cells per eye in the GCL. At both p19 and three months of age no significant difference could be found between *Aipl1*$^{-/-}$ and a wild-type retina (n=3 retinas, N=3 animals per strain; 2wayANOVA). **(C)** Quantification of relative expression of OPN4 showed that OPN4 is upregulated in early stages, with a reduction in expression being detected in *wild-type* animals by 3 months of age (**p<0.01, 2wayANOVA). *Aipl1*$^{-/-}$ animals showed a less drastic decrease in expression of OPN4, with a significant difference between *wild-type* and *Aipl1*$^{-/-}$ being detected, as *Aipl1*$^{-/-}$ retinas expressed nearly 3 times more OPN4 (*p<0.05, 2wayANOVA; n=4 retinas, N=4 animals per strain)(Scale bar 25µm).

Is not possible to determine for sure if the differences seen are due to upregulation of OPN4 or downregulation of Brn3. However, considering the data collected by immunohistochemistry and MEA analysis is more likely that the detected difference is due to changes in expression of OPN4 and not Bern3. Melanopsin staining seemed more intense in *Aipl1*$^{-/-}$ retinas, which could indicate that the overexpression of Opn4 detected by q-PCR could have resulted in more protein being present. Unfortunately, no other suitable housekeeping genes could be used, due to the overwhelming differences between *wild-type* and *Aipl1*$^{-/-}$ retinas.

In summary, *Aipl1*$^{-/-}$ did not shown any detectable visual function. Retinal function, assessed by MEA, revelled presence of light responses that were not photoreceptor-derived, being generated by ipRGCs. The percentage of ipRGCs recorded by MEA was higher than what has previously been reported in *wild-type* retinas. However, no difference in the total number of ipRGCs could be found. The antibodies available only detect one of several sub-types of ipRGCs, which could be a reason why no difference was identified. Over expression of melanopsin was detected by qPCR.

3.3.2.3 LOOM test

To evaluate and establish a base line for visual perception of *Aipl1*$^{-/-}$ mice, animals were place in a large arena and exposed to a circular stimulus designed to mimic a looming predator (N > 3, per time; *Aipl1*$^{-/-}$ and wild-type mice). Animals with visual perception should respond to such stimulus with a change in behaviour by wither freezing, rearing, or fleeing to a shelter placed in a corner of the arena. For a more detailed description of this technique please see the methods chapter.

At p18, 6 out of the 7 wild-type animals showed a responsive to the LOOM stimulus. None of the 7 age-matched *Aipl1*$^{-/-}$ animals responded to the same stimulus, resulting in a significant difference between strains at this age (**p = 0.005, Fisher's Exact test; N = 7 animals per strain). By three months of age this difference was still present, with all wild-types animals responded to the LOOM stimuli while none of the *Aipl1*$^{-/-}$ mice meet the requirement to be considered visually responsive to the same stimuli (**p = 0.003, Fisher's exact test; N=4, wild-type vs N=7*, Aipl1*$^{-/-}$) (Figure 38).

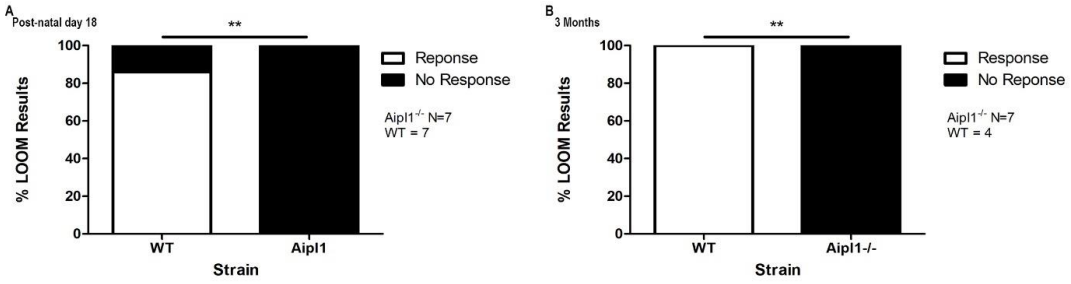

Figure 38 - Behaviour analysis following presentation of LOOM stimulus

(A) At p18, the response to LOOM stimulus was significantly different between strain, with over 80% of the wild-types animals presenting an identifiable response while age-matched *Aipl1*$^{-/-}$animals displayed no change in behaviour following stimulus presentation age (**p = 0.005, Fisher's exact test; N = 7 animals per strain). **(B)** At three month of age, animals all wild-types responded to LOOM stimulus presentation, while *Aipl1*$^{-/-}$ mice showed no response to the stimulus (**p = 0.003, Fisher's exact test; N = 4 animals , *wild-type* vs N=7, *Aipl1*$^{-/-}$).

3.3.2.4 Optomotor

The optomotor reflex in an innate reflex-driven behaviour, characterised by a slow head movement triggered by visual cues, such as a rotating slowly rotating stripe pattern. Mice follow the rotating pattern and visual perception can be assessed by how accurate that behaviour is. Patterns rotating clockwise will trigger a response of the left eye and patterns rotating anti-clockwise induce a response driven from the right eye, allowing assessment of each eye individually. This technique also allows to study contracts sensitive or visual acuity, by altering the contract, thickness, or rotation speed of the pattern. For the purposes of this project contrast sensitivity was accessed using a special component stimulus of 0.128 cycles per degree (c/d) and calculating according to the appropriate formula (see methods chapter for further detail). These experiments were only done in adult mice, 3 months of age, (N = 3, per strain), due to the hyperactivity seen in younger mice which made this assessment unviable for p18 animals.

Three months old wild-type mice were analysed for comparison and the values obtained for this strain varied between 13 and 25, each means wild-type mice can detect the visual stimulus with 5% or less contrast (see formula used in the Methods section 2.11.2). The values obtained for three months old *Aipl1*$^{-/-}$ animals were below 1, meaning this strain could not detect the visual stimulus, being significantly different from the values obtained for age-matched wild-type animals (***p<0.001, t-test; 23 ± 10.6 vs 1.04 ± 0.04, *wild-type* vs *Aipl1*$^{-/-}$ N = 3 animals) (Figure 39A). *Aipl1*$^{-/-}$ values for contrast sensitivity were similar to random calibration data collected by choosing “Right” or “Left” randomly in the absence of an animal. Only values significantly greater than this baseline can be interpreted as real behaviour in response to the stimulus. (Figure 39B), meaning that *Aipl1*$^{-/-}$ animals do not have contrast sensitivity detectable by optomotor test.

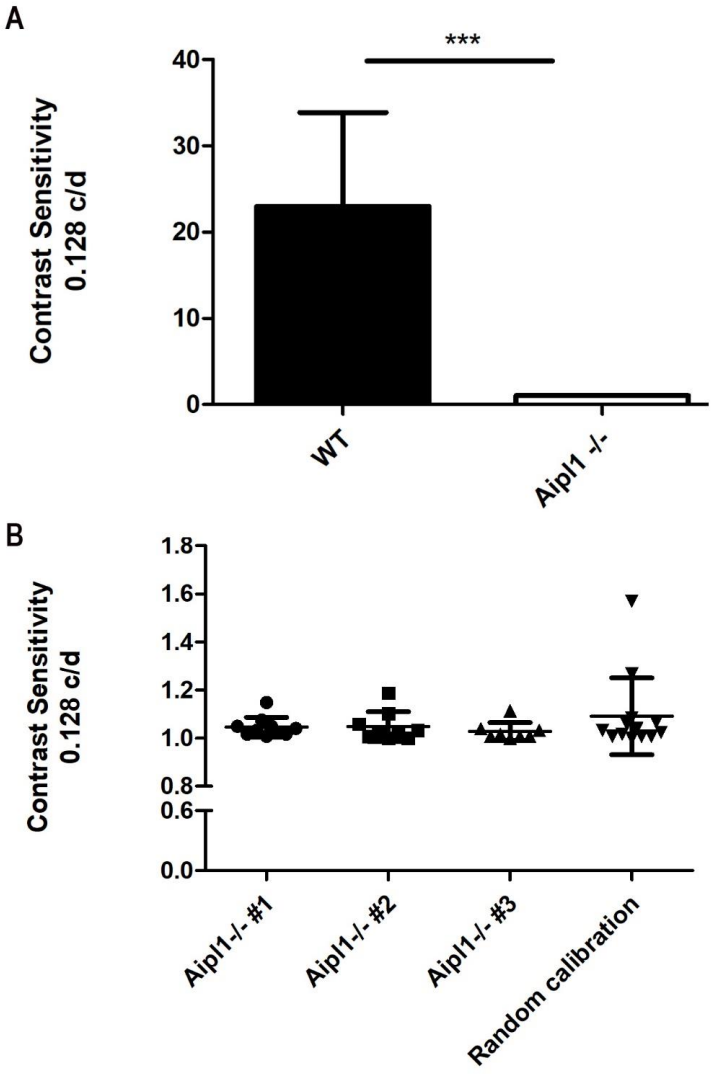

Figure 39 - Contrast sensitivity in *Aipl1*$^{-/-}$ mice

(A) *Wild-type* animals show a high contrast sensitivity, needing little contrast to be able to follow the stimulus presented. *Aipl1*$^{-/-}$ animals show a contrast sensitivity close to zero. The contrast sensitivity difference between strains is significant ($p<0.001$, 1Way ANOVA). **(B)** All the values obtained for each of the three *Aipl1*$^{-/-}$ mice analysed fall within the range of values obtained through random calibration of the Optomotor setup.

3.3.2.5 *Light avoidance test*

Light perception was tested in a light avoidance test that allowed animals to roam freely in an arena that comprises of a light and a dark compartment, relying on the natural tendency of (nocturnal) mice to prefer the dark when given the choice. Therefore, this test can be used to assess basic vision, since mice without light perception should not display a preference for the dark. Mice must be naïve to the arena in order to avoid a sense of safety which could interfere with the natural preference for darkness. As for optomotor test, only adult mice were use in these experiments due to the hyperactivity of younger mice.

The light avoidance test showed no difference between 3 months old wild-type animals (N = 7) and the advanced retinal degenerated, *Aipl1*$^{-/-}$ mice (N = 9). This was unexpected, as wild-type animals did not show a preference for the dark portion of the arena. Wild-type animals spent, on average, 46 ± 13% of their time in the dark portion of the area, and *Aipl1*$^{-/-}$ mice spent on average 38 ± 20% of their time in that dark. This different was not significant (t-test) (Figure 40).

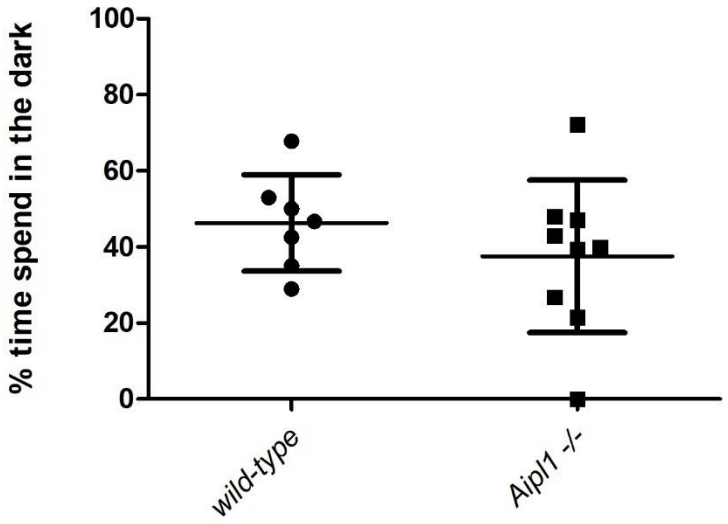

Figure 40 - Light avoidance behaviour
(A) No difference between 3 months old wild-type animals and *Aipl1*$^{-/-}$animals regarding the percentage of time spend in the dark was detected by using the Light avoidance test.

3.4 Conclusion

The detailed characterisation of *Aipl1*$^{-/-}$ retinas is particularly relevant to study the phenotype and to test new therapies for early onset retinal degenerative diseases. By having a detailed characterisation of the morphological and functional phenotype, extension of the number of parameters to assess following transplantation was achieved. This could allow identification a positive effect before visual rescue is achieved, being able to select more promising approaches and more effectively identify and troubleshoot limitations.

In this study *Aipl1*$^{-/-}$ mice generated by *Dyer et al.*, in 2004 were used. No assessment of retinal remodeling following photoreceptor degeneration had been reported for these animals. Here it was established that for this strain, rapid loss of rod photoreceptors occurs followed by loss of cone photoreceptors, in agreement to what had previously been reported (Dyer et al., 2004). This previous report showed that the remaining cones found at p12 displayed some morphological anomalies but preserved typical cone-like features(Dyer et al., 2004). Interestingly, was shown that, by p18 these remaining cone photoreceptors present severe morphological abnormalities, with no identifiable cone features, such as inner/outer segment or synaptic pedicle. Since it has been shown that the Aipl1 is a chaperone protein that is implicated in several cell functions, interacting with cell cycle(Hidalgo-de-Quintana et al., 2008, p. 1; Tan et al., 2012, p. 1; van der Spuy et al., 2003) and visual cycle proteins(Ramamurthy et al., 2003; Yadav and Artemyev, 2017, p. 1), is important to establish if photoreceptors develop normally or if the degeneration only takes part once the visual cycle is initiated. This data could suggest that that these cells initially develop normally and then surfer extremely rapid and severe degeneration following eye opening. Ramamurthy *et al*., who generated another *Aipl1*$^{-/-}$ strain, reported similar findings. By using electron microscopy, no differences in outer segment formation between *Aipl1*$^{-/-}$ and wild-type retinas were found at p8. However, *Aipl1*$^{-/-}$ retinas showed visible disruption of its outer segments by p11(Ramamurthy et al., 2004). Since this rapid photoreceptor degeneration takes place within days following eye opening, is likely that the compromised phototransduction process accelerated photoreceptor dead. However, due to the vast role of Aipl1 protein, is likely that other mechanisms contribute to the retinal degeneration.

The progression of remodeling events in the other layers of *Aipl1*$^{-/-}$ mice, was assessed considering morphology and quantification retinal interneurons. In this model, rod bipolar cells become displaced as the remodeling events progress.

However, no loss of total number of bipolar cells was seen, unlike what has been previously been reported for other *Aipl1*$^{-/-}$ strain (Singh et al., 2014a). Furthermore, severe changes in horizontal and amacrine cells were found. The number of horizontal cells to be significantly reduced in adult *Aipl1*$^{-/-}$ mice, and a severe reduction of amacrine cells was detected from p18 onwards. This data refutes the original report, where an increase in number of bipolar and amacrine cell was suggested(Dyer et al., 2004). The different results can be explained by the use of different techniques to assess the number of cells. Dyer *et al*. quantified the retinal cell types by staining dissociated 8-week-old retinas. The lack of specific and exclusive cell markers for most retinal cells makes the morphological features and location within the retinal layers essential for accurate quantification. Therefore, is likely that the quantification reported here is more accurate. Furthermore, these findings are supported by other reports which describe similar remodeling events in other retinal degeneration models(Jones et al., 2003; Jones and Marc, 2005; Singh et al., 2014b; Strettoi et al., 2003b). Further changes to the synaptic network are revealed by the absence of post-synaptic markers even at p18 when a full layer of cone photoreceptors still present. The maintenance of interneurons, which modulate the visual signal, and synaptic network is essential to achieve normal vision. The absence of these cells might impact the quality of visual rescue that can be achieved by strategies such as cell therapy, which aim to overcome the lack of photoreceptor cells but rely in the presence of a mostly intact inner retina. Presence of post-synaptic markers in the bipolar cells at p12 had been previously reported (Dyer et al., 2004), once again demonstrating the incredibly fast degeneration rate in *Aipl1*$^{-/-}$ retinas. Post-synaptic protein mGluR6, in normal developmental conditions, was first identified throughout the bipolar soma early in retinal development, p11, increasing gradually its levels and localising to the OPL where it should be evident by p14. By p21 mGluR6 should be confined to the ON bipolar cell post-synaptic terminals (Cao et al., 2015). In the *Aipl1*$^{-/-}$ strain at p18 very few positive structures could be identified in the OPL, suggesting that the formation of mature synaptic connections and establishment of synaptic network between the remaining photoreceptor cells and interneurons could be impaired. This could be due to the lack of LRIT1, a cell-adhesion molecule expressed selectively in cone photoreceptors, that binds to mGluR6 and has, recently, been shown essential for synaptic formation between cones and cone ON bipolar cells (Sarria et al., 2018; Ueno et al., 2018). Since *AIPL1* protein is responsible for stabilising of several proteins, it might have a role in stabilisation of LRIT1, therefore in this strain LRIT1 might be absent of miss localised. No studies regarding

the role of *Aipl1* in maintenance of LRIT1 have been published so far. It is also possible that the rapid loss of rod photoreceptors leads to lack of Elf1 or other proteins that are essential to induce expression and or localisation of post-synaptic receptors in the dendrites of bipolar (Tomioka et al., 2014). These are suitable hypothesis to justify the reduction of not only for mGluR6 but also other post-synaptic markers, as synaptogenesis requires specific contacts between pre and post-synaptic cells and presence of transmembrane adhesion proteins and/or secreted proteins that regulate distinct aspects of neuronal connectivity (for review see Williams et al., 2010).

As degeneration of the ONL happens so quickly, remodelling of the INL seems to be happening slightly earlier in this model than other similar advanced retinal degeneration model, such as *rd1* strain (Pignatelli and Strettoi, 2004; Veleri et al., 2015b). A representative example of the previous statement is the complete absence of dendrites of rod-bipolar cells in the OPL, that is described to take place in the r*d1* retina by the second or third month of life (Strettoi and Pignatelli, 2000), while in the *Aipl1*$^{-/-}$ retina the same event can be seen by 1 month of age. An even more striking difference can be identified in the presence of mGluR6 protein, that, though mislocalised, can still be found in 3 months old *rd1* mice (Strettoi and Pignatelli, 2000), but that is already mostly undetectable in *Aipl1*$^{-/-}$ retinas by p18. The similarities and differences between the phenotype of *rd1* and *Aipl1*$^{-/-}$ mice are summarised in table 4.

	***Rd1* mice**	***Aipl1*$^{-/-}$ mice (*Dyer et al*)**
Gene affected	PDE6β – affects rods	AIPL1 – affects rods and cones
Degeneration progression	Centre to periphery	Centre to periphery
Photoreceptor Degeneration	Complete rod degeneration and consequent cone degeneration	Both rods and cones degenerate simultaneously. Rod degeneration rate is faster
Complete degeneration rods degeneration	Virtually no rods by 4 weeks of age	Virtually no rods by post-natal day18
Remaining cone photoreceptors (degeneration plateau)	By 3 months of age degeneration plateaus (loss of 90% cones)	By 3 months of age degeneration plateaus (loss of >90% cones)
Cone morphology	Typical cone morphology seen until p25	Abnormal cone morphology from p18 (earliest time point analysed) onwards
Inner retina remodeling	Typical stage 2 (see Figure 14) remodeling features seen from ~3 month of age onwards	Typical stage 2 (see Figure 14) remodeling features seen from ~1 month of age onwards
Presence of mGLuR6	Mislocalised by ~3months of age	Undetectable by p18
Retinal function	ERG responses detected until postnatal day 21	No ERG responses detected

Table 4 - Summary of the phenotypical differences *rd1* vs *Aipl1*$^{-/-}$ mice

These differences make the use of *Aipl1*$^{-/-}$ mice for photoreceptor transplantation experiments extremely interesting, as achieving rescue of this model at 3 months of age would be a great advance and provide new evidence that cell therapy could be used to treat blindness, even in cases of extremely severe retinal degeneration. The rescue shown so far was obtained in *rd1* mice at 2 to 3 months old (Barnea-Cramer et al., 2016; MacLaren et al., 2006). In this strain the cone photoreceptors develop normally and degenerate as a consequence of the loss of rod photoreceptors. A full layer of cones remains in the *rd1* retinas until 1 month of age, unlike what is seen in the *Aipl1*$^{-/-}$ strain. The presence of a layer of healthy cones provides some input to the interneurons, supporting the synaptic layers. Therefore, the remodelling described in this model by 3 months of age is similar to the remodelling that *Aipl1*$^{-/-}$ retinas display by 1 month of age. Rescue of vision of an *Aipl1*$^{-/-}$ at 3 months of age would show that transplantation of photoreceptor cells can be used in cases where the remodelling events in the INL are more severe and the synaptic circuit has been lacking photoreceptor input for a longer period of time giving hope to treat patients with more severe retinal degeneration.

No visual function, assessed by ERG, optomotor and LOOM test, was detected at both of ages analysed. No optomotor data was collected for p18 mice, since it was not possible perform the test, due to the hyperactivity of young mice. Both behaviours, assessed by LOOM and optomotor test are complex behaviours that involve more than light perception. Therefore, light avoidance test would, in principle, be the simplest behavioural test to assess if the remaining photoreceptor cells in *Aipl1*$^{-/-}$ animals can drive a visual response. Despite the arena used for this test being the appropriate size, and the light levels being identical what has previously been published (Recober et al., 2009; Silva et al., 2017; Takao and Miyakawa, 2006), the light avoidance set up did not show the expected results for *wild-type* animals, as no preference for remaining in the dark was identified. It was hypothesised that the animals used, that had been born in the animal facility, might have been subjected a lot of handling and therefore no longer display the expected behaviour, of feeling safer in the dark and consequently avoiding light, when given free choice. Therefore, new wild-type animals were ordered in to test the setup, however those animals displayed a similar behaviour, not showing a preference for the dark portion of the arena. As we expect that in a bigger arena, mice will feel less safe and be more likely to show a preference to avoid the illuminated side of the arena, a new, bigger arena was ordered for future experiments. However, the lack of visual perception since p18 would not be unexpected, since previous studies had showed lack of ERG in this strain by this age

(Ramamurthy et al., 2004). The fact that with all the methods used, the animals showed no visual response at all, makes this strain a good model to study visual rescue following cell transplantation, as even a small improvement in vision should be distinguishable from the base line established.

Collecting MEA data in order to characterise this strain was extremely relevant. This data was necessary to establish the base line, how many responses are seen in an untreated animal and what is their profile. This was essential for an accurate interpretation of following transplantation experiments, as this would be the technique that would allow detection of retinal rescue over small areas, even if an overall visual rescue could not be achieved. It was important to establish if the remaining photoreceptors were able to detect and respond to a light stimulus, so that a baseline background would be in place and serve as comparison for future transplantation experiments. Unsurprisingly, no typical rod light response was detected, as very few rods were present. More interesting was the fact that even at p18 the cone photoreceptors, despite presenting presynaptic proteins, opsin proteins, in some cases localised to an outer segment-like structure, no response to the light stimulus was detected. A possible explanation for these results is the lack of post-synaptic proteins seen in this strain that could be responsible for the inability of propagation of a response throughout the synaptic network. Other possible explanation is that the cone photoreceptors cells are unable to detect light and initiate the visual cascade. Despite the required proteins being present, they might be miss localised or, most likely, the lack/reduction of PDE, as a consequence of absence of Aipl1 protein, impedes the phototransduction cascade. The fact that no micro-ERG could be detected could corroborate this hypothesis. All the light responses that were detected in the *Aipl1*$^{-/-}$ retinas, either at p19 or 3 months of age do not appear to be driven by photoreceptors, as they are slow to turn on and especially slow turning off, displaying a profile more consistent to typical melanopsin cell driven responses (Mure et al., 2016). Some cells were sensitive to short duration light flashes, something that has not been described for deafferent melanopsin responses. However, it is known that melanopsin positive cells do show some different responses in degenerated animals, as they appear to be more active once the photoreceptor input is lost (Fujii et al., 2016; Goo et al., 2011; Margolis et al., 2014; O'Hearn et al., 2006; Ruggiero et al., 2009). Furthermore, using pharmacology to block the synaptic pathways between photoreceptors and the rest of the synaptic network, the responses were maintained, corroborating that the responses seen were generated by ipRGCs cell and not by the remaining photoreceptor cells. It is known, in several strains, that melanopsin is

expressed in a greater number of ganglion cells in early stages and that that number is reduced once the retina is fully mature (Ruggiero et al., 2009; Sekaran et al., 2005).. There are several sub-types of melanopsin positive cells, and the available antibodies do not target to all types, making the quantification presented here probably an under estimation. The qPCR data that shows a significant increase in expression of *Opn4*, gene encoding melanopsin, in *Aipl1*$^{-/-}$ animals at 3 months of age when compared to age-matched *wild-type* retinas. Collectively, this data and the MEA recordings, that showed that the light responsive units identified as ipRGCs in *Aipl1*$^{-/-}$ responded to light flashes outside the normal temporal range of melanopsin (1 second light stimulus), suggest the presence of more photopigment available per cell or presence of more ipRGCs in *Aipl1*$^{-/-}$ retinas. If the increase seen is due to more cells expressing melanopsin or more melanopsin being express per cell still not clear. It is out of the scope of this project to investigate this possibility but, is an interesting finding that could, perhaps, generate further studies to investigate if this hypothesis could be used to develop future therapies for patients with LCA due to mutations in the *AIPL1* gene or other retinal dystrophies.

In view of the results described in this chapter transplantation experiments, described in the following chapters, will have 3 months old *Aipl1*$^{-/-}$ animals as hosts. The possibility of rescue due to material transfer between transplanted and host photoreceptor is dramatically reduced, as very few photoreceptors are left by 3 months of age. Moreover, by using *Aipl1*$^{-/-}$ mice at this age it would be possible to evaluate if transplantation of photoreceptor cells can stop or reverse the remodelling of the inner retina as well as rescue visual response. Despite ambitious, visual rescue or even identification of any changes in the INL, detected following transplantation, could improve and be relevant for future photoreceptor transplantation experiments.

Chapter 4: Transplantation of mESC an hESC-derived photoreceptor cells into *Aipl1*$^{-/-}$ mice

4.1 Introduction

In the previous chapter it was established that the *Aipl1*$^{-/-}$ retina is depleted of most photoreceptors cells and extensive remodelling has taken place by 3 months of age, with these animals not showing any detectable photoreceptor response to light. The current chapter describes efforts to rescue vision in these mice through transplantation of ESC-derived photoreceptors.

Initially, it would be important to investigate if transplanted photoreceptors cells are able to connect with the host retina. It was previously established that the *Aipl1*$^{-/-}$ retina lacks the post-synaptic protein, mGluR6, in bipolar cell dendrites, thus transplanted photoreceptors would need to stimulate its restoration. Evaluation of the impact transplanted photoreceptor cells have on the host retina and investigating if the remodelling events can be reversed could provide valuable information regarding treatment of advanced retinal degeneration conditions, such as AMD. The work described in this chapter attempted to optimise the transplantation of hESC-derived cone photoreceptor cells into *Aipl1*$^{-/-}$ mice. Due to the intense workload and cost associated with generating human retinal organoids (see methods, section 2.3), mESC-derived photoreceptors to provide guidance regarding the optimal number of hESC-derived cones for transplantation. Initially mESC-derived photoreceptors were used to investigate the consequences of increasing the number of transplanted cells. Whilst increasing the number of transplanted photoreceptor cells might improve the probability of rescue, a major concern was the possibility of an increase in immune rejection and retinal damage of the host's retina.

A short review of the two publications that most influenced the work described in this chapter is provided below.

4.1.1 Transplantation of mESC-derived photoreceptor cells

The mESC-derived photoreceptors, generated using the protocol described above were also transplanted into the advanced degeneration model *Aipl1*$^{-/-}$, where material transfer is not a complicating factor (Kruczek et al., 2017) (Figure 41). In this case, an AAV2/9 vector (2.1.GFP) encoding L/M cone OPSIN promoter was used to drive specific GFP expression in mouse cones cone precursors. The GFP positive cells

were sorted and transplanted, showing survival and cell maturation 3 weeks post-transplantation. Maturation was assessed by the presence of a panel of cone phototransduction-related proteins, including M-opsin, Gnat1, and CNG channel beta-3. The pre-synaptic protein, Ribeye, was also detected. Existence of rudimentary outer segment-like structures was supported by presence of Peripherin2 bud-like positive structures (Kruczek et al., 2017). However, this study did not establish whether the transplanted mESC-derived photoreceptor precursor cells were able to connect with the host retina and rescue of function.

Figure 41 - mESC-derived photoreceptors transplanted into *Aipl1*$^{-/-}$ animals

From Kruczek et al., 2017, under Creative Commons License

(A-C) The transplanted cells survive and present cone-specific phototransduction-related proteins. **(D)** Some of the transplanted cones show accumulation in distal processes of Peripherin2. **(E)** 2.1.GFP+ cells are in close proximity to CALBINDIN+ host horizontal cell dendrites. **(F and G)** Antibody staining for synaptic proteins Ribeye (CTBP2; F) and Synaptophysin (G) showing expression in transplanted GFP+ cells (arrowheads in F). Scale bars, 5 μm (F) and 10 μm (all other images).

4.1.2 Transplantation of hESC-derived photoreceptor cells

Our group recently published a 2D/3D differentiation protocol that generated neuroretinal-vesicles, also known as retinal embryonic bodies or retinal organoids, from hESC and hiPSC. These vesicles recapitulate the human retinal development and cone photoreceptor precursors can be generated, isolated and transplanted into mice models (Gonzalez-Cordero et al., 2017). Transplantation of 100K cells into the *Aipl1*$^{-/-}$ mouse strain, at 2 to 3 months of age, showed survival of these cells, with the cell mass forming an ONL-like patch in some regions of the subretinal space (Figure 42). Rosette formation by the transplanted photoreceptors was rare in this mouse strain, and the hPSC-derived cones formed a distinct layer adjacent to the host INL. The layer of transplanted cells was often a single-cell layer, but in some instances a thicker layer (around 2-3 cells), of transplanted cones could be seen (Figure 42 A, left image). Transplantation of these cells into *Nrl*$^{-/-}$ mice showed that some of the transplanted cells migrated into the host ONL, being incorporated into this layer (Figure 42B) Transplanted hPSC-derived cone photoreceptors showed ability to survive, up to 3 weeks following, displaying Peripherin2 in OS-like buds (Figure 42A) and pre-synaptic protein Ribeye sometimes located to a pedicle-like structure (Figure 42B) (Gonzalez-Cordero et al., 2017).

Figure 42 - Transplantation of hPSC-derived cones into mouse models of retinal degeneration

From Gonzalez-Cordero, 2017, under Creative Commons License

(A) 200K hPSC-derived cone photoreceptors, transplanted into adult *Aipl1*$^{-/-}$ mice, survive and form ONL-like regions, three weeks post transplantation (left). These cells produce the pre-synaptic protein, Ribeye (CtPB2) and in some cells small peripherin2 positive buds could be identified, suggesting formation of outer segment-like structures (centre and right, respectively). **(B)** Transplantation of 200,000 hPSC-derived cone photoreceptors into *Nrl*$^{-/-}$ mice. Widespread cell masses could be seen three weeks post-transplantation (left). Some of the transplanted cells were able to migrate and be incorporated by the host ONL (centre). Transplanted cells extend processes to the OPL and expressed pre-synaptic marker, Ribeye, at the photoreceptor synaptic terminal.

This study showed that the protocol established in our laboratory allows generation of neuroretina-vesicles, from hESC and hiPSC, that recapitulate the human retinal development. With a viral vector, it is possible to identify specific cell types, in this case L/M-opsin expressing cones. Moreover, the study demonstrates that is possible to dissociate and isolate the cone photoreceptors from these vesicles/retinal organoids, following FACS analysis for GFP positive cells. The cell suspension can be transplanted into *Aipl1*$^{-/-}$ animals, showing cell survival and some level of maturation. These results were encouraging, as they demonstrated that the established protocol allowed efficient differentiation of ES and iPS cells into retinal precursors. It also indicated the possibility of xenotransplantation of the photoreceptors derived using this protocol, with cells surviving 3 weeks following transplantation and expressing the necessary proteins to establish synapses with the host retina. However, further investigation regarding the capacity of the transplanted cells to restore function and their impact in the host retina is required.

4.2 Aims

The work developed in this chapter aims to (1) establish what is the best cell developmental stage for transplantation of mESC-derived photoreceptors into late degeneration *Aipl1*$^{-/-}$ mice; (2) investigate if increasing the number of transplanted mESC-derived photoreceptors impacts the transplantation outcome; (3) assess connectivity with host cells; (4) assess retinal and visual function following transplantation of mESC-derived photoreceptors; (5) transplant hESC-derived cone photoreceptors and evaluate transplantation outcome by assessing presence of synaptic markers and maturation of transplanted cells; and (6) evaluate retinal function following transplantation.

4.3 Results

4.3.1 Transplantation of dissociated mESC-derived photoreceptors

The work described in this chapter uses the transgenic mESC line, in which GFP expression is driven by the endogenous Crx promoter. *Crx* is expressed in the early stages of photoreceptor differentiation, soon after a cell commits to a photoreceptor cell fate, becoming a post-mitotic cell. Its expression is maintained in mature differentiated photoreceptors. Therefore, the Crx.GFP transgenic ESC line labels all post-mitotic developing and mature cone and rod photoreceptor cells. This cell line was previously differentiated using our adapted differentiation protocol, and full characterisation of photoreceptor development was performed. The expression of photoreceptor markers increased with time, with cells at dd26 resembling post-natal day eight photoreceptors. After dd28 the EBs started losing their structural integrity, with rosette formation taking place within the neuroepithelial region (Goh, 2016).

Here, 3 developmental stages were selected to evaluate the optimal transplantation stage: dd15 (n = 5 differentiations) an early developmental stage equivalent to post-natal retina day 4-8; dd 27 (n = 9 differentiations) and dd33 (n = 3 differentiations), a late developmental stage. Following dissociation of these mESC-derived retinal organoids, GFP-positive cells were isolated from these by FACS and resuspended to a concentration of 200,000 or 533,000 cells per µl. Using a Hamilton precision glass syringe and an 8mm, 34-gauge needle, cells were injected into the subretinal space of 3-4 months old *Aipl1*$^{-/-}$ mice.

The percentage of live cells at each developmental stage was assessed during the FACS experiments. Data showed that younger optical vesicles are healthy than older optical vesicles. The percentage of live cells at dd15 being significantly higher than that seen at dd33 (*$p<0.05$, 1way ANOVA; dd15 (55% ± 12, N = 5 differentiations) vs dd33 (13% ± 5; N = 3 differentiations)). No significant differences were found between cells at dd27 and the other developmental stages (Figure 43A). The percentage of photoreceptor precursors, *Crx*.GFP positive cells, at dd15 was significantly lower than the other two developmental stages (*$p<0.05$, 1way ANOVA; d15, 21% ± 16 vs dd27, 60% ± 10 vs dd33, 64% ± 9; N = 5 vs N= 9 vs N = 3 differentiations, respectively)(Figure 43B).

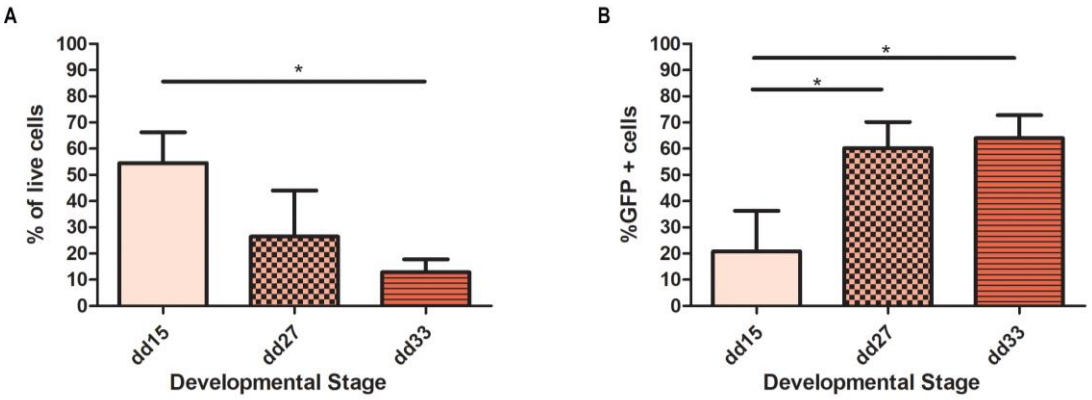

Figure 43 - Comparison of developmental stages of mESC-derived Optic Vesicles by FACS

Optic vesicles were dissociated and CRX.GFP positive cells were isolated by FACS. **(A)** Following dissociation of the mESC-derived retinal optical vesicles, the percentage of live cells identified by the FACS machine decreased with age. The percentage of live cells from optical vesical at dd15 being significantly different from optical vesicles at dd33 ($p<0.05$, 1wayANOVA). No significant differences between dd27 and the other developmental stages were identified. **(B)** The percentage of GFP positive cells was significantly lower at dd15 ($p<0.05$, 1wayANOVA).

Since the percentage of GFP-positive cells at dd27 was similar to that found at dd33 and the percentage of live cells was higher (25% ± 16 vs 13% ± 5), more GFP-positive cells were isolated per differentiation plate, resulting in a better yield of cells. Thus, dd27 proved, in terms of yield, to be the best developmental stage to use as source of mESC-derived photoreceptor precursors. However, survival and maturation of these cells following transplantation must also be evaluated as these are major criteria for achieving successful transplantation outcome.

The FACS data presented in Figure 43 includes all the cell differentiations and cell sorting data from all the transplantation experiments presented in rest of this chapter.

4.3.1.1 Increasing the number of transplanted mESC-derived photoreceptor precursors into *Aipl1*$^{-/-}$ mice

The number of transplanted cells was increased from ~200,000 cells, which had previously studied (Gonzalez-Cordero et al., 2013) to ~ 800,000 cells per eye, injecting 1.5 µl cell suspension at a ~ 533K cells/µl (see section 3.3). The amount of transplanted cells was chosen considering the maximum number of transplanted cell reported to date, between 500,000 and 750,000 hESC-derived retinal cells (Zhu et al., 2017) and the size difference between human and mouse photoreceptors.

The first three differentiations, at each of the developmental stages previously mentioned, were used to generate cells that were transplanted at a concentration of ~200,000 and ~800,000 cells per eye. This way a fair comparison between number of transplanted cells from the same differentiation was achieved. Three weeks following transplantation, cells could be detected in the subretinal space in 48% of the eyes that received ~200,000 cells and in 44% of the transplanted eyes that received ~800,000 cells. Cells transplanted at all developmental stages chosen, survived in the subretinal space, independently of the number of transplanted cells. Concerning cell survival following transplantation, eyes that received ~200,000 cells did not show much variability between developmental stages. The success rate, defined as number of eyes that presented a cell mass upon collection, for eyes that received cells at dd15 and dd33 was 50%, (3 out of 6 injected eyes, N = 3 mice, per developmental stage). Eyes receiving transplants of dd27 cells showed a success rate of 44% (4 out of 9 injected eyes, N = 5 mice). Eyes that received 800,000 cells showed similar results; 45% of transplants using cells at dd15 (7 out of 16 injected eyes, N = 8 mice) were successful; 44% of transplants using cells at dd27 cells (16 out of 36 injected eyes, N = 20 mice) and 43% for cells transplanted at dd33 (3 out of 7 injected eyes, N = 4 mice). Is important to note that due to the nature of the experiment, composed of discrete data, and difference in number of eyes injected between developmental stages the use of percentage might appear to reveal a small difference that is not real.

Transplantation of ~200,000 cells led to smaller cell masses in the subretinal space, independently of the developmental stage of the cells at time of transplantation (Figure 44). No obvious morphological differences were identified between cells transplanted at different developmental stages. The transplanted cells did not seem to organise themselves into a layer adjacent to the host's INL, with cells presenting variable orientation, some extending processes towards the host's INL (Figure 44 A, B) while others extended processes towards the RPE or parallel to the host's retina

(Figure 44F, H and I). Not all transplanted cells presented cell processes (Figure 44C, D and E). Next, the capability of these cells to form synaptic connections with the host retina and develop the required structures to be light sensitive were assessed. No pre-synaptic protein, Ribeye, (figure 44D-F) or outer segment-specific protein, Peripherin2, were detected in transplanted cells at any of the development stages used (Figure 44G-I).

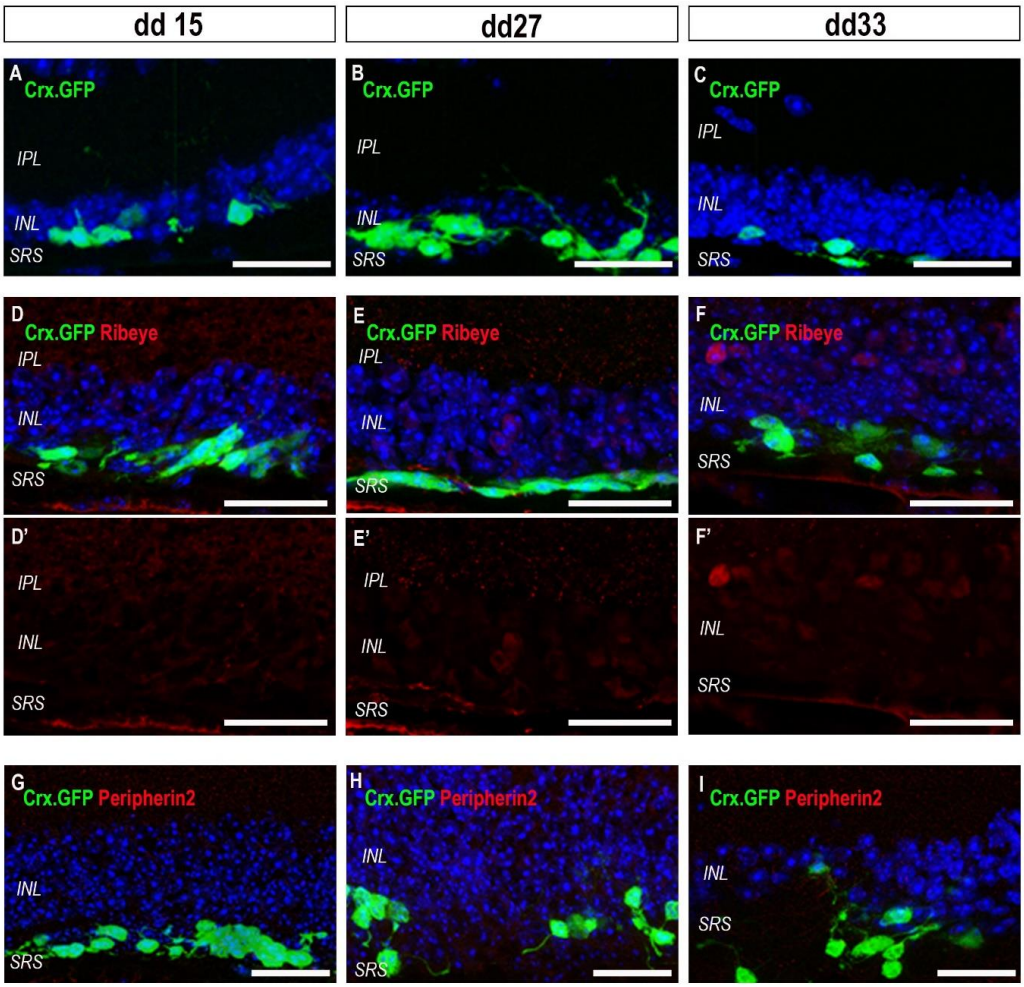

Figure 44 -mESC-derived Crx.GFP photoreceptor precursors, 3 weeks following transplantation of 200,000 cells, into Aipl1$^{-/-}$ mice

Representative confocal images showing spread and morphology of mESC-derived Crx.GFP photoreceptors precursors 3 weeks following transplantation of 200,000 cells, at dd15 (left column), dd27 (middle column) and dd33 (right column). **(A-C)** Presence of Crx.GFP positive cells in the subretinal space of a three-month-old *Aipl1*$^{-/-}$ mouse. Small cell masses containing GFP positive cells, showing cell survival, could be seen post-transplantation of all the chosen developmental stages **(D-F)** Staining for pre-synaptic protein Ribeye in transplanted cells. No signal for this marker was seen in cells transplanted at any of the developmental stages. This can more clearly be observed by isolation of red channel (D', E' and F'). Ribeye antibody is raised in mouse, which explains the background and positive staining of blood vessels. **(G-I)** No outer segment-like structures could be identified, with no Peripherin2 detected in the transplanted cells at any of the developmental stages transplanted. (Scale bar 25 µm)

Different results were seen when transplanting 800,000 mESC-derived photoreceptor precursors as the morphology of the transplanted cells was different between developmental stages. This was likely due to the bigger cell masses seen in eyes that received more cells, which allowed for such differences to become evident. Cells transplanted at dd15 showed some rosette formation (Figure 45A) and overall, fewer cells seem to extend processes into the host's INL (Figure 45B-C), when compared with cells transplanted at dd27 (Figure 45E-F). Cells transplanted at dd33 consistently showed a round or elongated morphology, had no identifiable cell polarity and extended no processes into the host's INL (Figure 45G-I). The spread of cell in the subretinal space and cell morphology was quite variable even within the same developmental stage, which is possibly due to variability between different differentiation batches.

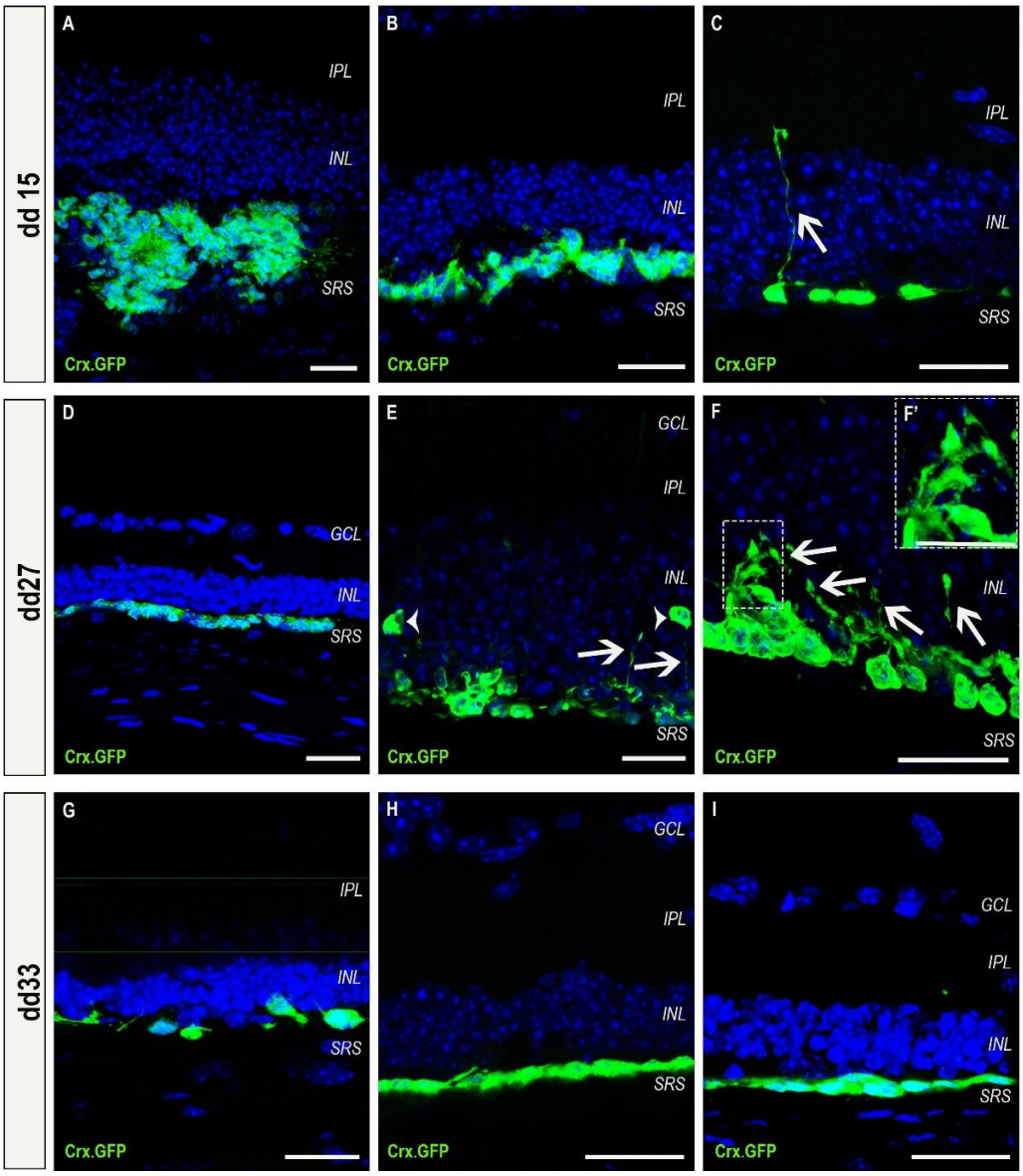

Figure 45 – mESC-derived Crx.GFP photoreceptor precursors, 3 weeks following transplantation of 800,000 cells, into *Aipl1*$^{-/-}$ mice

Representative confocal images showing the variability in spread and morphology of mESC-derived Crx.GFP photoreceptors precursors 3 weeks following transplantation of 800,000 cells, at dd15 (A-C), dd27 (D-F') and dd33 (G-I). **(A)** Cells transplanted at dd15 showed, occasionally, formation of rosettes in areas where the cell mass was denser. **(B)** Rosette formation was not seen in areas where the transplanted cells were spread apart, forming a less dense cell mass, at dd15. **(C)**Some cells transplanted at dd15 showed polarity, with a few cells extending processes into the host's INL (arrow). **(D)** Transplanted dd27 cells could be widely spread, covering a large area of the SRS and resembling an ONL of one or two nuclei in thickness. **(E-F)** Transplants showed several of the transplanted dd27 photoreceptors extending processes into the host's INL (arrows). A few transplanted photoreceptors could be seen displaced within int host's INL (arrowhead). **(G-I)** Transplanted eyes with cell mass of dd33 cells showed consistent cell morphology. Cell masses where widely spread, one to two nuclei thick and cells displayed a round or elongated morphology with no identifiable cell polarity or extension of process into the host's INL. (Scale bar 25µm; F' Scale bar 12.5µm)

The success rate was not greatly impacted by the increase in number of transplanted cells (48% vs 45%, transplanting 200,000 vs 800,000 cells, respectively), considering the biological variability inherent to these experiments. Furthermore, it appeared that when successful, transplants that received more cells led to bigger cell masses where cells appeared to extend more processes towards the host's INL. Consequently, it was decided that increasing the number of transplanted cells was likely to lead to better outcomes Therefore, all the results shown from this point on, in this chapter, were performed by transplanting 800,000 mESC-derived photoreceptor precursors into the subretinal space of 3-4 months old *Aipl1*$^{-/-}$ mice.

4.3.1.2 Characterisation of photoreceptor maturation and host interaction following transplantation of 800,000 mESC-derived photoreceptors into Aipl1$^{-/-}$ *mice*

Having established that the spread of cells in the subretinal space and cell morphology were quite variable between developmental stages, other differences were identified. The morphology and maturation, following transplantation, of photoreceptor cells of each developmental stage was evaluated by immunohistochemistry.

Since the majority of transplanted cells were rod photoreceptor precursors, which are more abundant in the mESC-derived retinal EBs, presence of Rhodopsin was used as a maturation marker. Rhodopsin, an essential protein for phototransduction, is localised to the outer segment region of mature rod photoreceptors, providing evidence regarding outer segment development. Cells transplanted at dd15 displayed areas where cells spread widely in the subretinal space, forming small clusters of GFP-positive cells. Such areas were rare and few of the transplanted photoreceptors were positive for Rhodopsin, presenting this protein throughout the cell body and not restricted to an outer segment-like region (Figure 46A). *In vitro* outer segment formation has not yet been demonstrated, as mESC-derived retinal EBs lose their structural integrity before such level of maturation is achieved (Goh, 2016). Interestingly, at dd15 in areas where rosette formation was observed, Rhodopsin was present and localised to restricted regions of outer segment-like structures. The outer segments grew towards the centre of the rosette (Figure 46B). These results demonstrate that the rod photoreceptors generated by this protocol are capable of further maturation and outer segment formation. However, to achieve such development *in vitro* culturing conditions need to be optimise. Rosette formation was frequently observed in eyes that received cell at dd15 but absent in eyes that received cell at a later stage of development. Cells transplanted at dd27 appeared to spread widely and evenly in areas of the subretinal space, in a single cell ONL-like

conformation. Most cells transplanted at dd27 presented Rhodopsin in their cell bodies and cell membranes (Figure 46C), but no outer segment-like structures were found (Figure 49). Similar cell mass conformation was seen in eyes which received dd33 mESC-derived photoreceptor precursors. However, unlike what was seen for cells transplanted at dd27, only a few Rhodopsin-positive cells were found. No localisation of this protein to outer segment-like structures were observed (Figured 46D).

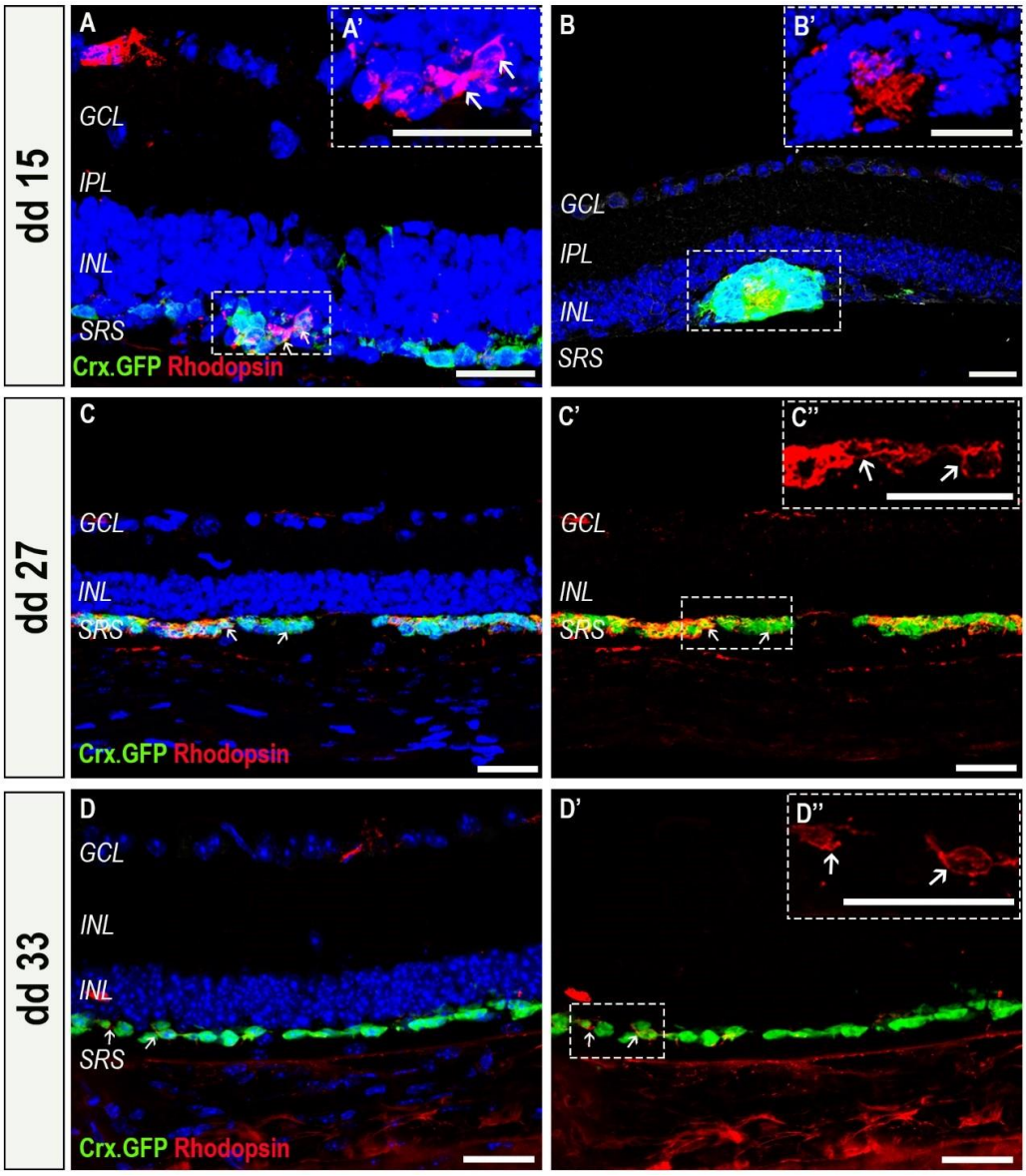

Figure 46 - Rhodopsin as a marker of cell maturation following transplantation of mESC-derived photoreceptor precursors at different developmental stages

Representative confocal images showing the presence of rhodopsin positive mESC-derived Crx.GFP photoreceptors, 3 weeks following transplantation of 800,000 cells, at dd 15 (A-B), dd 27 (C') and dd 33 (C). **(A)** In eyes where the cell mass spread in the SRS and no rosettes were formed, some of the cells transplanted at dd 15 stained positively for rhodopsin. Rhodopsin seemed to be present in the cell body and membrane of the transplanted cells (A'). Majority of the cells did not show presence of this marker. **(B)** Cells transplanted at dd 15 and that formed rosettes showed presence of rhodopsin positive structures, resembling OS. Staining was restricted to the OS-like structures in the centre of the rosettes (B''). **(C)** Majority of the cells transplanted at dd 27 were positive for rhodopsin, following transplantation. Rhodopsin was present in the cytoplasm and cell membrane, with no OS-like structures being identified (C''). **(D)** Few of the cells transplanted at dd 33 showed presence of rhodopsin in their cytoplasm and cell membrane (D''). (scale bar 25µm)

Cells transplanted at dd27 consistently showed some maturation, with majority of transplanted cells being positive for Rhodopsin (Figure 47).

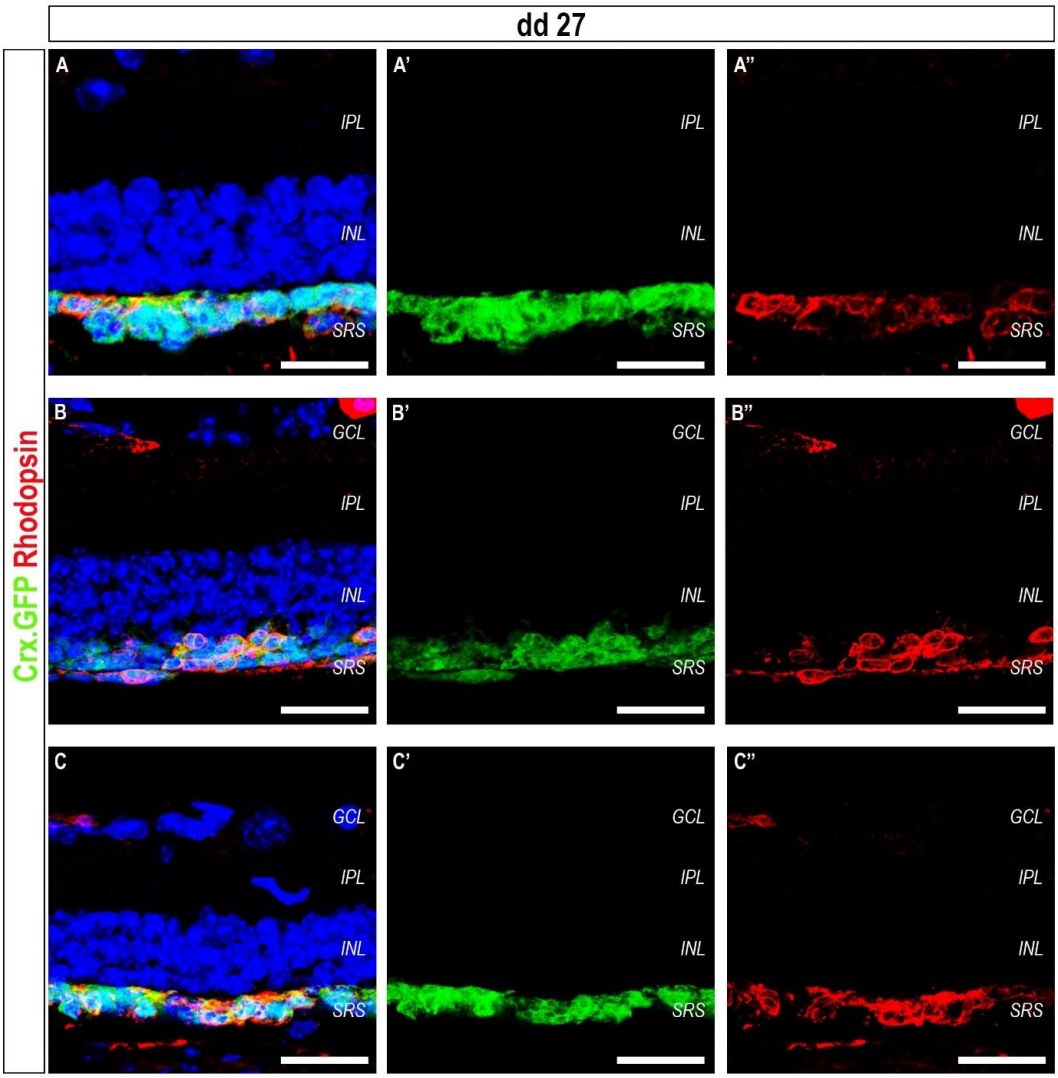

Figure 47 - Maturation of mESC-derived Crx.GFP photoreceptors transplanted at differentiation day 27

Representative confocal images showing maturation of majority of cells transplanted at dd 27, with cells being positive for rhodopsin 3 weeks following transplantation of 800,000 cells into *Aipl1*$^{-/-}$ mice. **(A-C)** Most of the cells transplanted at dd 27 were positive for rhodopsin. However, no OS-like structures were identified, with this protein being present in the cells' cytoplasm and membranes and not localising to an OS region. (Scale bar 25µm).

Maturation was also assessed by staining for Peripherin2 positive structures, indicating outer segment formation. Elongated Peripherin2 positive structures resembling outer segments were only observed in areas of rosette formation in cells transplanted at dd15 (Figure 48A). Similar to Rhodopsin, Peripherin2 positive outer segment-like structures were orientated towards the centre of the rosette. When cells were transplanted at dd27, rare Peripherin2 positive buds were identified (Figure 48B). These buds were extremely infrequent and only 2 out of the 16 eyes with cell masses displayed such structures. These buds were evidently different from what was seen in rosettes formed by dd15 cells, as they did not resemble a mature outer segment but rather an atrophic/underdeveloped one. No Peripherin2-positive structures were present in cells transplanted at dd33 (48C).

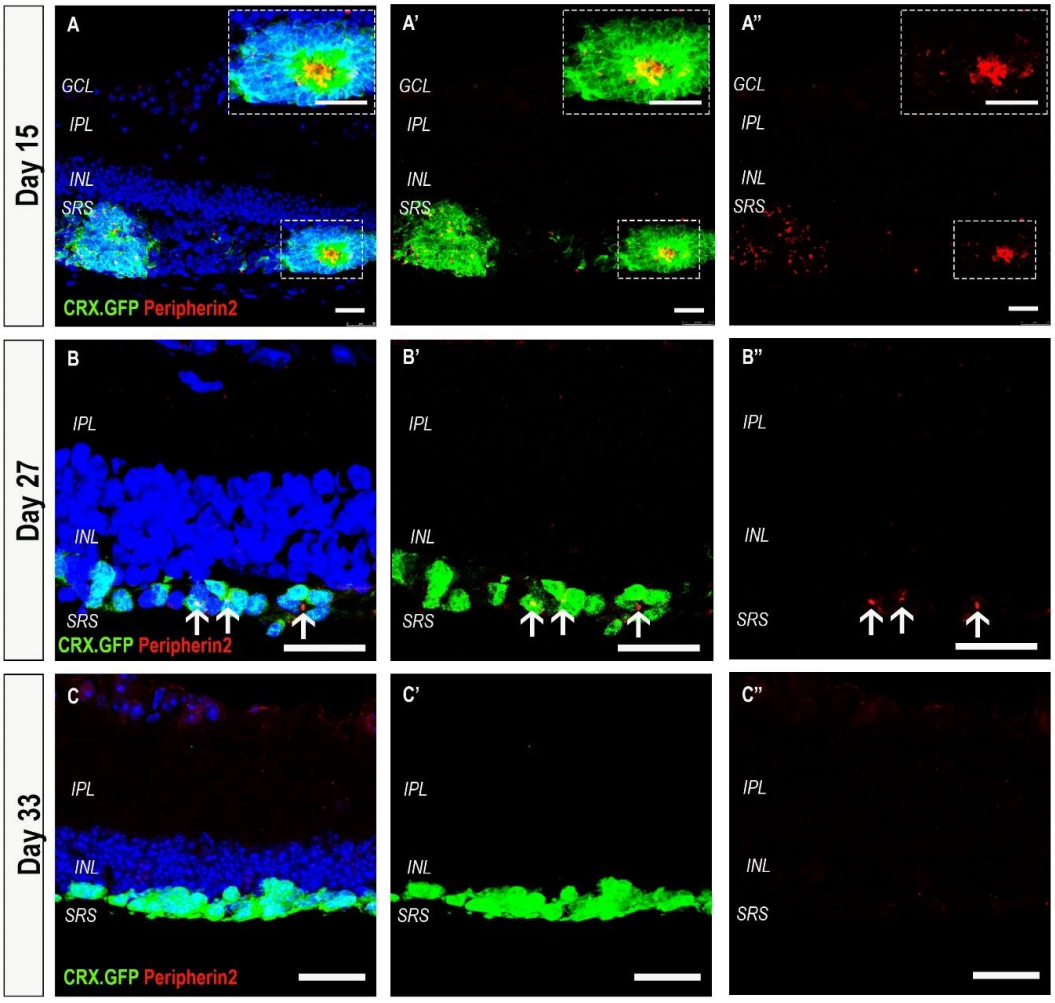

Figure 48 - Formation of Outer Segments following transplantation of mESC-derived photoreceptors

Representative confocal images of OS specific protein, peripherin2. **(A**) Long peripherin2 positive structures could be seen in cells transplanted at dd 15, exclusively in the centre of rosettes. **(B)** Very few of the cells transplanted at dd 27 developed peripherin2 positive buds, resembling an atrophic/underdeveloped OS-like structure (arrows). **(C)** No peripherin2 positive structures were identified in cells transplanted at dd 33, following transplantation. (Scale bar 25µm)

Following transplantation, dd27 was the developmental stage that showed best cell morphology, with several cells extending processes and displaying mature photoreceptor proteins, while no rosette formation was detected. Despite cell survival and maturation of cells transplanted at dd15, the rosette formation is not a desirable structure as it is not the natural arrangement of the retina and may prevent contact between host and transplanted cells. Therefore, dd27 was the stage chosen to analyse if synaptic connections between transplanted cells and host retina were established.

Transplanted cells showed Ribeye-positive structures (Figure 49A). However, there was no evidence of synaptic connectivity following staining for post-synaptic proteins. Presence of mGluR6 was difficult to evaluate, as the antibody seemed to bind to non-specific sites. Since mGluR6-positive structures did not co-localise with any of the PKC-α positive cells, it is likely that the majority of mGluR6-positive structures seen were due to background staining (Figure 49B). Samples were also stained for PSD95, another post-synaptic marker. No PSD95 positive structures were identified (Figure 49C). The evaluation of presence of this marker was not clear, as the antibody is raised in mouse and it seemed to bind to both host and transplanted cells.

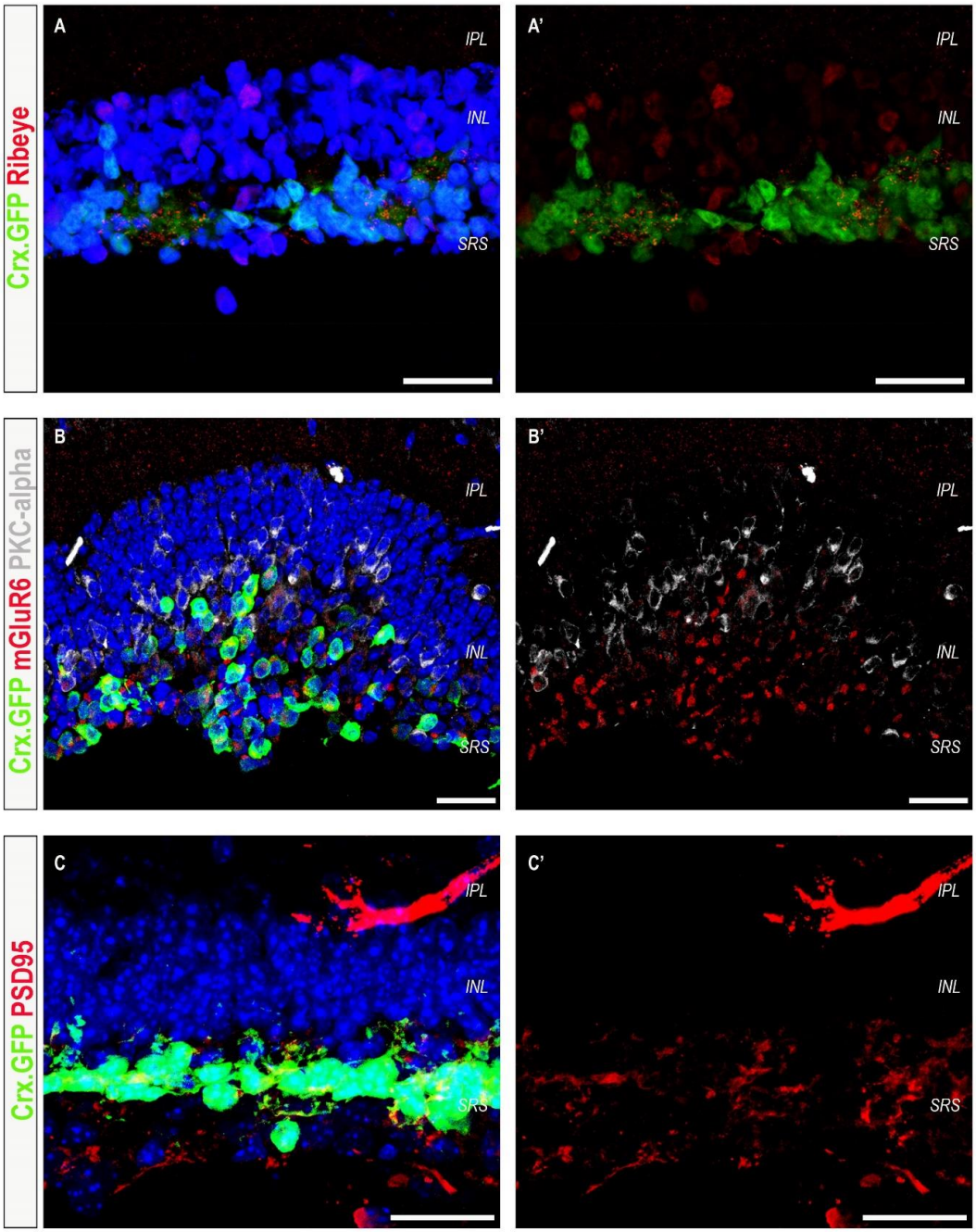

Figure 49 – Synaptic markers following dd 27 mESC-derived photoreceptor cells

Representative confocal images of pre-synaptic marker, Ribeye; post-synaptic marker mGluR6 and bipolar cell marker, PKC-α, as a reference to localise the synaptic marker to post-synaptic cells; and post synaptic marker PSD95. **(A)** Pre-synaptic protein Ribeye was present in some of transplanted cells. **(B)** Dotted pattern of mGluR6 positive structures can be seen in the IPL of the host. Positive mGluR6 staining was detected in the cell mass but did not co-localise with PKC-α positive rod bipolar cells. **(C)** PSD95 marker was detected in the subretinal space. As the antibody is anti-mouse, the host's blood vessels stained positively. (scale bar 25µm)

Additional optimisation of post-synaptic markers, as well as bipolar cell markers is required to determine with more certainty if the host retina is remodelling in response to the transplanted mESC-derived photoreceptors.

To further evaluate if the host retina reacted to the presence of transplanted photoreceptor cells, GFAP and PKC-α staining was performed. The activated Müller glia, also seen in un-injected 3 month old *Aipl1*$^{-/-}$ mice (see Figure 31), extend into the cell mass (Figure 50). However, no glial scar between host retina and transplanted cells was observed. Rare rod bipolar cells seem to extend short processes into the cell mass (Figure 50 A').

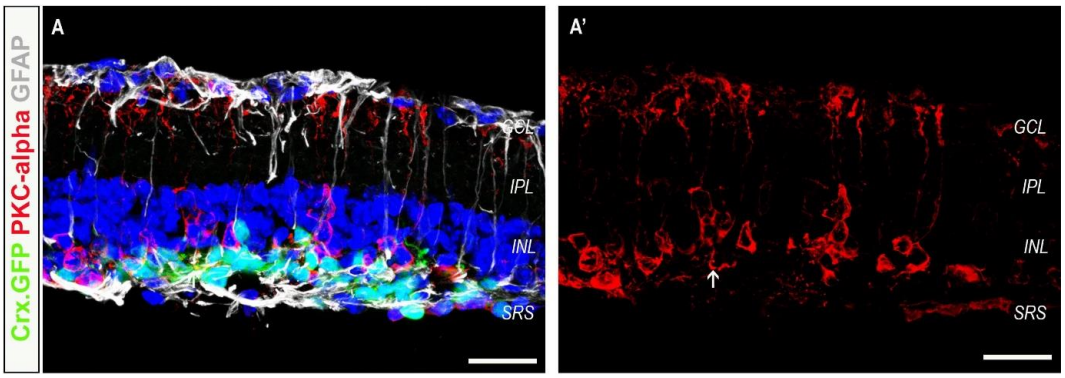

Figure 50 - Host Retina following Transplantation of dd27 mESC-derived photoreceptors

Representative confocal images with rod bipolar cell marker, PKC-α, and activated Müller Glia cell marker, Glial fibrillary acidic protein (GFAP). **(A)** Following transplantation, the Müller glia cells become activated and seem to engulf the cell mass. Rare rod bipolar cells appear to extend short post-synaptic processes towards the cell mass (arrow) (A'). (Scale bar 25µm)

Some animals that received dd27 photoreceptor precursors were kept until six weeks post-transplantation (n = 4 eyes, N= 4 animals, N = 2 differentiations). Only 1 of the 4 transplanted eyes showed a small number of surviving cells, but unlike what was seen at 3 weeks post-transplantation, the maturation marker, Rhodopsin, was not detected (Figure 51A). Some of the rare surviving cells that developed processes seem to preserve the pre-synaptic marker, Ribeye (Figure 51B).

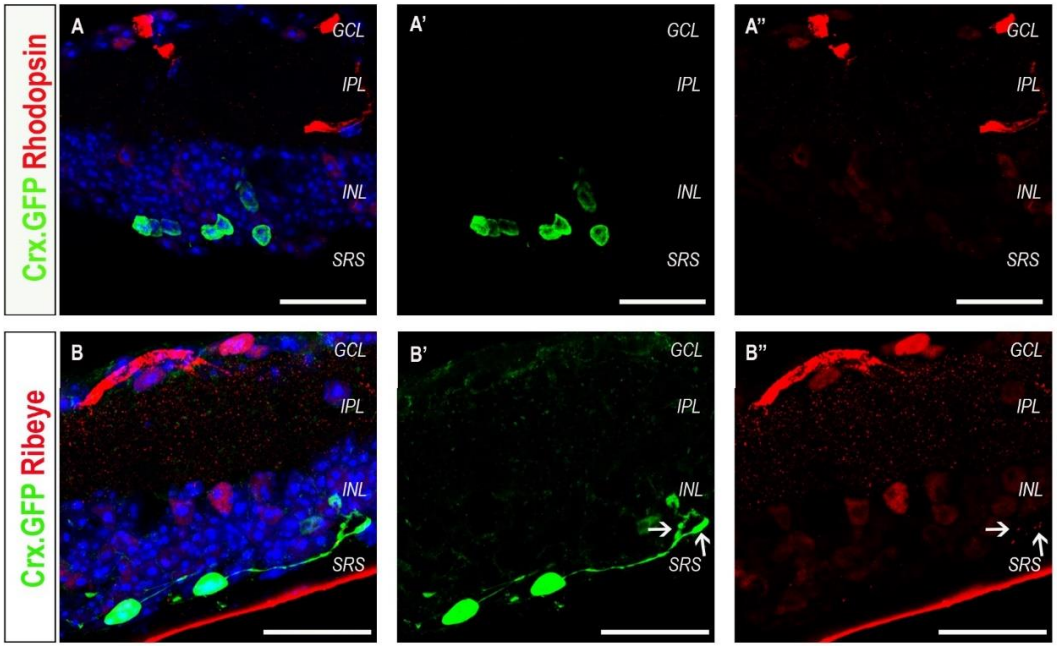

Figure 51 - mESC-derived Crx.GFP dd 27 cells, 6 weeks following transplantation

Representative confocal images of dd 27 cells, 6 weeks following transplantation. **(A)** Absence of rhodopsin in transplanted cells. **(B)** Ribeye was present in the synaptic pedicle of some of the transplanted cells (arrows). (Scale bar 25µm)

No functional analysis was attempted for these transplantation experiments due to the high failure rate and the immunohistochemistry data that did not show promising results regarding establishment of synapses or outer segment formation. The low intensity of the Crx.GFP signal made it very unreliable to identify the cell mass without staining and amplification of the signal. This was an impediment for MEA experiments, that depend in identification and correct placement of a GFP-positive area over the electrode array.

In brief, mESC-derived photoreceptors survive in the subretinal space of 3 month-old *Aipl1*$^{-/-}$ mice. Increasing the number of transplanted cells from 200,000 to 800,000 did not seem to greatly impact the transplantation success rate. However, it did appear to impact the morphology and cell maturation following transplantation. From the 3 differentiation stages analysed, dd27 appeared to be the best source of photoreceptors precursors. Cells transplanted at this developmental stage showed cell survival and maturation, extending processes towards the host retina, without rosette formation. The high failure rate, with less than 50% of the transplanted eyes presenting cell mass following transplantation, made analysis of retinal and visual function impractical. Furthermore, the variable cell morphology and the extremely rare and underdeveloped/atrophic outer segment-like structures indicated that improvement in visual function following transplantation would be unlikely.

4.3.2 Transplantation of dissociated hESC-derived cone photoreceptor precursors

With the aim of transplanting a pure population of hESC-derived cones it was necessary to consider that only 18% of cells in hESC-derived retinal organoids are cone photoreceptor cells (Gonzalez-Cordero et al., 2017). Since viral transduction is required for these cells to express the GFP protein, which is used to isolate them by FACS, is realistic to assume that only a portion of those 18% of cells will actually be isolated. Consequently, the number of required organoids to transplant 800,000 hESC-derived cones per eye would be impractical. Therefore, it was decided that ~500,000 hESC-derived cone photoreceptors would be transplanted into the subretinal space of 3-4 month old *Aipl1*$^{-/-}$ mice.

The RB2 hESC line was maintained, differentiated, dissociated, sorted and injected as previously described. Cells were labelled with GFP using a ShH10.2.1eGFP virus which specifically labels L/MOPSIN and a few S-OPSIN positive cone photoreceptors, at dd90 (see section 3.2 - 3.4) (Gonzalez-Cordero et al., 2018, 2017). Three to four weeks following viral infection, cells were dissociated. The percentage of isolated GFP positive hESC-derived cone photoreceptors was 9% ± 4.3%, measured by FACS experiments. A total of 9 eyes received hESC-derived cones at dd120, in over 6 independent experiments with 4 different batches of differentiations. Due to the effort and time required to grow hESC-derived retinal organoids no other developmental stages were tested. The stage chosen took into consideration the previous study where it was shown that at this stage cells are post-mitotic and fully committed to a cone photoreceptor fate (Gonzalez-Cordero et al., 2017). Furthermore, in some instances 2 or 3 batches of differentiations were combined per experiment, in order to achieve the number of cells required (n = 9 eyes, N = 9 animals; N = 6 injection days).

Eyes were collected 3 weeks following transplantation for immunohistochemistry (n=6) or MEA analyses (n=3). From the 3 eyes collected for MEA, only 2 had GFP-positive cell masses and 3 out of the 6 eyes collected for immunohistochemistry studies showed GFP-positive cells. Therefore, the success rate of transplantation (number of injected eyes that show cell mass of transplanted cells 3 weeks following transplantation) was 56%, which is consistent with what was previously reported when transplanting 100,000 cells per eye (Gonzalez-Cordero et al., 2017). This is further supporting evidence that increasing the number of cells injected does not appear to have a detrimental impact in transplantation success rate.

The transplanted cells formed a layer adjacent to the host INL. The amount and spread of these cells were variable (Figure 52), possibly due to quality of injection. Areas of thick layers of transplanted cells, consisting of more than 3 nuclei in thickness, could be identified in all the samples containing cell mass following transplantation. However, not all samples showed such a widespread area of cells as the one seen in Figure 52.

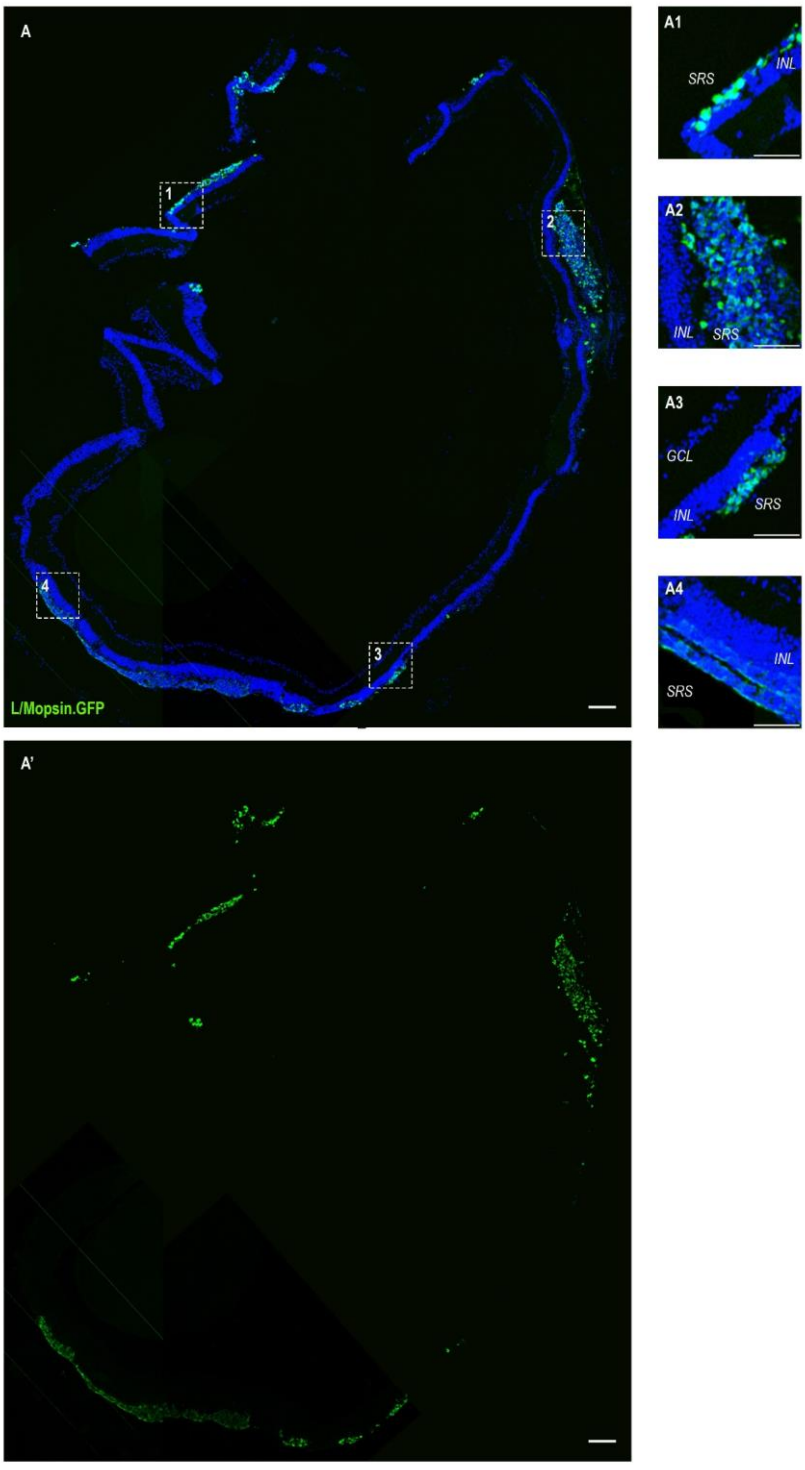

Figure 52 – Spread of hESC-derived cone-only cell mass in subretinal space of *Aipl1*$^{-/-}$ mice, 3 weeks following transplantation

Confocal image showing presence of L/Mopsin.GFP positive cells in the subretinal space of 3 months old *Aipl1*$^{-/-}$ mouse, 3 weeks following transplantation, representing the possible spread. **(A)** Wide spread of the cell mass occupying almost the entire eye circumference. GFP+ cells were more clearly seen in A'. Areas of few isolated single-cell spread (A1), layers over 5 cells thick (A2), layers of under 3 cells thick (A3) and continuous single-cell spread cell mass (A4) adjacent to the host's INL could be identified. (Scale bar 100µm, A and A'; 50µm A1-A4)

Next, the presence of pre-synaptic protein RIBEYE was analysed to confirm if the hESC-derived cones displayed the potential of forming synapses with the host retina. Interestingly, the presence of RIBEYE appeared to depend on size and spread of the cell mass (Figure 53). Isolated cells in the subretinal space were not positive RIBEYE (Figure 53A) while cells in areas where the transplanted cells were grouped, even if in a single-cell layer, RIBEYE positive structures were present (Figure 53B). These cells occasionally extended cell processes towards the host's INL (Figure 53C-D) and at the tip of those processes RIBEYE-positive structures could be identified (Figure 53c-d).

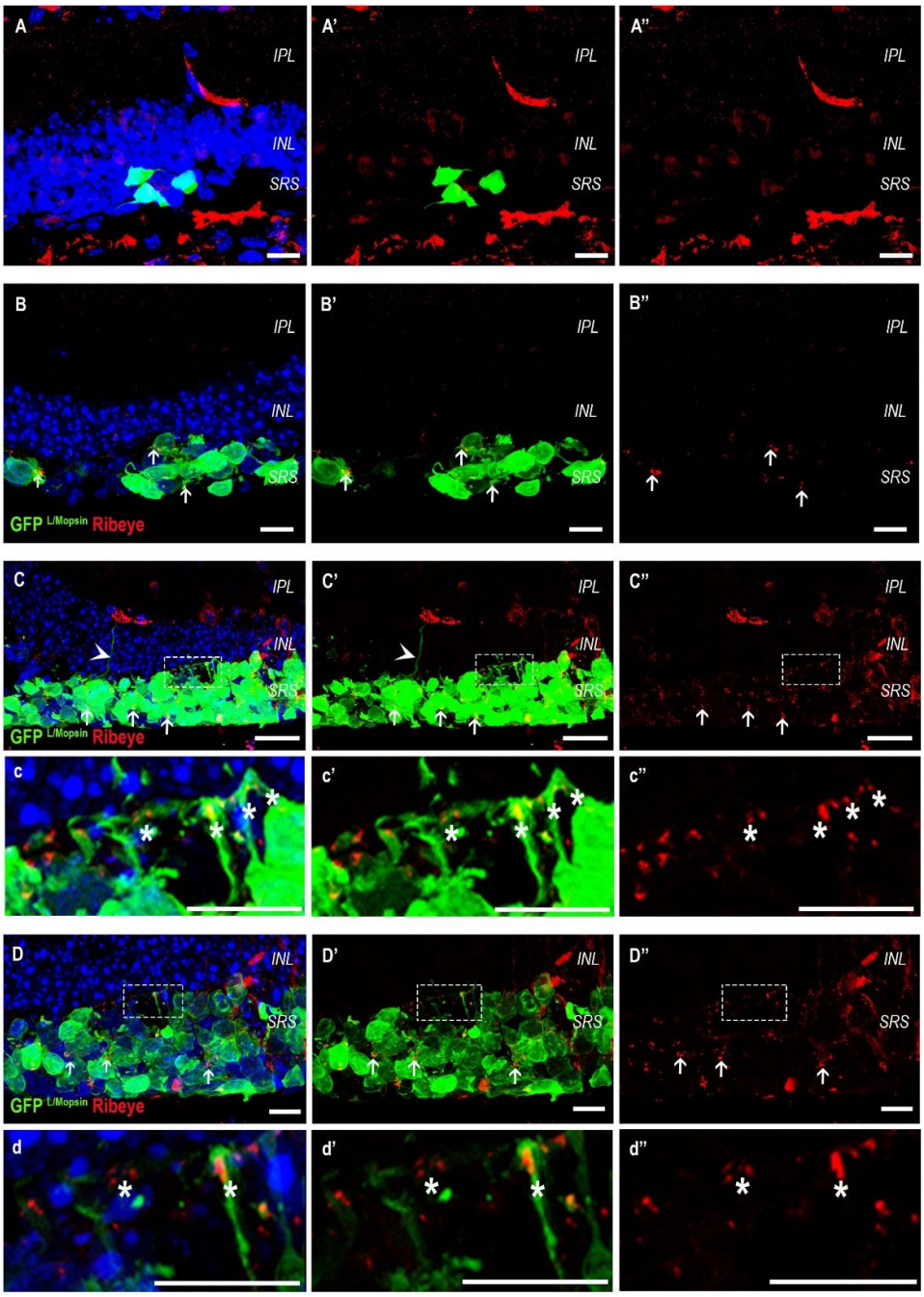

Figure 53 - Presence and localisation of pre-synaptic protein, Ribeye, in hESC-derived cones three weeks following transplantation into *Aipl1*$^{-/-}$ mice

Representative confocal projections showing presence of Ribeye and extension of processes into the host's INL, depending on the amount and spread of the transplanted hESC-derived cones following transplantation. **(A)** In areas where few hESC-derived cones were present no clear ribeye staining was identified. **(B)** In areas with a small cell mass, ribeye was present (arrows), even in cells forming a single-cell layer (arrow on the left). **(C-D)** Where the cell mass was denser more cells appear to be positive for ribeye (arrows) and occasionally extended processed into the host's INL (arrowhead) and in the tip some of those processes' ribeye could be found (dashed box area enlarged in c-d). (Scale bar 10µm, A, B, D and d; 25µm, C and c; 12.5µm).

Outer segment formation was used to assess photoreceptor maturation, by using specific marker PERIPHERIN2. Positive outer segment-like buds were identified and appear to be longer and more frequent in areas of dense cell mass (Figure 54).

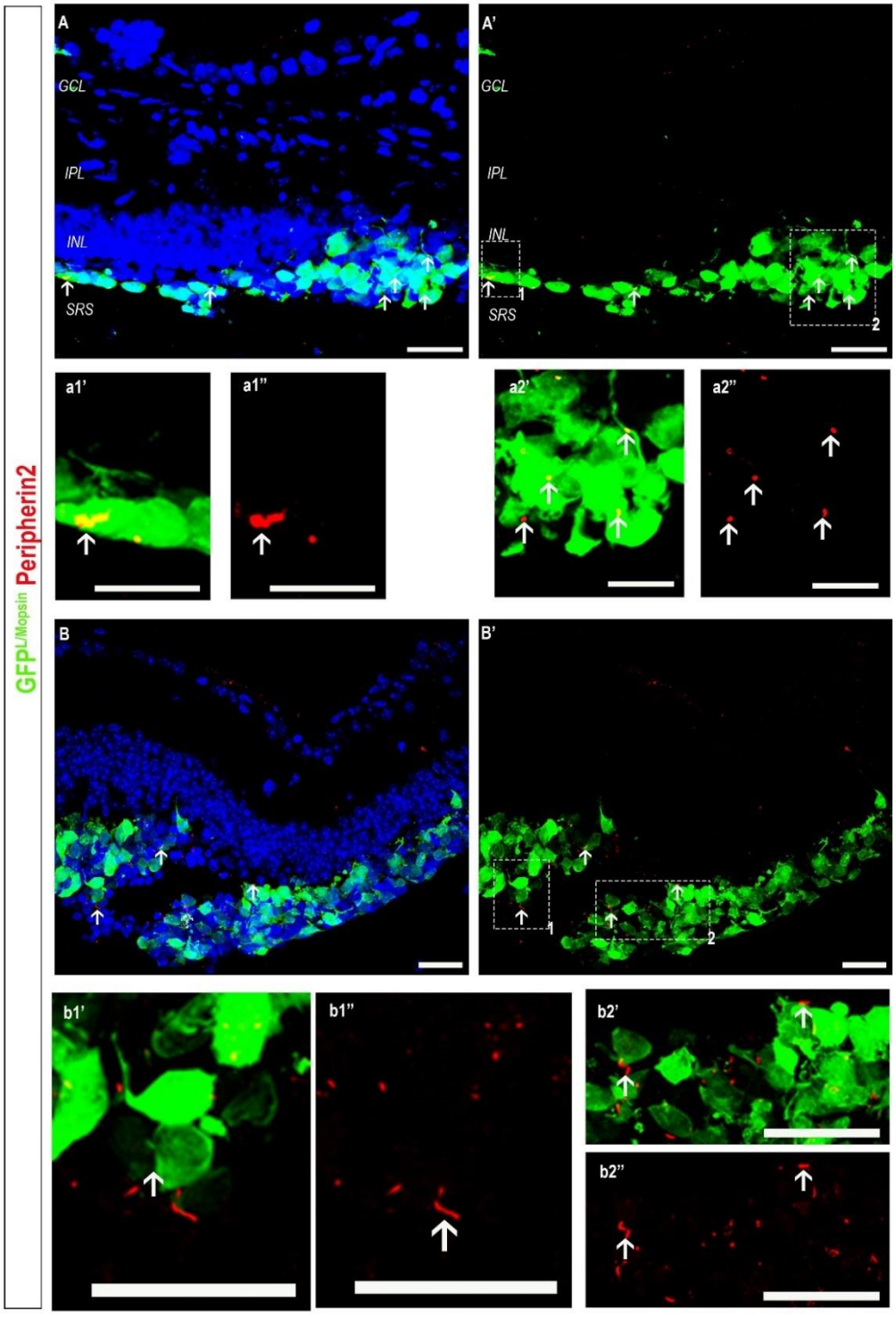

Figure 54 - Outer segment formation in hESC-derived cones following transplantation

Representative confocal projections showing presence of OS specific protein Peripherin2 in the transplanted hESC-derived cone photoreceptors. **(A)** In areas of large cell mass Peripherin2 positive buds was present, forming OS-like structures (arrows). These were more frequent and longer in areas where the cell mass was thicker (a2', a2'') but could also be found occasionally in cells where a single-cell layer of transplanted cones was seen (a1', a1''). **(B)** In large areas of dense cell mass most cells seem to develop the Peripherin2-positive buds (b1'- b2'') and several longer OS-like structures could be identified (arrows). (Scale bar 25 µm)

Interestingly, three weeks following transplantation L/Mopsin protein observed by immunohistochemistry was still present throughout the cytoplasm (Figure 55, Magenta) and not localised just to the outer segment-like regions as in mature cone photoreceptors. It is important to note that GFP expression is driven by an L/Mopsin promoter, but it is not linked to the L/Mopsin protein, therefore we would not expect to see GFP becoming localised to a specific area within the photoreceptor cells.

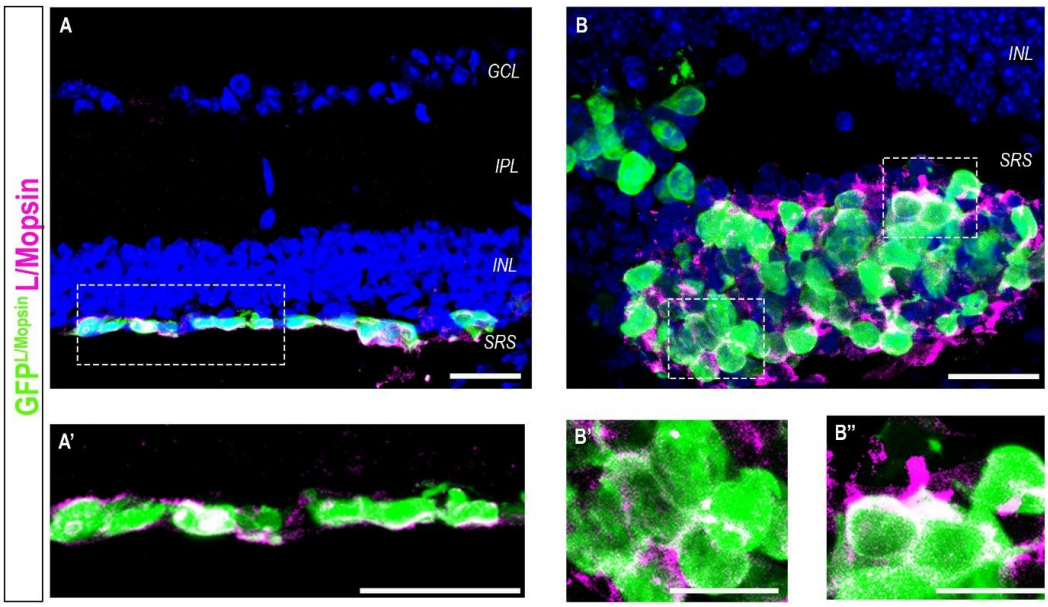

Figure 55 - Presence of L/Mopsin in hESC-derived cones following transplantation

Representative confocal projections showing the distribution of transplanted hESC-derived cone photoreceptors. **(A)** In areas where the transplanted cones formed a single-cell layer L/Mopsin protein was located in the cells' cytoplasm and membrane (A'). **(B)** Similar distributions were seen in areas were transplanted cells formed large and dense cell mass, with L/Mopsin presence in the cells' cytoplasm and membrane. No L/Mopsin rich buds were identified. (Scale bar 25 µm)

Transplanted cone photoreceptors appear not only to survive and mature in the subretinal space, but also to induce changes in the host's retina. Rod bipolar cells extended long processes into the cell mass, something that was not seen in areas where fewer transplanted cells were present (Figure 56). These processes were absent in untreated 3 month old *Aipl1*$^{-/-}$ retinas as described in the previous chapter (Figure 28). Additionally, more mGluR6-positive structures were present in areas with larger cell masses (Figure 56), while they were mostly absent in untreated 3 month old *Aipl1*$^{-/-}$ animals (Figure 33). Some of the mGluR6-positive structures co-localised with PKC-α-positive processes, as this post-synaptic protein is expressed in rod bipolar cells. In one out of the three samples analysed by immunohistochemistry, the presence of mGluR6 protein and long PKCα-positive processes was not detected. Interestingly, this eye presented a smaller cell mass than what was found in the other 2 samples. Similarly, in eyes that did have a larger cell mass, mGluR6 protein and long PKCα-positive processes were not observed in the areas without transplanted cells or in areas with very few transplanted cells (Figure 56B). Presence of mGluR6-positive structures that did not co-localise with PKC-α was not unexpected, as this protein is also expressed in cone bipolar cells which are not positive for PKC-α. The lack of a suitable marker for cone bipolar cells makes the assessment of potential contacts between host bipolar cells and transplanted hESC-derived cones incomplete.

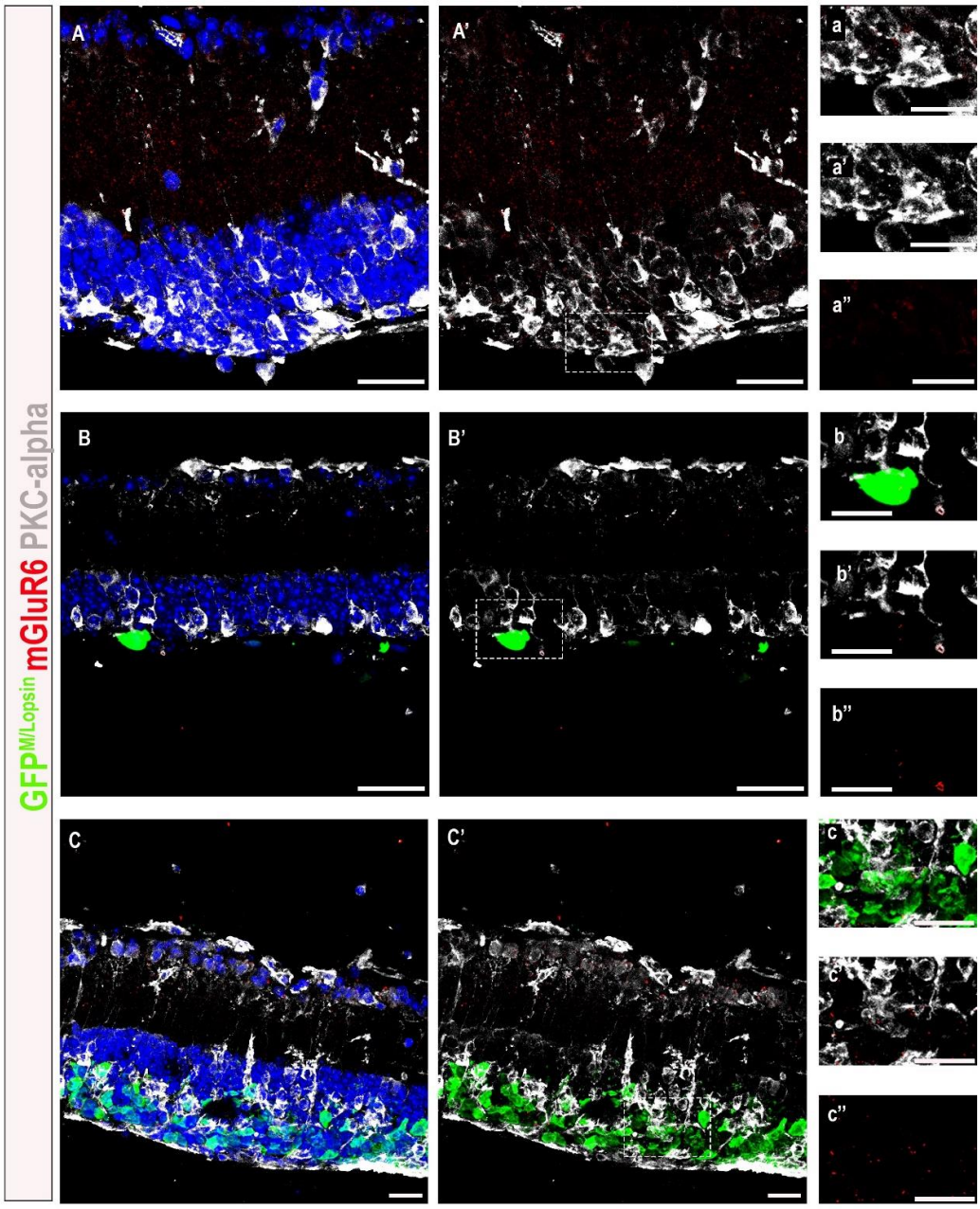

Figure 56 - Interaction between host *Aipl1*$^{-/-}$ retina and transplanted hESC-derived cones, 3 weeks following transplantation

Representative confocal projections identifying rod bipolar cells (PKCα-positive) and post-synaptic protein mGluR6. **(A**) mGluR6 post-synaptic receptor in an un-injected eye, showing a dotted pattern in the IPL but no signal was detected in close proximity to PKC-α positive cells. **(B)** Similar findings were true for areas of transplanted eyes where few hESC-derived cones were found, where signal for mGluR6 receptors was mostly absent in the OPL. Rare PKCα-positive processes colocalising with mGluR6 were present (b', b''). **(C)** mGluR6-positive structures were more abundant in areas of larger cell mass. Several rod bipolar cells extended processes into the cell mass (C')). Some of the mGluR6-positive structures co-localized with the PKCα processes, showing correct location of the post-synaptic protein (c'-c'''). (Scale bar 25µm, A-C'; 12.5µm a'-c''')

The extension of PKCα-positive processes and mGluR6-positive structures into areas with larger cell masses was consistent between samples (n=2 eyes, N=2) and between different areas of each sample (Figure 57).

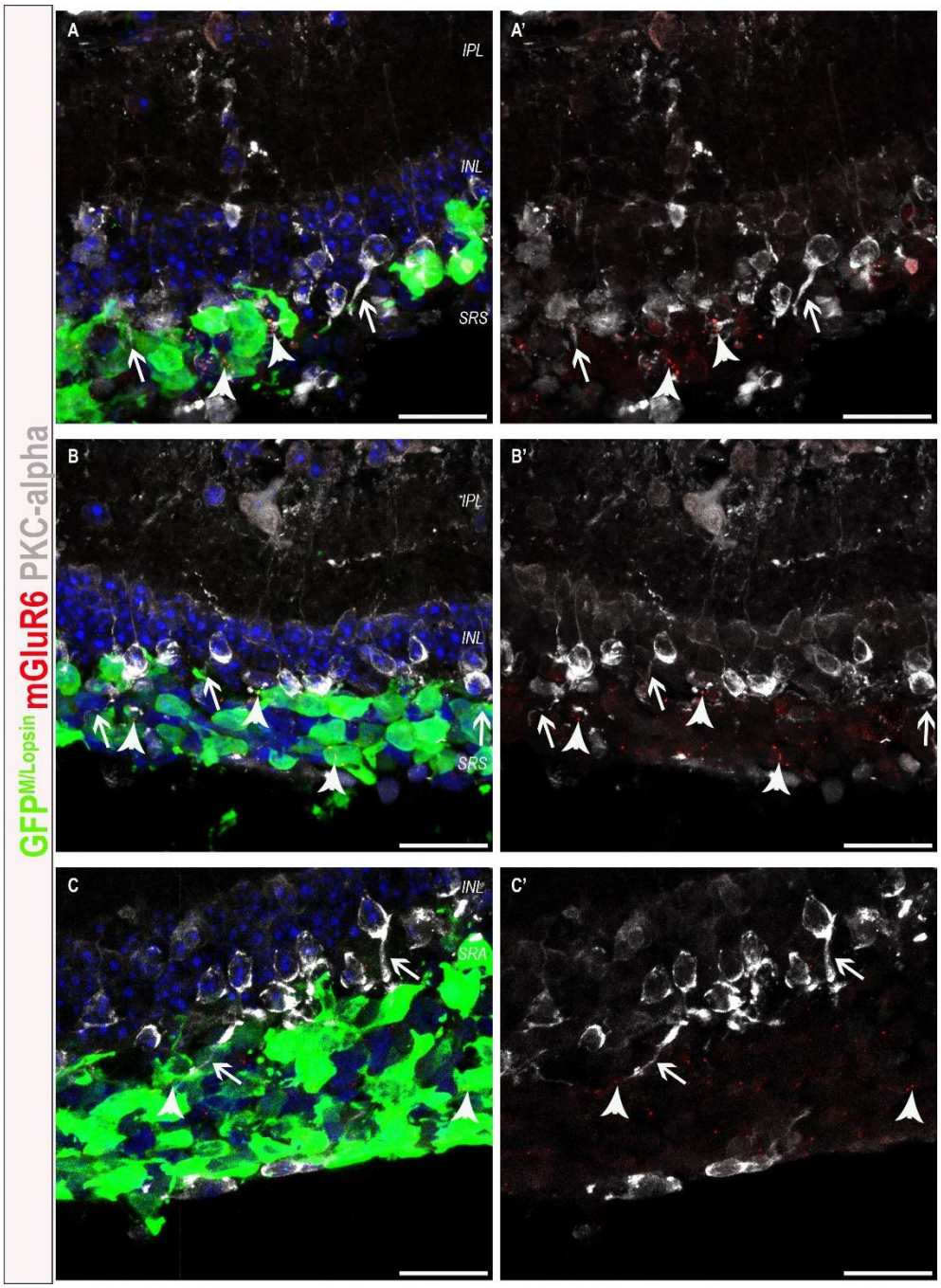

Figure 57 - Interaction between host *Aipl1*$^{-/-}$ retina and transplanted hESC-derived cones in areas with large cell masses, 3 weeks following transplantation

Confocal projections showing presence of rod bipolar cell processes (PKCα-positive) and post-synaptic protein mGluR6 in areas where transplanted hESC-derived cones formed a large cell mass in the subretinal space. mGluR6-positive structures were abundant in areas with larger cell masses (arrowheads). Rod bipolar cells extending processes into the cell mass was consistently seen across different samples and different areas within the same eye (arrows). (Scale bar 25µm)

Some of the mGluR6-positive structures were in close proximity to RIBEYE-positive structures which could suggest that some synaptic connections might be forming (Figure 58). These synaptic markers do not display the pattern seen in wild type retinas (Figure 26 A, B), but the orientation of the cell might be essential to recognise such pattern. Therefore, despite encouraging, this data does provide unambiguous proof of connections between host and graft, and if these are typical ribbon synapses.

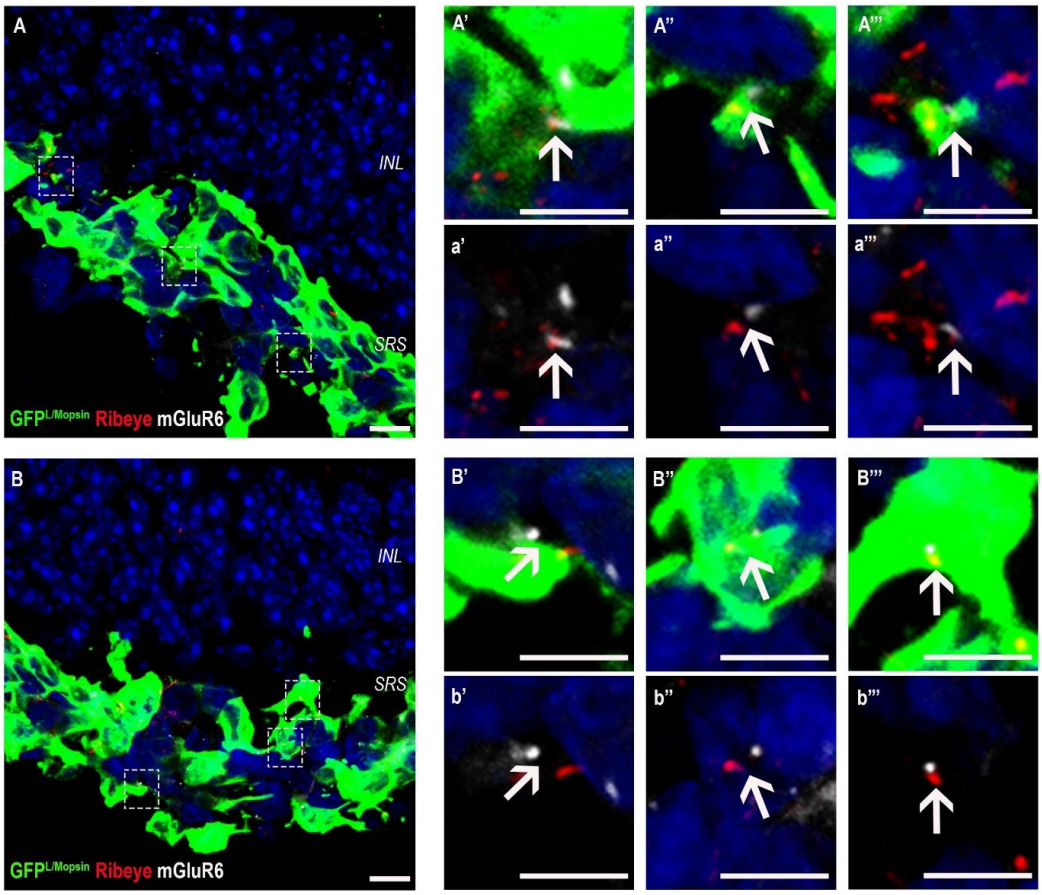

Figure 58 – Synaptic markers and possible connections between host and transplanted cells

Confocal projections showing presence of pre-synaptic protein Ribeye and post-synaptic protein, mGluR6 in areas where transplanted hESC-derived cones formed a large cell mass in the subretinal space. **(A, B)** Ribeye-positive structures present in transplanted hESC-derived cones were, occasionally, found in close proximity to mGluR6- positive structures. This is highlighted in the panel on the right (A'-B''') (arrows). Some of these structures seem to co-localise (A', B'''), by removing the GFP channel this becomes more evident (a', b'''). (Scale bar 10µm A, B; 5µ, A'-b''')

4.3.2.1 Assessing visual function following transplantation of hESC-derived cone photoreceptors

Prior to sacrificing the animals and collect the eye for immunohistochemistry analysis, ERGs, optomotor and LOOM experiments were performed (N = 6 animals). These experiments aimed to assess if retinal function and vision could be rescued following transplantation. Each animal only had one treated eye, with its un-injected acting as a control, to establish the internal base line of each animal. Eyes were randomly distributed at time of injection, with the author being unaware of which eye received cell transplantation.

4.3.2.1.1 ERGs

ERGs recordings were performed, by Justin Hoke and Aura Hare, at three weeks following transplantation, as described in the methods section (see 2.11.1). Electrodes were places in the corneas of both eyes and the changes of electrical potential, upon a light stimulus were recorded. No initial negative deflection, characteristic of an a-wave, or positive deflection from base line, typical of a b-wave could be identified in any of the animals. No difference between injected, eyes where later cell mass was found, and un-injected eyes. The traces showed spontaneous fluctuation of voltage, as seen in p18 *Aipl1*$^{-/-}$ animals (Figure 34). These results are exemplified by a representative ERG traces, recorded under photopic conditions, where the right eye was injected and later showed presence of large cell mass while the left eye of the same animal was not injected (Figure 59).

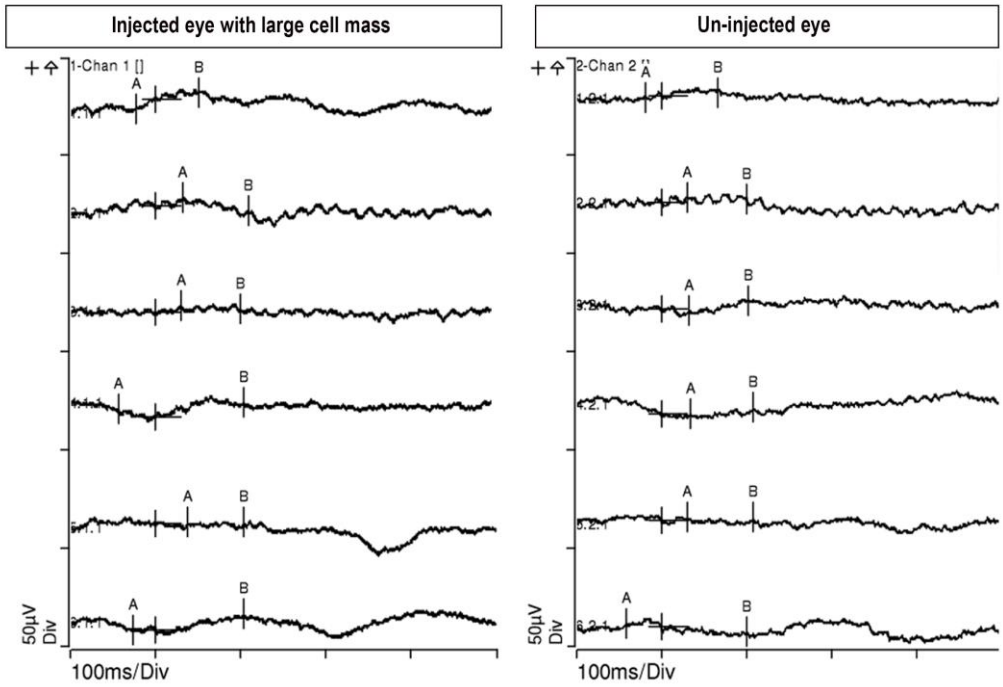

Figure 59 - Representative ERG trace under photopic conditions three weeks following transplantation of hESC-derived cones into *Aipl1*$^{-/-}$ mice

No a or b wave could be identified in the injected and un-injected eyes.

4.3.2.1.2 MEA

All MEA experiments were performed and analysed by Dr Christopher Procyk.

Only in two out of the three eyes collected for MEA analysis, a GFP positive cell mass was identified. However, one of those samples resulted in a null experiment, since the retina showed no spontaneous spiking. RGCs spontaneously spike and those electrical events are necessary to guaranty that the retinal is healthy at the time of recording. Since no spontaneous spiking was detected it was assumed that the retina was no longer alive by the time the recording started. This is most likely due to lack of oxygen supply during the preparation of the retina. Eyes with end stage degeneration tend to present with a thick vitreous which makes the removal of the retina and isolation of GFP positive areas more difficult. Despite frequent exchange of media, providing oxygenated solution, this sample did not survive the process. The other retina used for MEA experiments showed spontaneous spiking and ipRGC-derived light responses, which were used as an internal control for the viability of the retina and quality of the preparation. However, no obvious photoreceptor-like responses were detected in the raw data. Therefore, due to the time necessary to analyse MEA data, no further analysis was performed, with Dr Christopher Procyk's efforts being focused on the MEA analysis described in chapter five.

Summarising, hESC-derived cones survive in the subretinal space of 3 month-old *Aipl1*$^{-/-}$ mice. The success rate of transplanting hESC-derived cones was 56%. The hESC-derived cones spread differently in the subretinal space, with some areas showing a single cell layer of transplanted cells while other areas showed dense cell mass comprised of several hESC-derived cones. Most transplanted cells had pre-synaptic structures, positive for RIBEYE, and some extended processes into the host's INL. A proportion of transplanted cells matured following transplantation, presenting outer segment-like structures, positive for PERIPHERIN2. However, MOPSIN did not show such localisation, being present throughout the cell body of the transplanted cells. The host retina appears to react to the presence of hESC-derived cones, with rod bipolar cells extending processes deeply within the cell mass, strictly in areas where the cell mass was dense. Post-synaptic protein mGluR6, that was not seen in untreated 3-month-old *Aipl1*$^{-/-}$ animals, could also be identified in areas where a large/dense cell mass was present. Yet, no functional or visual rescue was detected. However, an increase in the number of samples with cell mass following transplantation is required in order to perform a more complete study of functional rescue.

4.3.2.1.3 LOOM Test

Videos of injected and un-injected *Aipl1*$^{-/-}$ animals were masked and analysed as described in the methods chapter (see 2.11.4). None of the animals showed changes in behaviour (freeze, flee or rearing) in response to the LOOM stimulus, which is a visual cue simulating a predator approaching. Even mice with eyes where later cell masses were found displayed, 5 out of the 6 tested animals, no changes in behaviour were observed. This was similar to what had been seen in age-matched un-injected *Aipl1*$^{-/-}$ mice, (See chapter 3, Figure 38).

4.3.2.1.4 Optomotor

Optomotor test allows evaluation of function of each eye from the same mouse separately, as the orientation of the rotation patter triggers a response derived exclusively from the right eye (anti-clockwise rotation) or left eye (clockwise rotation). Depending on the experimental conditions, both contrast sensitivity and visual acuity can be assessed. For this project it was decided to test contrast sensitivity, under photopic conditions using a special component stimulus of 0.128 cycles per degree (c/d). These same conditions were used in chapter 3 to characterise 3-month-old *Aipl1*$^{-/-}$ mice, which did not display a measurable contrast sensitivity, above random calibration range. Experiments were performed blinded to which eye was treated and showed no statistically significant difference between treated and untreated eyes (1way ANOVA) (Figure 60). One of the two eyes where a large cell mass was found later, mouse number 6, seemed to perform marginally better than the un-injected eye of the same animal (see box in Figure 60). To analyse specifically those eyes where a bigger cell mass was found, a t-test was conducted. No statistically significant differences were found. Furthermore, the results obtained were still within the range of random calibration (Figure 60).

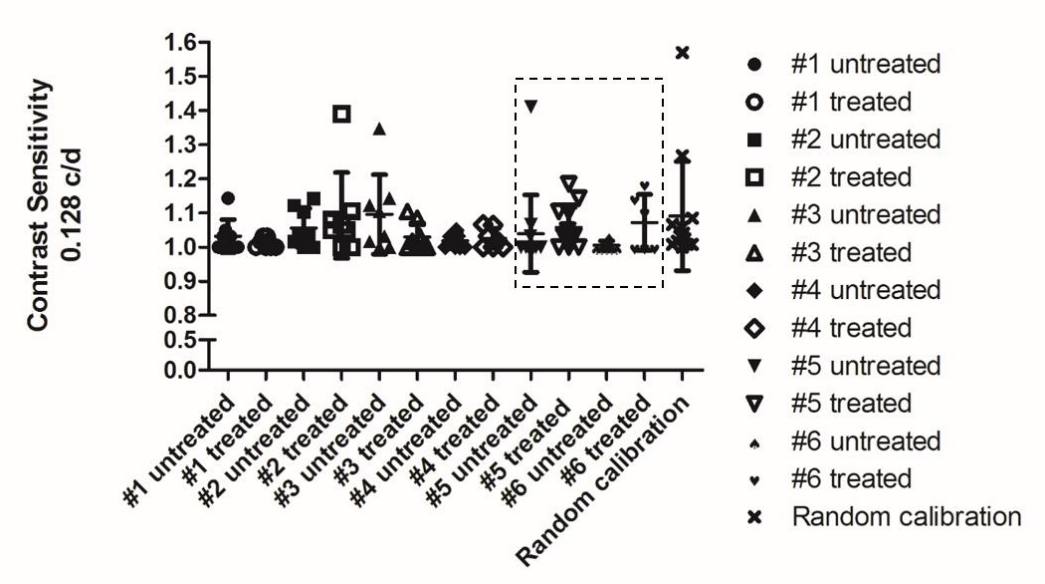

Figure 60 - Contrast sensitivity following transplantation of hESC-derived cone precursors

Contrast sensitivity, measured by optomotor, did not show a significant difference between treated and un-treated eye of the same animal. The treated eyes of mouse #5 and #6 (indicated by the box), were where larger cell masses were later found during immunohistochemistry analyses. All the values obtained in the injected animals were within the random calibration values.

4.3.3 Transplantation of hESC-derived retinal sheets

Currently there are two strategies, dissociated cells and retinal sheets, that different groups use in order to investigate if photoreceptor transplantation is a viable therapeutic strategy for retinal repair. However, no direct comparison between these two strategies has been reported, therefore hESC-derived retinal sheets were transplanted into 3 month old *Aipl1*$^{-/-}$ mice. These experiments hope to establish if different strategies lead to different transplantation outcomes. Retinal sheets were obtained by carefully dissecting the laminated neuroretinal layer from dd120 retinal organoids, under a light microscope. A needle blade microsurgical knife (Sharpoint) was used to cut these as accurately as possible, however variability in size (0.5-2mm diameter) and shape was inevitable. From a single hESC-derived retinal organoid up to 3 retinal sheets could be isolated. Retinal sheets were injected into the subretinal in a similar way to the dissociated cells, using up to 2µL of solution as a vehicle. A Hamilton precision glass syringe with an 8mm, 30-gauge needle were used to inject both eyes of 14 *Aipl1*$^{-/-}$ mice.

The success rate of transplantation of retinal sheets into 3 month-old *Aipl1*$^{-/-}$ mice was lower when compared with transplantation of dissociated cells. Only ~3% of the retinal sheet transplantation procedures were successful, with 1 out of 28 eyes showing GFP-positive retinal sheets in the subretinal space 3 weeks following transplantation. The retinal sheet was mainly formed of photoreceptor cells, as cells were positive for RECOVERIN, and a few GFP positive cones could be identified (Figure 61). Since the retinal sheets were dissected manually under a brightfield microscope, it is encouraging that the dissection appears to be mostly restricted to the photoreceptor layer of the NRVs. The donor cells did not seem to organise in layers or form rosettes, as previously publish by other groups (Iraha et al., 2018; Mandai et al., 2017a), most likely due to the short time between transplantation and collection of samples.

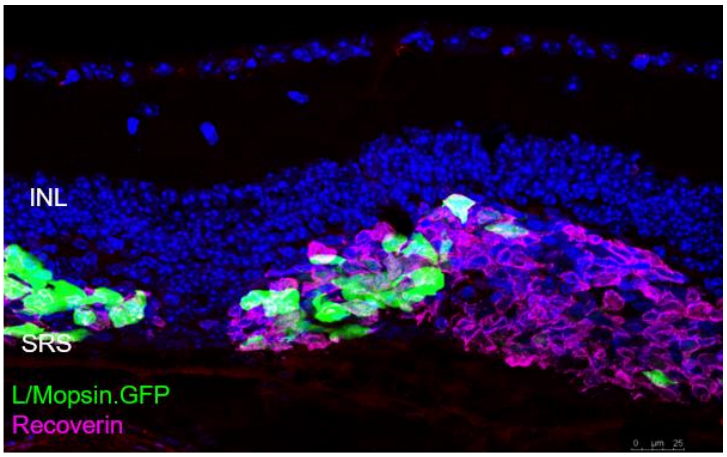

Figure 61 –hESC-derived retinal sheet, three weeks post-transplantation into a three-month-old *Aipl1*$^{-/-}$ mice

Representative confocal projection showing present of large hESC-derived retinal sheet in the subretinal space of a 3 month-old *Aipl1*$^{-/-}$ mouse. Most cells were positive for Recoverin. GFP-positive cones present. Cells did not show any morphological organisation and rosettes were not identified.

Is it unclear if the high number of unsuccessful transplants was the result of the hESC-derived retinal sheets being rejected, due to activation of the immune system or if the tissue refluxed out following injection. Unfortunately, further investigation regarding maturation of these cells, possible interaction between host interneurons and hESC-derived retinal sheet and possible activation of the host immune system was not possible. This is because the area where the retinal sheet was present was not spread across many of the cryo-sections. The sections that contained the retinal sheet were lost during the process of antigen retrieval required to unmask post-synaptic marker mGluR6 (see methods section 2.9.1). The presence of this synaptic marker was a priority, as it had not yet been described and could provide evidence for host/graft connections. Therefore, two out of three slides where a cell mass was present were used to try to stain for this marker and unfortunately were lost during the process.

Knowing that the failure rate is much greater when transplanting retinal sheets than when transplanting dissociated sorted cells, ~97%, versus ~45% respectively, it is imperative to improve cell survival. By improving the success rate, more samples could be collected, and a more complete characterisation would be possible. With the current success rate, it is not possible to compare transplantation of dissociated cells and retinal sheets, as there were not enough samples with transplanted retinal sheets to analyse cell maturation and expression of synaptic markers. Nevertheless, is fair to conclude that the surgical procedure for transplantation of retinal sheets is more complex requiring the use of a large gauge needle. As such, it results in more damage to the retina at the time of injection, which is likely to be a major contributing factor to the low success rate.

4.4 Conclusions

The work described in this chapter identified potential issues when transplanting photoreceptor cells into the severely degenerated retinas of *Aipl1*$^{-/-}$ mice. Some of the difficulties and results were expected, such as the complexity of the surgical procedure and the ability for both mESC and hESC-derived photoreceptors to survive in the subretinal space of this mouse strain, since previous studies had reported similar data (Gonzalez-Cordero et al., 2017; Kruczek et al., 2017). Regardless no detectable rescue of function being achieved the interaction seen between transplanted hESC-derived cones and hot retina were encouraging. Other studies have shown rescue of vision in advance degeneration mice, by transplantation of photoreceptor cells (see chapter 1.4 for further detail). However, all the studies performed in end-stage retinal degeneration used *rd1* mice as host for the transplantation. In *Aipl1*$^{-/-}$ mice both rods and cone degenerate at a faster rate, consequently the synaptic circuit and other remodelling events present a more severe phenotype at age of transplantation. The results described in this chapter suggest that despite the fast degeneration and severe remodeling seen in *Aipl1*$^{-/-}$ retinas by 3 months of age, cell transplantation might be able to reverse, at least some, of the remodeling events. Such findings present novelty and emphasise the potential of photoreceptor transplantation as a therapy for end-stage retinal degeneration.

4.4.1 Transplantation of dissociated mESC-derived photoreceptor precursors

Transplantation of a higher number of mESC-derived photoreceptor precursors, 800,000 instead of 200,000, led to larger cell masses with no major detriment to the transplantation success rate. These cell masses in many areas resembled an ONL composed of several rows of nuclei. Differentiation day 27 was shown to be the best source of photoreceptor precursors, not only taking into account the yield of photoreceptor precursors that could be sorted, but also the maturation of this cells following transplantation. For the CRX.GFP line, dd27 is within the established ideal developmental stage for transplantation, the equivalent of post-natal retina at day 4 to 8 (Goh, 2016; Gonzalez-Cordero et al., 2013). No quantification of number of cells present in the subretinal space following transplantation was performed. This is due to the morphology of the cells and density of cell masses which makes a manual quantification unreliable. This data could be collected by transplanting eyes and then collecting eyes for later FACS analysis, which would give the number of GFP-positive cells. However, these samples could not then be used for immunohistochemistry experiments. Due to the workload required to produce such samples it was decided

that knowing the number of cells surviving in the subretinal space of these mice was not the highest priority for the current project.

Is important to mention that the success rate of the transplantation of mESC-derived photoreceptor precursors was considerably lower than described previously by other members of this group using the same cell line and mouse strain. Previous studies resulted in the presence of cells in the subretinal space of *Aipl1*$^{-/-}$ mice 3 weeks following transplantation, in 75% of animals when transplanting 200,000 cells (N = 8 eyes) (Goh, 2016), and 100%, of animals when transplanting 100,000 cells (N = 12 eyes) (Kruczek et al., 2017). These transplantation success rates are substantially higher than that achieved during the present study. The results of Kruczec *et al.* (2017) could be disregarded, since the project objective was quite distinct from what I aimed to achieve in my project. Kruczec *et al.* (2017) project was focus on generation and transplantation of cones, and the mESC-derived EBs were screened, in order to select only the organoids with the very best morphology and virally transduced in order to transplant an enriched population of mESC-derived cone precursors. This led to the cell population being transplanted to be considerably different from the population used in this study. Rod precursors are more abundant in the EBs and therefore in the present study those were the majority of the transplanted cells. Cones are generated and mature first (Bassett and Wallace, 2012) and that could lead to the differences seen between this studies. Nevertheless, the experimental set up of the present study and the project developed by Goh (2016) is similar and consequently it would be expected that the transplantation outcome of transplanting 200,000 cells would be comparable across these projects. In the current project, even when transplanting 200,000 the success rate of transplantation was much lower than what was reported by Goh (2016), 48% vs 75% success rate. It is not possible to be certain why this difference occurred. However, at the time the mESC-derived EBs were grown for the present project, the cultures did not appear optimal. This was true for all mouse lines that were growing in the lab at the time and not limited to the Crx.GFP line. The specific issue was not identified, but the fact that not all the plated cells were aggregating and forming EBs, as reported by Gonzalez-Cordero *et al* in 2013, was indicative that something was not optimal. Maintenance cultures looked normal and the protocol was being followed so it was hypothesised that perhaps the constituents of the media, factors or plates were faulty, which would explain why the EB formation was not as efficient as previously. I cannot exclude that the EBs that were generated and used in the current transplantation study were less healthy than the ones generated in previous studies, due to suboptimal culture

conditions. This could explain the lower success rate of these experiments when compared with past projects.

Nevertheless, the experiments presented in this project were done simultaneously, having the same sorted cells being diluted and injected at 200,000 and 800,000 cells per eye. Therefore, the data presented here is consistent and comparable between groups. Thus, it is fair to conclude that increasing the number of transplanted cells showed no great impact on the transplantation outcome, but it did lead to larger cell masses and cells seemed to mature further than what was seen in the smaller cell masses produced by transplanting 200,000 cells. Furthermore, by increasing the number of transplanted cells, rare outer segment-like buds were present following transplantation. These were not reported in the previous study (Goh, 2016) and could suggest that the positive effect of increasing the number of injected cells was, possibly, underestimated due to the sub-optimal culture conditions.

The relatively low success rate of transplantation of mESC-derived photoreceptor precursors did not allow for all the initially set aims to be fulfilled. Retinal and visual function were not assessed. Studying the visual rescue by LOOM test or optomotor is time consuming and with the low success rate seen, it was decided that it would not be a good use of the time collecting and analysing that data, knowing that more than half the animals would not have any transplanted cells within their subretinal space. Considering the morphology and maturation, MEA seemed the most promising technique to identify any rare light responsive transplanted photoreceptors that had established synaptic connection with the host. However, the low success rate and additionally the low GFP intensity displayed by the transplanted cells following transplantation, without further antibody enhancement, made the identification of cell mass and its correct placement over the MEA unviable. Previous studies have claimed that despite the abnormal morphology and lack of proper outer segment formation, restoration of light sensitivity is possible (Barnea-Cramer et al., 2016; Lamba et al., 2009; Thompson et al., 2014). However, some of the results of those studies require reinterpretation, in light of the recent discoveries regarding material transfer between transplanted cells and host photoreceptors. Moreover, a previous study from our group, using the same cell line and host mouse strain, showed promising MEA data that suggests that some retinal function could be restored following transplantation of mESC-derived photoreceptor precursors into *Aipl1*$^{-/-}$ mice (Goh, 2016). It is likely that this lack of normal outer segment morphology in transplanted photoreceptor precursors would reduce their sensitivity to light, and a

higher number of cells may be required to compensate for the compromised light sensitivities of individual cells.

Therefore, further optimisation of the culture conditions and improvement of transplantation success rate are essential for future studies investigating the potential of retinal and visual rescue following the transplantation of mESC-derived photoreceptor precursors.

4.4.2 Transplantation of hESC-derived cone photoreceptors and retinal sheets

Regarding the transplantation of hESC-derived cones, a direct comparison between transplanting 100,000 or 500,000 cell per eye was not possible. This is due human photoreceptor cells taking longer to differentiate and the challenge to generate such a great number of hESC-derived cones, despite having a robust protocol. Since only 18% of cells in NRVs are cone photoreceptor cells (Gonzalez-Cordero et al., 2017) and using viral transduction we can only isolate half of those cones, it was not possible to generate enough cells to transplant and directly compare the outcome of injecting 100,000 or 500,000 hESC-derived cones. However, the success rate obtained in this study was in line with what had been previously published (Gonzalez-Cordero et al., 2017). While it is not possible to directly compare these two studies' findings, it is encouraging that the transplantation success rate did not seem to decrease greatly by injecting five times more hESC-derived cones into the same strain.

Interestingly, in samples where the cell masses were much larger than had previously been seen, the hESC-derived cones appeared to mature further, showing longer outer segment-like structures not seen in previous studies. Moreover, these cells also extended several pre-synaptic processes into the host's retina. In some areas the cell mass organisation resembled an ONL. The host retinas' bipolar cells invading the cell mass and the presence of post-synaptic protein mGluR6 suggested that the transplanted cells have an impact on the host INL, leading to renewed expression of post-synaptic receptors that were not present following photoreceptor loss in these mice (see chapter 3). This reaction of the host retinas to the presence of these large cell masses was unexpected, since it had not been reported previously and it was not seen when transplanting mouse ESC-derived photoreceptors. The presence of post-synaptic proteins that were absent before photoreceptor transplantation is very encouraging. This is evidence that transplanted cells impact the host retina. It shows that not only the transplanted cells attempt to establish connections but the host retina itself remodels in response to the presence of this new potential synaptic partners.

Despite some previous studies claiming similar results in other end-degeneration models, all of those were done based on the transplantation of human retinal sheets (Iraha et al., 2018; Mandai et al., 2017a). Since the retinal sheets are not a pure population of photoreceptors, it cannot be excluded that inner retinal cells present in culture, are part of the retinal sheet that was injected. Consequently, the presence of post-synaptic markers seen in those studies could be part of the retinal sheet and not necessarily on endogenous bipolar cells. Other studies have previously shown proximity between pre- and post-synaptic proteins, following transplantation of dissociated hESC-derived photoreceptors. However, in those studies the recipients were animal models in which the retina was functionally compromised, but in which the structural integrity was mostly intact and post-synaptic proteins were still present on endogenous interneurons (Lamba et al., 2009; Zhu et al., 2017).

The lack of detection of light responses or micro-ERGs by the MEA is not surprising; this is a challenging technique, requiring a greater number of experiments. It is important to mention that the MEA dimensions are small and only a patch of the transplanted graft can be recorded from, meaning that it is possible to miss the area where more cells might be connected or matured. It is also relevant that the *Aipl1*$^{-/-}$ retinas are very delicate, being thin and particularly adherent to the vitreous, due to the degeneration and remodelling. This, in turn, increased the processing time required from collecting the eye until recording. Therefore, a greater number of samples will be required in order to build a robust data set. Unsurprisingly, no rescue in visual function could be detected by ERG and LOOM test. Quantification of the survival of cells could be necessary, to establish how many transplanted cells are necessary to achieve visual rescue. It has been estimated that a reliable ERG response is achieved only when at least 150,000 photoreceptor cells are functional (Pearson et al., 2012), and it is possible that, even when transplanting ~500,000 cells, this minimal threshold of functional and connected cells was not achieved.

Since we showed in the previous chapter that the synaptic layers and some interneurons in the *Aipl1*$^{-/-}$ retinas are impaired, it is also possible that the synaptic circuit itself suffered remodelling changes that do not allow new functional synaptic connections to be established. Furthermore, Singh et al. (2014) observed that synapse development in *Aipl1*$^{-/-}$ retinas is compromised prior to photoreceptor degeneration, and synapses between photoreceptor terminals and second-order bipolar cells are not properly formed early on in development. Knowing that an intact photoreceptor's signals are required in order to establish the synaptic circuit (Dhingra and Vardi, 2012), it cannot be excluded that even if the first synaptic connections are

established between transplanted light responsive, cone photoreceptors and host's bipolar cells, the remaining circuit might still be impaired. This pattern of inner retinal degeneration in *Aipl1*$^{-/-}$ is unlike that in *rd1* mice where synaptic connections and the retinal circuit develops normally (Puthussery and Taylor, 2010) and rescue of visual function has been reported (Barnea-Cramer et al., 2016).

The success rate of transplantation of hESC-derived retinal sheets was so low that no conclusions can be drawn, other than that it results in more damage to the retina at the time of injection, which is likely to be a major contributing factor to the low success rate. In order to properly compare the transplantation outcome of dissociated cells and retinal sheets optimisation of the surgical procedure for the latest is necessary.

To properly assess if cell replacement therapies are suitable and able to rescue the phenotype seen in *Aipl1*$^{-/-}$ retinas further experiments are required. With more promising results depending on the size of the cell mass itself, further optimisation is required in order to consistently achieve such results. Furthermore, experiments such as MEA recordings and behavioural studies require a larger number of animals where the transplants were successful. To improve the transplantation outcome, it will be necessary an immune-compromised mouse model of retinal degeneration. By using an immuno-compromised model, it is anticipated the transplant outcome will improve. Using such a model would also allow assessing longer periods following transplantation, giving cells have more time to mature and establish synaptic connections. Consequently, in these animals an improvement in light sensitivity and/or visual rescue might be achieved.

Chapter 5: Transplantation of ESC-derived photoreceptor cells into immunodeficient, end-stage retinal degeneration mice

5.1 Introduction

In the context of this thesis, the absence of cell mass in the subretinal space following transplantation results in non-meaningful experiments as no data regarding cell maturation and synaptogenesis can be collected from those experiments. As described in the previous chapter, when transplanting into *Aipl*$^{-/-}$ mice, the transplantation success rate was approximately 50%. Furthermore, cell survival following transplantation appeared decrease after 3 weeks. To address this problem transplantation into immune deficient mice was performed. By using immunocompromised animals, the intention was to evaluate if the success rate could be improved and if the period following transplantation could be extended. It was hypothesised that by extending the period following transplantation, further maturation and synaptic formation could occur and, consequently, the likelihood of visual rescue would increase. The reason why the success rate was so low in the experiments described in the previous chapter, was unclear. However, possible contributing factors were immune rejection and the quality/viability of the cells at the time of transplantation.

5.1.1 Role of immune response in transplantation outcome

Immune rejection is a major problem in transplantation of any tissue (for review see Sanchez–Fuevo and Strom, 2011; Trivedi, 2007). Despite the immune privilege of the subretinal space (Jiang et al., 1993; Streilein et al., 2002), immune rejection is, most likely, a major contributor for the variability of transplantation outcome. The importance of immune modulation is further supported by a previous study from our lab which shown that immune suppression can improve the long-term survival of transplanted donor photoreceptor precursors in wild type retinas. In this study, the presence of macrophages and T-cells in the subretinal space, correlated with poor cell mass survival following transplantation. Upon treatment with cyclosporin in drinking water (50 mg/kg/day) for 1 week prior to and 3 weeks after transplantation, a significant reduction in number of T-cells was seen at 4 months following transplantation. In addition, the number of, what at the time was thought to be, integrated cells were also significantly increased (West et al., 2010). However, such

findings must be re-interpreted due to the recent discovery of material transfer. The increase in GFP-positive cells within the host ONL, could be due to the cell mass surviving for a longer period of time and, consequently, allowing for more material transfer to occur. Further work is necessary to accurately re-interpret these results. However, it was clear from these experiments that cyclosporin can increase cell survival following transplantation of photoreceptor precursors.

5.1.1.1 Immune compromised models as hosts for retinal cell transplantation

Several reports describe the use of immune compromised animals as a host for retinal cell transplantation, showing that such strains can sustain transplanted cells for up to six months following injection (Iraha et al., 2018; Mishra et al., 2017; Seiler et al., 2014; Shirai et al., 2016; Sugita et al., 2016). A cross of non-obese diabetic/severe-combined immunodeficiency (NOD.SCID) and *rd1* mice was recently generated. This strain lacks, B and T lymphocytes and NK cells. They display a similar retinal degeneration pattern to *rd1* mice and have been shown to be a useful model for allogenic and xenogenic cell-based therapies (Mishra et al., 2017). However, this strain is not yet commercially available. Moreover, due to their severely compromised immune system, the housing conditions required for these animals make them difficult to maintain. Another model that has been used for retinal cell transplantation is the SD-Foxn1 Tg(S334ter)3Lav (RD nude) rat. This strain was created and described by Seiler *et al* in 2014, and used by others for investigating transplanted retinal sheets to be kept for over 100 days post-transplantation, showing maturation of the transplanted cells (Shirai et al., 2016). These rats are commercially available however, the number of animals required, and issues reported in breeding this strain made their use too costly and therefore unviable for our study. Therefore, none of the available animal models were suitable and we decided to generate an alternative model.

The Crl:NU(NCr)-*Foxn1*^{nu} (*Foxn1*^{nu}) mice are mildly immunocompromised, since they lack mature T lymphocytes, but preserve other lymphocyte populations and their innate immune system. This phenotype is cause by a single gene defect, making it a more practical cross, unlike models that are completely immunocompromised, but would require several generations in order to knock out all the involved genes. *Foxn1*^{nu} mice are also more practical to maintain as a strain since they require less stringent sterility of the environment, they are kept in. Furthermore, as part of the phenotype caused by the mutation in the Foxn1 gene, these mice are hairless and consequently simple to genotype for this gene, by identifying this feature. Finally, immune rejection to transplanted grafts is a type IV hypersensitive type of response,

mostly mediated by T cells (reviewed in Streilein et al., 2002). This suggests that using *Foxn1*^{nu} mice should be sufficient to improve the transplantation outcome. Hence, *Foxn1*^{nu} mice were crossed with *Aipl1*$^{-/-}$ mice.

Due to the proximity in the chromosomal location, with the distance between Aipl1 and Foxn1 genes being only 2.93cM, there is a low chance of successful recombination (Figure 62). Consequently, an additional strain was generated by crossing *rd1* (C3H/HeN) with *Foxn1*^{nu} mice, to ensure that an immunocompromised strain with advance retinal degeneration would be available within this project's time frame.

Figure 62 - Genetic map of *AIPL1* and *FOXN1* genes, on mouse chromosome 11

Schematic representation of the location of the *Aipl1* and *Foxn1* genes, in close proximity on chromosome 11. The distance from the starting point (zero) is measured in cM, with *Aipl1* gene being at 43.81cM and *Foxn1* gene at 46.74cM.

In this chapter improvement of the transplantation outcome by using an immunocompromised strain as a host was explored. Due to time constraints only mESC-derived photoreceptor cells were transplanted into *Aipl*$^{-/-}$/Foxn1^{nu} mice, as the crossing of these strains did not allow sufficient time for experiments using hESC-derived cones. Instead, hESC-derived cones were transplanted into *rd1*/Foxn1^{nu} mice. Further experiments are necessary to assess the possibility of transplantation and rescue of visual vision of the immunocompromised *Aipl1*$^{-/-}$ strain.

The potential of *Foxn1*^{nu} animals as host for subretinal transplantation was evaluated by two pilot experiments. These experiments were done in visually intact animals. Firstly, hESC-derived RPE was transplanted to ascertain whether the lack of T lymphocytes was sufficient to allow prolonged graft survival. hESC-derived RPE cells were selected for this experiment due to the shorter differentiation protocol compared to hESC-derived photoreceptors, and their inability to survive in the subretinal space of immunocompetent mice for more than two weeks (Mehat, 2017). The second pilot experiment was intended to clarify the possibility of greatly improving the transplantation outcome of retinal sheets by using Foxn1^{nu} mice as hosts. Only by drastically increasing the success rate would it be possible to do a comparison study between transplantation of dissociated, sorted hESC-derived cone photoreceptors and hESC-derived retinal sheets, fulfilling one of the aims of this project.

5.1.2 Impact of photoreceptor quality in transplantation outcome

The impact of the condition of the cells at the time of transplantation cannot be excluded. Different differentiation batches may differ slightly. This might also have an impact on cell survival post transplantation. However, since within the same transplantation experiment variability was seen, it is not expected that those differences, if present, will be a major contributor to transplantation outcome. Moreover, all aspects of cell culture, cell dissociation and preparation, as well as the surgical procedure, were kept as constant as possible, by following standardised protocols (see section 2.1 – 2.8). Each of the required cell culture and cell preparation procedures were performed by the same investigator, the author of this thesis, and every time injections were executed by Professor Rachael Pearson. Nevertheless, it is important to note that, despite the efforts to keep the conditions constant, there is an intrinsic degree of biological variability that is not yet fully understood. For reasons thus far unknown, batches of hESC show variable differentiation potential, as only 52% of the differentiation generated retinal organoids. However, 23% of the

differentiation batches that work produce several retinal organoids (177 ± 65). Therefore, the range is wide as some differentiation will not produce a single retinal organoid while other produce over 200 organoids. All the retinal organoids, without exception, showed photoreceptor differentiation markers and recapitulate human development, but it is unknown if these cells show any epigenetic differences that could lead to different transplantation outcomes. When it comes to mESC cultures, the variability between the organoids generated appears to be less (Gonzalez-Cordero et al., 2013; Kruczek et al., 2017). However, as described in the last chapter, the differentiation of mESC was less efficient than previously reported. Without detailed genetic and epigenetics studies we cannot exclude that some differences are passing undetected and potentially affect transplantation outcome. Analysing the variability between differentiation batches could be greatly valuable in the future in order to optimize efficient GMP production of photoreceptors cells for future cell transplantation therapies in humans. However, despite its importance, this would involve long and complex experiments that are outside the scope of the current project.

5.2 Aims

By using immunocompromised animals in this study, we aim to first improve survival of cells providing the transplanted cells a longer period to mature and establish synaptic connections with the host retina.

The work described in this chapter aims to (1) evaluate whether the *Foxn1*^{nu} strain is a suitable host for retinal transplantation by assessing survival of hESC-derived RPE and retinal sheets following transplantation; (2) increase the period between mESC and hESC-derived cone transplantation and collection of samples from 3 to 6 or 12 weeks; (3) compare the two current strategies for photoreceptor transplantation, by transplanting dissociated cell suspension of hESC-derived cones and retinal sheets; (4) investigate if transplanted cells establish synaptic-connections with host INL; and (5) establish if hESC-derived photoreceptors, dissociated or as part of a retinal sheet, are able to rescue retinal/visual function of advanced retinal degeneration mice.

5.3 Results

5.3.1 Transplantation into the immunocompromised strain, Foxn1^{nu}

The current protocol generates a large number of RPE cells, and it was hypothesised that transplanting these cells would be a good indication for how long post-transplantation the hESC-derived photoreceptors could survive. RPE cells were cultured, dissociated and resuspended as described in the methods section. In this pilot experiment 50,000 hESC-derived RPE cells were transplanted (see section 2.7) into the subretinal space of adult *Foxn1^{nu}* mice, using the surgical method previously to inject dissociated photoreceptor cells. Eyes were collected at 4, 6, 8, 13, 16 and 24 weeks, following transplantation (n=2 per time point). hESC-derived RPE cells were present in all samples analysed, as shown by the pigmented cells staining positively for human nuclei (Figure 63). It is important to note that *Foxn1^{nu}* mice are albino so all pigmentation visible originates from transplanted cells.

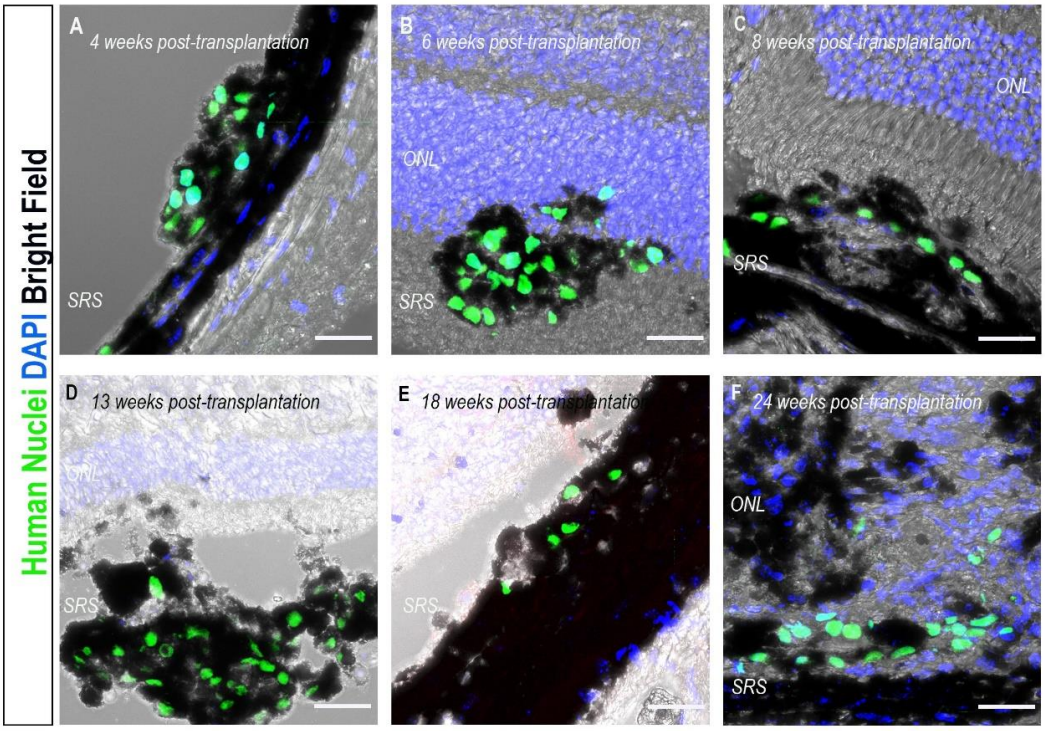

Figure 63 - Transplantation of hESC-RPE cells into immunocompromised mice

Representative confocal images showing presence of hESC-derived RPE cells in the subretinal space SRS) of the *Foxn1*^{nu} (n = 2 per time point). Cells were present at all time points analysed, showing widespread distribution in the subretinal space. **(A)** 4 weeks following transplantation, several pigmented cells could be found in the subretinal space. These cells were positive for human nuclear marker staining. In these animals, the retinal detachment prevented imaging of both cell mass and ONL in the same confocal image. **(B)** humans RPE cells were still present 6 weeks following transplantation, and some of the cells seem to invade the ONL. **(C, D)** By 8 and 13 weeks post-transplantation human RPE cells were still present. **(E)** Cells were still present 18 weeks post-transplantation. The amount of pigmentation visible, known to originate from the transplanted cells as the hot is albino, appears to increase. **(F)** By the last time point analysed, 24 weeks post-transplantation, donor cells were still present in the subretinal space of the host. (Scale bar 25µm)

To further study the potential of *Foxn1*^{nu} mice as a host strain for retinal cell transplantation, hESC-derived retinal sheets were cut and injected subretinally, as described in the previous chapter (n = 3 eyes, N = 3 animals). Cell survival and maturation were analysed 4 weeks following transplantation with 2 out of the 3 host eyes showing presence of hESC-derived retinal sheets. The hESC-derived retinal sheets were easily identified by their morphology and location, with a large mass of cells present in the subretinal space. Additionally, these cells were larger than the hosts' photoreceptors cells. Further confirmation regarding its origin was provided by the presence of GFP positive cone photoreceptors. Rosette formation was observed (Figure 64 and 65). Despite being manually cut, the hESC-derived retinal sheets appeared to be formed of mostly photoreceptors, as cells stained strongly for RECOVERIN (Figure 64A). All the cells within the retinal sheet were positive for human nuclei marker staining, which further confirms the origin of these cells (Figure 64B).

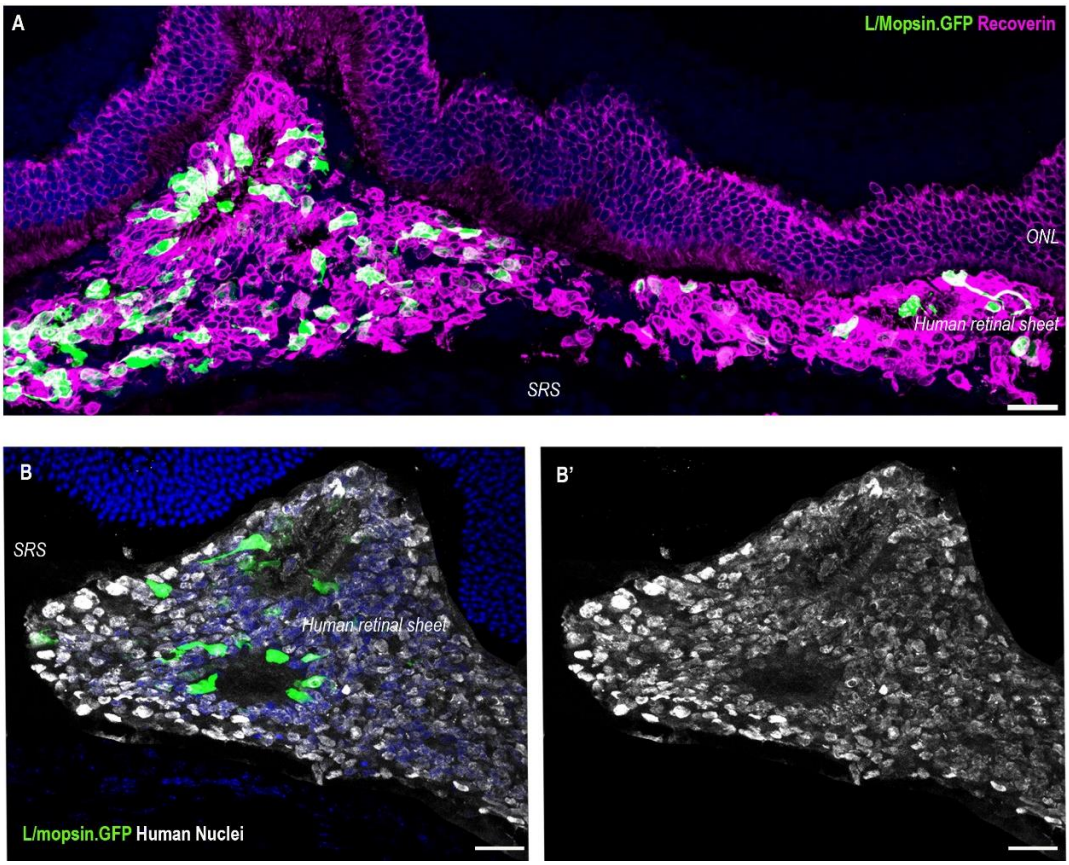

Figure 64 - *Foxn1^{nu}* as a host for transplantation of hESC-derived retinal sheets

hESC-derived retinal sheets in the subretinal space (SRS) of *Foxn1^{nu}* mice 4 weeks post-transplantation. **(A**) Majority of the cells within the retinal sheet were positive for recoverin. GFP positive L/M cones were present. Rosette formation was evident in different area of the retinal sheet. Note that the host's ONL also stained positive for recoverin, as the antibody is not specific to the human protein. **(B)** All the cells forming the retinal sheet were from human origin, staining positively for a human nuclei marker (B'). Rosette formation was observed. Few GFP positive cones were present. (scale bar 25µm).

Within rosettes, outer segment-like structures were positive for PERIPHERIN2 (Figure 65). The outer segment-like structures were longer and more abundant than those observed previously, when transplanting dissociated cones (see Figure 54). It is important to consider that when transplanting retinal sheets, both rods and cones were transplanted, while the dissociated cell suspension was a pure cone population. Because rod outer segments are longer than cone outer segments, the composition of the graft has to be taken into consideration when comparing the length of these structures. Since the host retinas were wild-type retinas, outer segments were also positive for Peripherin2. All the structures surrounding the hESC-derived retinal sheet were taken as belonging to the host, since the antibody does not allow distinction between mouse and human outer segments. Some of what was assumed to be the host outer segments could be seen on top of the transplanted tissue, probably due to disruption during the surgical procedure and retinal detachment.

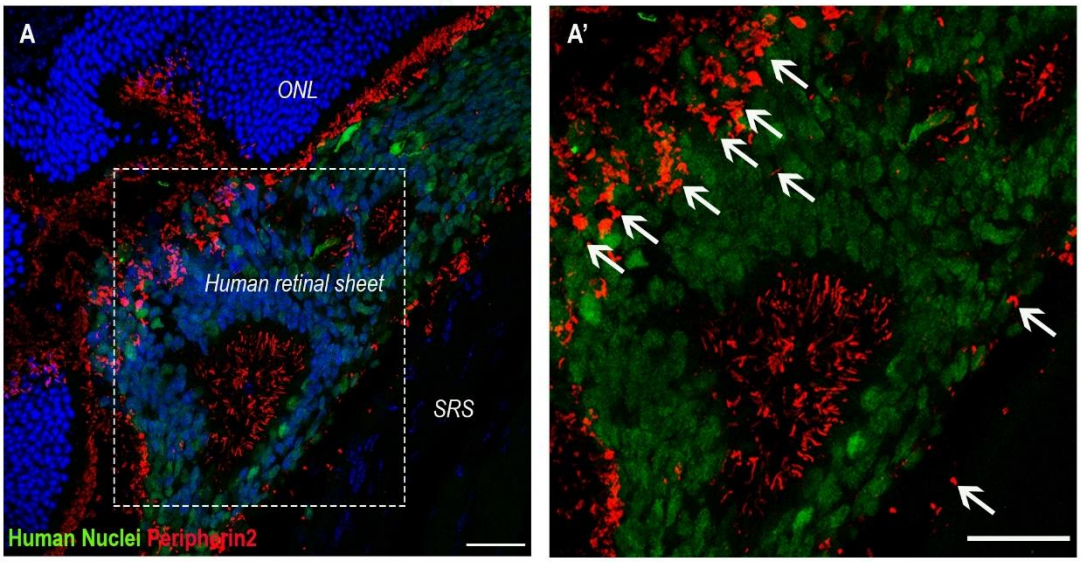

Figure 65 - Formation of outer segments in hESC-derived retinal sheet following transplantation

(A) A large hESC-derived retinal sheet could be seen in the subretinal space (SRS). All the cells within the retinal sheet were for human origin, confirming that that was the transplanted tissue. Large areas of rosette formation could be observed. In the centre of the rosettes, think and long peripherin positive OS-like structures formed (A'). In the periphery of the hESC-derived retinal sheet, broken OSs, that could be either from the host of graft, were identified by their more intense staining (white arrows).

Since the majority of the photoreceptor cells within the hESC-derived retinal sheet were rod, maturation of the transplanted cells was assessed by the presence of RHODOPSIN-positive outer segment-like structures (Figure 66). Presence of these RHODOPSIN-positive structures, which were seen developing towards the centre of the rosettes, was an indication of maturation. At time of transplantation, dd120, RHODOPSIN was seen throughout the cell body and not localised to outer segment region (Gonzalez-Cordero et al., 2017). These structures were elongated, demonstrating a typical rod outer segment morphology. SOPSIN cones were present in the ESC-derived retinal sheets and while some cells showed presence of SOPSIN throughout the cell body, as seen in culture, others appeared to have matured further with SOPSIN also being restricted to an outer segment-like structure. These structures were, as expected, shorter than the RHODOPSIN-positive structures. Cells within the ESC-derived retinal sheets did not seem to show any specific orientation, with exception of the rosette areas.

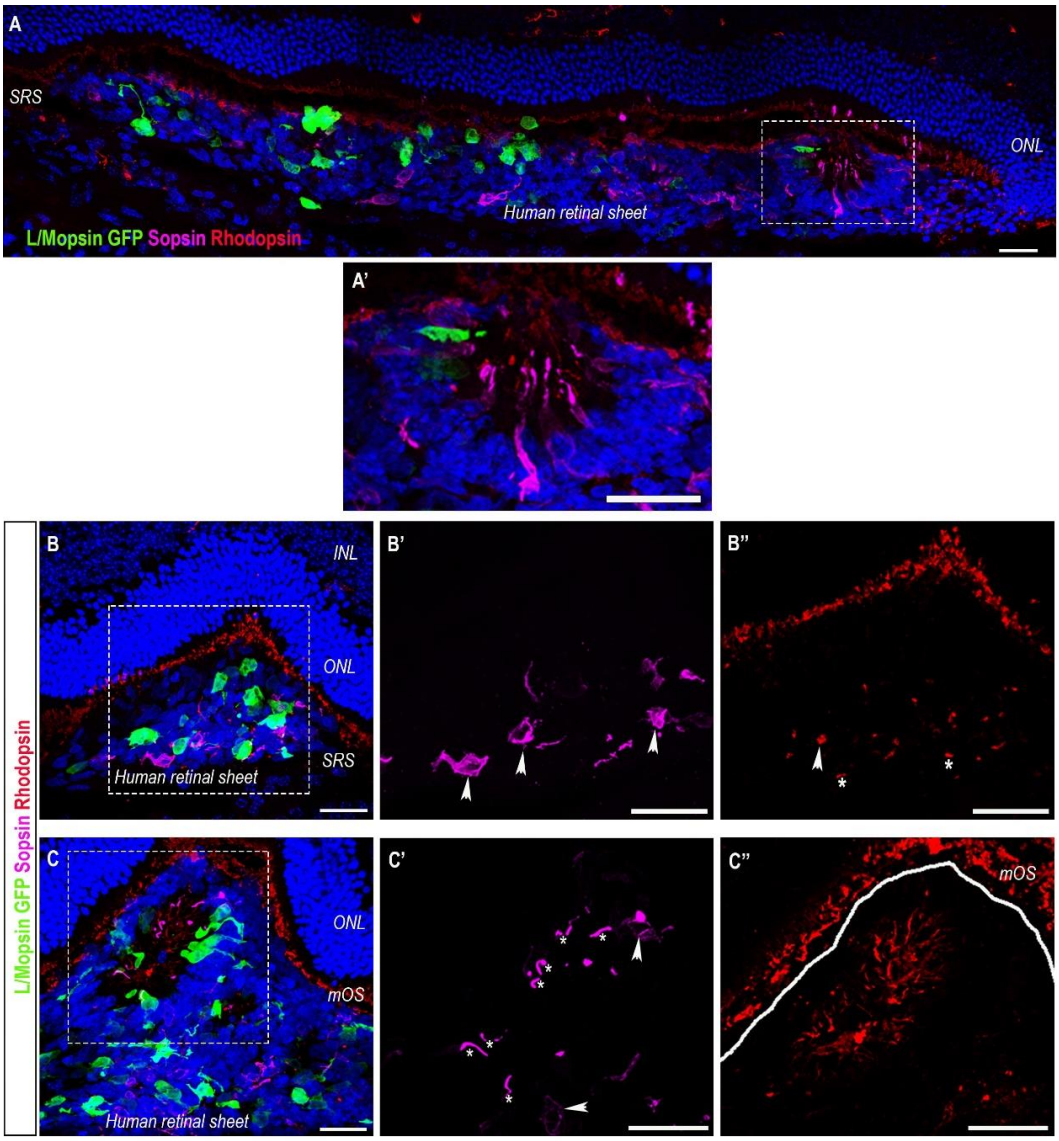

Figure 66 - Maturation of rods and S-opsin cones following transplantation of hESC-derived retinal sheets

(A) hESC-derived retinal sheets survived in the subretinal space (SRS) and showed presence of both L/M and S cones as well as rods. In areas of rosette formation, the cells seem to orientate and extend longer outer segment-like structures towards the centre of the rosette (A'). **(B)** In areas where no rosettes were formed, rods and cone were still present. However, S-opsin was not localised to outer segment-like structures, being present in the cell's cytoplasm (arrowheads). Rods seemed to mature further than cones, presenting some short and atrophic/underdeveloped rhodopsin positive outer segment-like structures. **(C)** In the centre of rosettes cells displayed further maturation. **(C')** Cells presenting S-opsin in the cell body were still present (arrow heads) but, several cells showed more localised S-opsin, forming an outer segment-like structure (asterisks). **(C'')** the rhodopsin positive outer segment-like structures appeared longer in the centre of the rosette. The rhodopsin positive structures in the periphery of the hESC-derived sheet (above white line) were the host outer segments (mOS = mouse outer segments). (scale bar 25µm)

Using the microglia and macrophage activation marker F4/80, which is present in macrophages and resting microglia, immune responses were evaluated. Some microglial cells were identified, but no major activation of the immune system was detected (Figure 67). No abnormal number of these cell types was detected.

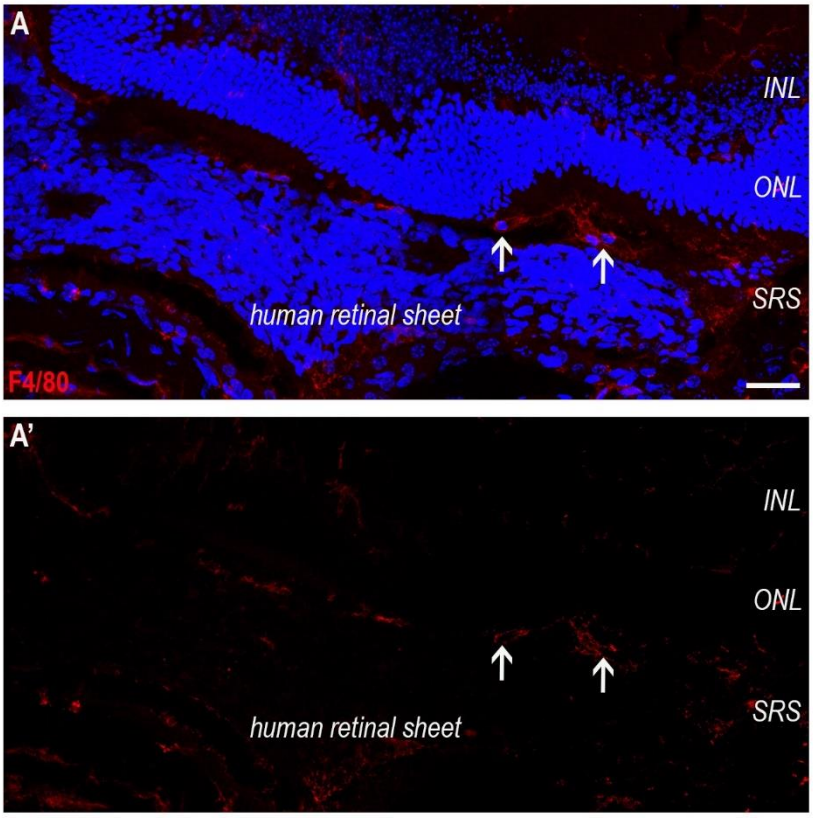

Figure 67 - F4/80 positive cells following transplantation of hESC-derived retinal sheets

A few F4/80 positive cells were present. These cells were morphological compatible with resting microglial cells and were seen in the SRS (arrows), between the host's ONL and the transplanted hESC-derived retinal sheet. (scale bar 25µm)

In summary, both the pilot experiments were successful and demonstrated the potential of *Foxn1^{nu}* mice as a host for retinal cell transplantation. Using this strain as a host improved the transplantation outcome, with over 90% of the eyes that received a transplant showing the presence of human cells many weeks following transplantation. The pilot experiment using hESC-derived RPE allowed us to study the possibility of extending the period between injection of cells and analysis. The results were encouraging as the hRPE was found at every one of the time points analysed in all the eyes that received a transplant. The post-transplantation period was extended from 2 weeks to 24 weeks, the last time point analysed in this pilot experiment. The pilot experiment transplanting hESC-derived retinal sheets also produced encouraging results despite the small sampling, with two out of the 3 transplants being successful. This was a great improvement, as previously only 1 out of 27 transplanted eyes led to a successful transplantation experiment. However, due to technical challenges, that will be discussed in the conclusions, transplantation of retinal sheets was not further explored.

Therefore, the following transplantation experiments focus on the use of dissociated and sorted photoreceptor cells and the transplantation of retinal sheets was not investigated further during this project.

5.3.2 Transplantation of mESC-derived photoreceptors into *Aipl1$^{-/-}$/Foxn1^{nu}*

Aipl1$^{-/-}$/Foxn1^{nu} retinas showed similar morphology to the ones described for *Aipl1$^{-/-}$* retinas of the similar age (see chapter three). In untreated control eyes (n = 3 eyes, N = 3 animals), no Rhodopsin-positive cells were found, and the retina was almost completely depleted of cone photoreceptors by 4.5 months of age (Figure 68A). Rare cone Arrestin-positive cells were present, but they did not show a typical cone morphology (Figure 68B). These findings were analogous to what was found in *Aipl1$^{-/-}$* retinas at the same age (Figure 23). As reported for *Aipl1$^{-/-}$* mice (Figure 33), mGluR6 was absent and a reduction in arborisation and disorganisation of the synaptic terminals at the OPL and IPL was evident in rod bipolar cells (Figure 68C). Morphology and distribution of amacrine cells appeared consistent with what was described for *Aipl1$^{-/-}$* animals (Figure 30); the unsystematic growth/rearrangement of the Calretinin positive processes of the synaptic network in the IPL was also present in this strain. No obvious morphological differences in ganglion cells, positive for HuC/D, was identified between *Aipl1$^{-/-}$* (Figure 30) and *Aipl1$^{-/-}$/Foxn1^{nu}* strains (Figure 68D).

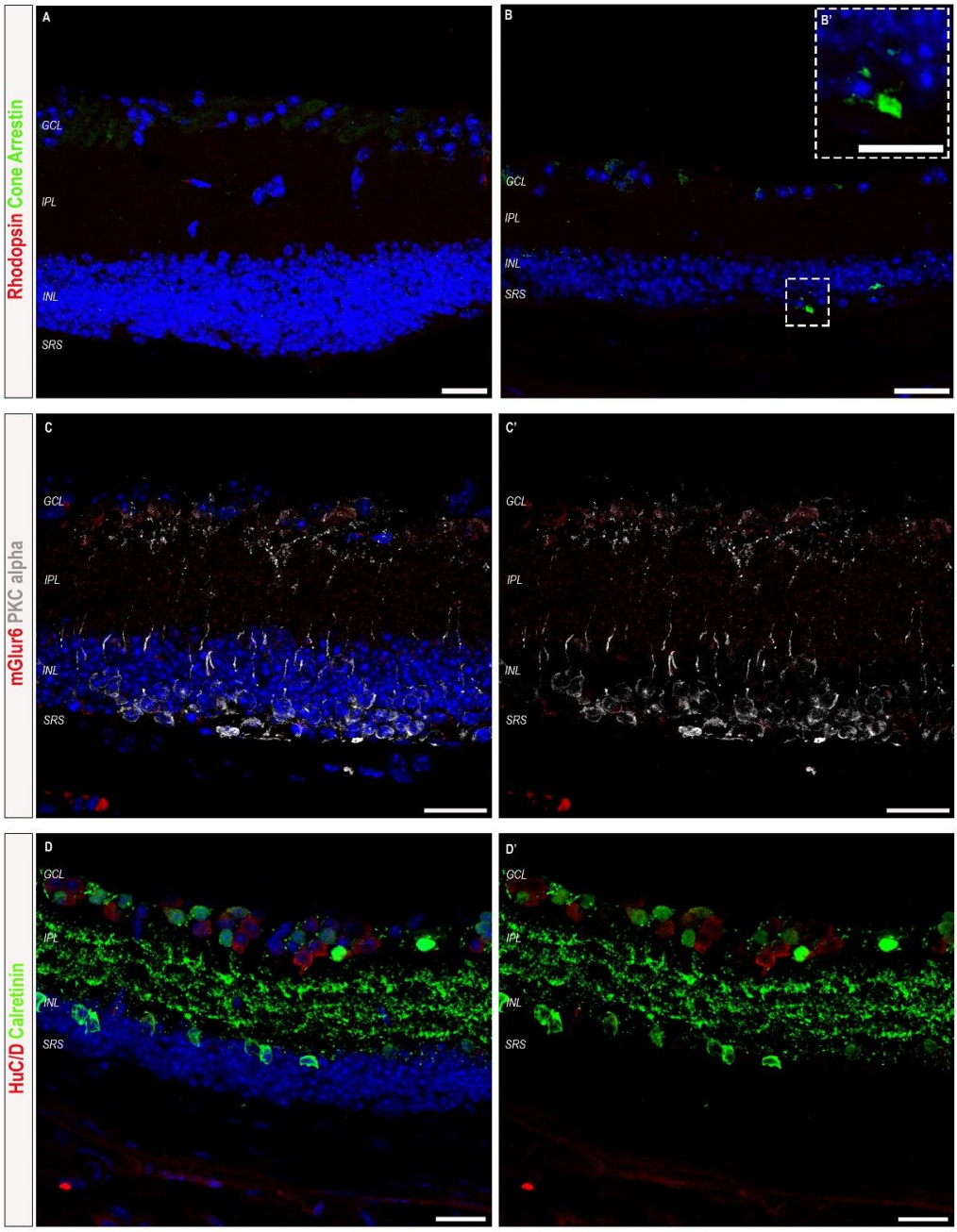

Figure 68 – Characterisation of *Aipl1*$^{-/-}$/*Foxn1*^{nu} retinas

Representative confocal images of immunohistochemistry for retinal cell markers. **(A)** At 4.5 months of age, most of the retina was depleted of any photoreceptor cells, rods and cones. **(B)** Rare photoreceptor cells could be identified. As only Cone Arrestin positive cells were found, the remaining photoreceptors were cones that showed loss of cell polarity and absent cell processes. **(C)** Some bipolar cells were seen within the INL and post-synaptic pedicles in the OPL were absent. Despite mGluR6 staining being visible in the IPL no mGluR6 positive structures were found between the INL and SRS. **(D)** Amacrine cells had unusual morphology, as they appeared fewer and smaller. Disorganisation of calretinin positive processes was visible in the IPL. Ganglion cells displayed typical morphology (Scale bar 12.5µm, B'; 25µm all other images)

In line with the experiments described in chapter four, 800,000 mESC-derived Crx.GFP positive photoreceptor precursors were isolated at dd27. Crx.GFP-positive cells were then transplanted in the subretinal space of 3 month old *Aipl1*$^{-/-}$*/Foxn1*^{nu} mice (n = 3 eyes, N=3 animals). Injected and un-injected eyes of each animal were collected 6 weeks following transplantation. Using the same batch of cells, in order to exclude the impact of cell quality in transplantation outcome, *Aipl1*$^{-/-}$ mice were also transplanted (n = 3 eyes, N = 2 mice). Those samples were collected at 3 week following transplantation and are part of the data set analysed in chapter 4. Such host eyes did not display cell mass 3 weeks following transplantation. Therefore, the comparisons described next were established having into account successfully transplanted samples.

The cell masses seen in *Aipl1*$^{-/-}$*/Foxn1*^{nu} animals were larger and cells displayed a more photoreceptor-like morphology, (Figure 69), when compared with the rounded cells seen in the subretinal space of *Aipl1*$^{-/-}$ mice, 6 weeks following transplantation (Figure 51A). However, these cell masses were smaller compared to the ones seen 3 weeks following transplantation into Aipl1-/- mice (Figure 45).

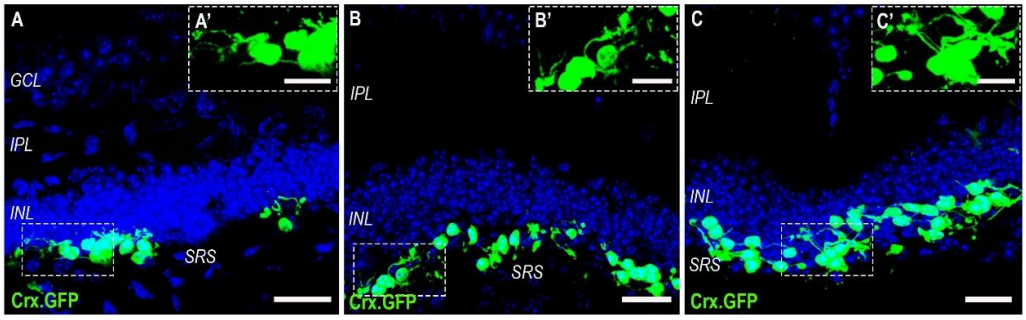

Figure 69 - mESC-derived Crx.GFP photoreceptor precursors, 6 weeks following transplantation into *Aipl1*$^{-/-}$/*Foxn1*^{nu} mice

Representative confocal images showing spread and morphology of mESC-derived Crx.GFP photoreceptors precursors 6 weeks following transplantation of 800,000 cells, at dd27 into an immunocompromised retinal degeneration host. **(A-C)** Crx.GFP positive cells were present in the subretinal space of four-month-old *Aipl1*$^{-/-}$*Foxn1*^{nu}. Post-transplantation the surviving cells extended several disorganised processes (A', B', C'). (Scale bar 25 µm A-C, 12.5 µm, A'-C')

Despite presenting a healthier morphology, features of mature photoreceptors were rare. Rare Peripherin2-positive buds were identified, and the majority of cells were not positive for the mature rod marker, Rhodopsin (Figure 70).

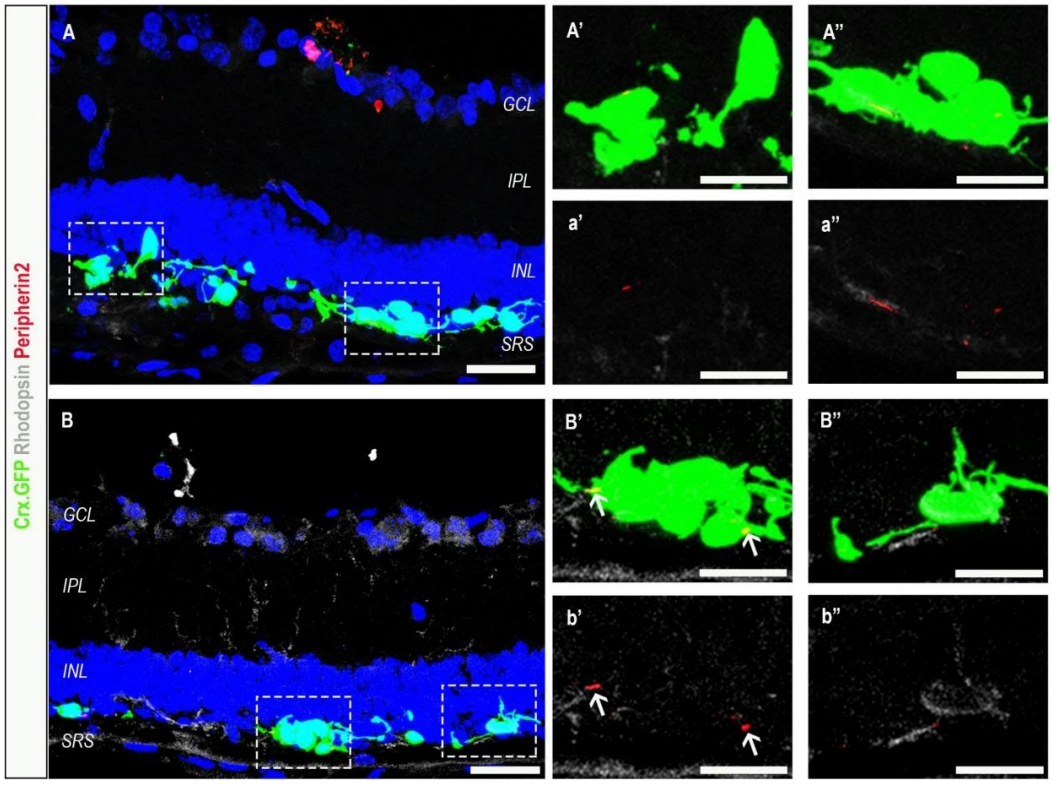

Figure 70 - Mature photoreceptor markers, Rhodopsin and Peripherin2, 6 weeks following transplantation into *Aip1*$^{-/-}$/*Foxn1*^{nu} mice

Representative confocal images of immunohistochemistry against mature rod marker, rhodopsin, and OS specific protein, Peripherin2. **(A)** Post-transplantation most of surviving cells did not show clear staining for rhodopsin (A'-A''). Some peripherin2 positive structures were present (a'-a''). **(B)** Rare rhodopsin positive cells were present (B'', b'') and occasional peripherin2 buds formed OS-like structures (arrows) (B', b'). (Scale bar 25 µm A, B; 12.5 µm, A'-b'')

To investigate if most of the surviving cells were cone photoreceptors, which would explain the lack of rhodopsin, immunohistochemistry for cone Arrestin was performed (Figure 71). Surprisingly, most of Crx.GFP positive cells were negative for cone Arrestin. In the few Crx.GFP positive cells that were positive, cone Arrestin, staining appeared to outline the cell. However, cone Arrestin-positive structures that did not co-localise with the GFP positive cells were also observed. Since those structures were only seen in specific areas, close to the cell mass and only in the subretinal space, it is likely that this is genuine staining. Cone Arrestin-positive cell debris from dead cells, either from the host or transplant, might be the source of this material. Due to the restriction in number of transplanted eyes, the source of this cone Arrestin positive strucures was not investigated further.

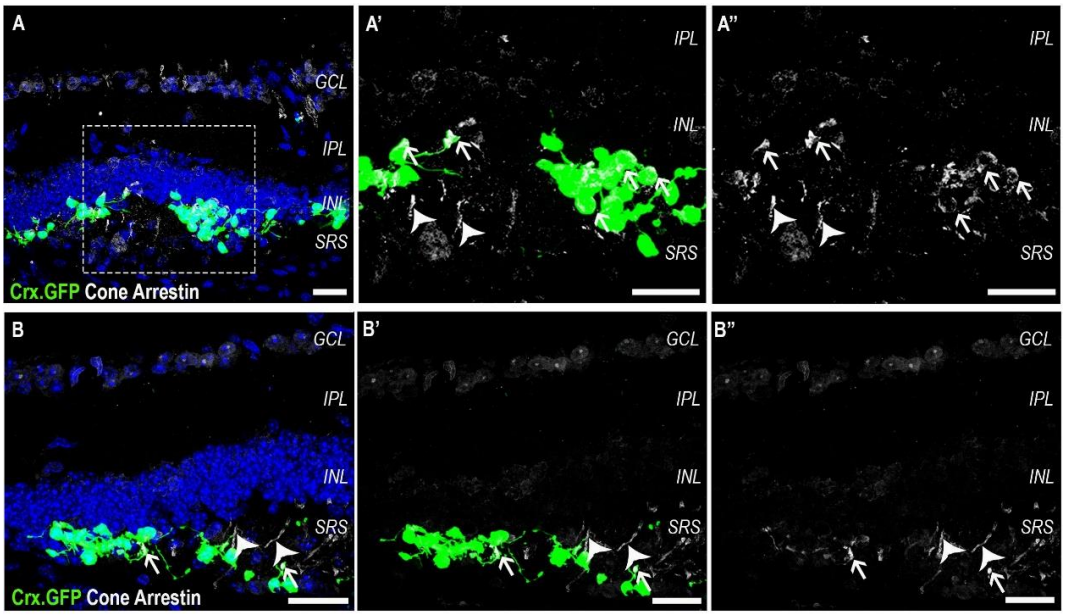

Figure 71 - Mature cone photoreceptor marker cone Arrestin, 6 weeks following transplantation into *Aip1*$^{-/-}$/*Foxn1*^{nu} mice

Representative confocal images of immunohistochemistry for mature cone marker, cone Arrestin. **(A, B)** Some of the Crx.GFP positive cells appear to be positive for cone Arrestin (arrows), however this staining was seen in the cell body and not localised to an outer segment-like structure. Staining was not associated with GFP positive cells was observed close to the cell the mass (arrowheads). (Scale bar 25 µm)

Transplanted cells showed presence of Ribeye-positive structures, in line with what was seen in samples collected 3 weeks following transplantation into immune competent mice (Figure 49B). Most Ribeye-positive structures displayed a dot shape (Figure 72A), but few horse-shoe shaped structures, typical for the Ribeye pattern in the OPL, were identified (Figure 72B).

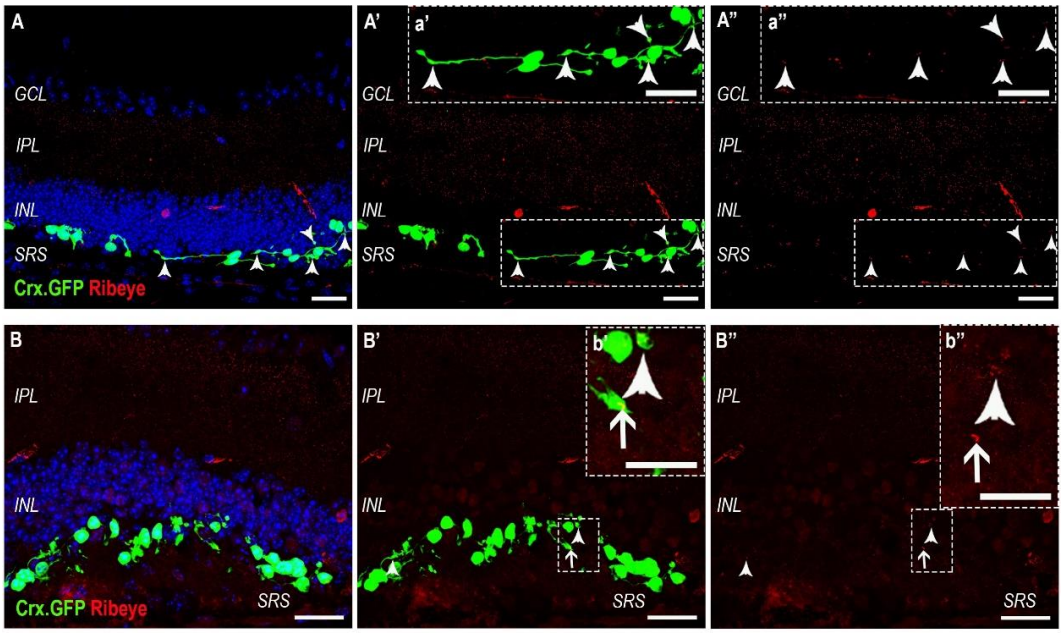

Figure 72 - Presence of Pre-synaptic protein ribeye, 6 weeks following transplantation into *Aipl1*$^{-/-}$/*Foxn1*^{nu} mice

Representative confocal images showing presence of pre-synaptic protein, ribeye, in transplanted cells, 6 weeks following transplantation into immune compromised *Aipl1*$^{-/-}$ mice. **(A)** Ribeye-positive dots were present in the synaptic pedicle of some of the transplanted cells (arrowheads). **(B)** Ribeye-positive dots were often found (arrowheads), however rare horse-shoe shaped ribeye-positive structures were identified within some of the transplanted cells' pedicles (b'', arrow). Since anti-ribeye antibody is raised in mouse, the secondary antibody results in staining of the host's blood vessels. (Scale bar 25µm, A-B; 12µm a'-b'')

To assess if, given more time following transplantation, the host retina would show further signs of interaction with the transplanted mESC-derived photoreceptors, immunohistochemistry for post-synaptic protein mGluR6 and rod bipolar cells, was performed. As discussed in the previous chapter the immunohistochemistry for mGluR6 in junction with PKCα is not ideal for mESC-derived cells. It was hypothesised that a longer post-transplantation period could improve the interaction between host retina and transplanted cells, which could translate in a stronger and more clear presence of these markers. Therefore, making the positive structures distinguishable from the background/unspecific staining. An mGluR6-positive dotted pattern could be identified in the host IPL, but no clear staining was seen within the cell mass. As previously seen, the transplanted cells displayed positive staining throughout their cell bodies, making the identification of post-synaptic mGluR6 structures unreliable (Figure 73). PKC-α positive processes extending into the cell mass were identified in areas where more transplanted cells were present (Figure 73B), but absent in areas where no transplanted cells were seen (Figure 73A).

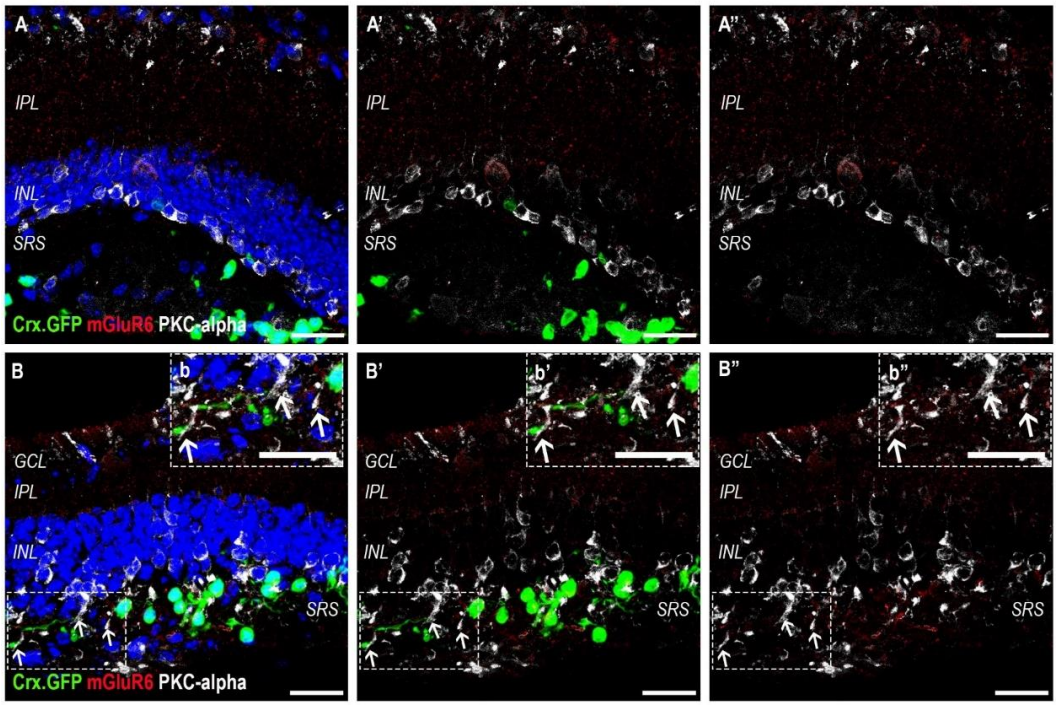

Figure 73 - Interaction between host 3-month-old *Aipl1*$^{-/-}$/*Foxn1*^{nu} retina and transplanted mESC-derived photoreceptor precursors, 6 weeks following transplantation

Representative confocal images of post-synaptic marker mGluR6 and bipolar cell marker, PKCα, as a reference to localise the synaptic marker to post-synaptic cells **(A)** A dotted pattern of mGluR6-positive structures can be seen in the IPL of the host. No positive mGluR6 staining was detected in the small cell mass. PKCα-positive rod bipolar cells did not extend processes towards the transplanted cells. **(B)** In areas where bigger cell masses were present, long PKCα-positive processes could be seen within the cell mass (arrows). No clear mGluR6-positive structures were identified, due to unspecific background staining (b', b''). (Scale bar 25µm, A, B; 12.5µm, b', b'')

Due to the small number of samples available all eyes were collected for immunohistochemistry characterisation and no MEA data was performed. Unfortunately, due to technical issues at the time of collection no LOOM or optomotor data could be collected.

In summary, the results were encouraging when it came to cell survival. However, extending the post-transplantation period did not seem to improve cell maturation of mESC-derived photoreceptors. Improving the quality of the cells transplanted could, possibly, improve such results. However, considering the overall goal of investigating cell therapy as a treatment for retinal degeneration, the use of mESC cultures and transplantation of mESC-derived photoreceptors was only used as a tool to optimise transplantation conditions. Optimisation of mESC cultures and differentiation would be a major investment in time and resources. Therefore, experiments using human ESC and iPSC-derived cones, the primary focus of this project, took priority and no further optimisation of mESC cultures was investigated.

5.3.3 Transplantation of hESC-derived photoreceptors into rd1/Foxn1^{nu}

Due to the length of the experiments using human cells and the time it was required to establish the cross between mouse strains, it was not possible to transplant hESC-derived photoreceptors into *Aipl1*$^{-/-}$*/Foxn1*^{nu} mice. Therefore, the following chapter uses *rd1/Foxn1*^{nu} mice as hosts for transplantation of hESC-derived cones.

A short immunohistochemistry characterisation of this strain was executed in order to established that the retinal degeneration phenotype of *rd1/Foxn1*^{nu} mice was consistent with previous reports of the retinal degeneration found in *rd1* mice (Jiménez et al., 1996; Kalloniatis et al., 2016; Lavail et al., 1997; M. García-Fernández et al., 1995). As this characterisation aimed to established if photoreceptor transplantation would have an impact on the host's retina, all samples used for this characterisation were collected at 3 months of age (n = 6 eyes, N = 3 animals), matching the age at which animals received transplants.

The phenotype seen was similar to that found for the *Aipl1*$^{-/-}$ mice. However, there were more areas where remaining cone photoreceptors could be found. These cells did not display typical morphology, as no processes were identified (Figure 74A). Additionally, the rod bipolar cells seemed more organised, with fewer displaced cells being seen in the INL (Figure 74B); however, no quantification was performed. Post synaptic protein, mGluR6 was present in the IPL, but no clear mGluR6-positive structures were found between INL and SRS (Figure 74B). Occasionally some mislocalised, mGluR6- positive structures were identified. Ganglion cells presented

normal morphology and amacrine cells appeared smaller and fewer (Figure 74D), but formal quantification would be required to confirm these findings. Disorganisation of the IPL was also present in the *rd1/Foxn1*^{nu} strain.

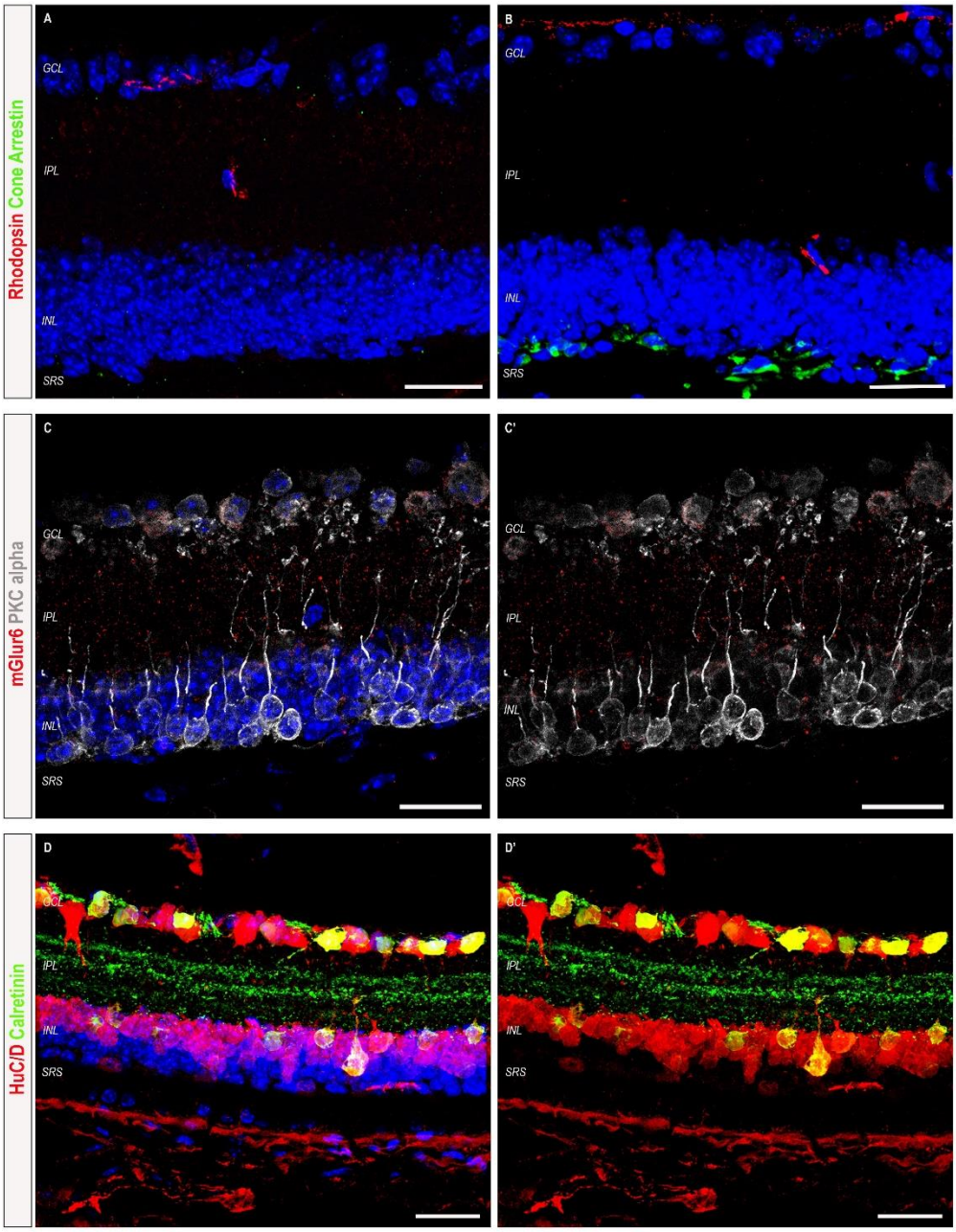

Figure 74 - Characterisation of 3 months old *rd1/Foxn1^{nu}* retinas

Representative confocal images of immunohistochemistry for retinal cell markers. **(A)** At 3 months of age, most of the retina did not show presence of any photoreceptor cells, rods or cones. **(B)** Some areas of the retina displayed an interrupted layer of cones. These cells did not present a typical cone morphology, with no identifiable processes being extended towards the INL, and were only identified by the presence of cone Arrestin. **(C)** Bipolar cells were seen mainly at the base of the INL. No post-synaptic processes were identified, and the pre-synaptic arborisation was reduced. While mGluR6 staining was visible in the IPL, no mGluR6-positive structures were found between the INL and SRS. Some staining could be seen between the cells in the INL, which appeared to be unspecific binding of the antibody to the cell nuclei. **(D)** Amacrine cells had unusual morphology, as they appeared fewer and smaller. Disorganisation of calretinin positive processes was visible in the IPL. Ganglion cells displayed typical morphology. (Scale bar 25µm)

5.3.3.1 Characterisation of CNGB3$^{-/-}$ iPS-derived photoreceptors at time of transplantation

To improve the experimental setup, a human iPS line with mutation in the *CNGB3* gene was differentiated into retinal organoids. Mutations in the *CNGB3* gene lead to absence of the β sub-unit of cone-specific cyclic nucleotide–gated ion channels (CNG channels), which prevents effective phototransduction (Johnson et al., 2004; Kohl et al., 2005). The use of this cell line allowed the production of healthy, but non-functional cone photoreceptors, that were transplanted and used as a negative control for all functional assays. These transplants will be called sham transplants and I will refer to this cell line as the CNGB3 line. A brief characterisation of the CNGB3 line, by immunohistochemistry, was done. This aimed to demonstrate that these cells develop similarly to the wild type hES line. Therefore, transplantation of cone photoreceptors derived from either cell line was expected to have the same impact on the host retina. However, since the iPS-derived cones have a *CNGB3* mutation, which impedes phototransduction, no rescue of function was expected in sham transplanted eyes.

The initial characterisation of this cell line was done by Dr Anai Gonzalez-Cordero. Data showed that the iPSCs have a one base pair deletion mutation in the *CNGB3* gene, c.1148deIC, which is the most common mutation reported (Kohl et al., 2005). Cells presented normal iPSC morphology, were positive for typical pluripotency markers and displayed normal karyotype (Figure 75).

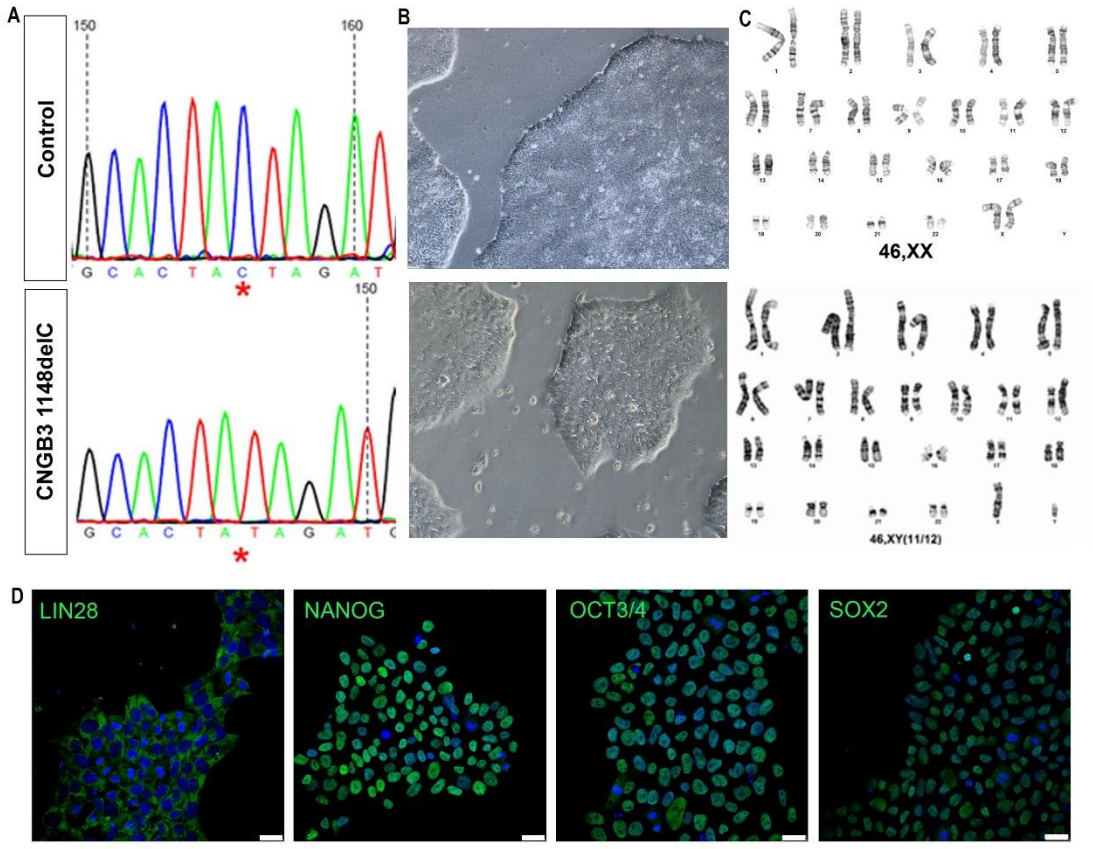

Figure 75 - CNGB3 iPS cell line characterisation, by Dr Anai Gonzalez-Cordero

(A) Sequencing data of the wildtype hESC RB2 line and the CNGB3 iPSC line showing the existence of a single base pair deletion in the CNGB3 iPS cell line (asterisk). **(B)** Bright field image of both cell lines presenting colonies with typical pluripotent cell morphology. **(C)** A normal karyotype was observed in both lines. **(D)** The CNGB3 cell line was positive for various pluripotency markers. (scale bar 25µm)

Following differentiation into retinal organoids, no obvious differences were seen between organoids derived from the wild-type RB2 or mutant CNGB3 cell lines (n = 5 retinal organoids, N = 5 differentiations, per cell line) . In both lines, human cone ARRESTIN (hCONE ARRESTIN) and RHOSOPSIN positive cells were seen at dd120 (Figure 76), as previously described (Gonzalez-Cordero *et al,* 2017). hCONE ARRESTIN was found throughout the cell bodies of the cone photoreceptors (Figure 76A'' and 76B''), which displayed characteristic cone morphology. Staining was more intense in the inner segment region. Some RHODOPSIN-positive cells were also found at this age. Similar to that seen for hCONE ARRESTIN, RHODOPSIN appeared to be found in the cell cytoplasm, not being localised, yet, to the developing outer segments (Figure 76A-B).

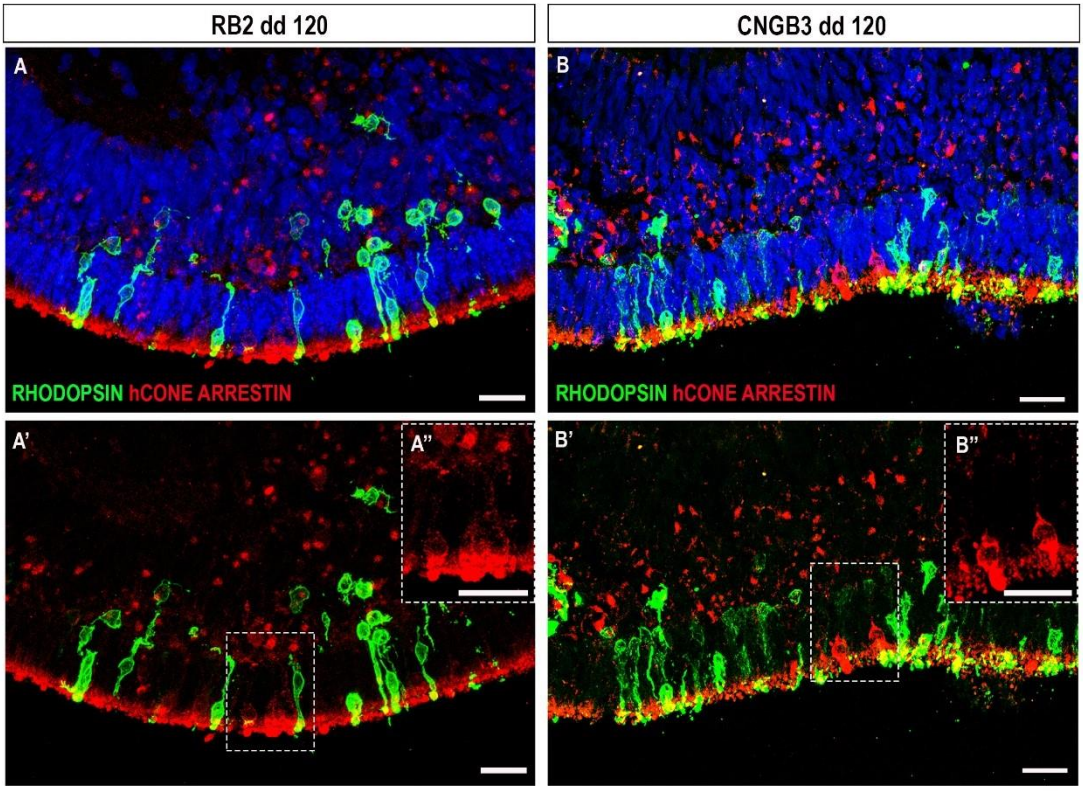

Figure 76 - Comparison between RB2 and CNGB3 retinal organoids: Photoreceptor markers

Representative confocal images showing presence of rod and cone photoreceptor precursors in retinal organoids derived from of both RB2 and CNGB3 lines. **(A, B)** Retinal organoids derived from both lines showed presence of HCONE ARRESTIN- and RHODOPSIN-positive cells. hCONE ARRESTIN-positive cells displayed typical cone morphology and are situated at the bottom of the photoreceptor layer (A'', B''). RHODOPSIN-positive cells are present throughout the photoreceptor layer and their morphology is consistent with those of rod photoreceptors. (Scale bar 25µm)

The CNGB3 mutation affects the ion channels in the outer segments and impairs phototransduction. However, it is expected that outer segments initially develop normally, despite ultimately degenerating as the mutation in the *CNGB3* gene leads to toxicity (Liu et al., 2013, p. 3). To evaluate the presence of outer segment-like structures at the time of transplantation, immunohistochemistry for PERIPHERIN2 protein was performed. Staining for a human mitochondrial marker was used to establish the extent of the inner segment area and assess if the PERIPHERIN2-positive structures were localised to the expected region. These experiments confirmed that PERIPHERIN2-positive structures, were present, small in size and localised to the expected region in photoreceptors from both cell lines (Figure 77). No obvious differences between cell lines was identified.

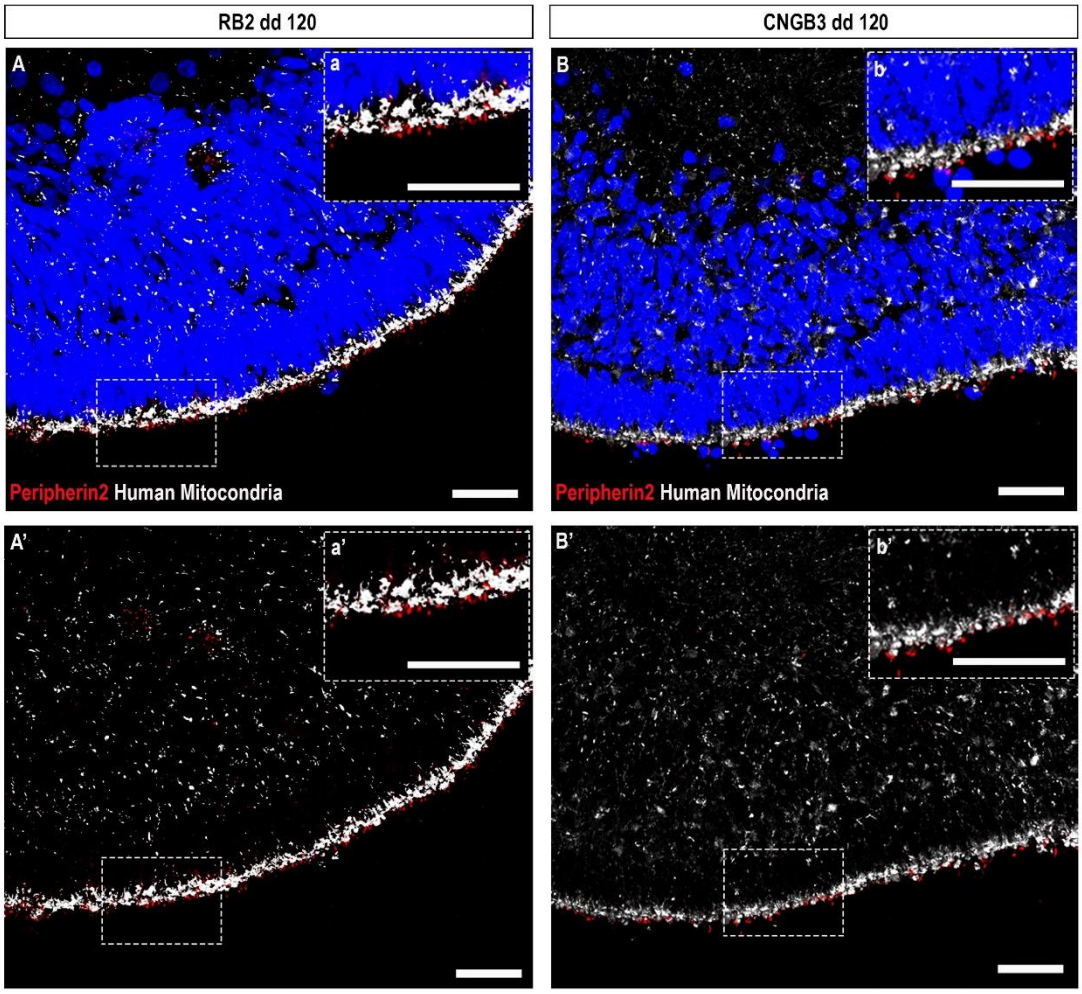

Figure 77 - Comparison between RB2 and CNGB3 retinal organoids: inner and outer segment formation

Representative confocal images showing IS-like region, rich in mitochondria, and outer segment-like region, where PERIPHERIN2-positive structures localise, in retinal organoids derived from of RB2 and CNGB3 lines. **(A)** Retinal organoids derived from the hESC line RB2 show an area rich in mitochondria, the inner segments-like region, followed by area rich in small PERIPHERIN2-positive structures, the outer segment-like region, (a and a'). **(B)** Retinal organoids derived from hiPSC line CNGB3 showed similar inner segment and outer segment-like regions, similar to the ones seen in RB2-derived retinal organoids. (Scale bar 25µm)

After establishing that retinal organoids derived from either cell lines appeared to be morphologically indistinguishable, a viral vector was used to infect L/M cone photoreceptors at dd90. Both RB2 hESC and CNGB3 hiPSC-derived retinal organoids showed presence of GFP positive cells at time of transplantation, dd120 (Figure 78A, B). The relative numbers of L/M cones were analysed by FACS, at the time of sorting prior to transplantation. A similar percentage of GFP-positive cells was found in both lines, with no significant difference being found between the yields of RB2 hESC-derived cones (15% ± 7, n = 9 FACS experiments) and CNGB3 hiPSC-derived cones (14% ± 4, n = 7 FACS experiments) (p=0.74, t-test) (Figure 78C).

In summary, the CNGB3 hiPSC line appeared to be a good source of non-functional cone photoreceptor cells.

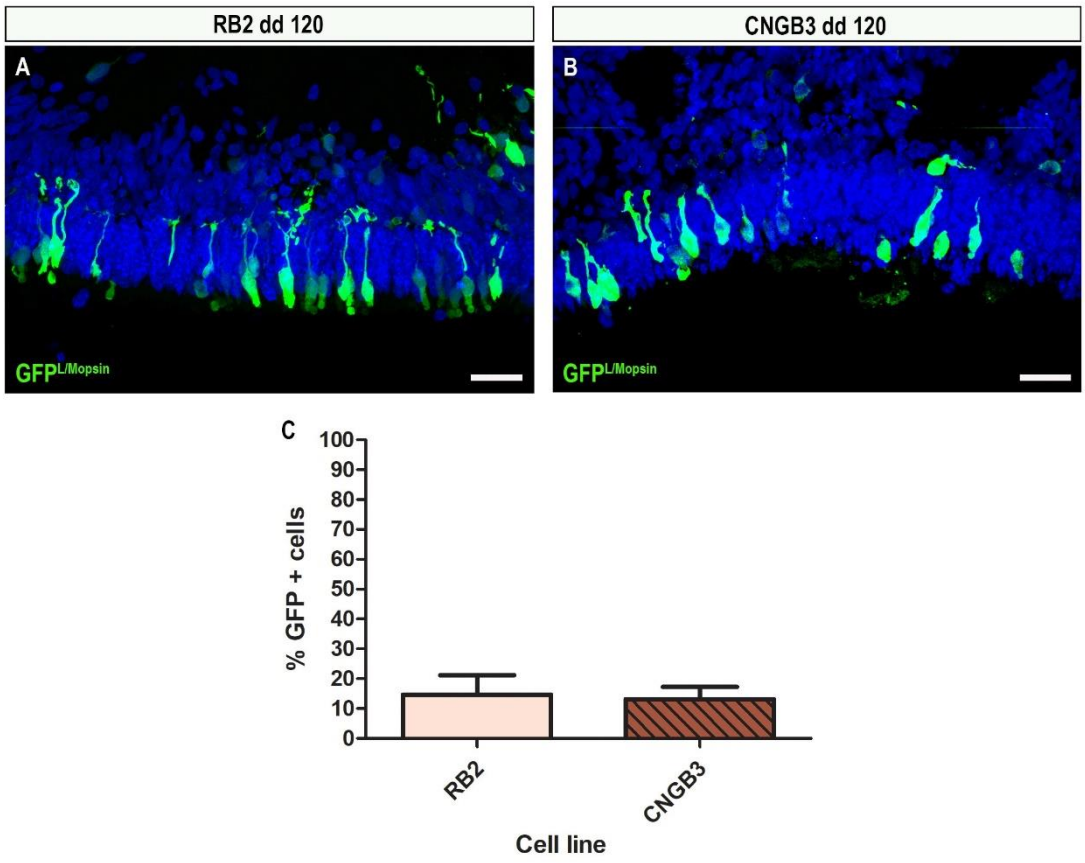

Figure 78 – Comparison of virally transduced cones in retinal organoids derived from RB2 and CNGB3 cell lines

(A-B) Representative confocal projection images showing presence of GFP-positive cells with cone morphology in retinal organoids derived from RB2 hESC (A) and CNGB3 hiPSC (B). (Scale bar 25µm) **(C**) At time of transplantation, the percentage of GFP positive cells, was not significantly different between retinal organoids derived from each cell line (t-test, RB2: 15% ± 7, n = 9; CNGB3: 14% ± 4, n = 7). The GFP-positive cells are the cones transduced by the ShH10.Mopsin.GPF vector.

5.3.3.2 Characterisation of photoreceptor maturation and host interaction following transplantation

GFP positive L/M hESC and hiPSC-derived photoreceptors were dissociated and sorted as described in chapter 4. A cell suspension of ~500,000 cones was transplanted into the subretinal space of 3 months old *rd1/Foxn1*^{nu} mice (n = 32 eyes, N = 31 animals received RB2 hESC-derived cones; n = 23 eyes, N = 20 animals received *CNGB3*$^{-/-}$ hiPSC-derived cones). Due to the shortage of animals some mice were injected in both eyes. However, whenever possible only one eye per animal was injected. Behaviour experiments, to assess visual function, were performed 12 weeks following transplantation. Eyes were then collected either for MEA experiments or immunohistochemistry experiments. When possible, retinas were collected following MEA experiments for morphological analysis by immunohistochemistry. For simplicity/clarity, all the immunohistochemistry data will be presented first, followed by the MEA and behavioural assessment of visual function.

Some injected animals were subjected to fundoscopy analyses, in order to identify any differences between cell masses *in vivo*. Both RB2 hESC-derived and CNGB3 hiPS-derived cones showed good survival and created a vast cell mass in the hosts' subretinal space, 12 weeks following transplantation. Some variability was seen regarding shape and spread of cell masses; however, this did not seem to be dependent on cell line (Figure 79). Fundoscopy data was collected by Dr Mark Bache.

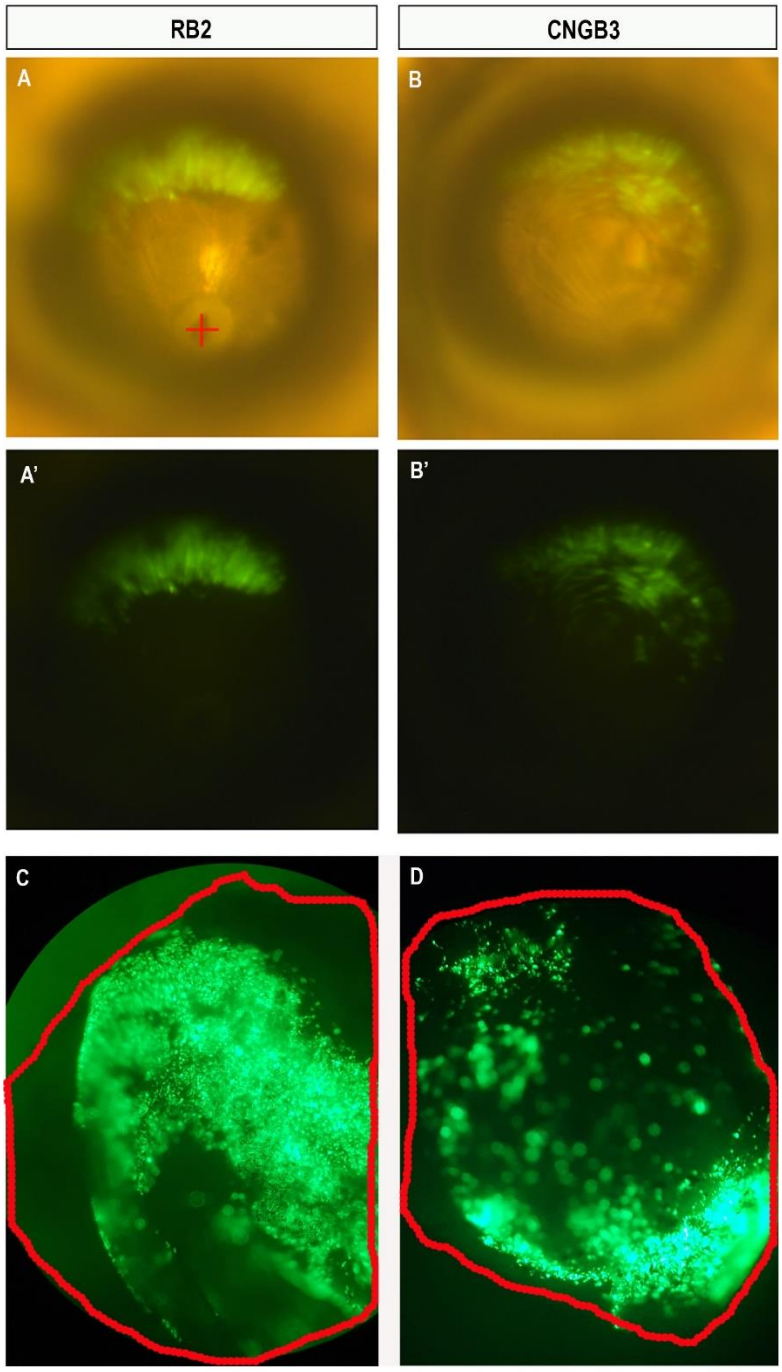

Figure 79 - Imaging of cell masses 12 weeks following transplantation into *Rd1/Foxn1^{nu}*

Representative images of fundoscopy and fluorescence microscopy showing the presence of vast GFP positive cell masses following transplantation. **(A,B)** Fundoscopy showed presence of GFP-positive region in superior retina of *Rd1/Foxn1^{nu}* animals injected with human cones derived from both cell lines, RB2 and CNGB3 **(C)** A vast cell mass could be seen in retinal explants of eyes that were injected with RB2 hESC-derived cones. The cells appeared to form a thick layer of photoreceptor cells. The red line shows the limit of the retinal explant. **(D)** The cell mass was equally large in retinal explants of eyes that were injected with CNGB3 hiPC-derived cones, despite the 3-dimensional nature of the tissue not allowing all of the cell mass to be in focus. However, the extensive spread of the cell mass can still be seen. The red line shows the limit of the retinal explant.

Following transplantation, 71% of the injected eyes showed a cell mass (n= 55 eyes, N=51 mice). This percentage includes both the RB2 and CNGB3 cell lines. Data was collected considering samples collected for immunohistochemistry, in which cell mass was identified following cryosection, samples collected for MEA experiments, in which cell masses were identified by immunofluorescence microscopy observation of the retinal explant, prior to MEA experiments. When analysing each cell line individually, RB2 transplants were less successful with a 66% success rate (n = 32 eyes, N = 31 animals), compared with CNGB3 with a 78% success rate (n = 23 eyes, N = 20 animals). It is important to mention that most eyes that did not show a cell mass corresponded to the first rounds of injections which were done using RB2 hESC-derived cones. Immunohistochemistry showed that not only the survival and spread of the cells was similar, but cells also displayed similar morphological features (Figure 80), with cells extending processes towards the host INL (n = 7, n = 13 eyes that received RB2 hESC or CNGB3 hiPSC-derived cones, respectively).

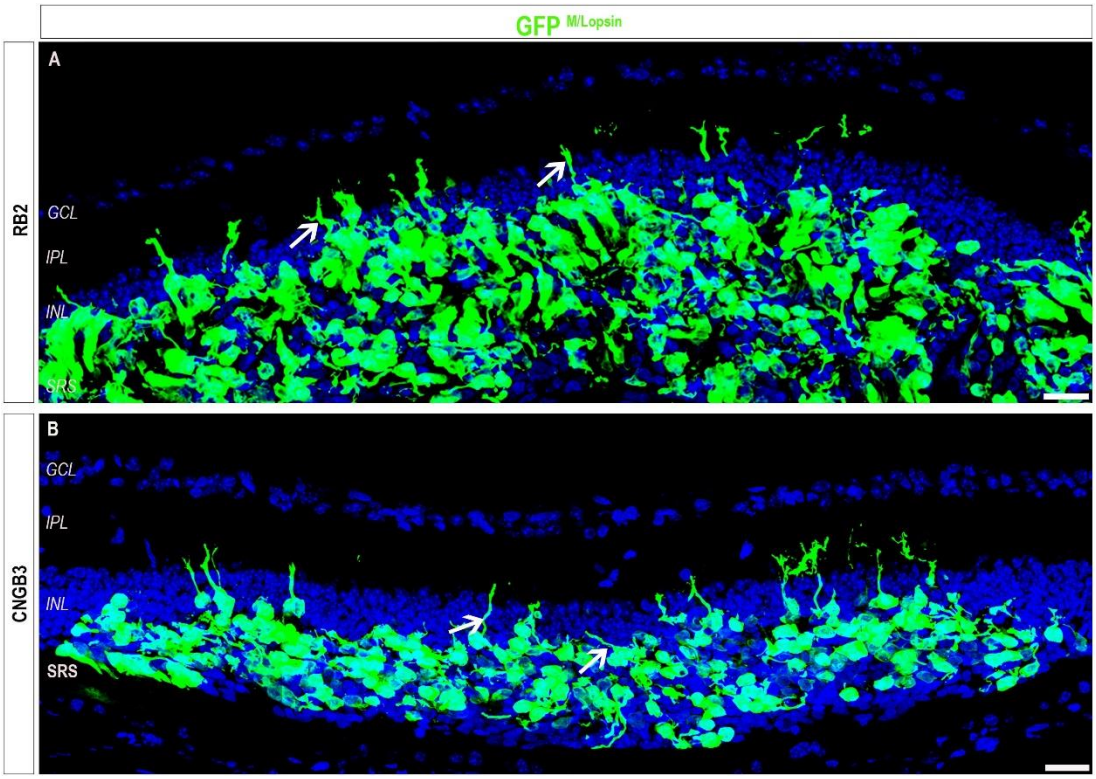

Figure 80 - Cell mass 12 weeks following transplantation into *Rd1/Foxn1^{nu}* mice

Confocal image showing presence of L/Mopsin.GFP-positive cells in the subretinal space of 7 month old *Rd1/Foxn1^{nu}* mice, 12 weeks following transplantation. **(A)** Human RB2 ESC-derived cones survived following transplantation forming a thick cell mass. Some of the cells extended processes towards the host retina (arrows). **(B)** Similar findings were seen for human CNGB3 iPSC-derived cones, that also showed good survival following transplantation and extended processes into the host INL. (Scale bar 25µm)

Development of outer segments, essential for light detection, was evaluated by the presence of PERIPHERIN2- positive structures. Cells within RB2 hESC-derived cone cell masses showed PERIPHERIN2-positive outer segment-like structures that were often elongated (Figure 81) rather than bud-like, as seen previously when transplanting into immune competent *Aipl1*$^{-/-}$ mice and collecting eyes 3 weeks following transplantation (Figure 54).

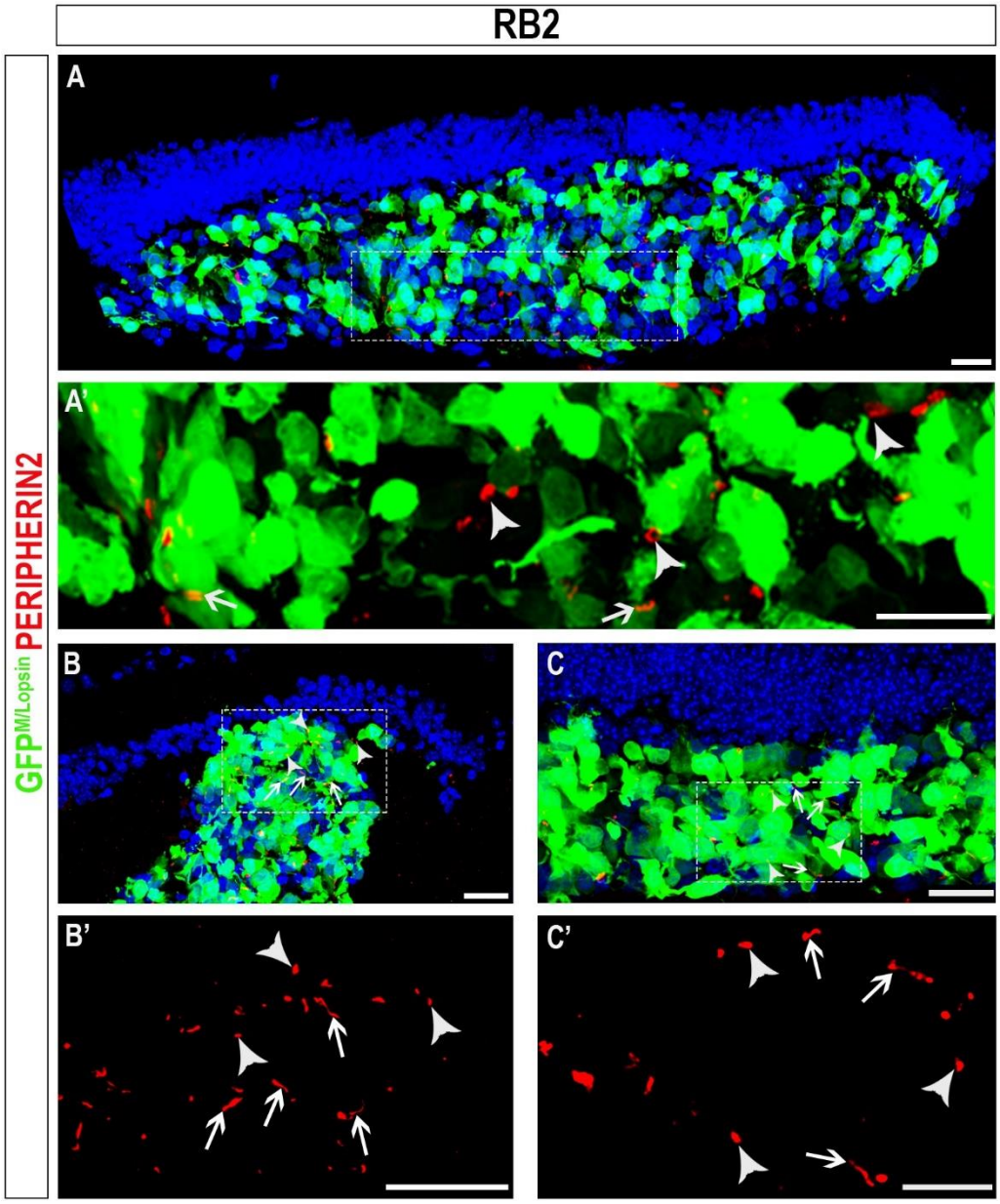

Figure 81 - Outer segment formation in RB2 hESC-derived cones 12 weeks following transplantation

Representative confocal projections showing presence of outer segment-specific protein PERIPHERIN2 in the transplanted RB2 hESC-derived cone photoreceptors. **(A-C)** Many transplanted cells in areas with a large cell mass displayed PERIPHERIN2-positive structures. As more visible in the close-up images, some of those structures were buds (arrow heads) while others were longer (arrows) resembling a more mature outer segment (Scale bar 25µm)

No obvious differences could be seen between RB2 hESC-derived and CNGB3 hiPS-derived cones, regarding presence of this outer segment specific marker. PHERIPHERIN2-positive outer segment-like structures were also present, in CNGB3$^{-/-}$ hiPSC-derived cones twelve weeks following transplantation (Figure 82).

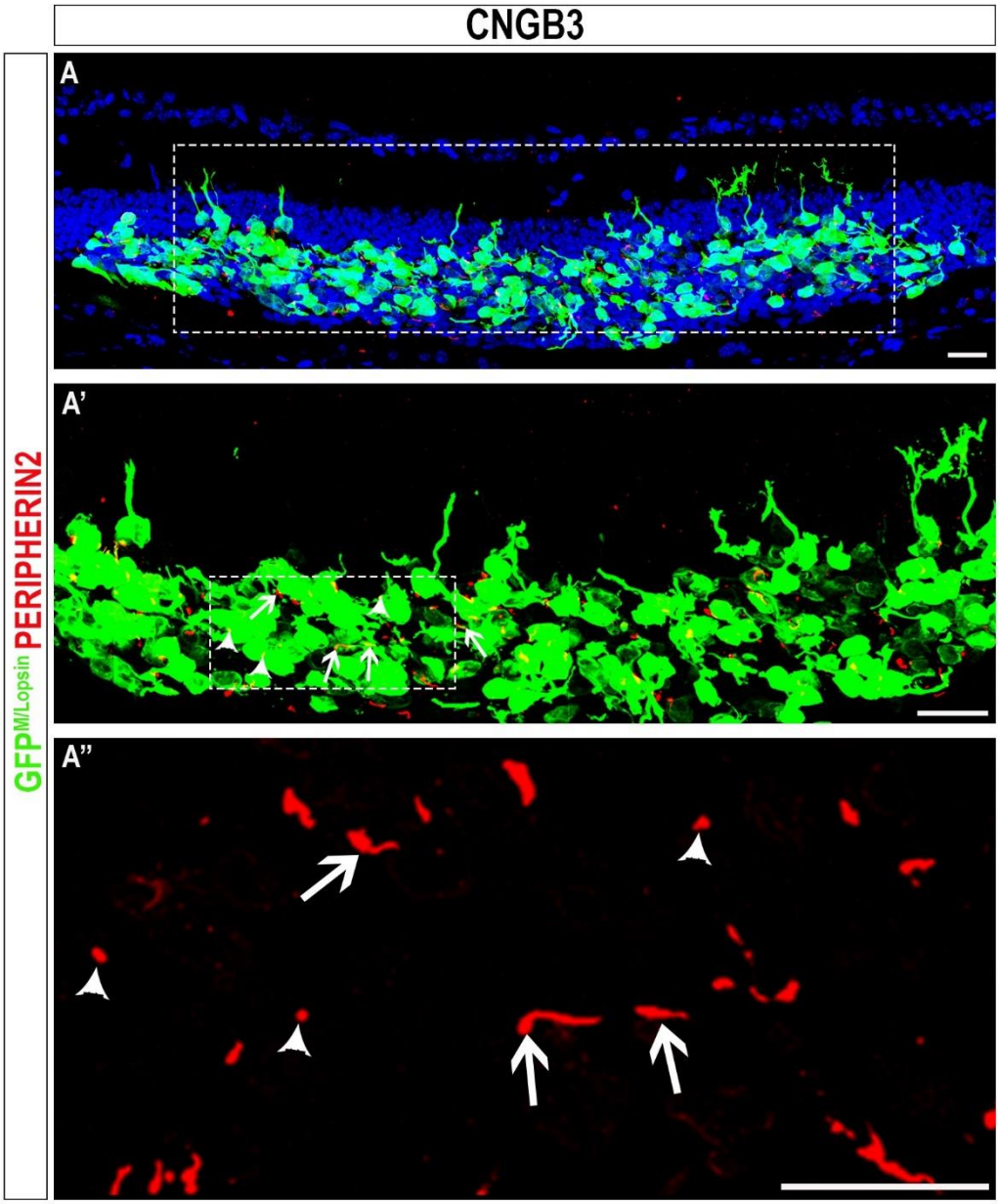

Figure 82 - Outer segment formation in *CNGB3* hiPSC-derived cones 12 weeks following transplantation

Representative confocal projections showing presence of outer segment specific protein PERIPHERIN2 in the transplanted CNGB3 hiPSC-derived cone photoreceptors. **(A)** Many transplanted cells in areas of large with a cell mass displayed PERIPHERIN2-positive structures. As more visible in A' and A'', some of those structures were buds (arrow heads) and others were longer (arrows) resembling a more mature outer segment. (Scale bar 25uµm)

To further evaluate cell maturation following transplantation, immunohistochemistry against L/M OPSIN was performed. By using this marker, a potential difference between RB2 hESC-derived and CNGB3 hiPS-derived cones was identified. Despite most transplanted cells being positive for L/M OPSIN and showing presence of this marker throughout the cell body, some cells showed localisation to an outer segment-like bud. These cells were a minority of the ones in the cell mass, however it appeared that only RB2 hESC-derived cones showed such L/MOPSIN localisation. Further analysis and formal quantification are necessary to further support this finding (Figure 83).

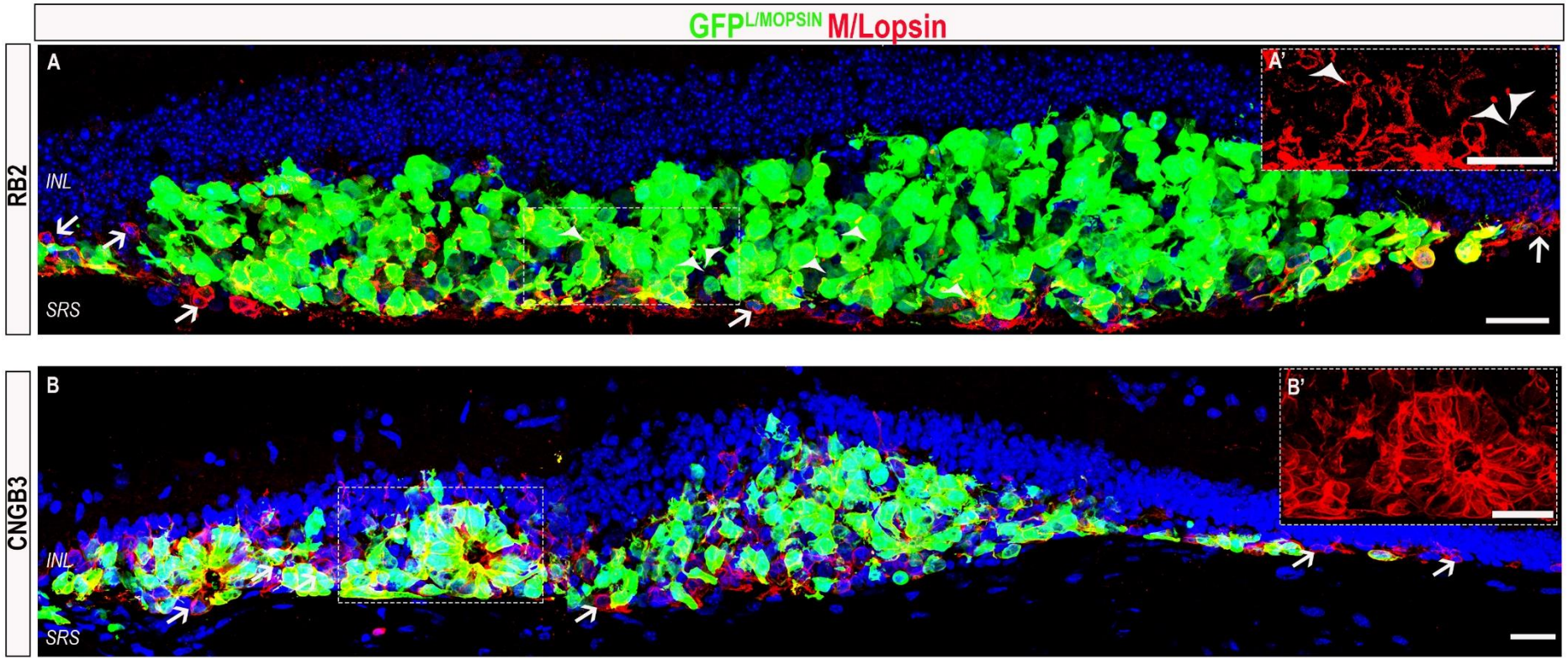

Figure 83 - Presence of L/MOPSIN in RB2 hESC and hiPSC-derived cones 12 weeks following transplantation

Representative confocal projections showing mature marker, L/MOPSIN, in transplanted cone photoreceptors. **(A)** Most RB2 hESC-derived cones showed Mopsin in the cell bodies. Rare cells appear to localise L/Mopsin to outer segment-like buds (A'). A few host Mopsin-positive cones were also identified (arrows) close to the cell mass, showing Mopsin in their cell bodies. **(B)** Similar results were seen in transplanted CNGB3 hiPSC-derived cones, with L/Mopsin presence in the cell bodies. No L/Mopsin rich buds were identified. Rare host Mopsin- positive cones were also present (arrows). (Scale bar 25 µm)

To study the interaction between transplanted hESC-derived cones and host retina rod bipolar cells specific marker, PKC-α, and post-synaptic protein, mGluR6 were analysed. As expected, due to the findings following transplantation into *Aipl1*$^{-/-}$ mice (see chapter 4, section 4.3.2), transplanted cells interacted with the host retina. The host's bipolar cells extended processes into the cell masses, sometimes measuring up to 55µm in length, seeking out terminals of transplanted cones (Figure 84, arrows). Such findings were only seen in areas where cell mass was identified. In un-injected eyes (Figure 74C) or in areas of injected eyes where no cell was present, no dendrites extension was observed. This supports the hypotheses that such axon growth is being guided by the transplanted hESC-derived cones, possibility by their pre-synaptic output. Presence of post-synaptic marker mGluR6 was also detected in areas where big cell masses were present. In *rd1/Foxn1*^{nu} mice, at 3 months of age, presence of this protein was only found at the IPL (Figure 74C').Presence of hESC-derived cones appear to induce synthesis and/or at least trafficking of mGluR6 protein to the post-synaptic terminals of bipolar cells. The plasticity revelled by the host retina, suggests major adjustments of the host synaptic circuit in response to the presence of hESC-derived cones, possibly due to changes in the microenvironment.

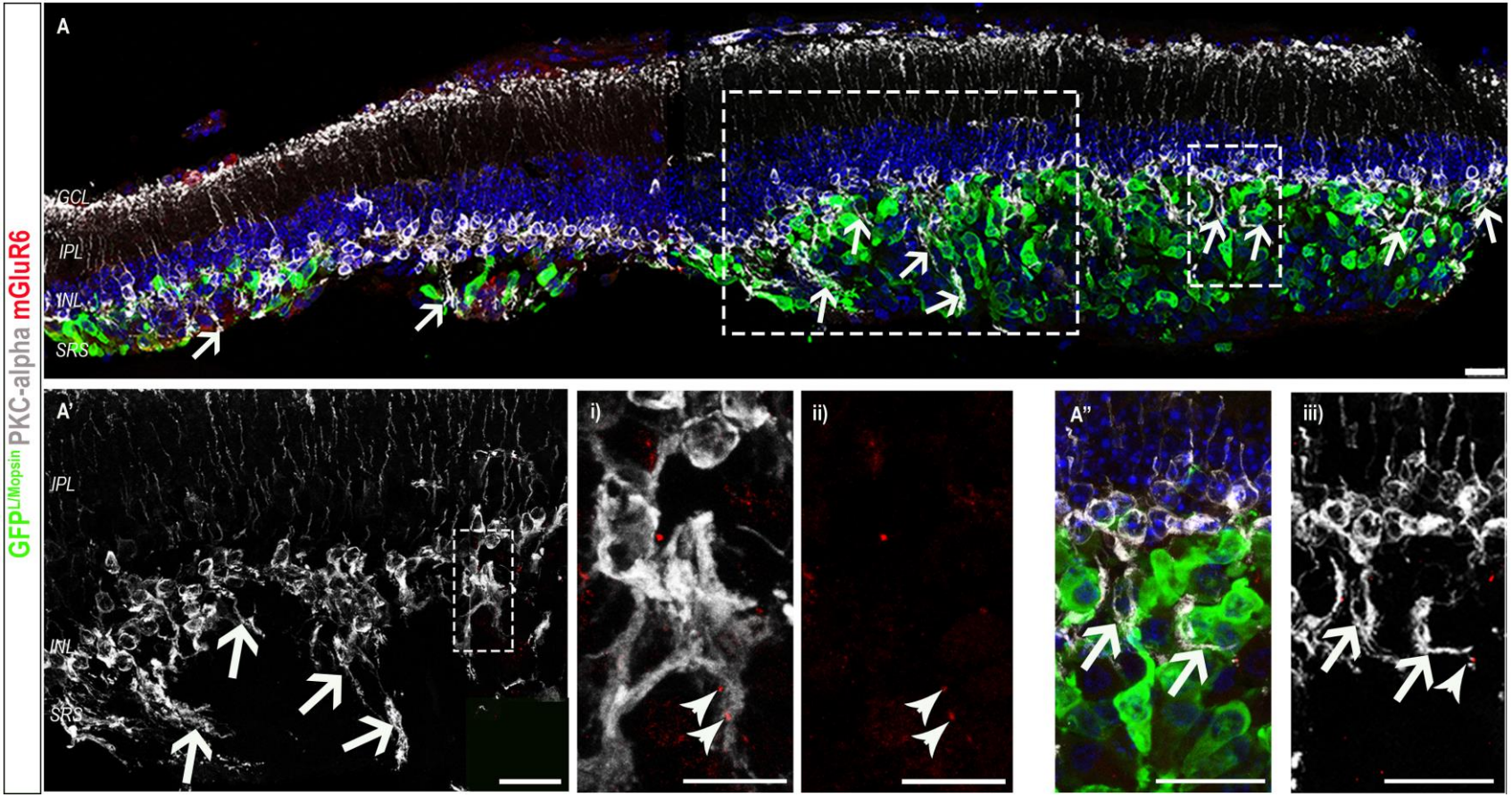

Figure 84 - Interaction between host retina and transplanted RB2 hESC-derived cones, 12 weeks following transplantation

Examples of confocal projections showing presence of rod bipolar cell processes (PKCα positive) and post-synaptic protein mGluR6 in areas where transplanted RB2 hESC-derived cones formed a large cell mass in the subretinal space. **(A**) Rod bipolar cells extended processes into the cell mass (arrow). mGluR6-positive structures were abundant and sometime co-localised with a rod bipolar cell's post-synaptic processes (arrowhead). (Scale bar 25µm)

Finally, indication of potential synaptic connections between transplanted cells and host retina was investigated. Pre- and post-synaptic markers, RIBEYE and mGluR6, were observed in the subretinal space of animals injected with hESC-derived cones. Their close proximity supported potential formation of synapses between host and transplanted cones (Figure 85).

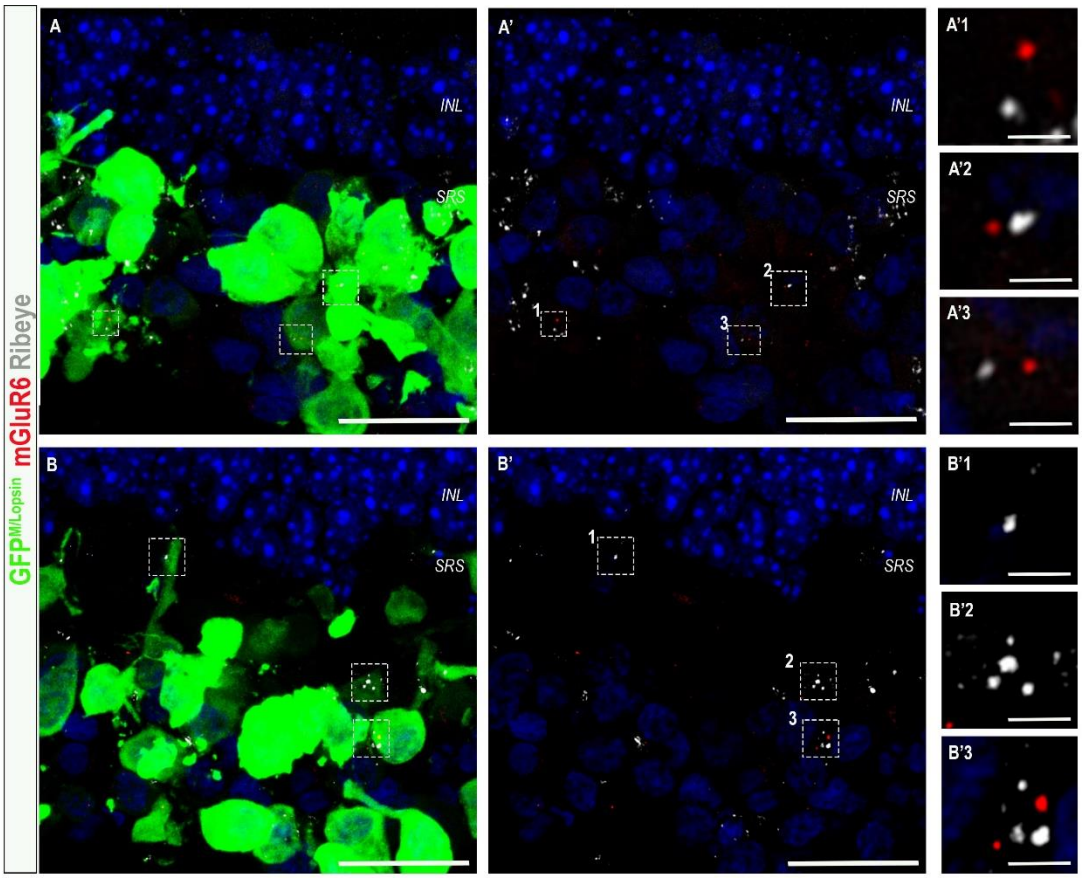

Figure 85 - Synaptic markers and possible connections between host and RB2 hESC-derived cones, 12 weeks following transplantation

Confocal projections showing presence of pre-synaptic protein RIBEYE and post-synaptic protein mGluR6 in areas of RB2 hESC-derived cones cell mass in the subretinal space of *Rd1/Foxn1*^{nu}. **(A, B)** RIBEYE positive structures present in transplanted RB2 hESC-derived cones were, occasionally, found in close proximity to mGluR6 positive structures (A'1-A'3, B'3). RIBEYE and mGluR6 were not always in close proximity (B'1, B'2) (Scale bar 25µm, A-B'; 3µm, A'1-B'3)

As expected, *CNGB3*$^{-/-}$ hiPSC-derived cones also interacted with the host retina, having the same morphological impact as the wild-type RB2 hESC-derived cones. This was not surprising because these cones, despite non-functional, developed and matured following transplantation, displaying no morphological differences. *CNGB3*$^{-/-}$ cones are unable to hyperpolarise in response to light, however they still able to produce neurotransmitters and other proteins which might contribute to the microenvironmental changes in the subretinal space of host animals. Therefore, transplantation of CNGB3 hiPSC-derived cones also led to extension of rod bipolar cell dendrites into the cell mass. Reappearance of mGluR6 protein in these dendrites and pre- and post-synaptic proteins in close proximity were also observed (Figure 86), similarly to the findings reported following transplantation of wild-type hESC-derived cones (Figure 84 and 85).

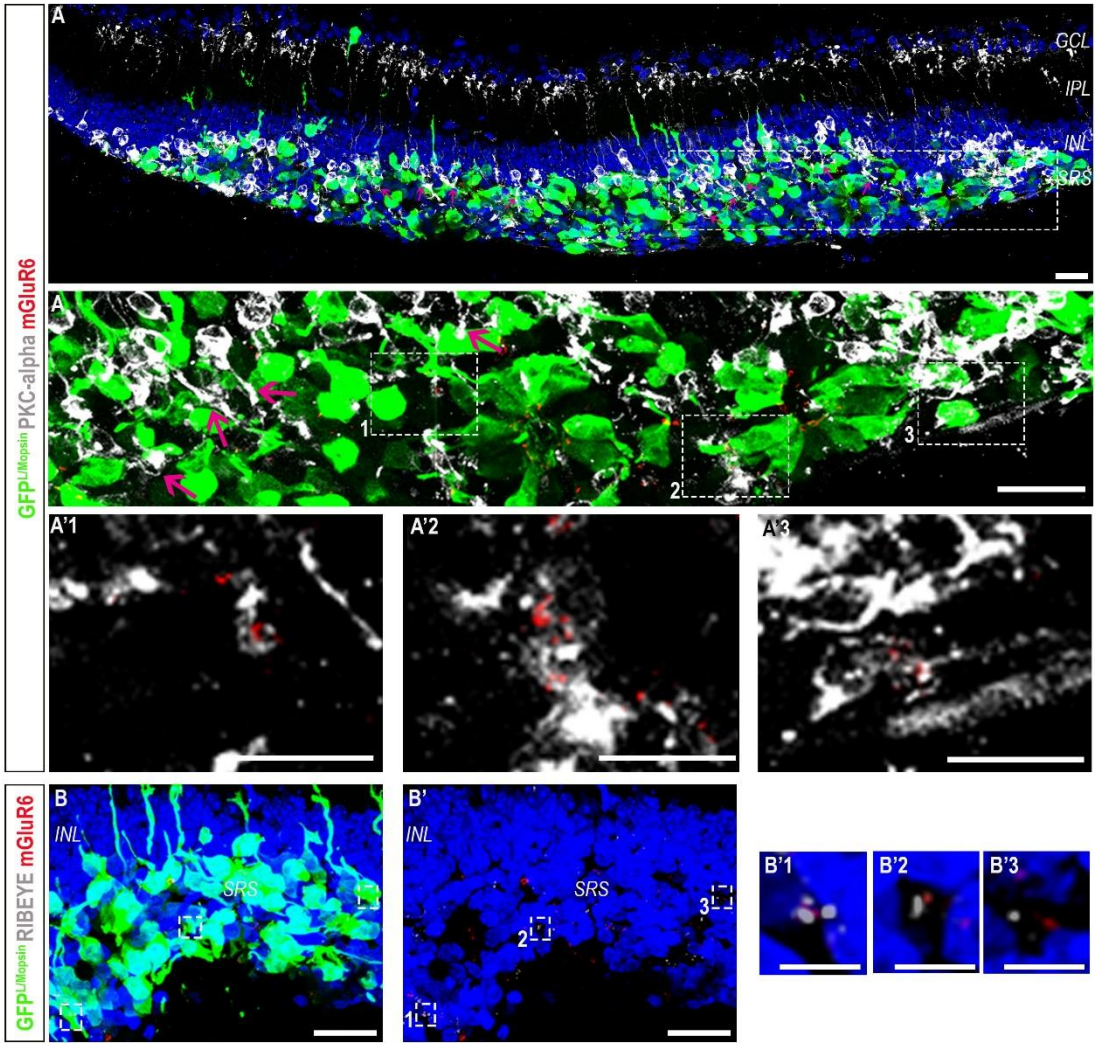

Figure 86 - Interaction between host retina and CNGB3 hiPSC-derived cones, 12 weeks following transplantation

Confocal projections examples showing presence of rod bipolar cell processes (PKCα-positive) and post-synaptic protein mGluR6 in areas where transplanted CNGB3 hiPSC-derived cones a formed large cell mass in the subretinal space. **(A**) Rod bipolar cells extended processes into the cell mass (pink arrows). mGluR6 positive structures were abundant and, in some instances, co-localised with a rod bipolar cell's post-synaptic process (A1'-A3'). **(B)** RIBEYE-positive structures were present in transplanted cones and could occasionally be found in close proximity to mGluR6-positive structures (B'1-B'3). (Scale bar 25µm, A-B'; 6.25µm, B'1-B'3)

5.3.3.2.1 Assessing Visual Function following transplantation

In order to establish if retinal and or visual rescue was now detectable, as extending the post-transplantation period allowed more time for transplanted cell and host retina to establish connections, behavioural and electrophysiology experiments were performed. With the benefit of the results described in previous chapters and the limitations of working with immune compromised animals, some of the experimental set-ups were altered or excluded.

5.3.3.2.1.1 ERG

All ERG data was collected by Aura Hare and analysed by the author of this thesis.

Twelve weeks following transplantation, ERG recordings were performed (N = 11; N = 10 animals recipients of RB2 hESC or CNGB3 hiPSC-derived cones, respectively), as previously described, by recording electrical changes at the corneal surface(see Methods, 2.11.1). No a-wave, which reflects the initial photoreceptor's hyperpolarisation and is seen in an ERG trace as a negative deflection of voltage, was observed. Is important to note that a recording artefact could be seen in the highest light levels under photopic conditions. This artefact resembled a negative deflection and could be confused with an a-wave. However, it was present in both injected and un-injected eyes across several animals independently of which cells – if any – they received. Furthermore, other colleagues in the laboratory reported the same findings in other mice strains, which excludes the possibility of these results being an abnormality of *rd1/Foxn1*^{nu} phenotype and corroborates that these observations were produced by a technical artefact. Similarly. no b-waves, a positive deflection which is produced by the depolarisation of bipolar cells, could be identified in any of the tested animals. Representative traces of an animals which received RB2 hESC-derived cones in its right eye, with left eye being un-injected, are shown in figure 87.

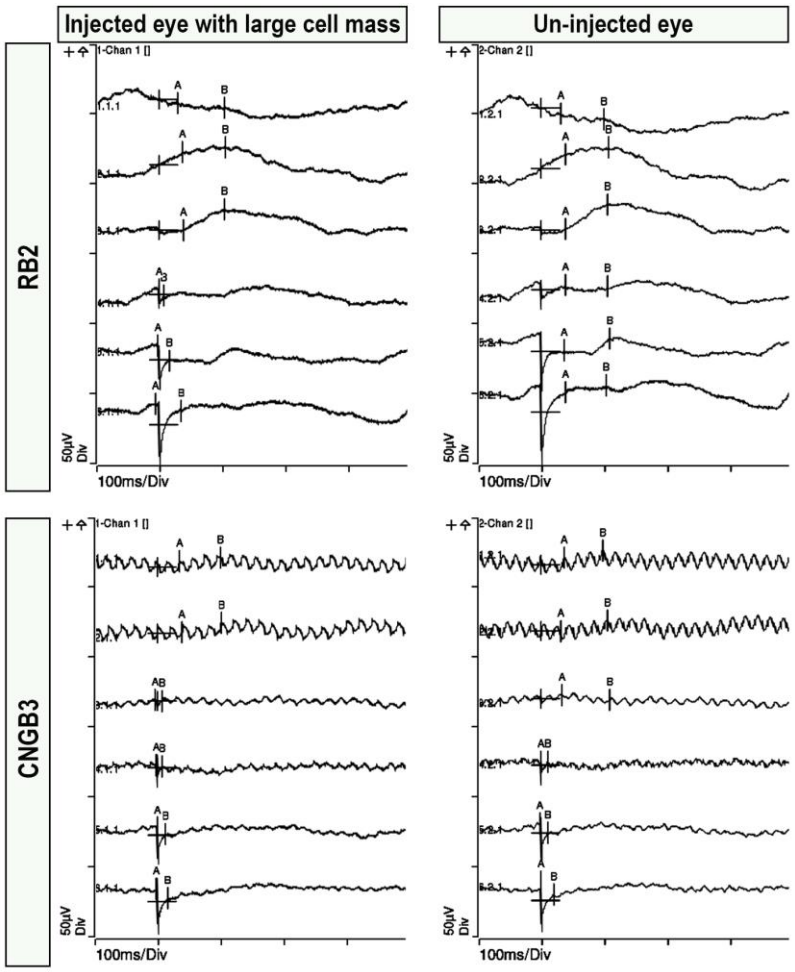

Figure 87 - Representative ERG traces under photopic conditions 12 weeks following transplantation into *Rd1/Foxn1*^{nu} mice

No a- or b- wave could be detected in any of the eyes, regardless whether eyes had received injections of sham transplant, wild-type cells or were un-injected. A recording artefact, voltage negative deflection at photopic light levels, was present across all tested animals.

5.3.3.2.1.2 MEA

All MEA data was collected and analysed by Dr Christopher Procyk.

As described previously (see chapter 3 and methods chapter), MEA is a state-of-the-art electrophysiology technique which utilises the same basic principles of an ERG, being often call a focal ERG. As in an ERG, MEA records extracellular electrical changes however, these are recorded directly from RGCs. Therefore, MEA is a more sensitive technique, able to detect smaller electrical changes, which cannot be detected by at the corneal surface by a full-field ERG. Furthermore, as experiments are performed *in vitro,* manipulation of the solution where retinal tissue is maintained is possible. This presents an opportunity to study synaptic connection by adding specific synaptic blockers to this solution. Since photoreceptor-derived responses require synaptic connection to reach RGCs, pharmacology can provide ambiguous evidence that synaptic connections between transplanted cones and host retina were established.

Briefly, eyes were collected, 12 weeks following transplantation, and kept in oxygenated medium. Retinas were carefully removed from the eye cups under a dissection microscope. For eyes which received cell transplantation, examination under a fluorescent microscope allowed identification of areas with GFP positive cells. These areas were selected and dissected from the retinal explants and placed on top of the electrodes, in contact with RGCs. Retinal tissue was left to dark adapt for up to an hour, with temperature control (~36°C) and oxygen being provided, in order to keep the tissue alive. RGCs spontaneous spiking was used as an indication of heath of the tissue and its presence was required to proceed with MEA experiments. Retinas were then exposed to the light stimulus. To identify transient, typical cone-derived responses, and sustained responses, typical of ipRGCs (see methods chapter and chapter 3 for further detail), shorter, 1 second, and longer, 10 seconds, light pulses were used (20 repeats). Recordings were initiated 2 seconds prior and terminated 5, to a 1 second stimulus, or 60, to a 10 seconds stimulus, seconds following to light stimulus.

Despite 14 eyes with RB2 transplants and 5 with CNGB3 transplants, all with cell masses, having been collected for MEA, not all preparations were successful. Furthermore, some of the samples that have been recorded from have not yet been spike sorted and analysed, since data analysing is a long and time-consuming process. Nonetheless, some conclusions can be drawn by examining the un-spike sorted data and the data sets that have been spiked sorted to date. Here the results

of these experiments are described in order to assess if transplanted RB2 hESC-derived cones can confer light invoked responses in the host retina. This data would support the previous results showing that transplantation of these cells can potentially lead to synaptic formation.

Untreated rd1/Foxn1^{nu} retinas, at 6 months of age (N = 4) were used to establish the base line responses in this strain. Retinas that received CNGB3 hiPSC-derived cones (N = 4), were used as sham controls, as these cells were not expected to rescue retinal function. Adult *GNAT1*$^{-/-}$ retinas (N = 4) were chosen as a positive control for these experiments, as in these retinas the rods are functionless and consequently all the photoreceptor-derived responses recorded up by the MEA were generated by cones. Therefore, these retinas provided an ideal comparison to retinas that received RB2 hESC-derived cones (N = 4). As expected, no transient-type responses (rapid changes in firing rate followed by a rapid return to base line) to a 1 second light stimulus were identified in either untreated rd1/Foxn1^{nu} retinas or retinas that received CNGB3 hiPSC-derived cones (Figure 88A, B). Importantly, no differences were identified between these 2 groups, which corroborated that no rescue of function of the host retina was achieved by neurotrophic preservation of the remaining host photoreceptors. In *GNAT1*$^{-/-}$ retinas clear light responses could be seen by quick changes in firing rate following the 1 second light stimulus (Figure 88C), displaying a very different profile to what was seen for untreated and sham transplanted retinas. Interestingly, retinas that received RB2 hESC-derived cones shown presence of transient light responses, similar to what was seen in *GNAT1*$^{-/-}$ retinas (Figure 88D). Despite presenting a similar profile, the responses seen in *GNAT1*$^{-/-}$ controls displayed higher frequency, with more impulses per second being recorded, than retinas transplanted with RB2 hESC-derived cones (note the different scales used in Figure 88).

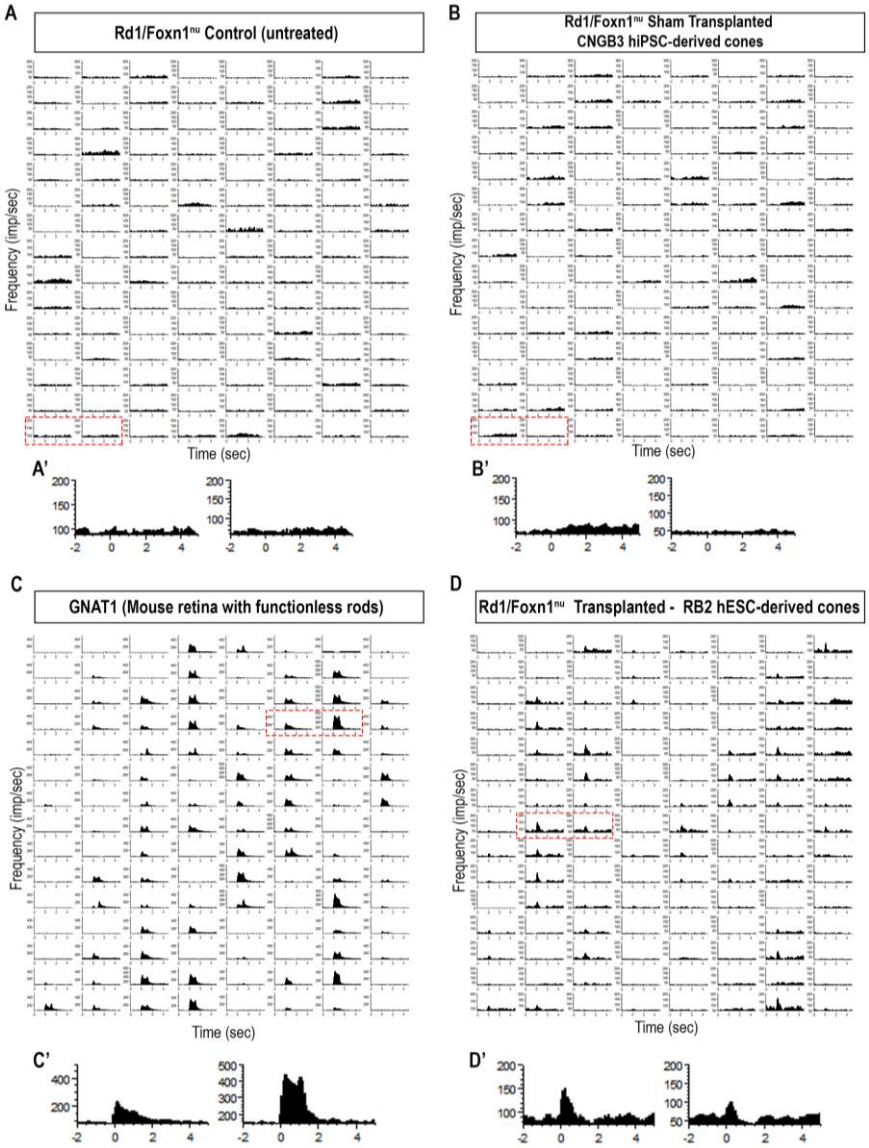

Figure 88 - Responses profiles in multi-unit MEA data

Peristimulus time histogram (PSTH) of representative experiments for each control and for transplanted retinas. Frequency of *GNAT1*$^{-/-}$ retinas is scale to a maximum of 500 and all other graphs are scaled to a maximum of 200 impulses/second. All graphs are base line subtracted. Light stimulus went on at 0 seconds. **(A)** *rd1*/Foxn1^{nu} retinas did not show an increase in spiking following light stimulus. Spontaneous spiking was recorded in these retinas. **(B)** RD1/Foxn1^{nu} retinas that received CNGB3 hiPSC-derived cones showed similar responses to what was seen in untreated RD1/Foxn1^{nu} retinas. **(C)** A different profile of responses was recorded in GNAT1$^{-/-}$ "cone only" retinas. An increase in frequency of spiking was recorded after the light stimulus was turned ON and in some cases another peak could be detected following the stimulus turning OFF. These changes in firing frequency were rapid. **(D)** RD1/Foxn1^{nu} retinas that received RB2 hESC-derived cones showed similar responses to what was seen in GNAT1$^{-/-}$ retinas, with spiking frequency changing rapidly following light stimulus and returning to base line in a similar time frame. The change in frequency was lower than what was seen in GNAT1$^{-/-}$ retinas. No increase in frequency could be seen, in this example, following light stimulus turning OFF. Each dashed box marks two representative channels that can be seen in more detail in A'-D'.

To confirm that the transient responses seen in RB2 hESC-derived cone injected eyes, were originated by photoreceptor cells, synaptic blockers were used (see methods 2.11.2) (Figure 89 A-F). All transient light responses seen in RB2 injected retinas were abolished upon addition of synaptic blockers. After washing out the synaptic blockers, the transient responses returned. The same was seen in *GNAT1*$^{-/-}$ retinas, which were used as positive controls for these experiments. Synaptic blockers did not obliterate the small non-transient responses seen in retinas that received *CNGB3*$^{-/-}$ hiPSC-derived cones (Figure 89 G-I). These responses were consistent with what would be expected from ipRGCs since they appear sustained and were not blocked by the addition of synaptic blockers.

This data provided a strong indication that the transient responses originated in transplanted photoreceptor cells. Nevertheless, it is important to be aware that that each channel could be recording from one or more cells and that responses seen in multi-unit data might not be spike sortable, due to the noise to response ratio. Therefore, the unsorted data should be taken as promising and supportive of retinal/visual rescue following photoreceptor transplantation, but further analysis is required to understand the extent of such rescue. The representative examples shown in figure 88 and 89 are consistent across all the recordings for each of the conditions.

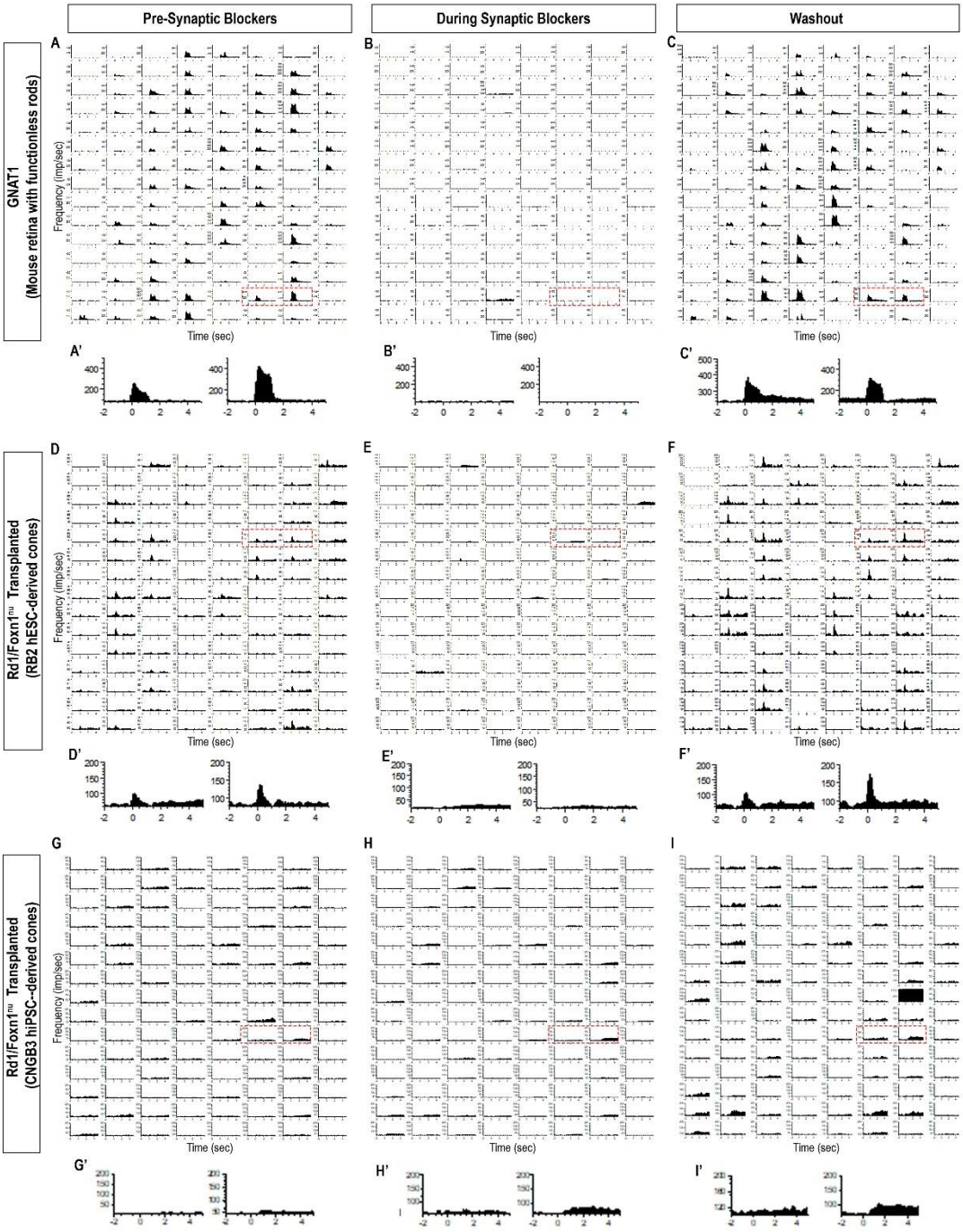

Figure 89 - Multi-unit MEA data in presence of synaptic blockers

Peristimulus time histogram (PSTH) of representative experiments GNAT1$^{-/-}$ control and RB2 transplanted retinas. Frequency of GNAT1$^{-/-}$ retinas is scaled to a maximum of 500 and RB2 transplant is scaled to a maximum of 200 impulses/second. Both graphs are base line subtracted. Light stimulus went on at 0 seconds. **(A, D)** Transient light responses were seen in both GNAT$^{-/-}$ eyes and RB2 injected eyes (see detailed description in figure 88). **(B, E)** After addition of synaptic blockers all transient responses were silenced. **(C, F)** Following washout of the synaptic blockers the transient responses returned. Each dashed box marks two representative channels that can be seen in more detail in A'-F'. **(G-I, D)** No **t**ransient light responses were seen in untreated Rd1/Foxn1^{nu} eyes. The responses seen were small in amplitude and were not obliterated upon addition of synaptic blockers.

The differences seen in the multi-unit data were strengthened following spike sorting. Further analysis of the data was done in the subset of experiments that have been spike sorted thus far. Each unit that could be isolated from the multi-unit data represents an individual RGC and was classified as light responsive or not light responsive, to a 1 second light stimulus. Light responsive units were further classified as Transient-ON, Transient-OFF, Transient-ON-OFF or transiently suppressed by light. Retinas that received RB2 hESC-derived cones showed a variety of responses to light, having LR units that fitted each of the categories described above, similar to what was seen in *GNAT1*$^{-/-}$ retinas (Figure 90). The percentage of non-light responsive units in retinas that received RB2 hESC-derived cones was 48%, which is higher than the 13% found in *GNAT1*$^{-/-}$ retinas. This is not unexpected as the immunohistochemistry showed that the transplanted cells are not organised like an ONL and the spread of the cell mass was variable between samples and different areas of the same sample. This could influence the ability of transplanted cells to establish synaptic connections with the host retinas, while in the *GNAT1*$^{-/-}$ retina all cone photoreceptors are connected to the synaptic network. The majority of light responsive units found were classified as ON responses, with 35% of the light responses found in *GNAT1*$^{-/-}$ retinas and 26% of the light responses found in RB2 host retinas showing this profile. OFF responses were the rarest in both *GNAT1*$^{-/-}$ and retinas that received RB2 hESC-derived cones, with only 13% and 3%, respectively, being classified as such. The firing rate appeared to be lower in retinas that received RB2 hESC-derived cones than in *GNAT1*$^{-/-}$, for both ON and OFF responses. The biggest difference between these groups appeared to be in the percentage of ON-OFF responses, with *GNAT1*$^{-/-}$ retinas showing this type of response in 17% of their light responsive units while retinas that received RB2 hESC-derived cones showed such response in only 4% of their light responsive units. Units that were supressed by light were present in both *GNAT1*$^{-/-}$ and RB2 transplanted host retinas, 22% and 19% of light responsive units, respectively. Retinas that received RB2 hESC-derived cones appeared to be more sensitive to light suppression, as their firing rate was lower than that seen for *GNAT1*$^{-/-}$ controls. However, RB2 transplanted host retinas seem to lack the OFF component seen in *GNAT1*$^{-/-}$ units that were suppressed by light (Figure 90).

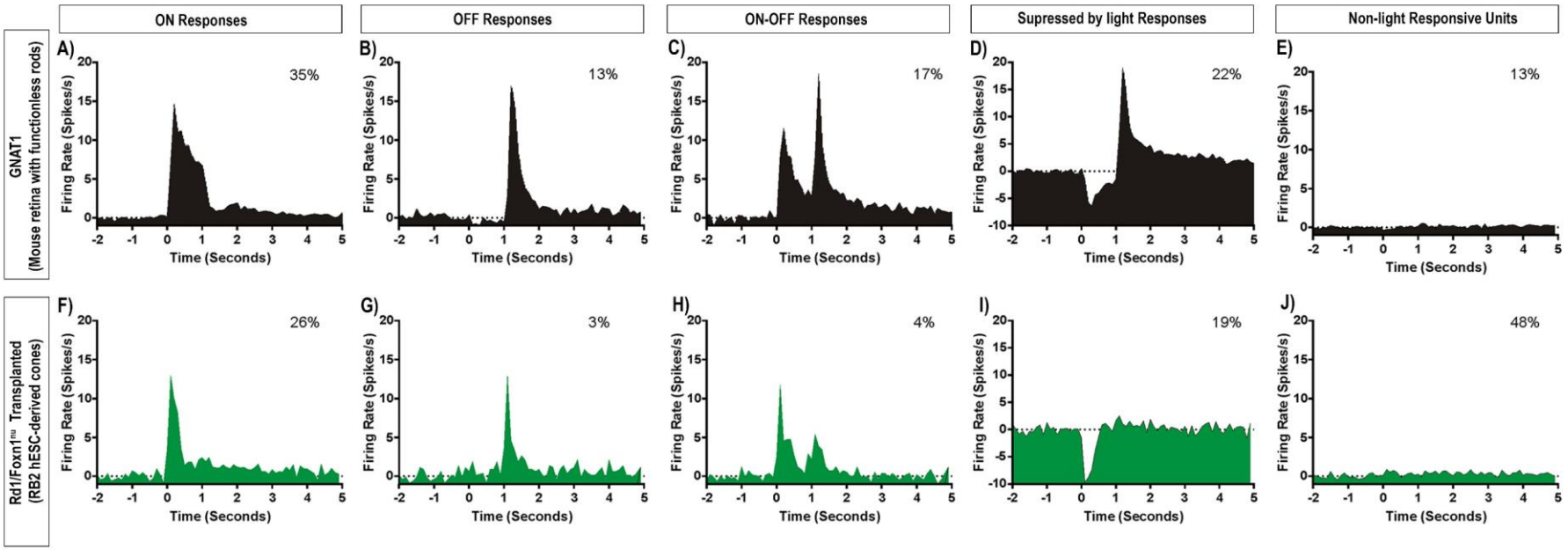

Figure 90 - MEA population data of single units from GNAT1 and RB2 transplanted retinas

Graphs show overlap of all units that were classified, upon spike sorting, in each category – Population Data. The percentages show the relative amount of each population. All graphs are base line subtracted. The 1s light stimulus went on at 0 seconds. **(A, F)** ON responses, with a rapid increase in firing rate following light stimulus, followed by a rapid return to base line were present in both control and transplanted retinas. **(B, G)** Both control and RB2 transplanted mice showed OFF responses, with a rapid increase in firing rate following light stimulus turning OFF, followed by a rapid return to base line. **(C, H)** ON-OFF responses, with a rapid increase in firing rate following light stimulus turning On, a rapid return to base line, followed by another rapid increase in firing rate and return to base line, when the stimulus was turned OFF were present. **(D, I)** Supressed by light responses, with a rapid decrease in firing rate following light stimulus, followed by a rapid return to base, present were present in both control and transplanted mice. $GNAT^{-/-}$ retinas had an OFF-component response that was not seen in RB2 transplanted retinas. Transplanted retinas showed a lower firing rate in all categories except cells supressed by light, where the change in firing rate appeared to be more pronounced. **(E, J)** Non LR units to the 1 second stimulus were found in both control and RB2 transplanted retinas.

Following spike sorting, no transient responses were found in either untreated *rd1*/Foxn1^{nu} control or sham transplanted retinas that received CNGB3 hiPSC-derived cones, confirming what had been seen in the raw data. Majority of these retinas were not light responsive. Nevertheless, a small proportion of cells, 24% for untreated retinas and 18% for sham transplanted retinas, showed sustained light responses (Figure 91). These profiles of light responses were consistent with the responses generated by ipRGCs. When plotted across 60 seconds instead of 5 seconds, the sustained profile of these cells can be more easily appreciated (Figure 91 A', C'). These response profiles and the previous multi-unit data under influence of synaptic blockers provided strong evidence that the responses seen in retinas that received CNGB3 hiPSC-derived cone photoreceptors were not generated by photoreceptor cells.

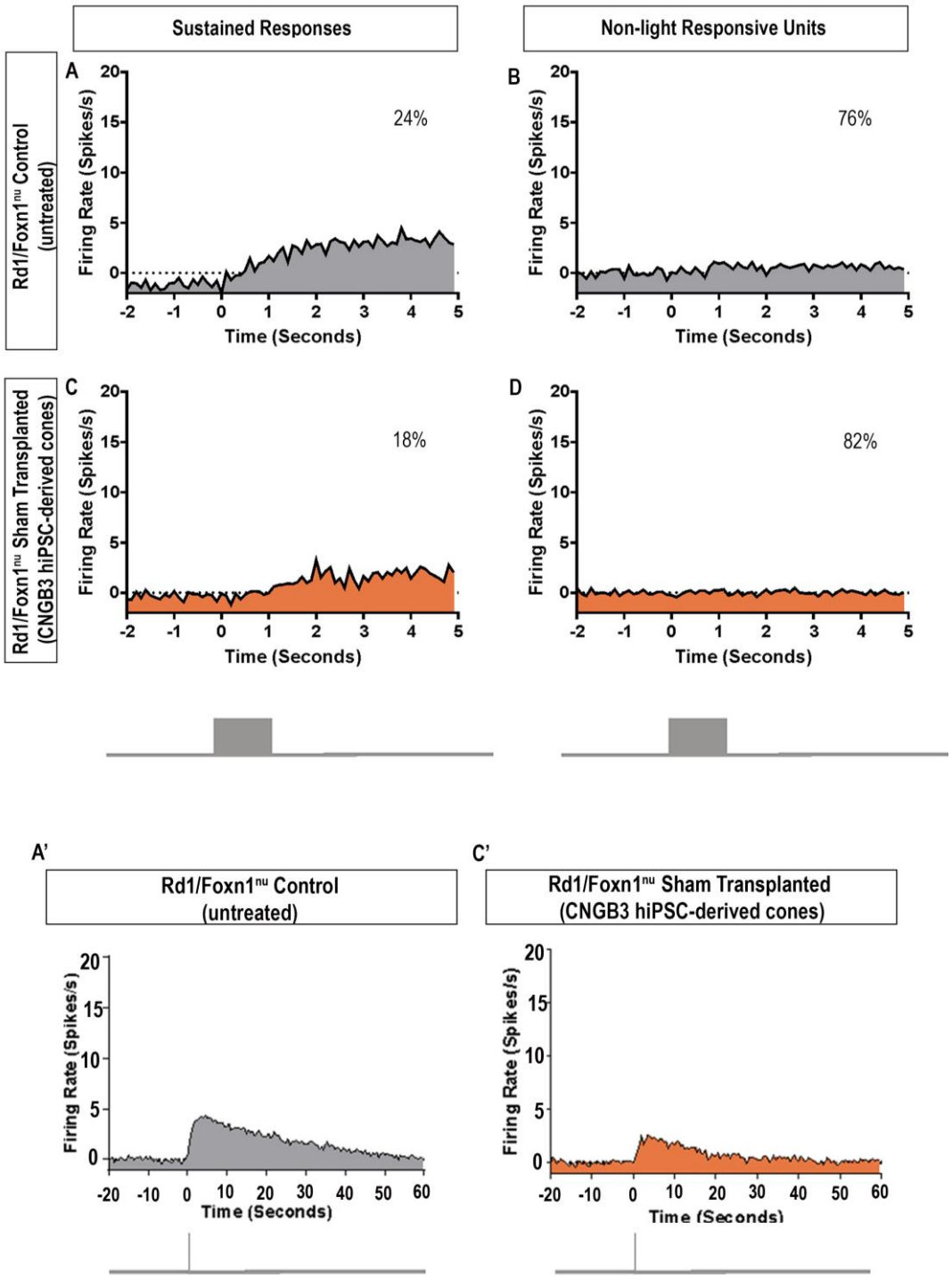

Figure 91 - MEA population data of single units from untreated Rd1/Foxn1^{nu} and CNGB3 transplanted retinas

Graphs show overlap of all units that were classified, upon spike sorting, in each category. The percentages show the relative amount of each population. All graphs are base line subtracted. The 1s light stimulus went on at 0 seconds. Grey bars at the bottom of graphs highlight the period of light stimulus. **(A, C)** LR units were present in both untreated and CNGB3 transplanted retinas. All LR units showed a profile consistent with sustained responses typical of ipRGCs. When the same data is plotted over 60 seconds following light stimulus a slow increase in firing rate followed by slow return to base line were identified (A', C'). **(B, D)** Non-light responsive units were present.

5.3.3.2.1.3 LOOM test and Optomotor

Due to technical issues with the Optomotor set up it was not possible to assess contrast sensitivity of these animals. The initial optomotor set up, described and used in previous chapters, broke down and a new set up, OptoDrum by Striatech, was acquired. In this set up the analysis is done by the software that already includes the base line random calibration data. This calibration data was acquired by analysing a that was much greater data set and therefore provides more reliable results. However, due to the lack of hair and natural leaning tendency seen in *rd1/Foxn1*^{nu} mice the software needs to be adjusted and a specific base line needs to be calculated. We are currently working with the company to establish such a base line. Ten videos of different Rd*1/Foxn1*^{nu} mice were recorded, inside the setup, with a stimulus of 0% contrast. Those videos were sent to the company and are currently being segmented and analysed in order to establish the base line for this strain. All transplanted animals were still tested, and the data was collected, however it cannot at this point be analysed. Once the new base line is set, we will analyse the data collected for all experiments described in this chapter.

LOOM experiments have been described in the previous chapters. Concerns regarding the safety of performing these experiments with immunocompromised mice were raised, as and the protocol requires mice to be exposed to a nonsterile environment for 5 days. Since the LOOM set up has not yet been fully characterised to use as a reliable tool to assess visual rescue, this method was not performed for the immune compromised animals, to minimise health risks. Currently, another PhD student within our group is working on a project that aims to fully characterise the LOOM test as an output for visual rescue. Results of this project will determine if future transplantation experiments, using *Foxn1*^{nu} animals, can be analysed using this method, considering the balance between health risk and evidence of visual function that can be determined by it.

5.3.3.2.1.4 Light Avoidance Test

As nocturnal animals, mice show preference for dark, especially when exposed to an unfamiliar environment. Therefore, this behaviour can be used to assess light detection in mice, providing evidence of basic vison. In chapter 3 concerns regarding the size of the arena where light avoidance experiments were performed was raised, as wild-type animals did not display the expected behaviour (see Chapter 3 section 3.3.2.5). Consequently, a new arena was built, and behavioural light avoidance experiments described next were performed using this new set up (see methods, section 2.11.5). By using a bigger arena, the light avoidance behaviour expected from visual intact animals was achieved. A schematic of the new set up is shown in Figure 92.

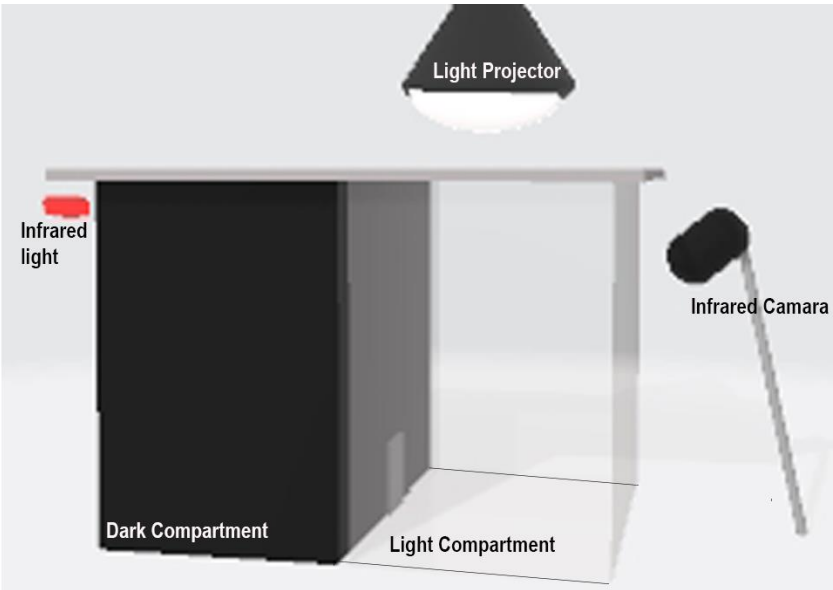

Figure 92 - Schematic representation of the new light avoidance arena

The arena was formed of 2 equal size compartments, made out of infrared transmitting acrylic. Mice could roam freely between compartment though an aperture. A light projector illuminated one of the compartments. Infrared illumination and use of infrared red camera allowed the movement of the mice to be recorded throughout both compartments.

Wild-type control mice showed a clear preference for the dark area while blind *rd1/Foxn1*^{nu} showed no preference (82 ±23%, wild-type, N = 10 mice vs 34 ±27%, untreated *rd1/Foxn1*^{nu}, N = 17 mice; ***p<0.001 1wayANOVA). Mice that received CNGB3 hiPSC-derived cone photoreceptors showed no preference between compartments and spent similar amount of time in the dark compartment as the untreated mice (43 ± 25 %; N = 15 mice). These animals also behaved significantly differently from wild-type animals (1way ANOVA, **p<0.01). In contrast, mice that received RB2 hESC-derived cone photoreceptors showed a clear preference for the dark compartment (68 ± 27 %; N = 16 mice) when compared to CNGB3 injected and untreated mice (CNGB3 transplanted vs RB2 transplanted, *p<0.05; Untreated vs RB2 transplanted, **p<0.01, 1wayANOVA,). Importantly, the time spent in the dark by RB2 transplanted animals was not significantly different from wild-type animals (Figure 93A). Latency to first cross between compartments was also analysed (Figure 93B). This is a further measurement of light aversive behaviour. In comparison to wild-type animals (0.02 ± 0.05 minutes, N= 10 mice), *Rd1/Foxn1*^{nu} mice (3.7 ±4 minutes, N = 17 mice) and mice that received CNGB3 hiPSC-derived cone photoreceptors (3.2 ±3 minutes, N = 14 mice) took considerably longer to cross into the dark compartment (*p<0.05, 1wayANOVA). Animals that received RB2 hESC-derived cone photoreceptors presented a shorter latency (1.2 ±2 minutes, N=15 mice) than untreated and sham transplant controls, but not as short as wild-type animals. The exploratory drive, as shown by representative tracking plots (Figure 93C) appeared to differ between groups, illustrating the results described previously. Untreated animals and animals which received CNGB3 hiPSC-derived cones, appeared, in most cases to explore the dark and light compartment with a similar approach, preferring to remain close to the walls of each compartment. In contrast, animals that received RB2 hESC-derived cones shown a pattern of exploration more similar to that seen in wild-type animals, which appeared to explore the centre of the dark compartment often. Overall, these results show that rescue of light detection was achieved in mice that received RB2 hESC-derived cones.

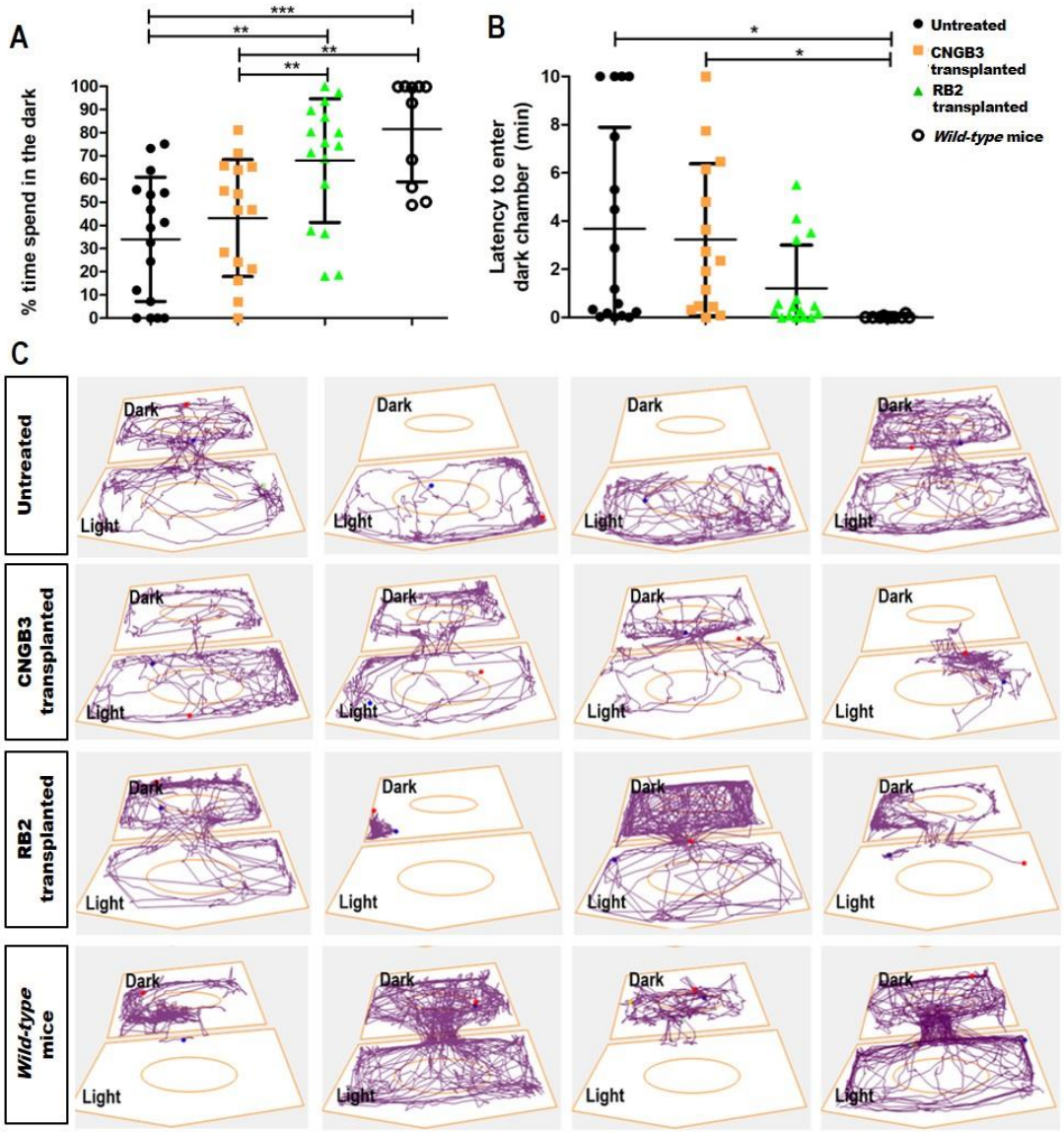

Figure 93 - Light Avoidance behaviour 12 weeks following transplantation

(A) Untreated rd1/Foxn1nu mice and mice that received CNGB3 hiPSC-derived cones showed no preference between the light or dark arenas. Mice that received RB2 hESC-derived cones showed aversion to light, showing preference for the dark arena, behaving similar to wild-type mice (mean ± SD; N = 17, untreated rd1/Foxn1^{nu} mice; N = 15, CNGB3 transplanted rd1/Foxn1^{nu} mice; RB2 transplanted rd1/Foxn1^{nu} mice, N = 16 mice; wild type, N = 10 mice; *p<0.05, **p<0.01, ***p<0.001; 1wayANOVA). **(B)** Untreated rd1/Foxn1nu mice and mice that received CNGB3 hiPSC-derived cones displayed similar latency to cross from light, where they were placed, to dark arena for the first time. RB2 transplanted mice made their first transition between the light chamber to the dark chamber faster than untreated and CNGB3 transplanted animals. Wild-type animals had much shorter latency time being significantly different from untreated and CNGB3 transplanted animals (mean ± SD; *p<0.05, 1wayANOVA). **(C)** Example tracking plots, of 4 different mice per group, showing the movement across light and dark compartments of the arena.

In summary, by using end-staged retinal degenerated, immune compromised mice it was possible to increase the transplantation success rate, when transplanting hESC/iPSC-derived cones. This allowed for more extensive analysis to take place. Both RB2 hESC-derived cones and CNGB3 hiPSC-derived cones survive in the subretinal space of r*d1/Foxn1*^{nu} mice for at least 12 weeks following transplantation. Functional and functionally-impaired human cones were morphologically similar at the time of transplantation and showed similar maturation features following transplantation, with pre-synaptic structures, extension of processes into the host INL and presence of outer segment-like structures. Similar to what was reported in the previous chapter, the host reacted to the presence of transplanted human cones, with rod bipolar cells extending processes deeply within the cell mass. Post-synaptic protein mGluR6, that was not seen in this mouse model at time of transplantation, was identified in areas of cell mass, occasionally in close proximity to pre-synaptic protein, RIBEYE. MEA data showed rescue of function, as light responses were found in retinas that were transplanted with RB2 hESC-derived cones. By pharmacologically blocking such responses, presence of synaptic connection between transplanted cones and host retinal circuit was established. The eyes which received *CNGB3*$^{-/-}$ hiPSC-derived cones were identical to un-treated eyes, displaying no photoreceptor-derived light responses. Additionally, light avoidance experiments show rescue of basic visual function, as mice that received RB2 hESC-derived cones behaved similar to wild-type animals, displaying a clear preference for the dark compartment. This behaviour was not seen in untreated of sham transplanted animals. Overall, the data presented here supports that transplantation of functional RB2 hESC-derived cones alters the synaptic circuit and rescues light perception.

5.4 Conclusions

The aims of this chapter were mostly accomplished. Rescue of function was achieved, and the results presented here allow a better understanding of the potential of cone replacement for macular degeneration.

5.4.1 Foxn1^{nu} strain as a host for photoreceptor cell transplantation

By using *Foxn1^{nu}* mice as a host it was possible to increase the survival period of hESC-derived RPE cells in the subretinal space, from up to 2 weeks (Mehat, 2017) to 24 weeks. It is relevant to mention that 24 weeks was the last time point analysed and longer experiments, to determine the upper limit of post-transplantation period, are required. The success rate of hESC-derived retinal sheets was also greatly improved by using this strain as a host, with an increase from ~3% to ~67%. Such results are not surprising since *Foxn1^{nu}* mice lack mature T-cells and immune rejection in the subretinal space is largely mediated by T-cells (West et al., 2010). However, it was important to initially establish if lack of T-cells would be sufficient to increase cell survival since other groups have used for more severely immune compromised models for similar experiments (Mishra et al., 2017). These mice present clear advantages over other available strains, by providing a more realist condition (complete immune deficiency cannot be used in a clinical set up). It is also more suited for research projects that require a large number of animals than the SD-Foxn1 Tg(S334ter)3Lav rats (Seiler et al., 2014), due to the cost associated. Furthermore, Foxn*1^{nu}* mice provide advantages over the use of immune suppressants, such as cyclosporin. Delivering immune suppressants to mice can be challenging, as when provided orally in drinking water for example, dosage cannot be measured with precision. Subcutaneous injections or endoscopy oral delivery are other methods that can be used. However, since treatment must be delivered daily for a course of several days it is extremely stressful for the animals. By crossing end-stage retinal degeneration models with immunocompromised *Foxn1^{nu}* mice we generated two new strains that can be very useful developing for photoreceptor transplantation approaches.

Additionally, interesting findings regarding the maturation of hESC-derived retinal sheets were observed. The results described in this chapter are similar to previous reports that showed development of outer segment-like structures in rosettes formed following transplantation of hESC and iPSC-retinal sheets (Iraha et al., 2018; Shirai et al., 2016). Interestingly, following transplantation, the cells generated using the protocol described in this thesis at dd163 to dd173 present mature structures similar

to those seen in cells generated by other protocols at dd215 to dd279 (Shirai et al., 2016). This could indicate that the culture condition of the protocol used during this project and published by *Gonzalez-Cordero et al* in 2017 could lead to faster photoreceptor maturation. However, the previous reports transplanting hESC or hiPSC-derived retinal-sheets, did not show earlier time points than dd215. Therefore, it is possible that such structures were present much earlier, but no data was collected. To establish if such results are true it would be necessary to directly compare both differentiation protocols, using the same facilities and cell lines.

The necessity of using a larger needle (see 2.8.2) to transplant retinal sheets makes the surgical procedure more challenging. After conferring with Professor Rachel Pearson, we established the larger needle and amount of pressure necessary to get though the sclera could induce too much damage and that the surgical intervention would require further optimisation. In view of the shortage of animals, as immunocompromised strains do not usually produce or are able to raise large numbers of healthy pups, optimisation of the surgical procedure was not something that could be accomplished within the time frame of this project. Another project was initiated to try to develop a more suitable tool, that will allow transplantation of the tissue without inducing as much damage to the eye. Furthermore, taking into account the results published so far, some pitfalls can be anticipated when transplanting retinal sheets that makes the use dissociated cells a more effective strategy. One disadvantage of retinal sheets is that these are cut manually. Consequently, the purity of the injected tissue is much less reliable and reproducible than when cells are dissociated and sorted for specific markers. This also makes analysis of established synaptic connections harder. In a retinal sheet, post-synaptic interneurons will almost certainly be transplanted as part of the retinal sheet. Thus, identifying pre and post synaptic markers in close proximity does not guarantee that those are the result of transplant/host possible contacts, as both cells can be part of the retinal sheet. Unfortunately, it was not possible to compare transplantation strategies, dissociated cells vs retinal sheets, leaving one of the aims of this thesis not accomplished.

The possibility of transplanting an organised layer of photoreceptors is clearly enticing and the ultimate goal of photoreceptor transplantation. Nevertheless, it is my opinion that such strategy will not be achieved by directly dissection of the retinal organoids. The size of the retinal organoids conditions the size of the sheets and it would not be possible to avoid variability between transplanted tissues. A more suitable approach, in my opinion, will bioengineering these sheets, by growing the organoids, dissociating and assemble an organised graft with sorted cells, in order to guarantee

that the composition of these sheet is consistent across experiments. This will require collaborative work with scientists from the biomaterial and bioengineering field.

5.4.2 Transplantation of mESC-derived photoreceptors into *Aipl1*$^{-/-}$/*Foxn1*^{nu}

Since it took several months to establish this mouse strain there were few mice available for these experiments and, consequently only one set of transplantation experiments was performed Consequently, it was not possible to draw strong conclusions regarding the effect of using these animals as host for transplantation of mESC-derived photoreceptor precursors. More experiments, using cells from different differentiation batches are necessary in order to evaluate possible sources of variability.

Nevertheless, it may be said that the use of *Aipl1*$^{-/-}$/*Foxn1*^{nu} mice showed promising results in improving the transplantation outcome regarding longer term survival of transplanted cells. A direct comparison, using the same batch of cells, differentiated, isolated and injected as part of the same transplantation experiment, showed that by using this immune compromised host, some of those cells were able to survive up to 6 weeks. Cells from the same differentiation batch were not present in immune competent mice, 3 week following transplantation. These results reinforced the hypotheses that immune rejection is a major cause for transplantation failure and that the use of *Aipl1*$^{-/-}$/*Foxn1*^{nu} mice improved transplantation outcome. This was encouraging because despite being immune compromised, these mice only lack mature T cells, having the remaining innate immune system and B cells completely functional. These results suggest that there would not be the requirement of further immune suppression for photoreceptor transplantation. This is a more realist and translational scenario than the use of SCID mice, that are completely depleted of immune system. Temporary modulation of T cell responses could be achieved in a clinical scenario while complete immunosuppression would not be appropriate for patients.

The cell masses seen were larger than that previously seen 6 weeks following transplantation into immune competent mice (see chapter 4), and cells displayed a healthier morphology. Interestingly, when transplanting into *Aipl1*$^{-/-}$/*Foxn1*^{nu} fewer Rhodopsin-positive cells were found, when compared with cells seen 3 weeks following transplantation into *Aipl1*$^{-/-}$ mice. However, more Rhodopsin-positive cells were found if compared with cells 6 weeks following transplantation into immune competent *Aipl1*$^{-/-}$ mice. These results suggest that the transplanted cells might, by six weeks following transplantation, downregulate mature markers, such as

Rhodopsin, but that the presence of bigger cell masses might influence the rate at each these events take place. Further experiments to establish if these results are reproducible are required. Improving the quality of the cells transplanted would, possibly, increase the number of surviving cells which could translate in more available cells to establish synaptic connections with the host retina. However, considering the overall goal of investigating cell therapy as a treatment for retinal degeneration, the use of mESC cultures and transplantation of mESC-derived photoreceptors was only used as a tool to optimise transplantation conditions. Therefore, optimisation of the mouse stem cell culture conditions and further assessments using mESC-derived photoreceptors was not pursued.

5.4.3 Transplantation of hESC-derived photoreceptors into *rd1/Foxn1^{nu}*

All aims initially proposed in this chapter were achieved, except for the comparison between the two current strategies for photoreceptor transplantation, dissociated cell suspension of hESC-derived cones and retinal sheets. This was due to technical limitations we encountered in transplanting sheets into such a small eye. A new PhD project is currently being developed to try to generate a more suitable tool (injector and bioengineered graft) that will, potentially, allow more successful transplantation of retinal sheets. Is also possible that a bigger animal, such as rabbit, will be necessary.

Reducing immune responses following transplantation was essential to the success of this project. However, other changes and optimisation of the experimental setup may also have been important. One of the improvements described in this chapter was the increase in efficiency of viral infection of retinal organoids, with an average of 15% GFP-positive cones being isolated per FACS experiment, as opposed to the 9% described in chapter 4 of this thesis and by Gonzalez-Cordero *et al*, 2017. One of the changes made during this study, that could have led to the difference seen is that viral vectors were filtered prior to titering. This possibly led to more accurate numbers of viral particles being added to the cultures and consequently a more effective viral transduction. In the first set of experiments, described in chapter 4, the virus was produced, titered and filtered only at the time of use. This was mainly because each vial of virus would usually be used to do more than one round of experiments. This was a simple, practical change that might have had a great impact on the overall experiment. Another potential improvement may have resulted from a few changes that were made to the culture medium composition (see methods section 2.3.3 and 2.4), which were part of a separate project that was not included in the present thesis as I was not directly involved. The results of that project are currently in preparation

for publication. That project showed no differences in cell development, other than better outer segments formation at later stages of cell culture, when photoreceptor cells are more mature (dd140 onwards). Although for the current project, retinal organoids are dissociated at an age where outer segments are just starting to form, it is possible that, despite no obvious morphological difference at this age, the small outer segment-like structures, present at dd120, were more organised and/or display more lipid-rich areas that enable more efficient viral transduction. Studies have shown that viruses utilise the lipids in cell membrane for entering the host cells, therefore if more of such structures are present/exposed viral infection could have been increased (Heaton and Randall, 2011; Mazzon and Mercer, 2014). Moreover, a recent study has shown, in rod photoreceptors, that outer segment development influences AAV-mediated transduction (Petit et al., 2017), further substantiating this hypotheses. The improvements in viral infection and consequent increase of GFP-positive cones may have allowed a more efficient use of retinal organoids and increased the number of transplanted samples/animals available for analysis.

Following transplantation, immunohistochemistry characterisation confirmed that, by re-introducing human ESC-derived cone photoreceptor cells, changes in the host retina were induced. Furthermore, graft and host cells appear to be able to establish *de novo* synaptic connections. By increasing the period following transplantation, transplanted cone photoreceptors developed further showing more mature features, such as longer outer segment-like structures. Transmission electronic microscopy (TEM) is now necessary to analyse the ultra-structure of these outer segments and establish if organised discs are being formed. TEM could also provide further information regarding the potential formation of synapses between transplanted cells and host retina. The results shown here were extremely promising. For the first time for a *rd1* phenotype, rescue of post-synaptic protein, mGluR6, in long processes extended by the host bipolar cells was shown. The processes extended by the host retina were surprising and might have a great implication regarding future approached to cell transplantation as a therapy for retinal degeneration. This is because the organisation and polarisation of the transplanted photoreceptor cells have been a challenge that appeared to be inevitable. The results shown here could open the possibility to such organisation being less relevant, as the host retina is adapting to the unorganised “layer” of photoreceptor cells. Obviously, organisation and polarisation of the photoreceptor cells is important and desirable, as we aim to recapitulate the ONL. However, the results shown here suggest that rescue is achievable even without such an organised ONL and that the host’s interneurons

might be of much more importance to achieve rescue. Formation of functional synapses, between transplanted cones and host retina, was suggested by the presence of pre- and post-synaptic proteins in close proximity. MEA data, using pharmacology, corroborated these findings and, together, very strong evidence of *de novo* synapses being formed were achieved. Currently I am optimising more synaptic markers in order to better characterise the host/graft synaptic network. Synaptic formation is, currently, seen as a major challenge to cell replacement therapies for retinal degeneration. By further characterising the synaptic connections we will provide a better understanding of how these synapses are being formed. We hope to understand and consequently stimulate formation of synaptic connections between transplanted photoreceptors and host bipolar cells, ultimately achieving a greater rescue of function.

The responses seen in MEA data were extremely encouraging, with transplanted cells providing light responses comparable, in amplitude and latency, to the host cones in *GNAT1*$^{-/-}$ retinas. The rescue of retinal function shown by MEA translated into visual rescue, as shown by light avoidance experiments. The light avoidance experiments allowed to confirm that transplantation of hESC-derived cones rescues light perception. Rescue of more complex visual function remains to be accessed. Videos of optomotor reflex were collected and can be analysed once the correct base line and threshold for this strain is established. Nevertheless, the clear results showing rescue of some level of vision were promising and is possible that rescue of vision was achieved but could not yet be tested/analysed.

The addition of sham transplants, by using non-functional/impaired cones derived from the *CNGB3*$^{-/-}$ hiPSC line, consolidates the rescue achieved by synaptic connection between transplanted *wild-type* hESC-derived cones and host retina. By including the sham transplants, we are able to exclude that functional outcomes were the result of a rescue of the host's surviving cones, given that sham and *wild-type* cones would provide the same structural and/or neurotrophic support. The possibility of material transfer was not a major concern when using *rd1/Foxn1*^{nu} mice, since the remaining cones in these retinas are not genetically affected by any mutation. For any future experiments using *Aipl1*$^{-/-}$*/Foxn1*^{nu} mice, the sham transplants will be a control for material transfer as well as structural support. Additionally, use of these non-functional cones presents a far better control than PBS injection, that was used as a sham injection previously (Barnea-Cramer et al., 2016). PBS injections have been used as a control for any possible changes induced by the surgical process however, these do not allow to exclude the possibility of material transfer and/or rescue of host

photoreceptors by providing structural or neurotrophic support. It was reassuring to see that the non-functional cones survived and matured following transplantation, with no morphological differences being identified between functional hESC-derived and non-functional hiPSC-derived cone photoreceptors. However, both light avoidance and MEA experiments revealed differences between mice that received either one. In fact, animals/retinas that received CNGB3 hiPSC-derived cones were more similar to untreated animals/retinas than to animals/retinas that received RB2 hESC-derived cones, which displayed rescue of function, measurable by behaviour and electrophysiology analysis.

Our results also showed the importance of using immunocompromised animals, which allowed not only improving the transplantation success rate, but also permitted extension of the post-transplantation period. Is now necessary to verify if this period can be extended further, since all experiments were terminated at 12 weeks following transplantation. Establishing how long human cone photoreceptors survive can following transplantation will be relevant to further optimise and evaluate the potential of photoreceptor replacement therapies in clinical setting. It is possible that the transplanted photoreceptors will, with time degenerate due to the microenvironment they were inserted in. The lack of host rod photoreceptor cells, that secrete a cone viability factors, may influence long-term survival of these cells (Hicks and Sahel, 1999; Léveillard et al., 2004; Mohand-Said et al., 1998). If longevity of the cells is compromised, it would be relevant to investigate if transplanting a mixed population of photoreceptors or introducing the rod-derived cone viability factor (RdCVF), either by external supplementation or even by genetically engineering the transplanted cones to produce such protein themselves, would improve survival of the transplanted cone photoreceptors. This possibility is supported by a publication that shown that by supplementing the *rd1* retina RdCVF, cone survival improved. This study showed that RdCVF mediates glucose uptake in cones. A portion of that glucose is, potentially, converted into lipid precursors and used for cone outer segment renewal, having a protective effect over these cells (Aït-Ali et al., 2015) Furthermore, one must consider the potential oxidative stress that the transplanted cells might be exposed to. Since in the *Aipl1*$^{-/-}$ and r*d1* retina loses the most abundant photoreceptor cells, rods, but the oxygen supply to the retina remains unaltered, it is possible that the microenvironment is not suitable for long term cell survival (Barnett and Handa, 2013; Bellezza, 2018). Interestingly rod-derived cone viability factor is involved in maintaining the appropriate intracellular redox state, reducing oxidative stress and consequent damage (reviewed by Léveillard and Sahel, 2010), which increases the

potential of using rod-derived cone viability factors to improve long-term survival of transplanted cone photoreceptor cells.

Overall, the results presented here were encouraging and further support the potential of photoreceptor transplantation for treating retinal degeneration.

Chapter 6: Discussion

6.1 How does this study fit in the current state-of-art?

The main aim of this study was to establish if, following transplantation, hESC-derived cones could establish synaptic connections with the host's advanced degenerated retina and rescue visual function. The study demonstrated that photoreceptor transplantation is a promising treatment strategy for advanced macular degeneration. It was demonstrated, for the first time, that a pure population of hESC-derived cone, generated *in vitro,* are functional and capable of integrating into the host synaptic circuit and rescue retinal function and basic visual function. Whilst the study presented in this thesis used isolated hESC-derived cone photoreceptors, other studies have claimed rescue of vision by adopting different strategies, such as transplantation of retinal sheets or mixed populations of dissociated retinal or photoreceptor cells.

The use of retinal sheets as a strategy for photoreceptor replacement and treatment for retinal degeneration has been intensively investigated. Clinical trials using human foetal retinas have shown long term-survival of the grafts with no adverse results has been reported (Das et al., 1999; Humayun et al., 2000; Radtke et al., 2008, 2002). However, the rescue of light detection reported were not maintained, disappearing within 3 to 13 months following transplantation (Humayun et al., 2000); or improvements were reported in both treated and untreated eyes of the same patient (Radtke et al., 2008), which suggests that the rescue cannot be interpreted as a consequence of transplantation. Furthermore, the use foetal human retinas as a source of cells for transplantation is restricted due to availability and raises controversial ethical issues. Such concerns would not apply to the strategy described in this thesis. Other sources of retinal sheets are hESC and hiPSC, overcome the availability and ethical issues previously mentioned. Long term-survival following transplantation, as well as rescue of visual function have been reported by using hESC and hiPSC-derived retinal sheets (Iraha et al., 2018; Shirai et al., 2016; Tu et al., 2019). However, I can anticipate some shortcomings when moving this strategy into a clinical setting. The most relevant disadvantage of retinal sheets is that these are cut manually. Consequently, the purity of the tissue injected is much less reliable and reproducible than when cells are dissociated and sorted for specific markers. The fact that other cell types, including bipolar cells, are introduced as part of the retinal sheets at time of transplantations also makes evaluation of established synaptic connections harder. At this stage, as the field progresses, is important to be able to

access, with certainty, formation of synapses between host/transplanted cells. By improving connectivity and promoting synaptic formation is likely that better visual rescue would be obtained, therefore accurate assessment of synapses is a desirable tool to improve transplantation conditions. A potential advantage of transplanting retinal sheets is that these grafts seem to enable the formation of long and mature outer segments, which have not yet been seen when transplanting dissociated photoreceptor precursors. However, in this project, outer segment formation was achieved by using dissociated hESC-derived cone photoreceptors. Furthermore, the use of dissociated cell appeared to achieve outer segment formation with the advantage of very rare rosette formation, structures that are often seen when transplanting retinal sheets (Iraha et al., 2018; Mandai et al., 2017a; Shirai et al., 2016). Another advantage of transplanting dissociated cells is that the area of treatment is not limited by the size of the retinal organoids generated. Transplanted dissociated cells can spread and potentially cover a larger area than retinal sheets. One can propose that by transplanting several retinal sheets a similar spread could be obtained. However, the surgical procedure to inject dissociated cells into the subretinal space of patients has already been established in the clinical trial using RPE cells (review in Zarbin et al., 2019), while the surgical procedure to deliver several retinal sheets into the human eye would still need to be developed and approved.

The dissociated cell suspension approach, similar to that used in this thesis, has also been used by other groups. However, there are few reports using human photoreceptor cells. The study by Barnea-Cramer *et al*., 2016 from which we can draw most similarities with what was described here, transplanted a mixed population of 200,000 photoreceptor rod and cone precursors, derived from either hESC or hiPSC, into 2.5 to 3 month old *rd1* mice. These mixed populations consisted mainly of rods (~95%), which is one of the biggest differences between that study and the one described in this thesis. They reported that hESC and hiPSC-derived rods survived in the subretinal space 3 weeks following transplantation. Long term survival of transplanted cells was not assessed. Furthermore, it was reported that the transplanted photoreceptor precursors did not adopt normal photoreceptor morphology and orientation, despite demonstrating maturation, by showing RHODOPSIN-positive structures (Barnea-Cramer et al., 2016). Presence and maturation of cones was also claimed, but that was not supported by the figures presented in the publication. Close proximity between transplanted cells and host retina was shown but the presence of post-synaptic markers was not investigated.

The pre-synaptic marker demonstrated by Barnea-Cramer *et al*. was SYNAPTOPHYSIN, which does not have a clear pattern, making the data set less comprehensive and clear than that shown in this thesis. Rescue of vision was shown by optomotor response, although the data was not presented in a typical way, as results were shown as "mean number of head tracks" and not as measure of contrast sensitivity or acuity. The light avoidance experiments performed only showed significant differences when smaller cell masses were removed, suggesting a correlation between number of cells and visual perception. Yet, removal of those animals from analyses of optomotor experiments was not required in order to find significant differences (Barnea-Cramer et al., 2016). This is surprising, as light detection, which is measured by light avoidance experiments, is required for optomotor experiments, which evaluate a more complex visual function. Therefore, the results shown were peculiar and difficult to interpret. Further evidence is required to strengthen these claims of visual rescue. Another major difference between our study and that of Barnea-Cramer *et al*. is our use of *CNGB3*$^{-/-}$ hiPSC-derived cones as sham controls, while Barnea-Cramer *et al*. used PBS injections as sham treatment. The PBS injection is a control for the surgical procedure but does not control for possible material transfer or neuroprotection of the remaining host photoreceptors. Therefore, despite some similarities, the experimental design described in this thesis surpasses the one used by Barnea-Cramer *et al*. and the use of a cone pure population makes it more relevant for future clinical applications.

In a recent study, by Garita-Hernandez *et al*., a cell suspension containing a mixed population of retinal cells was injected into the subretinal space of *Cpfl1/Rho*$^{-/-}$ (cone photoreceptor function loss 1 mice crossed with *Rhodopsin*$^{-/-}$ mice), 5 to 18 weeks of age at time of transplantation, and *rd1* mice, 4 to 11 weeks old at time of transplantation. Both these strains present advanced retinal degeneration. *Cpfl1/Rho*$^{-/-}$ mice are born with non-functional photoreceptors and present severe photoreceptor loss, with 2 to 3 rows of photoreceptors left by 9 weeks of age. The *rd1* mice phonotype is more severe, as has been described in this thesis, with a single row of cone photoreceptors remaining by 4 weeks of age. Within the mixed population transplanted in that study, were hiPSC-derived cones that were engineered by transducing the retinal organoids with an AAV virus with a cone Arrestin promotor expressing a hyperpolarising chloride pump, JAWS. These optogenetically engineered photoreceptors, which were more sensitive to red-light induced photocurrents, appeared to rescue retinal function measured by patch clamping and MEA recordings (Garita-Hernandez et al., 2019). The main idea behind this strategy

was that it was suggested that outer segment formation and rescue visual function would not be possible without RPE contact. Optogenetically engineered photoreceptors, which may function independent from RPE, would therefore be required in order to achieve rescue of visual function. However, this thesis has shown this to be unnecessary, as hESC-derived cones were able to form light responsive outer segments. Moreover, the negative control used by Garita-Hernandez *et al.* for those experiments were non-optogenetically modified cells, from which no rescue in function was detected. Rescue was not achieved most likely due to short follow up, as samples were collected 4 weeks following transplantation and probably by that time cell would not have had enough time to mature and form outer segments. According to the protocol they followed for differentiation of retinal organoids, by Reichman *et al.*, outer segment specific proteins only start to be present, in culture, by dd100 and the transplants were collected before this age. It is also important to mention that, according to the results described in this thesis, it is likely that to give cells enough time to mature following transplantation, modulation of the host's immune system would have been necessary. Another likely reason why rescue was not achieved by Garita-Hernandez *et al.* in their "control transplants" was the number of cells transplanted. The number of transplanted retinal cells was lower than the number of hESC-derived cones used for the work described in this thesis. More importantly, those 300,000 cells were a mixed population of dissociated retinal organoids and not a pure population of cone photoreceptor precursors. The percentage of cones present at the age of dissociation is not mentioned by Garita-Hernandez *et al* or covered in the original paper describing the protocol (Reichman et al., 2017). Having the protocol used in this thesis as a reference, at dd84, the closest time point to the dd70 used by Garita-Hernandez *et al,* less than 10% of the cells in retinal organoids are committed cones. Therefore, only 30,000 of the transplanted cells were in fact cone photoreceptors. Even ~30,000 is probably an over estimation having to account for the age of the cells and protocol used. Interestingly the results described in this thesis suggest that by transplanting a greater number of photoreceptor cells, survival and maturation are improved. Consequently, it is reasonable to hypothesise that the number of non-optogenetically modified cones transplanted by Garita-Hernandez *et al* is unlikely to be enough to rescue retina/visual function. This further reinforces the novelty of the results described in this thesis, where the conditions were established to rescue retinal and visual function, using a pure population of unmodified cones.

As previously mentioned, introducing cells that will not improve vision can create a barrier between host retina and transplanted photoreceptors and it could also increase the risk of immune response. Such cells would not add any benefits to transplantation outcome and therefore are not desirable. All of the studies previously mentioned, used hESC-derived retinal sheets or dissociated cells at earlier developmental stages, transplanting retinal or photoreceptor cell progenitors. This means that the cells might be committed to a retinal or photoreceptor cell fate but not specifically committed to a rod or cone cell fate, which will be a source of variability on the transplanted population. In a clinical setting it is essential that the population of cells that are transplanted is kept constant between subjects, so that comparisons can be drawn, and strong conclusions achieved. By using cells at a later stage of development this source of variability was eliminated, since only hESC-derived cone precursors were transplanted. Another clinically relevant detail revealed by this set of data is the response induced by the transplanted photoreceptors on the host's interneurons. Here, for the first time, it was shown that by replacing the missing photoreceptor cells it is possible to reverse some of the remodelling events, such as loss of post-synaptic protein in the terminals of bipolar cells. This has an impact when moving into a clinical setting, as remodelling of the host retina and its ability to establish *de novo* connections represents a major concern to the success of cell therapy.

In comparison with the results achieved in previous studies, the work described here provides an important advance to the field of cell therapy for retinal degeneration. New projects have arisen from the results described in this thesis and are currently being investigated by other researchers in our group. These include: the possibility of promoting axon formation and synaptogenesis by modulating presence of Wnt proteins, that have been shown to play a role in dendritic formations and synaptogenesis during retinal development (Fuhrmann, 2008; He et al., 2018); and use of biomaterials in order to transplant a more organised graft, by providing support, aid photoreceptor polarisation and possibly ensure an even spread of cells.

6.2 Future Directions: the road to clinical application

Despite the promising results and establishing hESC-derived cone precursors as a suitable and defined cell population to use in clinical trials, translation into clinical still requires further optimisation. Is also important to recognize that despite providing crucial validation for photoreceptor replacement therapy, the work described here should be performed in a larger mammal before a clinical trial is planned. The major requirement for the use of a bigger mammal, ideal a primate, would be necessity of a macula region. Unlike humans and other mammals, mice do not have a macula. Since the macula is more than a rod-free area of the retina, with a special connectivity and morphological arrangement, it is not possible to translate directly the results achieved in mice to the potential in humans. Nevertheless, the results achieved here are extremely promising, and justify the progression into a larger animal model. The use of a larger host, with more similarities to humans, would also be informative regarding the surgical procedure and long-term follow up. Furthermore, one can hypothesize that the potential and level of rescue achieved might be greater in a higher mammal, as the discrepancy between cell size, overall microenvironment, metabolic needs and connectivity will be more similar. The differences between wild-type mouse central retina (0°) and human macula are summarised in table 5.

	Wild-type mouse central retina	Human macula
Cone density	~13,000/mm^2 (similar to the periphery)	120,000 to 324,000 cones/mm^2 (~24x more than in the periphery)
Rods/Cones	~44	0
Cone morphology	Typical cone morphology (short and wide) as seen in the periphery	Elongated inner and outer segments due to being tightly packed
cone: bipolar (subtype specific): RGC	Midget bipolar and midget RG cells not present - 1:1:1 not possible	1:1:1 (Perifovea)
Metabolic needs	Similar to peripheral retina	More metabolic active than the periphery
RPE density	Slightly less densely packed than in the periphery (larger cells)	More densely packed than in the periphery (smaller cells)

Table 5 - Comparison between central mouse retina and human macula

There are other important aspects to consider. In the experimental design GFP was used as a marker to isolate this population of cells, however that would not be suitable for a clinical approach. Selection and isolation of cells will have to be done by surface antigens. Selection of the desired population and removal of proliferative cells and unwanted cells is a necessary safety measure as prevention of tumour formation could arise from transplanting unknown cell populations. Moreover, injection of other retinal cell types that will not improve vision, such as other interneurons that are present in the retinal organoids would increase the risk of immune response without having any benefit in the rescue of visual function(West et al., 2012b). The use of undifferentiated, proliferative cells has been proven to lead to adverse outcomes; patients who received intravitreal transplantation of cells that the authors claimed were ‘adipose tissue-derived stem cells’, suffered severe vision loss (Kuriyan et al., 2017).

Several studies have investigated the presence of such markers to enrich for photoreceptor precursors (Eberle et al., 2011; Gagliardi et al., 2018; Lakowski et al., 2015, 2011) and cone photoreceptor precursors (Welby et al., 2017). However, further investigation is necessary in order to improve the yield of cells, which still far lower than obtained by using a GFP reporter. Using peanut agglutinin (PNA) lectin beads, which selectively bind to cones, and magnetic cell isolation (MACS) could be a promising strategy (Balse et al., 2005) and other scientists in our group are currently testing and optimising this strategy.

The current differentiation protocol has proven to robustly generate a in numbers sufficiently large enough to permit the isolation of cones for transplantation (Gonzalez-Cordero et al., 2017). Nevertheless, the current protocol needs to be adapted in order to follow good manufacturing practices (GMP), such as use of defined xeno-free reagents and small molecules, which are required for clinical application. Other members of the group are currently working on establishing such protocols. As it will be undesirable to manufacture and perform quality control on individual batches of cells immediately prior to clinical transplantation, cryopreservation methods that will allow long-term cell storage, are also being investigated to aid the manufacturing process. Different cryopreservation methods of human retinal cells have been reported (Gagliardi et al., 2018; Nakano et al., 2012; Reichman et al., 2017; Slembrouck-Brec et al., 2018) and we are currently investigating which one would be the most suitable for a future clinical application.

The clinical trials using hESC or hiPSC-derived RPE cells (da Cruz et al., 2018; Mehat et al., 2018; Zarbin, 2016) will provide guidance regarding the clinical trial design, such as immunosuppression of the patients, delivery method and patient follow up. Is important to reiterate that a combined approach, to replace both photoreceptors and the RPE cells, will be required in certain degenerative retinal diseases, such as AMD and Stargardt's macular dystrophy, in order to achieve long-lasting rescue.

In summary, the results described in this thesis are promising and make a significant contribution to the field of cell therapy for the treatment of retinal disorders. In view of these results it is possible to start planning future clinical trial applications, which will probably identify further concerns that need to be addressed. If successful, cell replacement therapy for retinal degeneration could be widely applicable, representing hope to millions of patients.

Bibliography

Abdeljalil, J., Hamid, M., Abdel-mouttalib, O., Stéphane, R., Raymond, R., Johan, A., José, S., Pierre, C., Serge, P., 2005. The optomotor response: A robust first-line visual screening method for mice. Vision Res. 45, 1439–1446. https://doi.org/10.1016/j.visres.2004.12.015

Adler, R., Canto-Soler, M.V., 2007. Molecular mechanisms of optic vesicle development: complexities, ambiguities and controversies. Dev. Biol. 305, 1–13. https://doi.org/10.1016/j.ydbio.2007.01.045

Aït-Ali, N., Fridlich, R., Millet-Puel, G., Clérin, E., Delalande, F., Jaillard, C., Blond, F., Perrocheau, L., Reichman, S., Byrne, L.C., Olivier-Bandini, A., Bellalou, J., Moyse, E., Bouillaud, F., Nicol, X., Dalkara, D., van Dorsselaer, A., Sahel, J.-A., Léveillard, T., 2015. Rod-Derived Cone Viability Factor Promotes Cone Survival by Stimulating Aerobic Glycolysis. Cell 161, 817–832. https://doi.org/10.1016/j.cell.2015.03.023

Akimoto, M., Cheng, H., Zhu, D., Brzezinski, J.A., Khanna, R., Filippova, E., Oh, E.C.T., Jing, Y., Linares, J.-L., Brooks, M., Zareparsi, S., Mears, A.J., Hero, A., Glaser, T., Swaroop, A., 2006. Targeting of GFP to newborn rods by Nrl promoter and temporal expression profiling of flow-sorted photoreceptors. Proc. Natl. Acad. Sci. U. S. A. 103, 3890–3895. https://doi.org/10.1073/pnas.0508214103

Anchan, R.M., Reh, T.A., Angello, J., Balliet, A., Walker, M., 1991. EGF and TGF-alpha stimulate retinal neuroepithelial cell proliferation in vitro. Neuron 6, 923–936.

Andreazzoli, M., 2009. Molecular regulation of vertebrate retina cell fate. Birth Defects Res. Part C Embryo Today Rev. 87, 284–295. https://doi.org/10.1002/bdrc.20161

Armington, J.C., 1988. Electroretinogram, Electroretinography, in: Held, R. (Ed.), Sensory System I: Vision and Visual Systems, Readings from the Encyclopedia of Neuroscience. Birkhäuser Boston, Boston, MA, pp. 21–22. https://doi.org/10.1007/978-1-4899-6647-6_11

Assawachananont, J., Mandai, M., Okamoto, S., Yamada, C., Eiraku, M., Yonemura, S., Sasai, Y., Takahashi, M., 2014. Transplantation of embryonic and induced pluripotent stem cell-derived 3D retinal sheets into retinal degenerative mice. Stem Cell Rep. 2, 662–674. https://doi.org/mandai

Baehr, W., Karan, S., Maeda, T., Luo, D.-G., Li, S., Darin Bronson, J., Watt, C.B., Yau, K.-W., Frederick, J.M., Palczewski, K., 2007. The Function of Guanylate Cyclase

1 and Guanylate Cyclase 2 in Rod and Cone Photoreceptors. J. Biol. Chem. 282, 8837–8847. https://doi.org/10.1074/jbc.M610369200

Bain, G., Kitchens, D., Yao, M., Huettner, J.E., Gottlieb, D.I., 1995. Embryonic stem cells express neuronal properties in vitro. Dev. Biol. 168, 342–357. https://doi.org/10.1006/dbio.1995.1085

Bainbridge, J.W.B., Mehat, M.S., Sundaram, V., Robbie, S.J., Barker, S.E., Ripamonti, C., Georgiadis, A., Mowat, F.M., Beattie, S.G., Gardner, P.J., Feathers, K.L., Luong, V.A., Yzer, S., Balaggan, K., Viswanathan, A., de Ravel, T.J.L., Casteels, I., Holder, G.E., Tyler, N., Fitzke, F.W., Weleber, R.G., Nardini, M., Moore, A.T., Thompson, D.A., Petersen-Jones, S.M., Michaelides, M., van den Born, L.I., Stockman, A., Smith, A.J., Rubin, G., Ali, R.R., 2015. Long-term effect of gene therapy on Leber's congenital amaurosis. N. Engl. J. Med. 372, 1887–1897. https://doi.org/10.1056/NEJMoa1414221

Bainbridge, J.W.B., Smith, A.J., Barker, S.S., Robbie, S., Henderson, R., Balaggan, K., Viswanathan, A., Holder, G.E., Stockman, A., Tyler, N., Petersen-Jones, S., Bhattacharya, S.S., Thrasher, A.J., Fitzke, F.W., Carter, B.J., Rubin, G.S., Moore, A.T., Ali, R.R., 2008. Effect of Gene Therapy on Visual Function in Leber's Congenital Amaurosis. N. Engl. J. Med. 358, 2231–2239. https://doi.org/10.1056/NEJMoa0802268

Baker, C.K., Flannery, J.G., 2018. Innovative Optogenetic Strategies for Vision Restoration. Front. Cell. Neurosci. 12. https://doi.org/10.3389/fncel.2018.00316

Balse, E., Tessier, L.-H., Fuchs, C., Forster, V., Sahel, J.A., Picaud, S., 2005. Purification of Mammalian Cone Photoreceptors by Lectin Panning and the Enhancement of Their Survival in Glia-Conditioned Medium. Invest. Ophthalmol. Vis. Sci. 46, 367–374. https://doi.org/10.1167/iovs.04-0695

Banin, E., Obolensky, A., Idelson, M., Hemo, I., Reinhardtz, E., Pikarsky, E., Ben-Hur, T., Reubinoff, B., 2006. Retinal incorporation and differentiation of neural precursors derived from human embryonic stem cells. Stem Cells Dayt. Ohio 24, 246–257. https://doi.org/10.1634/stemcells.2005-0009

Barber, A.C., Hippert, C., Duran, Y., West, E.L., Bainbridge, J.W.B., Warre-Cornish, K., Luhmann, U.F.O., Lakowski, J., Sowden, J.C., Ali, R.R., Pearson, R.A., 2013. Repair of the degenerate retina by photoreceptor transplantation. Proc. Natl. Acad. Sci. 110, 354–359. https://doi.org/10.1073/pnas.1212677110

Barnea-Cramer, A.O., Wang, W., Lu, S.-J., Singh, M.S., Luo, C., Huo, H., McClements, M.E., Barnard, A.R., MacLaren, R.E., Lanza, R., 2016. Function of human pluripotent stem cell-derived photoreceptor progenitors in blind mice. Sci. Rep. 6, 29784. https://doi.org/10.1038/srep29784

Barnett, B.P., Handa, J.T., 2013. Retinal microenvironment imbalance in dry age-related macular degeneration: a mini-review. Gerontology 59, 297–306. https://doi.org/10.1159/000346169

Bassett, E.A., Wallace, V.A., 2012. Cell fate determination in the vertebrate retina. Trends Neurosci. 35, 565–573. https://doi.org/10.1016/j.tins.2012.05.004

Bauer, P.J., 2013. The Complex of cGMP-gated Channel and Na/Ca2+, K Exchanger in Rod Photoreceptors. Landes Bioscience.

Beebe, D.C., 1986. Development of the ciliary body: a brief review. Trans. Ophthalmol. Soc. U. K. 105 (Pt 2), 123–130.

Bellezza, I., 2018. Oxidative Stress in Age-Related Macular Degeneration: Nrf2 as Therapeutic Target. Front. Pharmacol. 9. https://doi.org/10.3389/fphar.2018.01280

Blanks, J.C., Adinolfi, A.M., Lolley, R.N., 1974. Synaptogenesis in the photoreceptor terminal of the mouse retina. J. Comp. Neurol. 156, 81–93. https://doi.org/10.1002/cne.901560107

Bloch, E., Luo, Y., da Cruz, L., 2019. Advances in retinal prosthesis systems. Ther. Adv. Ophthalmol. 11. https://doi.org/10.1177/2515841418817501

Bodnarenko, S.R., Jeyarasasingam, G., Chalupa, L.M., 1995. Development and regulation of dendritic stratification in retinal ganglion cells by glutamate-mediated afferent activity. J. Neurosci. Off. J. Soc. Neurosci. 15, 7037–7045.

Borghuis, B.G., Looger, L.L., Tomita, S., Demb, J.B., 2014. Kainate Receptors Mediate Signaling in Both Transient and Sustained OFF Bipolar Cell Pathways in Mouse Retina. J. Neurosci. 34, 6128–6139. https://doi.org/10.1523/JNEUROSCI.4941-13.2014

Boucherie, C., Mukherjee, S., Henckaerts, E., Thrasher, A.J., Sowden, J.C., Ali, R.R., 2013. Brief Report: Self-Organizing Neuroepithelium from Human Pluripotent Stem Cells Facilitates Derivation of Photoreceptors. STEM CELLS 31, 408–414. https://doi.org/10.1002/stem.1268

Boye, S.E., Boye, S.L., Lewin, A.S., Hauswirth, W.W., 2013. A comprehensive review of retinal gene therapy. Mol. Ther. J. Am. Soc. Gene Ther. 21, 509–519. https://doi.org/10.1038/mt.2012.280

Brown, N.L., Patel, S., Brzezinski, J., Glaser, T., 2001. Math5 is required for retinal ganglion cell and optic nerve formation. Dev. Camb. Engl. 128, 2497–2508.

Busskamp, V., Picaud, S., Sahel, J.A., Roska, B., 2012. Optogenetic therapy for retinitis pigmentosa. Gene Ther. 19, 169–175. https://doi.org/10.1038/gt.2011.155

Cao, Y., Masuho, I., Okawa, H., Xie, K., Asami, J., Kammermeier, P.J., Maddox, D.M., Furukawa, T., Inoue, T., Sampath, A.P., Martemyanov, K.A., 2009. Retina-specific GTPase accelerator RGS11/G beta 5S/R9AP is a constitutive heterotrimer selectively targeted to mGluR6 in ON-bipolar neurons. J. Neurosci. Off. J. Soc. Neurosci. 29, 9301–9313. https://doi.org/10.1523/JNEUROSCI.1367-09.2009

Cao, Y., Sarria, I., Fehlhaber, K.E., Kamasawa, N., Orlandi, C., James, K.N., Hazen, J.L., Gardner, M.R., Farzan, M., Lee, A., Baker, S., Baldwin, K., Sampath, A.P., Martemyanov, K.A., 2015. Mechanism for Selective Synaptic Wiring of Rod Photoreceptors into the Retinal Circuitry and Its Role in Vision. Neuron 87, 1248–1260. https://doi.org/10.1016/j.neuron.2015.09.002

Carpenter, M.K., Rao, M.S., 2015. Concise Review: Making and Using Clinically Compliant Pluripotent Stem Cell Lines. Stem Cells Transl. Med. 4, 381–388. https://doi.org/10.5966/sctm.2014-0202

Carter-Dawson, L.D., LaVail, M.M., Sidman, R.L., 1978. Differential effect of the rd mutation on rods and cones in the mouse retina. Invest. Ophthalmol. Vis. Sci. 17, 489–498.

Chalupa, L.M., Günhan, E., 2004. Development of On and Off retinal pathways and retinogeniculate projections. Prog. Retin. Eye Res. 23, 31–51. https://doi.org/10.1016/j.preteyeres.2003.10.001

Chapple, J.P., Grayson, C., Hardcastle, A.J., Saliba, R.S., van der Spuy, J., Cheetham, M.E., 2001. Unfolding retinal dystrophies: a role for molecular chaperones? Trends Mol. Med. 7, 414–421.

Chen, C.K., Burns, M.E., Spencer, M., Niemi, G.A., Chen, J., Hurley, J.B., Baylor, D.A., Simon, M.I., 1999. Abnormal photoresponses and light-induced apoptosis in rods lacking rhodopsin kinase. Proc. Natl. Acad. Sci. U. S. A. 96, 3718–3722.

Chen, J., Simon, M.I., Matthes, M.T., Yasumura, D., LaVail, M.M., 1999. Increased Susceptibility to Light Damage in an Arrestin Knockout Mouse Model of Oguchi Disease (Stationary Night Blindness). Invest. Ophthalmol. Vis. Sci. 40, 2978–2982.

Chen, S., Li, H., Gaudenz, K., Paulson, A., Guo, F., Trimble, R., Peak, A., Seidel, C., Deng, C., Furuta, Y., Xie, T., 2013. Defective FGF signaling causes coloboma formation and disrupts retinal neurogenesis. Cell Res. 23, 254–273. https://doi.org/10.1038/cr.2012.150

Colella, P., Trapani, I., Cesi, G., Sommella, A., Manfredi, A., Puppo, A., Iodice, C., Rossi, S., Simonelli, F., Giunti, M., Bacci, M.L., Auricchio, A., 2014. Efficient gene delivery to the cone-enriched pig retina by dual AAV vectors. Gene Ther. 21, 450–456. https://doi.org/10.1038/gt.2014.8

Cook, J.E., 1996. Spatial properties of retinal mosaics: an empirical evaluation of some existing measures. Vis. Neurosci. 13, 15–30.

Cruess, A.F., Zlateva, G., Xu, X., Soubrane, G., Pauleikhoff, D., Lotery, A., Mones, J., Buggage, R., Schaefer, C., Knight, T., Goss, T.F., 2008. Economic burden of bilateral neovascular age-related macular degeneration: multi-country observational study. PharmacoEconomics 26, 57–73.

da Cruz, L., Coley, B.F., Dorn, J., Merlini, F., Filley, E., Christopher, P., Chen, F.K., Wuyyuru, V., Sahel, J., Stanga, P., Humayun, M., Greenberg, R.J., Dagnelie, G., Argus II Study Group, 2013. The Argus II epiretinal prosthesis system allows letter and word reading and long-term function in patients with profound vision loss. Br. J. Ophthalmol. 97, 632–636. https://doi.org/10.1136/bjophthalmol-2012-301525

da Cruz, L., Fynes, K., Georgiadis, O., Kerby, J., Luo, Y.H., Ahmado, A., Vernon, A., Daniels, J.T., Nommiste, B., Hasan, S.M., Gooljar, S.B., Carr, A.-J.F., Vugler, A., Ramsden, C.M., Bictash, M., Fenster, M., Steer, J., Harbinson, T., Wilbrey, A., Tufail, A., Feng, G., Whitlock, M., Robson, A.G., Holder, G.E., Sagoo, M.S., Loudon, P.T., Whiting, P., Coffey, P.J., 2018. Phase 1 clinical study of an embryonic stem cell–derived retinal pigment epithelium patch in age-related macular degeneration. Nat. Biotechnol. 36, 328–337. https://doi.org/10.1038/nbt.4114

da Silva, S., Cepko, C.L., 2017. Fgf8 Expression and Degradation of Retinoic Acid Are Required for Patterning a High-Acuity Area in the Retina. Dev. Cell 42, 68-81.e6. https://doi.org/10.1016/j.devcel.2017.05.024

Dacheux, R.F., Raviola, E., 1986. The rod pathway in the rabbit retina: a depolarizing bipolar and amacrine cell. J. Neurosci. Off. J. Soc. Neurosci. 6, 331–345.

Das, S.R., Bhardwaj, N., Kjeldbye, H., Gouras, P., 1992. Muller cells of chicken retina synthesize 11-cis-retinol. Biochem. J. 285, 907–913. https://doi.org/10.1042/bj2850907

Das, T., del Cerro, M., Jalali, S., Rao, V.S., Gullapalli, V.K., Little, C., Loreto, D.A., Sharma, S., Sreedharan, A., del Cerro, C., Rao, G.N., 1999. The transplantation of human fetal neuroretinal cells in advanced retinitis pigmentosa patients: results of a long-term safety study. Exp. Neurol. 157, 58–68. https://doi.org/10.1006/exnr.1998.6992

de Melo, J., Peng, G.-H., Chen, S., Blackshaw, S., 2011. The Spalt family transcription factor Sall3 regulates the development of cone photoreceptors and retinal horizontal interneurons. Dev. Camb. Engl. 138, 2325–2336. https://doi.org/10.1242/dev.061846

Decembrini, S., Koch, U., Radtke, F., Moulin, A., Arsenijevic, Y., 2014. Derivation of Traceable and Transplantable Photoreceptors from Mouse Embryonic Stem Cells. Stem Cell Rep. 2, 853–865. https://doi.org/10.1016/j.stemcr.2014.04.010

De Franceschi, G., Vivattanasarn, T., Saleem, A.B., Solomon, S.G., 2016. Vision Guides Selection of Freeze or Flight Defense Strategies in Mice. Curr. Biol. 26, 2150–2154. https://doi.org/10.1016/j.cub.2016.06.006

Devries, S.H., Baylor, D.A., 1997. Mosaic arrangement of ganglion cell receptive fields in rabbit retina. J. Neurophysiol. 78, 2048–2060. https://doi.org/10.1152/jn.1997.78.4.2048

Dhingra, A., Vardi, N., 2012. “mGlu Receptors in the Retina” - WIREs Membrane Transport and Signaling. Wiley Interdiscip. Rev. Membr. Transp. Signal. 1, 641–653. https://doi.org/10.1002/wmts.43

Donovan, S.L., Dyer, M.A., 2004. Developmental defects in Rb-deficient retinae. Vision Res. 44, 3323–3333. https://doi.org/10.1016/j.visres.2004.08.007

D’Orazi, F.D., Suzuki, S.C., Wong, R.O., 2014. Neuronal remodeling in retinal circuit assembly, disassembly, and reassembly. Trends Neurosci. 37, 594–603. https://doi.org/10.1016/j.tins.2014.07.009

Dyer, M.A., Donovan, S.L., Zhang, J., Gray, J., Ortiz, A., Tenney, R., Kong, J., Allikmets, R., Sohocki, M.M., 2004. Retinal degeneration in Aipl1-deficient mice: a new genetic model of Leber congenital amaurosis. Mol. Brain Res., Neurogenomics 132, 208–220. https://doi.org/10.1016/j.molbrainres.2004.10.011

Eberle, D., Schubert, S., Postel, K., Corbeil, D., Ader, M., 2011. Increased integration of transplanted CD73-positive photoreceptor precursors into adult mouse retina. Invest. Ophthalmol. Vis. Sci. 52, 6462–6471. https://doi.org/10.1167/iovs.11-7399

Einthoven, W., Jolly, W.A., 1908. The Form and Magnitude of the Electrical Response of the Eye to Stimulation by Light at Various Intensities. Q. J. Exp. Physiol. 1, 373–416. https://doi.org/10.1113/expphysiol.1908.sp000026

Eiraku, M., Adachi, T., Sasai, Y., 2012. Relaxation-expansion model for self-driven retinal morphogenesis. Bioessays 34, 17–25. https://doi.org/10.1002/bies.201100070

Eiraku, M., Sasai, Y., 2012. Mouse embryonic stem cell culture for generation of three-dimensional retinal and cortical tissues. Nat. Protoc. 7, 69–79. https://doi.org/10.1038/nprot.2011.429

Eiraku, M., Takata, N., Ishibashi, H., Kawada, M., Sakakura, E., Okuda, S., Sekiguchi, K., Adachi, T., Sasai, Y., 2011. Self-organizing optic-cup morphogenesis in three-dimensional culture. Nature 472, 51–56. https://doi.org/10.1038/nature09941

Emerson, M.M., Surzenko, N., Goetz, J.J., Trimarchi, J., Cepko, C.L., 2013. Otx2 and Onecut1 promote the fates of cone photoreceptors and horizontal cells and repress rod photoreceptors. Dev. Cell 26, 59–72. https://doi.org/10.1016/j.devcel.2013.06.005

Euler, T., Haverkamp, S., Schubert, T., Baden, T., 2014. Retinal bipolar cells: elementary building blocks of vision. Nat. Rev. Neurosci. 15, 507–519. https://doi.org/10.1038/nrn3783

Evans, M.J., Kaufman, M.H., 1981. Establishment in culture of pluripotential cells from mouse embryos. Nature 292, 154–156. https://doi.org/10.1038/292154a0

Fain, G.L., Lisman, J.E., 1999. Light, Ca2+, and Photoreceptor Death: New Evidence for the Equivalent-Light Hypothesis from Arrestin Knockout Mice. Invest. Ophthalmol. Vis. Sci. 40, 2770–2772.

Fain, G.L., Lisman, J.E., 1993. Photoreceptor degeneration in vitamin A deprivation and retinitis pigmentosa: the equivalent light hypothesis. Exp. Eye Res. 57, 335–340. https://doi.org/10.1006/exer.1993.1132

Fisher, L.J., 1979. Development of synaptic arrays in the inner plexiform layer of neonatal mouse retina. J. Comp. Neurol. 187, 359–372. https://doi.org/10.1002/cne.901870207

Forrester, J., Dick, A., McMenamin, P., Lee, W., 1996. The Eye, Basic Sciences in pratice, 1st ed. W. B. saunders Company Ltd, London.

Franklin, J.L., Johnson, E.M., 1994a. Block of neuronal apoptosis by a sustained increase of steady-state free Ca2+ concentration. Philos. Trans. R. Soc. Lond. B. Biol. Sci. 345, 251–256. https://doi.org/10.1098/rstb.1994.0102

Franklin, J.L., Johnson, E.M., 1994b. Elevated intracellular calcium blocks programmed neuronal death. Ann. N. Y. Acad. Sci. 747, 195–204.

Fuhrmann, S., 2010. Eye Morphogenesis and Patterning of the Optic Vesicle. Curr. Top. Dev. Biol. 93, 61–84. https://doi.org/10.1016/B978-0-12-385044-7.00003-5

Fuhrmann, S., 2008. Wnt signaling in eye organogenesis. Organogenesis 4, 60–67.

Fuhrmann, S., Zou, C., Levine, E.M., 2014. Retinal pigment epithelium development, plasticity, and tissue homeostasis (Invited review for Experimental Eye Research). Exp. Eye Res. 0, 141–150. https://doi.org/10.1016/j.exer.2013.09.003

Fujii, M., Sunagawa, G.A., Kondo, M., Takahashi, M., Mandai, M., 2016. Evaluation of micro Electroretinograms Recorded with Multiple Electrode Array to Assess Focal Retinal Function. Sci. Rep. 6, 30719. https://doi.org/10.1038/srep30719

Gagliardi, G., M'Barek, K.B., Chaffiol, A., Slembrouck-Brec, A., Conart, J.-B., Nanteau, C., Rabesandratana, O., Sahel, J.-A., Duebel, J., Orieux, G., Reichman, S., Goureau, O., 2018. Characterization and Transplantation of CD73-Positive Photoreceptors Isolated from Human iPSC-Derived Retinal Organoids. Stem Cell Rep. 0. https://doi.org/10.1016/j.stemcr.2018.07.005

Garita-Hernandez, M., Lampič, M., Chaffiol, A., Guibbal, L., Routet, F., Santos-Ferreira, T., Gasparini, S., Borsch, O., Gagliardi, G., Reichman, S., Picaud, S., Sahel, J.-A., Goureau, O., Ader, M., Dalkara, D., Duebel, J., 2019. Restoration of visual function by transplantation of optogenetically engineered photoreceptors. Nat. Commun. 10, 1–13. https://doi.org/10.1038/s41467-019-12330-2

Gauthier, J.L., Field, G.D., Sher, A., Greschner, M., Shlens, J., Litke, A.M., Chichilnisky, E.J., 2009. Receptive fields in primate retina are coordinated to sample visual space more uniformly. PLoS Biol. 7, e1000063. https://doi.org/10.1371/journal.pbio.1000063

Ghosh, K.K., Bujan, S., Haverkamp, S., Feigenspan, A., Wässle, H., 2004. Types of bipolar cells in the mouse retina. J. Comp. Neurol. 469, 70–82. https://doi.org/10.1002/cne.10985

Glaser, T., Jepeal, L., Edwards, J.G., Young, S.R., Favor, J., Maas, R.L., 1994. PAX6 gene dosage effect in a family with congenital cataracts, aniridia, anophthalmia and central nervous system defects. Nat. Genet. 7, 463–471. https://doi.org/10.1038/ng0894-463

Goh, D., 2016. PhD Thesis - Assessing visual function following transplantation of mouse ES cell-derived rod photoreceptor precursors.

Gonzalez-Cordero, A., Goh, D., Kruczek, K., Naeem, A., Fernando, M., Kleine Holthaus, S.-M., Takaaki, M., Blackford, S.J.I., Kloc, M., Agundez, L., Sampson, R.D., Borooah, S., Ovando-Roche, P., Mehat, M.S., West, E.L., Smith, A.J., Pearson, R.A., Ali, R.R., 2018. Assessment of AAV Vector Tropisms for Mouse and Human Pluripotent Stem Cell-Derived RPE and Photoreceptor Cells. Hum. Gene Ther. 29, 1124–1139. https://doi.org/10.1089/hum.2018.027

Gonzalez-Cordero, A., Kruczek, K., Naeem, A., Fernando, M., Kloc, M., Ribeiro, J., Goh, D., Duran, Y., Blackford, S.J.I., Abelleira-Hervas, L., Sampson, R.D., Shum, I.O., Branch, M.J., Gardner, P.J., Sowden, J.C., Bainbridge, J.W.B., Smith, A.J., West, E.L., Pearson, R.A., Ali, R.R., 2017. Recapitulation of Human Retinal Development from Human Pluripotent Stem Cells Generates Transplantable Populations of Cone Photoreceptors. Stem Cell Rep. 9, 820–837. https://doi.org/10.1016/j.stemcr.2017.07.022

Gonzalez-Cordero, A., West, E.L., Pearson, R.A., Duran, Y., Carvalho, L.S., Chu, C.J., Naeem, A., Blackford, S.J.I., Georgiadis, A., Lakowski, J., Hubank, M., Smith, A.J., Bainbridge, J.W.B., Sowden, J.C., Ali, R.R., 2013. Photoreceptor precursors derived from three-dimensional embryonic stem cell cultures integrate and mature within adult degenerate retina. Nat. Biotechnol. 31. https://doi.org/10.1038/nbt.2643

Goo, Y.S., Ahn, K.N., Song, Y.J., Ahn, S.H., Han, S.K., Ryu, S.B., Kim, K.H., 2011. Spontaneous Oscillatory Rhythm in Retinal Activities of Two Retinal Degeneration

(rd1 and rd10) Mice. Korean J. Physiol. Pharmacol. Off. J. Korean Physiol. Soc. Korean Soc. Pharmacol. 15, 415–422. https://doi.org/10.4196/kjpp.2011.15.6.415

Gotch, F., 1903. The time relations of the photo-electric changes in the eyeball of the frog. J. Physiol. 29, 388–410. https://doi.org/10.1113/jphysiol.1903.sp000965

Gouras, P., Du, J., Gelanze, M., Lopez, R., Kwun, R., Kjeldbye, H., Krebs, W., 1991. Survival and synapse formation of transplanted rat rods. J. Neural Transplant. Plast. 2, 91–100. https://doi.org/10.1155/NP.1991.91

Graham, D.M., Wong, K.Y., 1995. Melanopsin-expressing, Intrinsically Photosensitive Retinal Ganglion Cells (ipRGCs), in: Kolb, H., Fernandez, E., Nelson, R. (Eds.), Webvision: The Organization of the Retina and Visual System. University of Utah Health Sciences Center, Salt Lake City (UT).

Greenlund, L.J., Deckwerth, T.L., Johnson, E.M., 1995. Superoxide dismutase delays neuronal apoptosis: a role for reactive oxygen species in programmed neuronal death. Neuron 14, 303–315.

Günhan-Agar, E., Kahn, D., Chalupa, L.M., 2000. Segregation of on and off bipolar cell axonal arbors in the absence of retinal ganglion cells. J. Neurosci. Off. J. Soc. Neurosci. 20, 306–314.

Gust, J., Reh, T.A., 2011. Adult Donor Rod Photoreceptors Integrate into the Mature Mouse Retina. Invest. Ophthalmol. Vis. Sci. 52, 5266–5272. https://doi.org/10.1167/iovs.10-6329

Hao, W., Wenzel, A., Obin, M.S., Chen, C.-K., Brill, E., Krasnoperova, N.V., Eversole-Cire, P., Kleyner, Y., Taylor, A., Simon, M.I., Grimm, C., Remé, C.E., Lem, J., 2002. Evidence for two apoptotic pathways in light-induced retinal degeneration. Nat. Genet. 32, 254–260. https://doi.org/10.1038/ng984

Hatakeyama, J., Kageyama, R., 2004. Retinal cell fate determination and bHLH factors. Semin. Cell Dev. Biol. 15, 83–89. https://doi.org/10.1016/j.semcdb.2003.09.005

He, chun-wei, Liao, C.-P., Pan, C.-L., 2018. Wnt signalling in the development of axon, dendrites and synapses. Open Biol.

Heaton, N.S., Randall, G., 2011. Multifaceted roles for lipids in viral infection. Trends Microbiol. 19, 368–375. https://doi.org/10.1016/j.tim.2011.03.007

Heavner, W., Pevny, L., 2012. Eye Development and Retinogenesis. Cold Spring Harb. Perspect. Biol. 4. https://doi.org/10.1101/cshperspect.a008391

Helmstaedter, M., Briggman, K.L., Turaga, S.C., Jain, V., Seung, H.S., Denk, W., 2013. Connectomic reconstruction of the inner plexiform layer in the mouse retina. Nature 500, 168–174. https://doi.org/10.1038/nature12346

Hennig, A.K., Peng, G.-H., Chen, S., 2008. Regulation of photoreceptor gene expression by Crx-associated transcription factor network. Brain Res. 1192, 114–133. https://doi.org/10.1016/j.brainres.2007.06.036

Hicks, D., Sahel, J., 1999. The Implications of Rod-Dependent Cone Survival for Basic and Clinical Research. Invest. Ophthalmol. Vis. Sci. 40, 3071–3074.

Hidalgo-de-Quintana, J., Evans, R.J., Cheetham, M.E., Spuy, J. van der, 2008. The Leber Congenital Amaurosis Protein AIPL1 Functions as Part of a Chaperone Heterocomplex. Invest. Ophthalmol. Vis. Sci. 49, 2878–2887. https://doi.org/10.1167/iovs.07-1576

Hinds, J.W., Hinds, P.L., 1983. Development of retinal amacrine cells in the mouse embryo: evidence for two modes of formation. J. Comp. Neurol. 213, 1–23. https://doi.org/10.1002/cne.902130102

Hinds, J.W., Hinds, P.L., 1978. Early development of amacrine cells in the mouse retina: an electron microscopic, serial section analysis. J. Comp. Neurol. 179, 277–300. https://doi.org/10.1002/cne.901790204

Hippert, C., Graca, A.B., Barber, A.C., West, E.L., Smith, A.J., Ali, R.R., Pearson, R.A., 2015. Müller Glia Activation in Response to Inherited Retinal Degeneration Is Highly Varied and Disease-Specific. PLOS ONE 10, e0120415. https://doi.org/10.1371/journal.pone.0120415

Ho, A.C., Humayun, M.S., Dorn, J.D., da Cruz, L., Dagnelie, G., Handa, J., Barale, P.-O., Sahel, J.-A., Stanga, P.E., Hafezi, F., Safran, A.B., Salzmann, J., Santos, A., Birch, D., Spencer, R., Cideciyan, A.V., de Juan, E., Duncan, J.L., Eliott, D., Fawzi, A., Olmos de Koo, L.C., Brown, G.C., Haller, J.A., Regillo, C.D., Del Priore, L.V., Arditi, A., Geruschat, D.R., Greenberg, R.J., Argus II Study Group, 2015. Long-Term Results from an Epiretinal Prosthesis to Restore Sight to the Blind. Ophthalmology 122, 1547–1554. https://doi.org/10.1016/j.ophtha.2015.04.032

Holt, C.E., Bertsch, T.W., Ellis, H.M., Harris, W.A., 1988. Cellular determination in the Xenopus retina is independent of lineage and birth date. Neuron 1, 15–26.

Hopkins, J.M., Boycott, B.B., 1997. The cone synapses of cone bipolar cells of primate retina. J. Neurocytol. 26, 313–325. https://doi.org/10.1023/A:1018504718282

Hosoya, T., Baccus, S.A., Meister, M., 2005. Dynamic predictive coding by the retina. Nature 436, 71–77. https://doi.org/10.1038/nature03689

Hsu, Y.T., Molday, R.S., 1993. Modulation of the cGMP-gated channel of rod photoreceptor cells by calmodulin. Nature 361, 76–79. https://doi.org/10.1038/361076a0

Humayun, M.S., de Juan, E., del Cerro, M., Dagnelie, G., Radner, W., Sadda, S.R., del Cerro, C., 2000. Human neural retinal transplantation. Invest. Ophthalmol. Vis. Sci. 41, 3100–3106.

Iraha, S., Tu, H.-Y., Yamasaki, S., Kagawa, T., Goto, M., Takahashi, R., Watanabe, T., Sugita, S., Yonemura, S., Sunagawa, G.A., Matsuyama, T., Fujii, M., Kuwahara, A., Kishino, A., Koide, N., Eiraku, M., Tanihara, H., Takahashi, M., Mandai, M., 2018. Establishment of Immunodeficient Retinal Degeneration Model Mice and Functional Maturation of Human ESC-Derived Retinal Sheets after Transplantation. Stem Cell Rep. 10, 1059–1074. https://doi.org/10.1016/j.stemcr.2018.01.032

Jacobs, G.H., Williams, G.A., Cahill, H., Nathans, J., 2007. Emergence of novel color vision in mice engineered to express a human cone photopigment. Science 315, 1723–1725. https://doi.org/10.1126/science.1138838

Jadhav, A.P., Mason, H.A., Cepko, C.L., 2006. Notch 1 inhibits photoreceptor production in the developing mammalian retina. Dev. Camb. Engl. 133, 913–923. https://doi.org/10.1242/dev.02245

Jensen, A.M., Wallace, V.A., 1997. Expression of Sonic hedgehog and its putative role as a precursor cell mitogen in the developing mouse retina. Dev. Camb. Engl. 124, 363–371.

Jia, L., Oh, E.C.T., Ng, L., Srinivas, M., Brooks, M., Swaroop, A., Forrest, D., 2009. Retinoid-related orphan nuclear receptor RORbeta is an early-acting factor in rod photoreceptor development. Proc. Natl. Acad. Sci. U. S. A. 106, 17534–17539. https://doi.org/10.1073/pnas.0902425106

Jiang, L.Q., Jorquera, M., Streilein, J.W., 1993. Subretinal space and vitreous cavity as immunologically privileged sites for retinal allografts. Invest. Ophthalmol. Vis. Sci. 34, 3347–3354.

Jiménez, A.J., García-Fernández, J.M., González, B., Foster, R.G., 1996. The spatio-temporal pattern of photoreceptor degeneration in the aged rd/rd mouse retina. Cell Tissue Res. 284, 193–202. https://doi.org/10.1007/s004410050579

Johnson, S., Michaelides, M., Aligianis, I.A., Ainsworth, J.R., Mollon, J.D., Maher, E.R., Moore, A.T., Hunt, D.M., 2004. Achromatopsia caused by novel mutations in both CNGA3 and CNGB3. J. Med. Genet. 41, e20–e20. https://doi.org/10.1136/jmg.2003.011437

Jones, B.W., Marc, R.E., 2005. Retinal remodeling during retinal degeneration. Exp. Eye Res. 81, 123–137. https://doi.org/10.1016/j.exer.2005.03.006

Jones, B.W., Marc, R.E., Watt, C.B., Vaughan, D.K., Organisciak, D.T., 2006. Neural plasticity revealed by light-induced photoreceptor lesions. Adv. Exp. Med. Biol. 572, 405–410. https://doi.org/10.1007/0-387-32442-9_57

Jones, B.W., Watt, C.B., Frederick, J.M., Baehr, W., Chen, C.-K., Levine, E.M., Milam, A.H., Lavail, M.M., Marc, R.E., 2003. Retinal remodeling triggered by photoreceptor degenerations. J. Comp. Neurol. 464, 1–16. https://doi.org/10.1002/cne.10703

Kalloniatis, M., Nivison-Smith, L., Chua, J., Acosta, M.L., Fletcher, E.L., 2016. Using the rd1 mouse to understand functional and anatomical retinal remodelling and treatment implications in retinitis pigmentosa: A review. Exp. Eye Res., Special Issue: Cellular remodeling in the retina and optic nerve following injury and disease 150, 106–121. https://doi.org/10.1016/j.exer.2015.10.019

Kawasaki, H., Mizuseki, K., Nishikawa, S., Kaneko, S., Kuwana, Y., Nakanishi, S., Nishikawa, S.I., Sasai, Y., 2000. Induction of midbrain dopaminergic neurons from ES cells by stromal cell-derived inducing activity. Neuron 28, 31–40.

Kay, J.N., Roeser, T., Mumm, J.S., Godinho, L., Mrejeru, A., Wong, R.O.L., Baier, H., 2004. Transient requirement for ganglion cells during assembly of retinal synaptic layers. Dev. Camb. Engl. 131, 1331–1342. https://doi.org/10.1242/dev.01040

Kaylor, J.J., Cook, J.D., Makshanoff, J., Bischoff, N., Yong, J., Travis, G.H., 2014. Identification of the 11-cis-specific retinyl-ester synthase in retinal Müller cells as multifunctional O-acyltransferase (MFAT). Proc. Natl. Acad. Sci. U. S. A. 111, 7302–7307. https://doi.org/10.1073/pnas.1319142111

Kedzierski, W., Bok, D., Travis, G.H., 1998. Non-Cell-Autonomous Photoreceptor Degeneration in rdsMutant Mice Mosaic for Expression of a Rescue Transgene. J. Neurosci. 18, 4076–4082. https://doi.org/10.1523/JNEUROSCI.18-11-04076.1998

Kefalov, V.J., 2010. Phototransduction: Phototransduction in Cones, in: Dartt, D.A. (Ed.), Encyclopedia of the Eye. Academic Press, Oxford, pp. 389–396. https://doi.org/10.1016/B978-0-12-374203-2.00189-5

Keller, G., 2005. Embryonic stem cell differentiation: emergence of a new era in biology and medicine. Genes Dev. 19, 1129–1155. https://doi.org/10.1101/gad.1303605

Klassen, H.J., Ng, T.F., Kurimoto, Y., Kirov, I., Shatos, M., Coffey, P., Young, M.J., 2004. Multipotent retinal progenitors express developmental markers, differentiate into retinal neurons, and preserve light-mediated behavior. Invest. Ophthalmol. Vis. Sci. 45, 4167–4173. https://doi.org/10.1167/iovs.04-0511

Klimczak, R.R., Koerber, J.T., Dalkara, D., Flannery, J.G., Schaffer, D.V., 2009. A Novel Adeno-Associated Viral Variant for Efficient and Selective Intravitreal Transduction of Rat Müller Cells. PLOS ONE 4, e7467. https://doi.org/10.1371/journal.pone.0007467

Kohl, S., Varsanyi, B., Antunes, G.A., Baumann, B., Hoyng, C.B., Jägle, H., Rosenberg, T., Kellner, U., Lorenz, B., Salati, R., Jurklies, B., Farkas, A., Andreasson, S., Weleber, R.G., Jacobson, S.G., Rudolph, G., Castellan, C., Dollfus, H., Legius, E., Anastasi, M., Bitoun, P., Lev, D., Sieving, P.A., Munier, F.L., Zrenner, E., Sharpe, L.T., Cremers, F.P.M., Wissinger, B., 2005. CNGB3 mutations account for 50% of all cases with autosomal recessive achromatopsia. Eur. J. Hum. Genet. EJHG 13, 302–308. https://doi.org/10.1038/sj.ejhg.5201269

Kosmaoglou, M., Schwarz, N., Bett, J.S., Cheetham, M.E., 2008. Molecular chaperones and photoreceptor function. Prog. Retin. Eye Res. 27, 434–449. https://doi.org/10.1016/j.preteyeres.2008.03.001

Kruczek, K., Gonzalez-Cordero, A., Goh, D., Naeem, A., Jonikas, M., Blackford, S.J.I., Kloc, M., Duran, Y., Georgiadis, A., Sampson, R.D., Maswood, R.N., Smith, A.J., Decembrini, S., Arsenijevic, Y., Sowden, J.C., Pearson, R.A., West, E.L., Ali, R.R., 2017. Differentiation and Transplantation of Embryonic Stem Cell-Derived Cone Photoreceptors into a Mouse Model of End-Stage Retinal Degeneration. Stem Cell Rep. 8, 1659–1674. https://doi.org/10.1016/j.stemcr.2017.04.030

Kuriyan, A.E., Albini, T.A., Townsend, J.H., Rodriguez, M., Pandya, H.K., Leonard, R.E., Parrott, M.B., Rosenfeld, P.J., Flynn, H.W., Goldberg, J.L., 2017. Vision Loss after Intravitreal Injection of Autologous “Stem Cells” for AMD. N. Engl. J. Med. 376, 1047–1053. https://doi.org/10.1056/NEJMoa1609583

L. Kalbaugh, T., Zhang, J., S. Diamond, J., 2009. Coagonist Release Modulates NMDA Receptor Subtype Contributions at Synaptic Inputs to Retinal Ganglion Cells. J. Neurosci. https://doi.org/10.1523/JNEUROSCI.4240-08.2009

Lakowski, J., Baron, M., Bainbridge, J., Barber, A.C., Pearson, R.A., Ali, R.R., Sowden, J.C., 2010. Cone and rod photoreceptor transplantation in models of the childhood retinopathy Leber congenital amaurosis using flow-sorted Crx-positive donor cells. Hum. Mol. Genet. 19, 4545–4559. https://doi.org/10.1093/hmg/ddq378

Lakowski, J., Gonzalez-Cordero, A., West, E.L., Han, Y.-T., Welby, E., Naeem, A., Blackford, S.J.I., Bainbridge, J.W.B., Pearson, R.A., Ali, R.R., Sowden, J.C., 2015. Transplantation of Photoreceptor Precursors Isolated via a Cell Surface Biomarker Panel From Embryonic Stem Cell-Derived Self-Forming Retina. Stem Cells Dayt. Ohio 33, 2469–2482. https://doi.org/10.1002/stem.2051

Lakowski, J., Han, Y.-T., Pearson, R.A., Gonzalez-Cordero, A., West, E.L., Gualdoni, S., Barber, A.C., Hubank, M., Ali, R.R., Sowden, J.C., 2011. Effective transplantation of photoreceptor precursor cells selected via cell surface antigen expression. Stem Cells Dayt. Ohio 29, 1391–1404. https://doi.org/10.1002/stem.694

Lamb, T.D., Collin, S.P., Pugh, E.N., 2007. Evolution of the vertebrate eye: opsins, photoreceptors, retina and eye cup. Nat. Rev. Neurosci. 8, 960–976. https://doi.org/10.1038/nrn2283

Lamba, D.A., Gust, J., Reh, T.A., 2009. Transplantation of Human Embryonic Stem Cell-Derived Photoreceptors Restores Some Visual Function in Crx-Deficient Mice. Cell Stem Cell 4, 73–79. https://doi.org/10.1016/j.stem.2008.10.015

Lamba, D.A., Karl, M.O., Ware, C.B., Reh, T.A., 2006. Efficient generation of retinal progenitor cells from human embryonic stem cells. Proc. Natl. Acad. Sci. U. S. A. 103, 12769–12774. https://doi.org/10.1073/pnas.0601990103

Lamba, D.A., McUsic, A., Hirata, R.K., Wang, P.-R., Russell, D., Reh, T.A., 2010. Generation, Purification and Transplantation of Photoreceptors Derived from Human Induced Pluripotent Stem Cells. PLOS ONE 5, e8763. https://doi.org/10.1371/journal.pone.0008763

Larhammar, D., Nordström, K., Larsson, T.A., 2009. Evolution of vertebrate rod and cone phototransduction genes. Philos. Trans. R. Soc. Lond. B Biol. Sci. 364, 2867–2880. https://doi.org/10.1098/rstb.2009.0077

Lavail, M.M., Matthes, M.T., Yasumura, D., Steinberg, R.H., 1997. Variability in Rate of Cone Degeneration in the Retinal Degeneration (rd/rd) Mouse. Exp. Eye Res. 65, 45–50. https://doi.org/10.1006/exer.1997.0308

Lee, C.J., Huie, P., Leng, T., Peterman, M.C., Marmor, M.F., Blumenkranz, M.S., Bent, S.F., Fishman, H.A., 2002. Microcontact printing on human tissue for retinal cell transplantation. Arch. Ophthalmol. Chic. Ill 1960 120, 1714–1718.

Lees, M.B., 1994. Basic neurochemistry, 5th edition, edited by G.J. Siegel, B.W. Agranoff, R.W. Albers, and P.B. Molinoff. Raven Press, New York, 1994, ISBN 0-7817-0104-x, 1104 pp, $67.00. J. Neurosci. Res. 39, 512–512. https://doi.org/10.1002/jnr.490390418

Léveillard, T., Mohand-Saïd, S., Lorentz, O., Hicks, D., Fintz, A.-C., Clérin, E., Simonutti, M., Forster, V., Cavusoglu, N., Chalmel, F., Dollé, P., Poch, O., Lambrou, G., Sahel, J.-A., 2004. Identification and characterization of rod-derived cone viability factor. Nat. Genet. 36, 755–759. https://doi.org/10.1038/ng1386

Léveillard, T., Sahel, J.-A., 2010. Rod-derived cone viability factor for treating blinding diseases: from clinic to redox signaling. Sci. Transl. Med. 2, 26ps16. https://doi.org/10.1126/scitranslmed.3000866

Lillien, L., 1995. Changes in retinal cell fate induced by overexpression of EGF receptor. Nature 377, 158–162. https://doi.org/10.1038/377158a0

Lillien, L., Cepko, C., 1992. Control of proliferation in the retina: temporal changes in responsiveness to FGF and TGF alpha. Dev. Camb. Engl. 115, 253–266.

Lin, B., Masland, R.H., Strettoi, E., 2009. Remodeling of cone photoreceptor cells after rod degeneration in rd mice. Exp. Eye Res. 88, 589–599. https://doi.org/10.1016/j.exer.2008.11.022

Lipton, S.A., Kater, S.B., 1989. Neurotransmitter regulation of neuronal outgrowth, plasticity and survival. Trends Neurosci. 12, 265–270.

Lisman, J., Fain, G., 1995. Support for the equivalent light hypothesis for RP. Nat. Med. 1, 1254–1255.

Liu, C., Sherpa, T., Varnum, M.D., 2013. Disease-associated mutations in CNGB3 promote cytotoxicity in photoreceptor-derived cells. Mol. Vis.

Liu, X., Bulgakov, O.V., Wen, X.-H., Woodruff, M.L., Pawlyk, B., Yang, J., Fain, G.L., Sandberg, M.A., Makino, C.L., Li, T., 2004. AIPL1, the protein that is defective in

Leber congenital amaurosis, is essential for the biosynthesis of retinal rod cGMP phosphodiesterase. Proc. Natl. Acad. Sci. U. S. A. 101, 13903–13908. https://doi.org/10.1073/pnas.0405160101

Livesey, F.J., Cepko, C.L., 2001. Vertebrate neural cell-fate determination: lessons from the retina. Nat. Rev. Neurosci. 2, 109–118. https://doi.org/10.1038/35053522

London, A., Benhar, I., Schwartz, M., 2013. The retina as a window to the brain-from eye research to CNS disorders. Nat. Rev. Neurol. 9, 44–53. https://doi.org/10.1038/nrneurol.2012.227

Lu, A., Ng, L., Ma, M., Kefas, B., Davies, T.F., Hernandez, A., Chan, C.-C., Forrest, D., 2009. Retarded developmental expression and patterning of retinal cone opsins in hypothyroid mice. Endocrinology 150, 1536–1544. https://doi.org/10.1210/en.2008-1092

M. García-Fernández, J., Jimenez, A.J., Foster, R.G., 1995. The persistence of cone photoreceptors within the dorsal retina of aged retinally degenerate mice (rdrd): implications for circadian organization. Neurosci. Lett. 187, 33–36. https://doi.org/10.1016/0304-3940(95)11330-Y

MacLaren, R.E., Pearson, R.A., MacNeil, A., Douglas, R.H., Salt, T.E., Akimoto, M., Swaroop, A., Sowden, J.C., Ali, R.R., 2006. Retinal repair by transplantation of photoreceptor precursors. Nature 444, 203. https://doi.org/10.1038/nature05161

MacNeil, M.A., Heussy, J.K., Dacheux, R.F., Raviola, E., Masland, R.H., 2004. The population of bipolar cells in the rabbit retina. J. Comp. Neurol. 472, 73–86. https://doi.org/10.1002/cne.20063

Maddox, D.M., Vessey, K.A., Yarbrough, G.L., Invergo, B.M., Cantrell, D.R., Inayat, S., Balannik, V., Hicks, W.L., Hawes, N.L., Byers, S., Smith, R.S., Hurd, R., Howell, D., Gregg, R.G., Chang, B., Naggert, J.K., Troy, J.B., Pinto, L.H., Nishina, P.M., McCall, M.A., 2008. Allelic variance between GRM6 mutants, Grm6nob3 and Grm6nob4 results in differences in retinal ganglion cell visual responses. J. Physiol. 586, 4409–4424. https://doi.org/10.1113/jphysiol.2008.157289

Maeda, A., Palczewski, K., 2013. Retinal degeneration in animal models with a defective visual cycle. Drug Discov. Today Dis. Models 10, e163–e172. https://doi.org/10.1016/j.ddmod.2014.01.001

Maeder, M.L., Gersbach, C.A., 2016. Genome-editing Technologies for Gene and Cell Therapy. Mol. Ther. J. Am. Soc. Gene Ther. 24, 430–446. https://doi.org/10.1038/mt.2016.10

Mancuso, K., Hauswirth, W.W., Li, Q., Connor, T.B., Kuchenbecker, J.A., Mauck, M.C., Neitz, J., Neitz, M., 2009. Gene therapy for red-green colour blindness in adult primates. - PubMed - NCBI [WWW Document]. URL https://www.ncbi.nlm.nih.gov/pubmed/19759534 (accessed 3.11.19).

Mandai, M., Fujii, M., Hashiguchi, T., Sunagawa, G.A., Ito, S., Sun, J., Kaneko, J., Sho, J., Yamada, C., Takahashi, M., 2017a. iPSC-Derived Retina Transplants Improve Vision in rd1 End-Stage Retinal-Degeneration Mice. Stem Cell Rep. 8, 69–83. https://doi.org/10.1016/j.stemcr.2016.12.008

Mandai, M., Watanabe, A., Kurimoto, Y., Hirami, Y., Morinaga, C., Daimon, T., Fujihara, M., Akimaru, H., Sakai, N., Shibata, Y., Terada, M., Nomiya, Y., Tanishima, S., Nakamura, M., Kamao, H., Sugita, S., Onishi, A., Ito, T., Fujita, K., Kawamata, S., Go, M.J., Shinohara, C., Hata, K.-I., Sawada, M., Yamamoto, M., Ohta, S., Ohara, Y., Yoshida, K., Kuwahara, J., Kitano, Y., Amano, N., Umekage, M., Kitaoka, F., Tanaka, A., Okada, C., Takasu, N., Ogawa, S., Yamanaka, S., Takahashi, M., 2017b. Autologous Induced Stem-Cell-Derived Retinal Cells for Macular Degeneration. N. Engl. J. Med. 376, 1038–1046. https://doi.org/10.1056/NEJMoa1608368

Marc, R.E., Jones, B.W., 2003. Retinal remodeling in inherited photoreceptor degenerations. Mol. Neurobiol. 28, 139–147. https://doi.org/10.1385/MN:28:2:139

Marc, R.E., Jones, B.W., Watt, C.B., Strettoi, E., 2003a. Neural remodeling in retinal degeneration. Prog. Retin. Eye Res. 22, 607–655.

Marc, R.E., Jones, B.W., Watt, C.B., Strettoi, E., 2003b. Neural remodeling in retinal degeneration. Prog. Retin. Eye Res. 22, 607–655.

Marc, R.E., Jones, B.W., Watt, C.B., Vazquez-Chona, F., Vaughan, D.K., Organisciak, D.T., 2008. Extreme retinal remodeling triggered by light damage: implications for age related macular degeneration. Mol. Vis. 14, 782–806.

Margolis, D.J., Gartland, A.J., Singer, J.H., Detwiler, P.B., 2014. Network Oscillations Drive Correlated Spiking of ON and OFF Ganglion Cells in the rd1 Mouse Model of Retinal Degeneration. PLOS ONE 9, e86253. https://doi.org/10.1371/journal.pone.0086253

Marquardt, T., Ashery-Padan, R., Andrejewski, N., Scardigli, R., Guillemot, F., Gruss, P., 2001. Pax6 is required for the multipotent state of retinal progenitor cells. Cell 105, 43–55.

Marquardt, T., Gruss, P., 2002. Generating neuronal diversity in the retina: one for nearly all. Trends Neurosci. 25, 32–38. https://doi.org/10.1016/S0166-2236(00)02028-2

Martin, G.R., 1981. Isolation of a pluripotent cell line from early mouse embryos cultured in medium conditioned by teratocarcinoma stem cells. Proc. Natl. Acad. Sci. U. S. A. 78, 7634–7638.

Martinez-Morales, J.R., Wittbrodt, J., 2009. Shaping the vertebrate eye. Curr. Opin. Genet. Dev., Differentation and gene regulation 19, 511–517. https://doi.org/10.1016/j.gde.2009.08.003

Masland, R.H., 2012. The neuronal organization of the retina. Neuron 76, 266–280. https://doi.org/10.1016/j.neuron.2012.10.002

Masu, M., Iwakabe, H., Tagawa, Y., Miyoshi, T., Yamashita, M., Fukuda, Y., Sasaki, H., Hiroi, K., Nakamura, Y., Shigemoto, R., 1995. Specific deficit of the ON response in visual transmission by targeted disruption of the mGluR6 gene. Cell 80, 757–765.

Mata, N.L., Radu, R.A., Clemmons, R.S., Travis, G.H., 2002. Isomerization and Oxidation of Vitamin A in Cone-Dominant Retinas: A Novel Pathway for Visual-Pigment Regeneration in Daylight. Neuron 36, 69–80. https://doi.org/10.1016/S0896-6273(02)00912-1

Matsuo, I., Kuratani, S., Kimura, C., Takeda, N., Aizawa, S., 1995. Mouse Otx2 functions in the formation and patterning of rostral head. Genes Dev. 9, 2646–2658.

Mazzon, M., Mercer, J., 2014. Lipid interactions during virus entry and infection. Cell. Microbiol. 16, 1493–1502. https://doi.org/10.1111/cmi.12340

Mehat, M.S., 2017. PhD Thesis - Investigation of Stem cell-derived Retinal pigmented Epithelium (RPE) Transplantation.

Mehat, M.S., Sundaram, V., Ripamonti, C., Robson, A.G., Smith, A.J., Borooah, S., Robinson, M., Rosenthal, A.N., Innes, W., Weleber, R.G., Lee, R.W.J., Crossland, M., Rubin, G.S., Dhillon, B., Steel, D.H.W., Anglade, E., Lanza, R.P., Ali, R.R., Michaelides, M., Bainbridge, J.W.B., 2018. Transplantation of Human Embryonic

Stem Cell-Derived Retinal Pigment Epithelial Cells in Macular Degeneration. Ophthalmology 125, 1765–1775. https://doi.org/10.1016/j.ophtha.2018.04.037

Meister, M., Berry, M.J., 1999. The neural code of the retina. Neuron 22, 435–450. https://doi.org/10.1016/s0896-6273(00)80700-x

Meister, M., Pine, J., Baylor, D.A., 1994. Multi-neuronal signals from the retina: acquisition and analysis. J. Neurosci. Methods 51, 95–106. https://doi.org/10.1016/0165-0270(94)90030-2

Mellough, C.B., Collin, J., Khazim, M., White, K., Sernagor, E., Steel, D.H.W., Lako, M., 2015. IGF-1 Signaling Plays an Important Role in the Formation of Three-Dimensional Laminated Neural Retina and Other Ocular Structures From Human Embryonic Stem Cells. Stem Cells Dayt. Ohio 33, 2416–2430. https://doi.org/10.1002/stem.2023

Meyer, J.S., Shearer, R.L., Capowski, E.E., Wright, L.S., Wallace, K.A., McMillan, E.L., Zhang, S.-C., Gamm, D.M., 2009. Modeling early retinal development with human embryonic and induced pluripotent stem cells. Proc. Natl. Acad. Sci. U. S. A. 106, 16698–16703. https://doi.org/10.1073/pnas.0905245106

Michaelides, M., Hardcastle, A.J., Hunt, D.M., Moore, A.T., 2006. Progressive cone and cone-rod dystrophies: phenotypes and underlying molecular genetic basis. Surv. Ophthalmol. 51, 232–258. https://doi.org/10.1016/j.survophthal.2006.02.007

Michaelides, M., Hunt, D.M., Moore, A.T., 2004. The cone dysfunction syndromes. Br. J. Ophthalmol. 88, 291–297.

Mishra, A., Das, B., Nath, M., Iyer, S., Kesarwani, A., Bhattacharjee, J., Arindkar, S., Sahay, P., Jain, K., Sahu, P., Sinha, P., Velpandian, T., Nagarajan, P., Upadhyay, P., 2017. A novel immunodeficient NOD.SCID-rd1 mouse model of retinitis pigmentosa to investigate potential therapeutics and pathogenesis of retinal degeneration. Biol. Open 6, 449–462. https://doi.org/10.1242/bio.021618

Mohand-Said, S., Deudon-Combe, A., Hicks, D., Simonutti, M., Forster, V., Fintz, A.C., Léveillard, T., Dreyfus, H., Sahel, J.A., 1998. Normal retina releases a diffusible factor stimulating cone survival in the retinal degeneration mouse. Proc. Natl. Acad. Sci. U. S. A. 95, 8357–8362.

Morgan, J., Wong, R., 1995. Development of Cell Types and Synaptic Connections in the Retina, in: Kolb, H., Fernandez, E., Nelson, R. (Eds.), Webvision: The

Organization of the Retina and Visual System. University of Utah Health Sciences Center, Salt Lake City (UT).

Morgan, J.L., Soto, F., Wong, R.O.L., Kerschensteiner, D., 2011. Development of cell type-specific connectivity patterns of converging excitatory axons in the retina. Neuron 71, 1014–1021. https://doi.org/10.1016/j.neuron.2011.08.025

Moulder, K.L., Cormier, R.J., Shute, A.A., Zorumski, C.F., Mennerick, S., 2003. Homeostatic effects of depolarization on Ca2+ influx, synaptic signaling, and survival. J. Neurosci. Off. J. Soc. Neurosci. 23, 1825–1831.

Münch, T.A., da Silveira, R.A., Siegert, S., Viney, T.J., Awatramani, G.B., Roska, B., 2009. Approach sensitivity in the retina processed by a multifunctional neural circuit. Nat. Neurosci. 12, 1308–1316. https://doi.org/10.1038/nn.2389

Muniz, A., Villazana-Espinoza, E.T., Thackeray, B., Tsin, A.T.C., 2006. 11-cis-Acyl-CoA:Retinol O-Acyltransferase Activity in the Primary Culture of Chicken Muller Cells. Biochemistry 45, 12265–12273. https://doi.org/10.1021/bi060928p

Mure, L.S., Hatori, M., Zhu, Q., Demas, J., Kim, I.M., Nayak, S.K., Panda, S., 2016. Melanopsin-encoded response properties of intrinsically photosensitive retinal ganglion cells. Neuron 90, 1016–1027. https://doi.org/10.1016/j.neuron.2016.04.016

Nakano, T., Ando, S., Takata, N., Kawada, M., Muguruma, K., Sekiguchi, K., Saito, K., Yonemura, S., Eiraku, M., Sasai, Y., 2012. Self-Formation of Optic Cups and Storable Stratified Neural Retina from Human ESCs. Cell Stem Cell 10, 771–785. https://doi.org/10.1016/j.stem.2012.05.009

Nasonkin, I.O., Merbs, S.L., Lazo, K., Oliver, V.F., Brooks, M., Patel, K., Enke, R.A., Nellissery, J., Jamrich, M., Le, Y.Z., Bharti, K., Fariss, R.N., Rachel, R.A., Zack, D.J., Rodriguez-Boulan, E.J., Swaroop, A., 2013. Conditional knockdown of DNA methyltransferase 1 reveals a key role of retinal pigment epithelium integrity in photoreceptor outer segment morphogenesis. Dev. Camb. Engl. 140, 1330–1341. https://doi.org/10.1242/dev.086603

Nelson, R., Kolb, H., 1983. Synaptic patterns and response properties of bipolar and ganglion cells in the cat retina. Vision Res. 23, 1183–1195.

Nishiguchi, K.M., Carvalho, L.S., Rizzi, M., Powell, K., Holthaus, S.-M. kleine, Azam, S.A., Duran, Y., Ribeiro, J., Luhmann, U.F.O., Bainbridge, J.W.B., Smith, A.J., Ali, R.R., 2015. Gene therapy restores vision in *rd1* mice after removal of a confounding mutation in *Gpr179*. Nat. Commun. 6, 6006. https://doi.org/10.1038/ncomms7006

Nomura, A., Shigemoto, R., Nakamura, Y., Okamoto, N., Mizuno, N., Nakanishi, S., 1994. Developmentally regulated postsynaptic localization of a metabotropic glutamate receptor in rat rod bipolar cells. Cell 77, 361–369. https://doi.org/10.1016/0092-8674(94)90151-1

Obien, M.E.J., Deligkaris, K., Bullmann, T., Bakkum, D.J., Frey, U., 2015. Revealing neuronal function through microelectrode array recordings. Front. Neurosci. 8. https://doi.org/10.3389/fnins.2014.00423

Oh, E.C.T., Cheng, H., Hao, H., Jia, L., Khan, N.W., Swaroop, A., 2008. Rod differentiation factor NRL activates the expression of nuclear receptor NR2E3 to suppress the development of cone photoreceptors. Brain Res. 1236, 16–29. https://doi.org/10.1016/j.brainres.2008.01.028

O'Hearn, T.M., Sadda, S.R., Weiland, J.D., Maia, M., Margalit, E., Humayun, M.S., 2006. Electrical stimulation in normal and retinal degeneration (rd1) isolated mouse retina. Vision Res. 46, 3198–3204. https://doi.org/10.1016/j.visres.2006.03.031

Olney, J.W., 1968. An electron microscopic study of synapse formation, receptor outer segment development, and other aspects of developing mouse retina. Invest. Ophthalmol. 7, 250–268.

Ortin-Martinez, A., Tsai, E.L.S., Nickerson, P.E., Bergeret, M., Lu, Y., Smiley, S., Comanita, L., Wallace, V.A., 2017. A Reinterpretation of Cell Transplantation: GFP Transfer From Donor to Host Photoreceptors. Stem Cells Dayt. Ohio 35, 932–939. https://doi.org/10.1002/stem.2552

Osakada, F., Ikeda, H., Mandai, M., Wataya, T., Watanabe, K., Yoshimura, N., Akaike, Akinori, Akaike, Akiori, Sasai, Y., Takahashi, M., 2008. Toward the generation of rod and cone photoreceptors from mouse, monkey and human embryonic stem cells. Nat. Biotechnol. 26, 215–224. https://doi.org/10.1038/nbt1384

Owen, C.G., Jarrar, Z., Wormald, R., Cook, D.G., Fletcher, A.E., Rudnicka, A.R., 2012. The estimated prevalence and incidence of late stage age related macular degeneration in the UK. Br. J. Ophthalmol. 96, 752–756. https://doi.org/10.1136/bjophthalmol-2011-301109

Palczewski, K., 2012. Chemistry and Biology of Vision. J. Biol. Chem. 287, 1612–1619. https://doi.org/10.1074/jbc.R111.301150

Parvini, M., Satarian, L., Parivar, K., Javan, M., Tondar, M., Ahmad, S., Baharvand, H., 2014. Human Pluripotent Stem Cell-Derived Retinal Pigmented Epithelium in

Retinal Treatment: from Bench to Bedside. Mol. Neurobiol. 50, 597–612. https://doi.org/10.1007/s12035-014-8684-y

Pearson, R.A., Barber, A.C., Rizzi, M., Hippert, C., Xue, T., West, E.L., Duran, Y., Smith, A.J., Chuang, J.Z., Azam, S.A., Luhmann, U.F.O., Benucci, A., Sung, C.H., Bainbridge, J.W., Carandini, M., Yau, K.-W., Sowden, J.C., Ali, R.R., 2012. Restoration of vision after transplantation of photoreceptors. Nature 485, 99. https://doi.org/10.1038/nature10997

Pearson, R.A., Gonzalez-Cordero, A., West, E.L., Ribeiro, J.R., Aghaizu, N., Goh, D., Sampson, R.D., Georgiadis, A., Waldron, P.V., Duran, Y., Naeem, A., Kloc, M., Cristante, E., Kruczek, K., Warre-Cornish, K., Sowden, J.C., Smith, A.J., Ali, R.R., 2016. Donor and host photoreceptors engage in material transfer following transplantation of post-mitotic photoreceptor precursors. Nat. Commun. 7, 13029. https://doi.org/10.1038/ncomms13029

Petit, L., Ma, S., Cheng, S.-Y., Gao, G., Punzo, C., 2017. Rod Outer Segment Development Influences AAV-Mediated Photoreceptor Transduction After Subretinal Injection. Hum. Gene Ther. 28, 464–481. https://doi.org/10.1089/hum.2017.020

Pignatelli, V., Strettoi, E., 2004. Bipolar cells of the mouse retina: A gene gun, morphological study. J. Comp. Neurol. 476, 254–266. https://doi.org/10.1002/cne.20207

Pin, J.-P., Duvoisin, R., 1995. The metabotropic glutamate receptors: Structure and functions. Neuropharmacology 34, 1–26. https://doi.org/10.1016/0028-3908(94)00129-G

Pittler, S.J., Keeler, C.E., Sidman, R.L., Baehr, W., 1993. PCR analysis of DNA from 70-year-old sections of rodless retina demonstrates identity with the mouse rd defect. Proc. Natl. Acad. Sci. U. S. A. 90, 9616–9619.

Pontikos, N., Arno, G., Jurkute, N., Schiff, E., Ba-Abbad, R., Malka, S., Gimenez, A., Georgiou, M., Wright, G., Armengol, M., Knight, H., Katz, M., Moosajee, M., Yu-Wai-Man, P., Moore, A.T., Michaelides, M., Webster, A.R., Mahroo, O.A., 2020. Genetic Basis of Inherited Retinal Disease in a Molecularly Characterized Cohort of More Than 3000 Families from the United Kingdom. Ophthalmology 0. https://doi.org/10.1016/j.ophtha.2020.04.008

Portera-Cailliau, C., Sung, C.H., Nathans, J., Adler, R., 1994. Apoptotic photoreceptor cell death in mouse models of retinitis pigmentosa. Proc. Natl. Acad. Sci. U. S. A. 91, 974–978.

Prada, C., Puelles, L., Genis-Gálvez, J.M., Ramírez, G., 1987. Two modes of free migration of amacrine cell neuroblasts in the chick retina. Anat. Embryol. (Berl.) 175, 281–287.

Pugh, E.N., Lamb, T.D., 2000. Chapter 5 Phototransduction in vertebrate rods and cones: Molecular mechanisms of amplification, recovery and light adaptation, in: Stavenga, D.G., DeGrip, W.J., Pugh, E.N. (Eds.), Handbook of Biological Physics, Molecular Mechanisms in Visual Transduction. North-Holland, pp. 183–255. https://doi.org/10.1016/S1383-8121(00)80008-1

Puthussery, T., Taylor, W.R., 2010. Functional changes in inner retinal neurons in animal models of photoreceptor degeneration. Adv. Exp. Med. Biol. 664, 525–532. https://doi.org/10.1007/978-1-4419-1399-9_60

Quesada, A., Prada, F., Armengol, J.A., Génis-Gálvez, J.M., 1981. Early morphological differentiation of the bipolar neurons in the chick retina. A Golgi analysis. Anat. Histol. Embryol. 10, 328–341.

Radtke, N.D., Aramant, R.B., Petry, H.M., Green, P.T., Pidwell, D.J., Seiler, M.J., 2008. Vision Improvement in Retinal Degeneration Patients by Implantation of Retina Together with Retinal Pigment Epithelium. Am. J. Ophthalmol. 146, 172-182.e1. https://doi.org/10.1016/j.ajo.2008.04.009

Radtke, N.D., Aramant, R.B., Seiler, M., Petry, H.M., 1999. Preliminary report: indications of improved visual function after retinal sheet transplantation in retinitis pigmentosa patients. Am. J. Ophthalmol. 128, 384–387.

Radtke, N.D., Seiler, M.J., Aramant, R.B., Petry, H.M., Pidwell, D.J., 2002. Transplantation of intact sheets of fetal neural retina with its retinal pigment epithelium in retinitis pigmentosa patients. Am. J. Ophthalmol. 133, 544–550. https://doi.org/10.1016/s0002-9394(02)01322-3

Ramamurthy, V., Niemi, G.A., Reh, T.A., Hurley, J.B., 2004. Leber congenital amaurosis linked to AIPL1: a mouse model reveals destabilization of cGMP phosphodiesterase. Proc. Natl. Acad. Sci. U. S. A. 101, 13897–13902. https://doi.org/10.1073/pnas.0404197101

Ramamurthy, V., Roberts, M., Akker, F. van den, Niemi, G., Reh, T.A., Hurley, J.B., 2003. AIPL1, a protein implicated in Leber's congenital amaurosis, interacts with and aids in processing of farnesylated proteins. Proc. Natl. Acad. Sci. 100, 12630–12635. https://doi.org/10.1073/pnas.2134194100

Recober, A., Kuburas, A., Zhang, Z., Wemmie, J.A., Anderson, M.G., Russo, A.F., 2009. Role of Calcitonin Gene-Related Peptide in Light-Aversive Behavior: Implications for Migraine. J. Neurosci. 29, 8798–8804. https://doi.org/10.1523/JNEUROSCI.1727-09.2009

Reese, B.E., Raven, M.A., Stagg, S.B., 2005. Afferents and homotypic neighbors regulate horizontal cell morphology, connectivity, and retinal coverage. J. Neurosci. Off. J. Soc. Neurosci. 25, 2167–2175. https://doi.org/10.1523/JNEUROSCI.4876-04.2005

Reichman, S., Slembrouck, A., Gagliardi, G., Chaffiol, A., Terray, A., Nanteau, C., Potey, A., Belle, M., Rabesandratana, O., Duebel, J., Orieux, G., Nandrot, E.F., Sahel, J.-A., Goureau, O., 2017. Generation of Storable Retinal Organoids and Retinal Pigmented Epithelium from Adherent Human iPS Cells in Xeno-Free and Feeder-Free Conditions. Stem Cells Dayt. Ohio 35, 1176–1188. https://doi.org/10.1002/stem.2586

Reichman, S., Terray, A., Slembrouck, A., Nanteau, C., Orieux, G., Habeler, W., Nandrot, E.F., Sahel, J.-A., Monville, C., Goureau, O., 2014. From confluent human iPS cells to self-forming neural retina and retinal pigmented epithelium. Proc. Natl. Acad. Sci. U. S. A. 111, 8518–8523. https://doi.org/10.1073/pnas.1324212111

Reinhard, K., Tikidji-Hamburyan, A., Seitter, H., Idrees, S., Mutter, M., Benkner, B., Münch, T.A., 2014. Step-By-Step Instructions for Retina Recordings with Perforated Multi Electrode Arrays. PLOS ONE 9, e106148. https://doi.org/10.1371/journal.pone.0106148

Ribelayga, C., 2010. Vertebrate Vision: TRP Channels in the Spotlight. Curr. Biol. 20, R278–R280. https://doi.org/10.1016/j.cub.2010.02.012

Rice, D.S., Nusinowitz, S., Azimi, A.M., Martínez, A., Soriano, E., Curran, T., 2001. The reelin pathway modulates the structure and function of retinal synaptic circuitry. Neuron 31, 929–941.

Ripamonti, C., Henning, G.B., Robbie, S.J., Sundaram, V., van den Born, L.I., Casteels, I., de Ravel, T.J.L., Moore, A.T., Smith, A.J., Bainbridge, J.W., Ali, R.R.,

Stockman, A., 2015. Spectral sensitivity measurements reveal partial success in restoring missing rod function with gene therapy. J. Vis. 15, 20. https://doi.org/10.1167/15.15.20

Roberts, M.R., Srinivas, M., Forrest, D., Morreale de Escobar, G., Reh, T.A., 2006. Making the gradient: Thyroid hormone regulates cone opsin expression in the developing mouse retina. Proc. Natl. Acad. Sci. U. S. A. 103, 6218–6223. https://doi.org/10.1073/pnas.0509981103

Rockhill, R.L., Euler, T., Masland, R.H., 2000. Spatial order within but not between types of retinal neurons. Proc. Natl. Acad. Sci. U. S. A. 97, 2303–2307. https://doi.org/10.1073/pnas.030413497

Rodrigues, M.M., Bardenstein, D., Wiggert, B., Lee, L., Fletcher, R.T., Chader, G., 1987. Retinitis pigmentosa with segmental massive retinal gliosis. An immunohistochemical, biochemical, and ultrastructural study. Ophthalmology 94, 180–186.

Roska, B., Werblin, F., 2003. Rapid global shifts in natural scenes block spiking in specific ganglion cell types. Nat. Neurosci. 6, 600–608. https://doi.org/10.1038/nn1061

Rowan, S., Chen, C.-M.A., Young, T.L., Fisher, D.E., Cepko, C.L., 2004. Transdifferentiation of the retina into pigmented cells in ocular retardation mice defines a new function of the homeodomain gene Chx10. Dev. Camb. Engl. 131, 5139–5152. https://doi.org/10.1242/dev.01300

Rudnicka, A.R., Kapetanakis, V.V., Jarrar, Z., Wathern, A.K., Wormald, R., Fletcher, A.E., Cook, D.G., Owen, C.G., 2015. Incidence of Late-Stage Age-Related Macular Degeneration in American Whites: Systematic Review and Meta-analysis. Am. J. Ophthalmol. 160, 85-93.e3. https://doi.org/10.1016/j.ajo.2015.04.003

Ruggiero, L., Allen, C.N., Brown, R.L., Robinson, D.W., 2009. The development of melanopsin-containing retinal ganglion cells in mice with early retinal degeneration. Eur. J. Neurosci. 29, 359–367. https://doi.org/10.1111/j.1460-9568.2008.06589.x

Sakamoto, K., McCluskey, M., Wensel, T.G., Naggert, J.K., Nishina, P.M., 2009. New mouse models for recessive retinitis pigmentosa caused by mutations in the Pde6a gene. Hum. Mol. Genet. 18, 178–192. https://doi.org/10.1093/hmg/ddn327

Samson, M., Emerson, M.M., Cepko, C.L., 2009. Robust marking of photoreceptor cells and pinealocytes with several reporters under control of the Crx gene. Dev. Dyn. Off. Publ. Am. Assoc. Anat. 238, 3218–3225. https://doi.org/10.1002/dvdy.22138

Sanchez–Fueyo, A., Strom, T.B., 2011. Immunologic Basis of Graft Rejection and Tolerance Following Transplantation of Liver or Other Solid Organs. Gastroenterology 140. https://doi.org/10.1053/j.gastro.2010.10.059

Santos-Ferreira, T., Llonch, S., Borsch, O., Postel, K., Haas, J., Ader, M., 2016. Retinal transplantation of photoreceptors results in donor–host cytoplasmic exchange. Nat. Commun. 7, 13028. https://doi.org/10.1038/ncomms13028

Sanyal, S., Zeilmaker, G.H., 1984. Development and degeneration of retina in rds mutant mice: Light and electron microscopic observations in experimental chimaeras. Exp. Eye Res. 39, 231–246. https://doi.org/10.1016/0014-4835(84)90011-3

Sarria, I., Cao, Y., Wang, Y., Ingram, N.T., Orlandi, C., Kamasawa, N., Kolesnikov, A.V., Pahlberg, J., Kefalov, V.J., Sampath, A.P., Martemyanov, K.A., 2018. LRIT1 Modulates Adaptive Changes in Synaptic Communication of Cone Photoreceptors. Cell Rep. 22, 3562–3573. https://doi.org/10.1016/j.celrep.2018.03.008

Schmitz, F., Natarajan, S., Venkatesan, J.K., Wahl, S., Schwarz, K., Grabner, C.P., 2012. EF hand-mediated Ca2+- signalling in photoreceptor synaptic terminals. Front. Mol. Neurosci. 5. https://doi.org/10.3389/fnmol.2012.00026

Schnetkamp, P.P., Basu, D.K., Li, X.B., Szerencsei, R.T., 1991. Regulation of intracellular free Ca2+ concentration in the outer segments of bovine retinal rods by Na-Ca-K exchange measured with fluo-3. II. Thermodynamic competence of transmembrane Na+ and K+ gradients and inactivation of Na(+)-dependent Ca2+ extrusion. J. Biol. Chem. 266, 22983–22990.

Schwartz, S.D., Regillo, C.D., Lam, B.L., Eliott, D., Rosenfeld, P.J., Gregori, N.Z., Hubschman, J.-P., Davis, J.L., Heilwell, G., Spirn, M., Maguire, J., Gay, R., Bateman, J., Ostrick, R.M., Morris, D., Vincent, M., Anglade, E., Del Priore, L.V., Lanza, R., 2015. Human embryonic stem cell-derived retinal pigment epithelium in patients with age-related macular degeneration and Stargardt's macular dystrophy: follow-up of two open-label phase 1/2 studies. The Lancet 385, 509–516. https://doi.org/10.1016/S0140-6736(14)61376-3

Schwartz, S.D., Tan, G., Hosseini, H., Nagiel, A., 2016. Subretinal Transplantation of Embryonic Stem Cell–Derived Retinal Pigment Epithelium for the Treatment of

Macular Degeneration: An Assessment at 4 Years. Investig. Opthalmology Vis. Sci. 57, ORSFc1. https://doi.org/10.1167/iovs.15-18681

Seiler, M.J., Aramant, R.B., 2012. Cell replacement and visual restoration by retinal sheet transplants. Prog. Retin. Eye Res. 31, 661–687. https://doi.org/10.1016/j.preteyeres.2012.06.003

Seiler, M.J., Aramant, R.B., Jones, M.K., Ferguson, D.L., Bryda, E.C., Keirstead, H.S., 2014. A new immunodeficient pigmented retinal degenerate rat strain to study transplantation of human cells without immunosuppression. Graefes Arch. Clin. Exp. Ophthalmol. Albrecht Von Graefes Arch. Klin. Exp. Ophthalmol. 252, 1079–1092. https://doi.org/10.1007/s00417-014-2638-y

Sekaran, S., Lupi, D., Jones, S.L., Sheely, C.J., Hattar, S., Yau, K.-W., Lucas, R.J., Foster, R.G., Hankins, M.W., 2005. Melanopsin-Dependent Photoreception Provides Earliest Light Detection in the Mammalian Retina. Curr. Biol. CB 15, 1099–1107. https://doi.org/10.1016/j.cub.2005.05.053

Semo, M., Gias, C., Ahmado, A., Sugano, E., Allen, A.E., Lawrence, J.M., Tomita, H., Coffey, P.J., Vugler, A.A., 2010. Dissecting a role for melanopsin in behavioural light aversion reveals a response independent of conventional photoreception. PloS One 5, e15009. https://doi.org/10.1371/journal.pone.0015009

Sernagor, E., Mehta, V., 2001. The role of early neural activity in the maturation of turtle retinal function. J. Anat. 199, 375–383.

Sexton, T.J., Golczak, M., Palczewski, K., Van Gelder, R.N., 2012. Melanopsin Is Highly Resistant to Light and Chemical Bleaching in Vivo. J. Biol. Chem. 287, 20888–20897. https://doi.org/10.1074/jbc.M111.325969

Shen, Y., Liu, X., Yang, X., 2006. N-methyl-D-aspartate receptors in the retina. Mol. Neurobiol. https://doi.org/10.1385/MN:34:3:163

Shi, C., Yuan, X., Chang, K., Cho, K.-S., Xie, X.S., Chen, D.F., Luo, G., 2018. Optimization of Optomotor Response-based Visual Function Assessment in Mice. Sci. Rep. 8, 1–10. https://doi.org/10.1038/s41598-018-27329-w

Shirai, H., Mandai, M., Matsushita, K., Kuwahara, A., Yonemura, S., Nakano, T., Assawachananont, J., Kimura, T., Saito, K., Terasaki, H., Eiraku, M., Sasai, Y., Takahashi, M., 2016. Transplantation of human embryonic stem cell-derived retinal tissue in two primate models of retinal degeneration. Proc. Natl. Acad. Sci. 113, E81–E90. https://doi.org/10.1073/pnas.1512590113

Silva, S.R.D., Barnard, A.R., Hughes, S., Tam, S.K.E., Martin, C., Singh, M.S., Barnea-Cramer, A.O., McClements, M.E., During, M.J., Peirson, S.N., Hankins, M.W., MacLaren, R.E., 2017. Long-term restoration of visual function in end-stage retinal degeneration using subretinal human melanopsin gene therapy. Proc. Natl. Acad. Sci. 201701589. https://doi.org/10.1073/pnas.1701589114

Singh, M.S., Charbel Issa, P., Butler, R., Martin, C., Lipinski, D.M., Sekaran, S., Barnard, A.R., MacLaren, R.E., 2013. Reversal of end-stage retinal degeneration and restoration of visual function by photoreceptor transplantation. Proc. Natl. Acad. Sci. U. S. A. 110, 1101–1106. https://doi.org/10.1073/pnas.1119416110

Singh, R.K., Kolandaivelu, S., Ramamurthy, V., 2014a. Early Alteration of Retinal Neurons in Aipl1−/− Animals. Invest. Ophthalmol. Vis. Sci. 55, 3081–3092. https://doi.org/10.1167/iovs.13-13728

Singh, R.K., Kolandaivelu, S., Ramamurthy, V., 2014b. Early Alteration of Retinal Neurons in Aipl1−/− Animals. Invest. Ophthalmol. Vis. Sci. 55, 3081–3092. https://doi.org/10.1167/iovs.13-13728

Slaughter, M.M., Miller, R.F., 1983. The role of excitatory amino acid transmitters in the mudpuppy retina: an analysis with kainic acid and N-methyl aspartate. J. Neurosci. Off. J. Soc. Neurosci. 3, 1701–1711.

Slaughter, M.M., Miller, R.F., 1981. 2-amino-4-phosphonobutyric acid: a new pharmacological tool for retina research. Science 211, 182–185.

Slembrouck-Brec, A., Nanteau, C., Sahel, J.-A., Goureau, O., Reichman, S., 2018. Defined Xeno-free and Feeder-free Culture Conditions for the Generation of Human iPSC-derived Retinal Cell Models. J. Vis. Exp. JoVE. https://doi.org/10.3791/57795

Smith, W., Assink, J., Klein, R., Mitchell, P., Klaver, C.C., Klein, B.E., Hofman, A., Jensen, S., Wang, J.J., de Jong, P.T., 2001. Risk factors for age-related macular degeneration: Pooled findings from three continents. Ophthalmology 108, 697–704.

Sokolov, M., Lyubarsky, A.L., Strissel, K.J., Savchenko, A.B., Govardovskii, V.I., Pugh, E.N., Arshavsky, V.Y., 2002. Massive light-driven translocation of transducin between the two major compartments of rod cells: a novel mechanism of light adaptation. Neuron 34, 95–106.

Song, W.K., Park, K.-M., Kim, H.-J., Lee, J.H., Choi, J., Chong, S.Y., Shim, S.H., Del Priore, L.V., Lanza, R., 2015. Treatment of Macular Degeneration Using Embryonic Stem Cell-Derived Retinal Pigment Epithelium: Preliminary Results in

Asian Patients. Stem Cell Rep. 4, 860–872. https://doi.org/10.1016/j.stemcr.2015.04.005

Specht, D., Wu, S.-B., Turner, P., Dearden, P., Koentgen, F., Wolfrum, U., Maw, M., Brandstätter, J.H., Dieck, S. tom, 2009. Effects of Presynaptic Mutations on a Postsynaptic Cacna1s Calcium Channel Colocalized with mGluR6 at Mouse Photoreceptor Ribbon Synapses. Invest. Ophthalmol. Vis. Sci. 50, 505–515. https://doi.org/10.1167/iovs.08-2758

Srinivas, M., Ng, L., Liu, H., Jia, L., Forrest, D., 2006. Activation of the blue opsin gene in cone photoreceptor development by retinoid-related orphan receptor beta. Mol. Endocrinol. Baltim. Md 20, 1728–1741. https://doi.org/10.1210/me.2005-0505

Stett, A., Barth, W., Weiss, S., Haemmerle, H., Zrenner, E., 2000. Electrical multisite stimulation of the isolated chicken retina. Vision Res. 40, 1785–1795. https://doi.org/10.1016/S0042-6989(00)00005-5

Stett, A., Egert, U., Guenther, E., Hofmann, F., Meyer, T., Nisch, W., Haemmerle, H., 2003. Biological application of microelectrode arrays in drug discovery and basic research. Anal. Bioanal. Chem. 377, 486–495. https://doi.org/10.1007/s00216-003-2149-x

Stingl, K., Bartz-Schmidt, K.U., Besch, D., Braun, A., Bruckmann, A., Gekeler, F., Greppmaier, U., Hipp, S., Hörtdörfer, G., Kernstock, C., Koitschev, A., Kusnyerik, A., Sachs, H., Schatz, A., Stingl, K.T., Peters, T., Wilhelm, B., Zrenner, E., 2013. Artificial vision with wirelessly powered subretinal electronic implant alpha-IMS. Proc R Soc B 280, 20130077. https://doi.org/10.1098/rspb.2013.0077

Streilein, J.W., Ma, N., Wenkel, H., Ng, T.F., Zamiri, P., 2002. Immunobiology and privilege of neuronal retina and pigment epithelium transplants. Vision Res. 42, 487–495.

Strettoi, E., 2015. A Survey of Retinal Remodeling. Front. Cell. Neurosci. 9. https://doi.org/10.3389/fncel.2015.00494

Strettoi, E., Pignatelli, V., 2000. Modifications of retinal neurons in a mouse model of retinitis pigmentosa. Proc. Natl. Acad. Sci. 97, 11020–11025. https://doi.org/10.1073/pnas.190291097

Strettoi, E., Pignatelli, V., Rossi, C., Porciatti, V., Falsini, B., 2003a. Remodeling of second-order neurons in the retina of rd/rd mutant mice. Vision Res. 43, 867–877.

Strettoi, E., Pignatelli, V., Rossi, C., Porciatti, V., Falsini, B., 2003b. Remodeling of second-order neurons in the retina of rd/rd mutant mice. Vision Res. 43, 867–877.

Strettoi, E., Porciatti, V., Falsini, B., Pignatelli, V., Rossi, C., 2002. Morphological and Functional Abnormalities in the Inner Retina of the rd/rd Mouse. J. Neurosci. 22, 5492–5504. https://doi.org/10.1523/JNEUROSCI.22-13-05492.2002

Sugita, S., Iwasaki, Y., Makabe, K., Kamao, H., Mandai, M., Shiina, T., Ogasawara, K., Hirami, Y., Kurimoto, Y., Takahashi, M., 2016. Successful Transplantation of Retinal Pigment Epithelial Cells from MHC Homozygote iPSCs in MHC-Matched Models. Stem Cell Rep. https://doi.org/10.1016/j.stemcr.2016.08.010

Sung, C.-H., Chuang, J.-Z., 2010. The cell biology of vision. J. Cell Biol. 190, 953–963. https://doi.org/10.1083/jcb.201006020

Swaroop, A., Kim, D., Forrest, D., 2010. Transcriptional regulation of photoreceptor development and homeostasis in the mammalian retina. Nat. Rev. Neurosci. 11, 563–576. https://doi.org/10.1038/nrn2880

Takao, K., Miyakawa, T., 2006. Light/dark Transition Test for Mice. J. Vis. Exp. JoVE. https://doi.org/10.3791/104

Tan, M.H., Mackay, D.S., Cowing, J., Tran, H.V., Smith, A.J., Wright, G.A., Dev-Borman, A., Henderson, R.H., Moradi, P., Russell-Eggitt, I., MacLaren, R.E., Robson, A.G., Cheetham, M.E., Thompson, D.A., Webster, A.R., Michaelides, M., Ali, R.R., Moore, A.T., 2012. Leber Congenital Amaurosis Associated with AIPL1: Challenges in Ascribing Disease Causation, Clinical Findings, and Implications for Gene Therapy. PLOS ONE 7, e32330. https://doi.org/10.1371/journal.pone.0032330

Tan, M.H., Smith, A.J., Pawlyk, B., Xu, X., Liu, X., Bainbridge, J.B., Basche, M., McIntosh, J., Tran, H.V., Nathwani, A., Li, T., Ali, R.R., 2009. Gene therapy for retinitis pigmentosa and Leber congenital amaurosis caused by defects in AIPL1: effective rescue of mouse models of partial and complete Aipl1 deficiency using AAV2/2 and AAV2/8 vectors. Hum. Mol. Genet. 18, 2099–2114. https://doi.org/10.1093/hmg/ddp133

Taranova, O.V., Magness, S.T., Fagan, B.M., Wu, Y., Surzenko, N., Hutton, S.R., Pevny, L.H., 2006. SOX2 is a dose-dependent regulator of retinal neural progenitor competence. Genes Dev. 20, 1187–1202. https://doi.org/10.1101/gad.1407906

Thaung, C., Arnold, K., Jackson, I.J., Coffey, P.J., 2002. Presence of visual head tracking differentiates normal sighted from retinal degenerate mice. Neurosci. Lett. 325, 21–24. https://doi.org/10.1016/s0304-3940(02)00223-9

Thompson, S., Blodi, F.R., Lee, S., Welder, C.R., Mullins, R.F., Tucker, B.A., Stasheff, S.F., Stone, E.M., 2014. Photoreceptor Cells With Profound Structural Deficits Can Support Useful Vision in Mice. Invest. Ophthalmol. Vis. Sci. 55, 1859–1866. https://doi.org/10.1167/iovs.13-13661

Thomson, J.A., Itskovitz-Eldor, J., Shapiro, S.S., Waknitz, M.A., Swiergiel, J.J., Marshall, V.S., Jones, J.M., 1998. Embryonic stem cell lines derived from human blastocysts. Science 282, 1145–1147.

Tomioka, N.H., Yasuda, H., Miyamoto, H., Hatayama, M., Morimura, N., Matsumoto, Y., Suzuki, T., Odagawa, M., Odaka, Y.S., Iwayama, Y., Won Um, J., Ko, J., Inoue, Y., Kaneko, S., Hirose, S., Yamada, K., Yoshikawa, T., Yamakawa, K., Aruga, J., 2014. Elfn1 recruits presynaptic mGluR7 in trans and its loss results in seizures. Nat. Commun. 5, 4501. https://doi.org/10.1038/ncomms5501

Travis, G.H., 1998. Mechanisms of cell death in the inherited retinal degenerations. Am. J. Hum. Genet. 62, 503–508.

Trifonov, Yu.A., 1968. Study of synaptic transmission between photoreceptor and horizontal cell by means of electrical stimulation of the retina. [Study of synaptic transmission between photoreceptor and horizontal cell by means of electrical stimulation of the retina.]. Biofizika 13, 809–817.

Trivedi, H.L., 2007. Immunobiology of rejection and adaptation. Transplant. Proc. 39, 647–652. https://doi.org/10.1016/j.transproceed.2007.01.047

Tu, H.-Y., Watanabe, T., Shirai, H., Yamasaki, S., Kinoshita, M., Matsushita, K., Hashiguchi, T., Onoe, H., Matsuyama, T., Kuwahara, A., Kishino, A., Kimura, T., Eiraku, M., Suzuma, K., Kitaoka, T., Takahashi, M., Mandai, M., 2019. Medium- to long-term survival and functional examination of human iPSC-derived retinas in rat and primate models of retinal degeneration. EBioMedicine 39, 562–574. https://doi.org/10.1016/j.ebiom.2018.11.028

Turner, D.L., Cepko, C.L., 1987. A common progenitor for neurons and glia persists in rat retina late in development. Nature 328, 131–136. https://doi.org/10.1038/328131a0

Turner, D.L., Snyder, E.Y., Cepko, C.L., 1990. Lineage-independent determination of cell type in the embryonic mouse retina. Neuron 4, 833–845.

Ueno, A., Omori, Y., Sugita, Y., Watanabe, S., Chaya, T., Kozuka, T., Kon, T., Yoshida, S., Matsushita, K., Kuwahara, R., Kajimura, N., Okada, Y., Furukawa, T., 2018. Lrit1, a Retinal Transmembrane Protein, Regulates Selective Synapse Formation in Cone Photoreceptor Cells and Visual Acuity. Cell Rep. 22, 3548–3561. https://doi.org/10.1016/j.celrep.2018.03.007

van der Spuy, J., Kim, J.H., Yu, Y.S., Szel, A., Luthert, P.J., Clark, B.J., Cheetham, M.E., 2003. The expression of the Leber congenital amaurosis protein AIPL1 coincides with rod and cone photoreceptor development. Invest. Ophthalmol. Vis. Sci. 44, 5396–5403.

Vardi, N., Duvoisin, R., Wu, G., Sterling, P., 2000. Localization of mGluR6 to dendrites of ON bipolar cells in primate retina. J. Comp. Neurol. 423.

Vardi, N., Morigiwa, K., 1997. ON cone bipolar cells in rat express the metabotropic receptor mGluR6. Vis. Neurosci. 14, 789–794.

Veleri, S., Lazar, C.H., Chang, B., Sieving, P.A., Banin, E., Swaroop, A., 2015a. Biology and therapy of inherited retinal degenerative disease: insights from mouse models. Dis. Model. Mech. 8, 109–129. https://doi.org/10.1242/dmm.017913

Veleri, S., Lazar, C.H., Chang, B., Sieving, P.A., Banin, E., Swaroop, A., 2015b. Biology and therapy of inherited retinal degenerative disease: insights from mouse models. Dis. Model. Mech. 8, 109–129. https://doi.org/10.1242/dmm.017913

Vitillo, L., Tovell, V.E., Coffey, P., 2020. Treatment of Age-Related Macular Degeneration with Pluripotent Stem Cell-Derived Retinal Pigment Epithelium. Curr. Eye Res. 45, 361–371. https://doi.org/10.1080/02713683.2019.1691237

Waldron, P.V., Di Marco, F., Kruczek, K., Ribeiro, J., Graca, A.B., Hippert, C., Aghaizu, N.D., Kalargyrou, A.A., Barber, A.C., Grimaldi, G., Duran, Y., Blackford, S.J.I., Kloc, M., Goh, D., Zabala Aldunate, E., Sampson, R.D., Bainbridge, J.W.B., Smith, A.J., Gonzalez-Cordero, A., Sowden, J.C., Ali, R.R., Pearson, R.A., 2018. Transplanted Donor- or Stem Cell-Derived Cone Photoreceptors Can Both Integrate and Undergo Material Transfer in an Environment-Dependent Manner. Stem Cell Rep. https://doi.org/10.1016/j.stemcr.2017.12.008

Wang, J.-S., Estevez, M.E., Cornwall, M.C., Kefalov, V.J., 2009. Intra-retinal visual cycle required for rapid and complete cone dark adaptation. Nat. Neurosci. 12, 295–302. https://doi.org/10.1038/nn.2258

Wang, J.-S., Kefalov, V.J., 2011. The cone-specific visual cycle. Prog. Retin. Eye Res. 30, 115–128. https://doi.org/10.1016/j.preteyeres.2010.11.001

Wang, S.W., Kim, B.S., Ding, K., Wang, H., Sun, D., Johnson, R.L., Klein, W.H., Gan, L., 2001. Requirement for math5 in the development of retinal ganglion cells. Genes Dev. 15, 24–29. https://doi.org/10.1101/gad.855301

Wang, Y., Macke, J.P., Merbs, S.L., Zack, D.J., Klaunberg, B., Bennett, J., Gearhart, J., Nathans, J., 1992. A locus control region adjacent to the human red and green visual pigment genes. Neuron 9, 429–440. https://doi.org/10.1016/0896-6273(92)90181-C

Warre-Cornish, K., Barber, A.C., Sowden, J.C., Ali, R.R., Pearson, R.A., 2014. Migration, integration and maturation of photoreceptor precursors following transplantation in the mouse retina. Stem Cells Dev. 23, 941–954. https://doi.org/10.1089/scd.2013.0471

Wässle, H., Peichl, L., Boycott, B.B., 1981. Dendritic territories of cat retinal ganglion cells. Nature 292, 344–345.

Wässle, H., Puller, C., Müller, F., Haverkamp, S., 2009. Cone contacts, mosaics, and territories of bipolar cells in the mouse retina. J. Neurosci. Off. J. Soc. Neurosci. 29, 106–117. https://doi.org/10.1523/JNEUROSCI.4442-08.2009

Wässle, H., Riemann, H.J., 1978. The mosaic of nerve cells in the mammalian retina. Proc. R. Soc. Lond. B Biol. Sci. 200, 441–461. https://doi.org/10.1098/rspb.1978.0026

Watanabe, K., Kamiya, D., Nishiyama, A., Katayama, T., Nozaki, S., Kawasaki, H., Watanabe, Y., Mizuseki, K., Sasai, Y., 2005. Directed differentiation of telencephalic precursors from embryonic stem cells. Nat. Neurosci. 8, 288–296. https://doi.org/10.1038/nn1402

Welby, E., Lakowski, J., Di Foggia, V., Budinger, D., Gonzalez-Cordero, A., Lun, A.T.L., Epstein, M., Patel, A., Cuevas, E., Kruczek, K., Naeem, A., Minneci, F., Hubank, M., Jones, D.T., Marioni, J.C., Ali, R.R., Sowden, J.C., 2017. Isolation and Comparative Transcriptome Analysis of Human Fetal and iPSC-Derived Cone

Photoreceptor Cells. Stem Cell Rep. 9, 1898–1915. https://doi.org/10.1016/j.stemcr.2017.10.018

Werblin, F.S., Dowling, J.E., 1969. Organization of the retina of the mudpuppy, Necturus maculosus. II. Intracellular recording. J. Neurophysiol. 32, 339–355. https://doi.org/10.1152/jn.1969.32.3.339

West, E.L., Gonzalez-Cordero, A., Hippert, C., Osakada, F., Martinez-Barbera, J.P., Pearson, R.A., Sowden, J.C., Takahashi, M., Ali, R.R., 2012a. Defining the integration capacity of embryonic stem cell-derived photoreceptor precursors. Stem Cells Dayt. Ohio 30, 1424–1435. https://doi.org/10.1002/stem.1123

West, E.L., Gonzalez-Cordero, A., Hippert, C., Osakada, F., Martinez-Barbera, J.P., Pearson, R.A., Sowden, J.C., Takahashi, M., Ali, R.R., 2012b. Defining the integration capacity of embryonic stem cell-derived photoreceptor precursors. Stem Cells Dayt. Ohio 30, 1424–1435. https://doi.org/10.1002/stem.1123

West, E.L., Pearson, R.A., Barker, S.E., Luhmann, U.F.O., Maclaren, R.E., Barber, A.C., Duran, Y., Smith, A.J., Sowden, J.C., Ali, R.R., 2010. Long-Term Survival of Photoreceptors Transplanted into the Adult Murine Neural Retina Requires Immune Modulation. Stem Cells Dayt. Ohio 28, 1997–2007. https://doi.org/10.1002/stem.520

Williams, M.E., de Wit, J., Ghosh, A., 2010. Molecular Mechanisms of Synaptic Specificity in Developing Neural Circuits. Neuron 68, 9–18. https://doi.org/10.1016/j.neuron.2010.09.007

Wong, K.A., Trembley, M., Abd Wahab, S., Viczian, A.S., 2015. Efficient retina formation requires suppression of both Activin and BMP signaling pathways in pluripotent cells. Biol. Open 4, 573–583. https://doi.org/10.1242/bio.20149977

Wong, W.T., Faulkner-Jones, B.E., Sanes, J.R., Wong, R.O., 2000. Rapid dendritic remodeling in the developing retina: dependence on neurotransmission and reciprocal regulation by Rac and Rho. J. Neurosci. Off. J. Soc. Neurosci. 20, 5024–5036.

Woodruff, M.L., Wang, Z., Chung, H.Y., Redmond, T.M., Fain, G.L., Lem, J., 2003. Spontaneous activity of opsin apoprotein is a cause of Leber congenital amaurosis. Nat. Genet. 35, 158–164. https://doi.org/10.1038/ng1246

Xiang, M., 2013. Intrinsic control of mammalian retinogenesis. Cell. Mol. Life Sci. CMLS 70, 2519–2532. https://doi.org/10.1007/s00018-012-1183-2

Xu, J., Dodd, R.L., Makino, C.L., Simon, M.I., Baylor, D.A., Chen, J., 1997. Prolonged photoresponses in transgenic mouse rods lacking arrestin. Nature 389, 505–509. https://doi.org/10.1038/39068

Xu, X., Li, S., Xiao, X., Wang, P., Guo, X., Zhang, Q., 2009. Sequence variations of GRM6 in patients with high myopia. Mol. Vis. 15, 2094–2100.

Yadav, R.P., Artemyev, N.O., 2017. AIPL1: a specialized chaperone for the phototransduction effector. Cell. Signal. 40, 183–189. https://doi.org/10.1016/j.cellsig.2017.09.014

Yang, X.-L., 2004. Characterization of receptors for glutamate and GABA in retinal neurons. Prog. Neurobiol. 73, 127–150. https://doi.org/10.1016/j.pneurobio.2004.04.002

Yilmaz, M., Meister, M., 2013. Rapid innate defensive responses of mice to looming visual stimuli. Curr. Biol. CB 23, 2011–2015. https://doi.org/10.1016/j.cub.2013.08.015

Yonehara, K., Farrow, K., Ghanem, A., Hillier, D., Balint, K., Teixeira, M., Jüttner, J., Noda, M., Neve, R.L., Conzelmann, K.-K., Roska, B., 2013. The first stage of cardinal direction selectivity is localized to the dendrites of retinal ganglion cells. Neuron 79, 1078–1085. https://doi.org/10.1016/j.neuron.2013.08.005

Zarbin, M., 2016. Cell-Based Therapy for Degenerative Retinal Disease. Trends Mol. Med. 22, 115–134. https://doi.org/10.1016/j.molmed.2015.12.007

Zarbin, M., Sugino, I., Townes-Anderson, E., 2019. Concise Review: Update on Retinal Pigment Epithelium Transplantation for Age-Related Macular Degeneration. Stem Cells Transl. Med. 8, 466–477. https://doi.org/10.1002/sctm.18-0282

Zeitz, C., van Genderen, M., Neidhardt, J., Luhmann, U.F.O., Hoeben, F., Forster, U., Wycisk, K., Mátyás, G., Hoyng, C.B., Riemslag, F., Meire, F., Cremers, F.P.M., Berger, W., 2005. Mutations in GRM6 cause autosomal recessive congenital stationary night blindness with a distinctive scotopic 15-Hz flicker electroretinogram. Invest. Ophthalmol. Vis. Sci. 46, 4328–4335. https://doi.org/10.1167/iovs.05-0526

Zhang, Houbin, Huang, W., Zhang, Haikun, Zhu, X., Craft, C.M., Baehr, W., Chen, C.-K., 2003. Light-dependent redistribution of visual arrestins and transducin subunits in mice with defective phototransduction. Mol. Vis. 9, 231–237.

Zhao, X., Liu, J., Ahmad, I., 2002. Differentiation of embryonic stem cells into retinal neurons. Biochem. Biophys. Res. Commun. 297, 177–184.

Zhong, X., Gutierrez, C., Xue, T., Hampton, C., Vergara, M.N., Cao, L.-H., Peters, A., Park, T.S., Zambidis, E.T., Meyer, J.S., Gamm, D.M., Yau, K.-W., Canto-Soler, M.V., 2014. Generation of three-dimensional retinal tissue with functional photoreceptors from human iPSCs. Nat. Commun. 5, 4047. https://doi.org/10.1038/ncomms5047

Zhu, J., Cifuentes, H., Reynolds, J., Lamba, D.A., 2017. Immunosuppression via Loss of IL2rγ Enhances Long-Term Functional Integration of hESC-Derived Photoreceptors in the Mouse Retina. Cell Stem Cell 20, 374-384.e5. https://doi.org/10.1016/j.stem.2016.11.019

Zuber, M.E., Gestri, G., Viczian, A.S., Barsacchi, G., Harris, W.A., 2003. Specification of the vertebrate eye by a network of eye field transcription factors. Dev. Camb. Engl. 130, 5155–5167. https://doi.org/10.1242/dev.00723